UNIVERSITA' DEGLI STUDI DI NAPOLI FEDERICO II

PH.D. PROGRAMME IN SEISMIC RISK

COORDINATOR: PROF. ALDO ZOLLO

XXVI CYCLE

GIOVANNI FORTE

Ph.D. thesis

Integrated approach to the analysis of earthquake-triggered landslides and their impact on road infrastructures

TUTORS: FILIPPO SANTUCCI DE MAGISTRIS
FRANCESCO SILVESTRI

COTUTOR: SILVIA FABBROCINO

MARCH 2014

ACKNOWLEDGMENTS

This Ph. D. thesis represents the closure of a very difficult chapter of my life. At certain point its accomplishment became a challenge with me, which seems... I succeeded.

At the end of a path it becomes unavoidable to watch back and reflect on what happened during this three years period, but as this is a moment of joy I will only mention the happiest memories, which probably will be the only ones to last for life.

I am extremely grateful to Professor Filippo Santucci de Magistris, who was a tutor, but also a friend, who encouraged me, read the whole dissertation and gave me relevant advices to improve its quality. I will always remember the good time we shared in the very long days spent in Termoli village.

My gratitude also goes to Professor Francesco Silvestri, whose advices put me on the right path. I think it is impossible to not remain astonished by the passion he always put in his work. He is really inspiring.

I also want to thank Professor Silvia Fabbrocino and Professor Giovanni Fabbrocino, they gave me this important opportunity. In particular, I want to thank them to have me involved within scientific topics, whose I completely ignored the existence, which are the earthquake engineering geology and the seismic engineering. I hope the experiment they attempted had satisfactory results in the end.

I also wish to thank the geotechnical community, which I don't know whether acknowledged me, but at least became accustomed to the presence of a geologist among them.

My thanks also are for the colleagues and friends of StreGa Laboratory, Giovanni Lanzano and Antonio Panico, and the colleagues and friends of DISTAR department Pasquale Paduano, Nicola Mondillo and Mara Cesarano who supported and tolerated me many times. We always found the way to make a laugh and joke in the time spent together.

I am grateful to the students of University of Molise, who helped me in collecting and organizing some of the data reported in this dissertation.

A thank is also deserved to my Ph. D. colleagues Sergio, Crescenzo, Marianna and Barbara; we spent a nice time together during the several courses we attended.

Sincere thanks also to Daniela Manganaro and Fabio Todisco, who feeded my passion for Geology.

I also have to thank all my friends, who supported me and who maybe could do more.

Lastly, I would like to thank my wonderful family for all their love. And most of all my loving, supportive, encouraging and patient Francesca, whose faithful support during all the stages of this Ph.D., was so appreciated and relevant... Thank you.

ABSTRACT

This thesis dealt with one of the side-phenomena, which can occur during or after a seismic event, namely earthquake-triggered landslides. These phenomena involve both natural and man-made slopes, whose occurrence is very common and widespread as testified by several recent earthquakes. Their consequences can be dramatic, as they can strongly contribute to the death toll, since they often affect buildings and infrastructures, preventing effective post-emergency strategies. Hence it appears relevant to consider into the framework of seismic risk studies also the evaluation of slope stability, which can also be carried out from regional to the scale of the single slope.

The area selected for the present study is the Molise Region, (Central-Southern Italy) within the Southern Apennines, which is one of the Italian areas struck by earthquakes in the last decade, suffering damages both in building heritage and physical environment. It is characterized by medium-high seismicity and high landslide susceptibility. In particular, the most abundant landslides are represented by coherent landslides, i.e. rotational and translative slides, on which this dissertation focused. The main issues concerned the development of stability analysis at territorial scale; within this framework several side-issues were explored. In particular, the implementation of a database of geological and geotechnical tests permitted to characterize the soil strength behavior, produce seismic soil class map and empirical correlations between geotechnical parameters. The stability analyses were calculated as PGD at regional scale through two methodologies, which found validation in the detailed analysis of a case study.

KEYWORDS: Earthquake-triggered landslides, Geotechnical characterization, Seismic Permanent Ground Deformations (PGD), Highway vulnerability, GIS, Molise (Italy).

TABLE OF CONTENTS

INTRODUCTION

Recent and historical seismic events showed that the vulnerability of structures and lifelines is dependent on both the transient (TGD) and the permanent ground deformation (PGD). TGD is the dynamic ground response due to the propagation of elastic waves. PGD is the irrecoverable displacement that persists after the end of shaking (O'Rourke, 1998). The latter encompasses soil liquefaction, surface faulting, ground settlements and landslides. In particular, the latter is the most common phenomenon which can occur in a country as Italy, constituted by a relatively "young" geological setting, whose natural morphoevolution is mainly committed through landslides. The impact of those events can affect strategical infrastructures, as roadways, which directly prevent effective post-earthquake emergency strategies.

From the above premises, it appears relevant to consider into the framework of seismic risk studies also the evaluation of slope stability. This study focused on this concept and it was aimed at developing slope stability analysis in seismic conditions performed at regional scale, in order to also account for the vulnerability of the roadway network to those phenomena. This research also pointed out the possibility to expand the scale of the studies from regional to the scale of the single slope.

An essential part of this work was also devoted to the collection and organization of the pre-existing knowledge through the constitution of a database of geological and geotechnical investigations, as it represents the backbone of every small scale project aimed at territorial analysis.

The area selected for the present study is the Molise Region, (Central-Southern Italy), which is one of the Italian areas struck by earthquakes in the last decade, suffering damages both in building heritage and physical environment and naturally prone to landslides.

The work developed through different stages:

- Collection and study of the reference literature on the phenomenon of earthquake triggered landslides and the way in which this topic is studied into the international literature.
- Collection and study of the main geological and geotechnical technical-scientific literature of Molise Region and the materials which crop out, also in analog geological contexts of Southern Apennines.
- Analysis of the database investigation aimed at characterizing the soil strength behavior, producing seismic soil class map and correlation between geotechnical parameters.
- Implementation of two methodologies for the analysis of the PGD at regional scale and evaluation of the impact on the roadway network.
- Validation of the proposed approach and characterization of a landslide phenomenon at detailed scale.

The flowchart of Figure 1 summarizes the main step of the research activity with the main accomplished results.

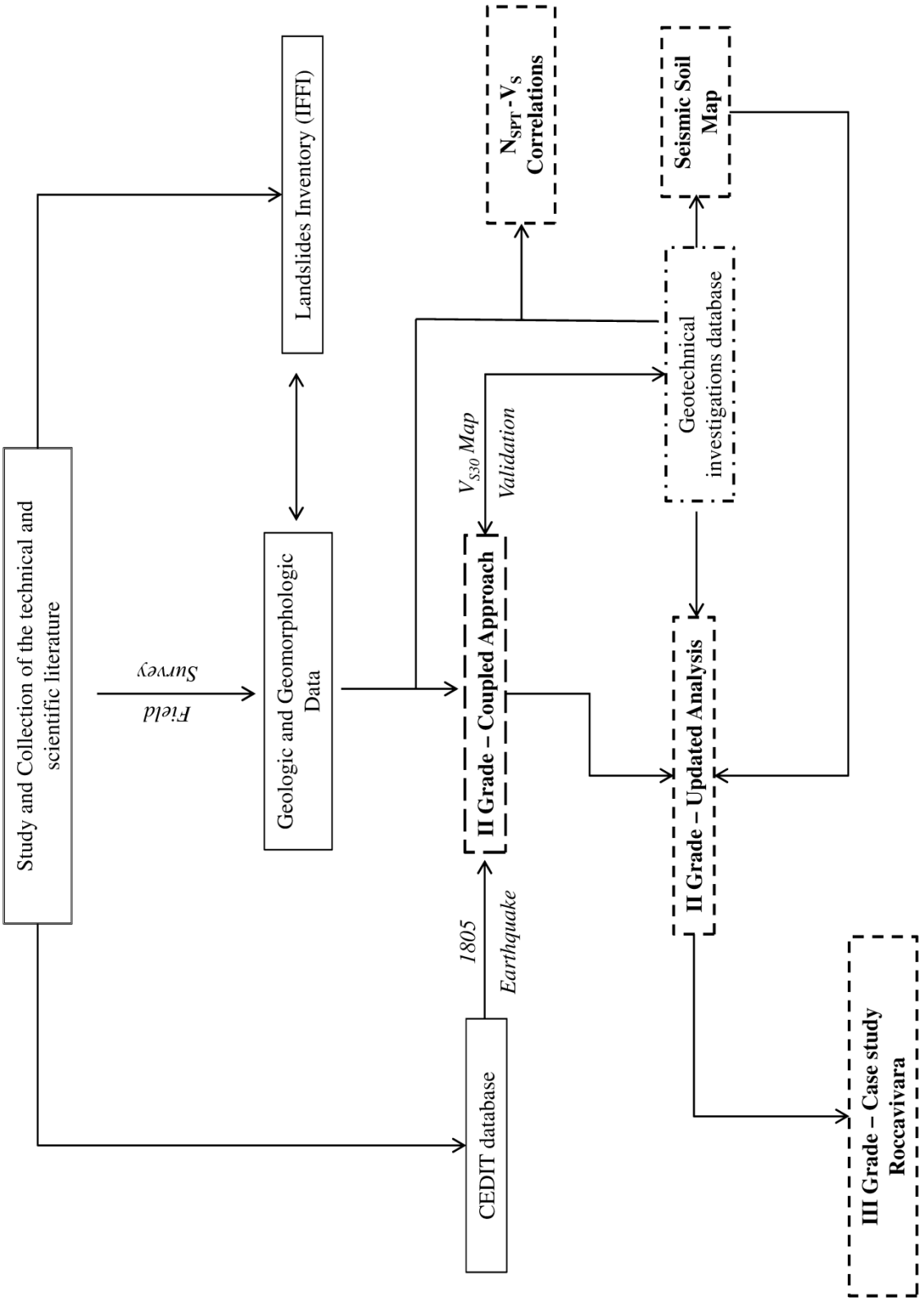

Figure 1. . Flowchart of the approach followed in this research with the obtained results.

The text was organized into five chapters, corresponding to the above mentioned aspects of the research.

In *Chapter 1*, after a brief explanation of the mechanisms of seismic-induced landslides and the category to which they can be classified, a representative case history of damages to roadways due to landslides during recent earthquakes are widely described. They were subdivided into worldwide and italian case histories and reported in chronological order.

Chapter 2 summarizes some of the main geological knowledge about the Southern Apennines and in particular the Molise Region. The latter is described subdividing the chain into three paleogeographic domains, which are (West-Eastward): the Carbonate domain, the Flysch and the Foredeep-Foreland Successions. Then the chapter continues with the description of the geomorphological features of the Region and its seismological setting, with a list of the main historical earthquakes, which affected the area.

In Chapter 3, the organization of the database of geological and geotechnical investigation collected is described, together with the engineering geological classification and the shear strength characterization of the structurally complex formations. The dissertation is followed by a focus on the seismic soil classification approaches at regional scale, with the verification of the applicability of simplified methods in the area and culminates with the production of an original seismic soil class map. Finally, the relationships between N_{SPT} and V_S are explored and new empirical correlations based on a lithostratigraphic approach is proposed and validated.

Chapter 4 describes the two seismic stability methods implemented for the territorial analysis. The first is based on a geomorphological-geotechnical coupled approach, which was compared with another widespread simplified procedure, i.e. the HAZUS (2003) method.

The second is an engineering geology approach based on the soil characterization described in Chapter 3. The suitability of the proposed approach was successfully checked, since it well-predicted the location of the landslides triggered by the Maximum Historical Earthquake (MHE) with the highest displacements. The seismic performance of the roadway network was evaluated through fragility curves and vulnerability thresholds.

In Chapter 5, a detailed slope stability analysis in seismic conditions was carried out. The investigated phenomenon affected the neighboring roadway and it is typical of the earthslides which seasonally occur in Molise. The geological and geomorphological features were identified by field surveys and permitted to describe the subsoil model, which was validated by the geotechnical characterization by laboratory tests on undisturbed soil samples. The stability analysis was performed solving the rigorous Newmark approach for two different conditions, which are pre-failure and incipient failure. The calculated displacements compared with the results of chapter 4 validated both approaches.

1. EARTHQUAKE-TRIGGERED LANDSLIDES

Damage induced by large earthquakes is generally due to strong ground shaking, but also to ground failure. The Northridge earthquake in 1994 (M_w 6.7) triggered more than 11,000 landslides (Harp & Jibson, 1996); while the El Salvador earthquake in 2001 (M_w 7.6) triggered only one landslide in Las Colinas, which killed about 400 people (Lomnitz & Rodríguez, 2001). Those examples are sufficient to remind that, in many earthquakes, landslides have been responsible for as much damage as all other seismic hazards. It is therefore evident the relevance of the evaluation of seismic slope stability within studies of seismic hazard assessment.

The term *earthquake-triggered landslide* encompasses several failure phenomena, whose occurrence and destructiveness depends on geologic environmental and mechanical factors. The interest in this topic is shared among several branches of engineering and geosciences. As noted in Fell et al. (2000), a number of researchers proposed different landslide classification, as function of their concern. Engineering geologists developed descriptive terminology (i.e. Hutchinson 1988; Cruden & Varnes, 1996), as mainly concerned with landslide identification and hazard assessment, while geotechnical engineers focused on material behavior (i.e. Skempton & Hutchinson, 1969; Morgenstern 1992), because as designers, are interested in factor of safety assessment and slope stabilization. The Commission on Landslides and Other Mass Movements of the International Association for Engineering Geology and the Environment (IAEG 1990) and the UNESCO Working Party on the World Landslide Inventory (WP/WL1) suggested a standard set of terms for description of landslides, starting from its definition as: "*the movement of a mass of rock, debris, or earth (soil) down a slope (under the influence of gravity)*". So the earthquake together with rainfalls represents the natural triggering factors responsible for the onset of the downhill movement.

In particular as summarized in Tropeano (2010), the interaction between slope and seismic waves is responsible for the decrease of the resistant forces and the increase of the destabilizing ones. The former is due to the cyclical degradation of the strength parameters (φ'; c'; s_u) for rock joints and soils, but also to the pore pressure buildup. The latter are due to the seismic amplification, for stratigraphic and topographic effects. The kinematics of their movement is quite similar to non-seismic slope failure; this is the reason why the most widespread seismic triggered landslide classification, introduced by Keefer (1984), adopts the same organization than that by Varnes (1978). Specifically, Keefer (1984) assembled the different landslides typologies into 3 categories, depending on the triggering mechanism and ensuing movement.

- Category I: disrupted slides and falls. It encompasses rock and soil falls, rock and disrupted soil slides, rock and soil avalanches (Figure 1.1a). Landslides in this category typically originate on steep slopes, travel relatively fast, and are capable of transporting material far beyond the bases of the steep slopes on which they originate. Except for rock avalanches, all of which have volumes greater than 0.5 × 106 m^3, landslides in this category are also typically thin, with initial failure depths of less than 3 m.
- Category II: coherent slides. It encompasses rock and soil slumps, rock and soil block slides, slow earthflows (Figure 1.1b). These landslides exhibit a slight to moderate amount of internal disruption, typically consisting of a few moving blocks, each of which may be little deformed except for localized internal fissuring. These types of landslides occur most commonly on moderately steep slopes, typically move relatively slowly, and displace material less than 100 m. These landslides are also relatively thick, with typical initial failure depths greater than 3 m.
- Category III: lateral spreads and flows (Figure 1.1c). It includes those landslides for which fluid-like flow is the predominant movement mechanism. Landslides in this category initiate only in soil materials and involve either blocks of relatively intact

material moving on a subsurface liquefied zone (soil lateral spreads) or more completely liquefied masses that move by fluid-like flow throughout (rapid soil flows). In many cases, these landslides are the results of soil liquefaction in saturated sands, gravels, or silts; occasionally they result from seismically-induced disturbance in sensitive (i.e., thixotropic) clays. Also included in this category are all underwater ("subaqueous") landslides, most of which are complex and can involve elements of rotational or translational sliding as well as lateral spreading or flow. Landslides in this category commonly initiate and move on gentle to nearly level slopes, move rapidly, and can transport material large distances.

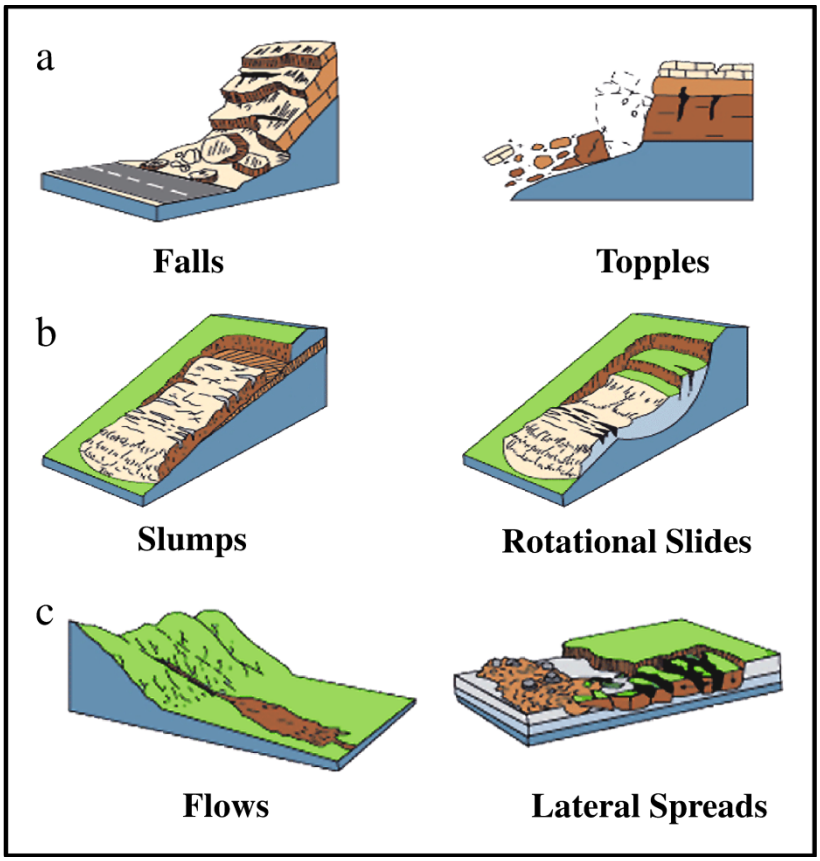

Figure 1.1. Landslide Classification by Keefer (1984). **a)** I Category. **b)** II Category. **c)** III Category.

In the next section a concise description of the main case histories of seismic-induced landslides worldwide and for the Italian territory is proposed.

1.1 WORLDWIDE CASE HISTORIES

Before about 200 years ago, reports of earthquake triggered landslides in historical documents were incomplete, as the information about locations of landslides were imprecise and vague about the kind of material and movement, although valuable historical information could be retrieved. The first formal scientific study of the effects of a large earthquake dated back to the Calabria (Italy) Earthquake in 1783 (MI = 7), when the Neapolitan Academy of Sciences and Fine Letters appointed a commission to conduct field studies in the epicentral area (Sarconi, 1784). These reports indicate that among other effects, at least 215 landslide-dammed lakes were documented (Cotecchia et al., 1986). Throughout the nineteenth and early twentieth centuries, various other scientific commissions carried out field investigations after several other major earthquakes and landslides were commonly documented along with other earthquake effects. Examples of these early reports include those on the MI 7.3 Charleston, South Carolina, earthquake of 1886, the M 8.3 Assam, India, earthquake of 1897, the M 7.8 San Francisco, California, earthquake of 1906 and the M 8.1 Bihar, India-Nepal, earthquake of 1934 (Keefer, 2002 and referenced papers).

In the following, some of the main worldwide earthquakes occurred in the last century are described, with special reference to the slope failures they caused.

1.1.1 THE BIG ONE - SAN FRANCISCO EARTHQUAKE (1906)

It was a major earthquake (M_w 7.8), originated by the St. Andrea's fault, which struck San Francisco and the coast of Northern California on April 18, 1906. It is quite famous for the

devastating fires, which followed the event and lasted for several days. As a result of the quake and fires, about 3,000 people died and over 80% of San Francisco was destroyed (Gilbert et al., 1907). This event triggered ground failures at numerous locations throughout 600 km long segment of the Coast Ranges extending from southern Monterey County on the south to Eureka on the north. These movements considerably damaged bridges and pipelines that crossed the rivers and highways and railroads that paralleled the rivers Figure 1.2 shows historical photos of the triggered landslides (Youd & Hoose, 1978).

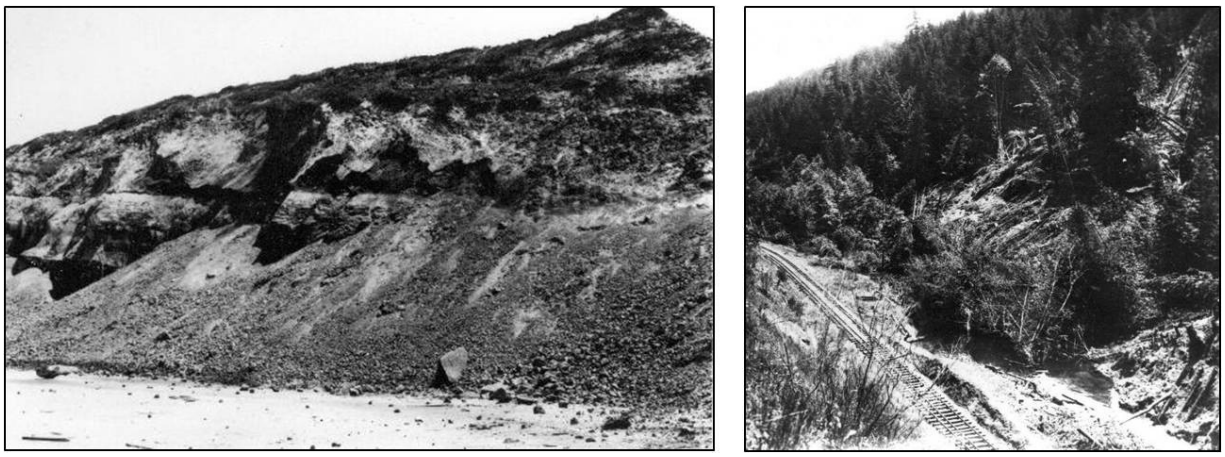

Figure 1.2. Left) Rockfalls along coastal bluffs between Ocean Avenue and Mussel Rock. ***Right)*** Hillside landslide in redwood forest about 6.4 km above Alma, the landslide has dammed Los Gatos Creek from the south (Youd & Hoose, 1978).

1.1.2 THE GREAT ALASKA EARTHQUAKE (1964)

On March, 27, 1964 a great earthquake of M_w 9.2, also known as the Good Friday Earthquake, occurred in Prince William Sound region of Alaska. This event is the second largest earthquake ever recorded in the world, after a M_w 9.5 earthquake in Chile in 1960. The epicenter was located at 120 km from the city of Anchorage. It had an extraordinary duration of 3 to 4 minutes, took 137 lives and caused 350-500 million $ in property damage. Property damage from slides in the mountains was generally limited to roads and railroads (Eckel, 1970). The maximum uplift recorded was 10 m on land and as much as 15 m on the sea floor. The uplift destroyed or greatly

affected many harbors. The strong ground motion induced many landslides, in Anchorage, the most infamous occurred in Government Hill and the Turnagain Heights areas (Figure 1.3).

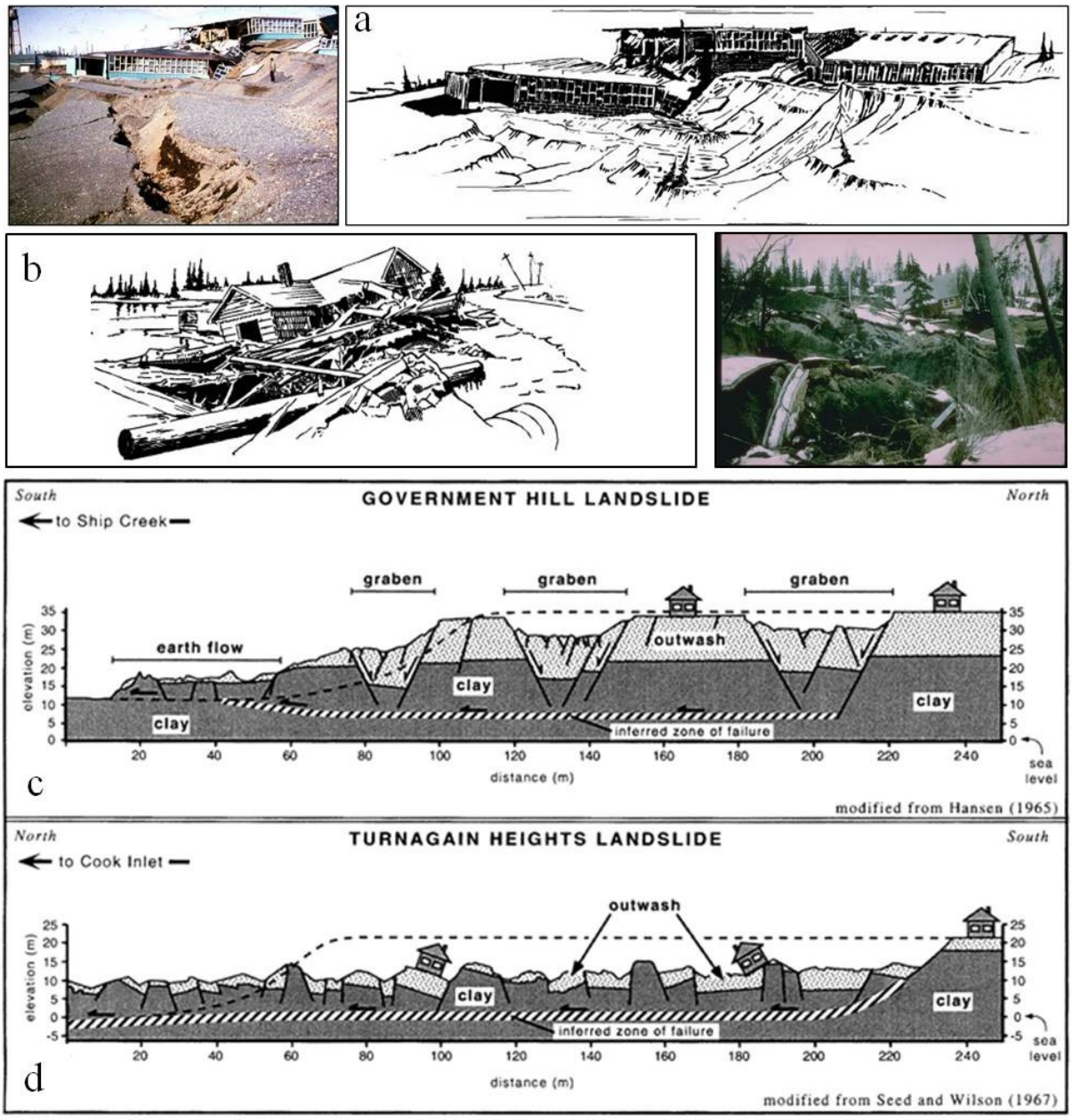

Figure 1.3. a) Government Hill landslide (modified after Eckel, 1970). ***b)*** Turnagain Heights landslide (modified after Eckel, 1970). ***c) d)*** Landslides cross-section after Barnhardt & Kayen (2000).

In both cases the landslides were characterized by the presence of a surface sandy stratum placed on marine clays. This was one of the first cases in which the slope failure was clearly related to cyclic softening phenomena in cohesive materials. Indeed, post-earthquake measurement put in

evidence a 1/30 ratio between the peak and the residual shear strength before and after the earthquake, respectively. Moreover, an important role is likely to have been played by the liquefaction of several sandy inclusions within the clayey soils, as well as by the interaction between inertial effects and the initial shear stress state (Seed, 1968).

1.1.3 LOMA PRIETA EARTHQUAKE (1989)

On October 17, 1989 at 5:04 P.M., a magnitude 6.9 earthquake struck the San Francisco Bay area and lasted for 15 to 20 seconds. The earthquake happened along the San Andreas Fault, with the epicenter happening near the Loma Prieta peak within the Santa Cruz Mountains. It produced slides throughout an area of about 15,000 km^2. The western portion of the bay sits on soft mud; this amplified the shaking by 5 to 8 times in this area and the "interstate route 880" collapsed. This portion of the freeway was 90 kilometers away from the epicenter but experienced severe shaking due to the ground it was built over and the vibration frequency of the structure matching the frequency of the ground motion: 2 to 4 lateral cycles per second. The earthquake also caused ground failure which led to mudslides, fires, and broken water lines. The most spectacular landslides occurred along the coast, as seen in Figure 1.4.

Figure 1.4. A huge landslide triggered along the coast.

The area with the most reported damage was the Marina District because of the liquefaction of saturated sandy and uncompacted soil. A total of about 1280 landslides were identified throughout an area of approximately 2000 km^2 in the southern Santa Cruz Mountains, whereas additional 80 landslides occurred along the adjacent coastal cliffs (Keefer, 2000).

1.1.4 THE HOKKAIDO-NANSEI-OKI EARTHQUAKE (1993)

In the evening of 12 July 1993, a 7.8 Magnitude earthquake occurred in the Sea of Japan, offshore of the Hokkaido Island. Most of the loss was to due to the Tsunami, which followed the event, but liquefaction, rockfall and landslides (14) were also reported in Southern Hokkaido and on the Okushiri Island. The landslide protection system built along the coastal road presented meshes heavily damaged, concrete gravity walls overturned or smashed, and many embankments also failed (Butcher et al. 1993). Yamagishi (2000) recognized rock/soil slides, debris slumps, rock/debris avalanches and rockfall triggered by this event. The most destructive was the Okushiri-port Slide (Figure 1.5), with 20-30 m of thickness, 200 m wide and a mobilized volume of 10^5 m^3, which occurred in Miocene Sandstones.

Figure 1.5. Okushiri-port Slide induced by the Hokkaido-Nansei-oki Earthquake (after Yamagishi, 2000)

1.1.5 THE NORTHRIDGE EARTHQUAKE (1994)

The Northridge earthquake (M_w 6.7) occurred on January 17, 1994 and was centered in the north-central San Fernando Valley Region, Los Angeles, California. It was one of the most costly natural disaster of the United States history; damages involved structural failure in residential, commercial, industrial and transportation facilities, several breaks in water, gas and sewer pipelines, poor performance of geotechnical structure as dam and landfill, thousands of landslides in mountainous areas surrounding the epicenter. The death toll was 61, with more than 18,500 injured and more than $15 billion in damage (Stewart et al., 1994). The triggered landslides were distributed along an area approximately radiating 25 km from the epicenter, including Simi Hills, Big Mountain, Santa Monica, San Gabriel and Santa Susana Mountains in areas of known high landslide susceptibility (Figure 1.6).

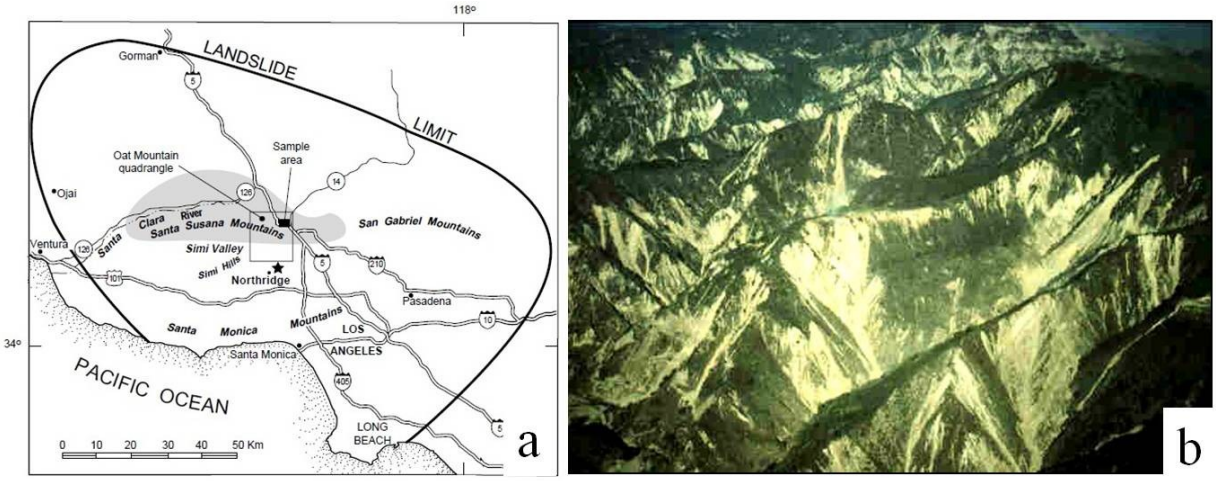

Figure 1.6. a) Location of landslides triggered by Northridge earthquake, shaded area shows zone of greatest landslide concentration (after Jibson et al. 1998). ***b)*** Aerial view of the triggered landslides in Santa Susana Mts.

1.1.6 KOBE EARTHQUAKE (1995)

The 1995 Hyogoken-Nambu (Kobe) earthquake (M_W 7.2) was one of major earthquakes to directly hit a modern city with a high concentration of civil engineering facilities. The development of landslides was reviewed based on air photo interpretation, revealing landslides to be almost linearly distributed along the line of aftershocks. Most of them showed limited motion, probably due to the very dry season in which the earthquake occurred. A conspicuous exception was the Nikawa rapid landslide (Figure 1.7), which, with a volume of about 110,000 m^3, moved in just a few seconds over more than 100 m, destroyed 11 residential buildings and killed 34 people (Japanese Geotechnical Society, 1998). As observed by Sassa et al. (1996), the significant distance and runoff speed were unexpected because (a) the slope inclination barely exceeded 20°, (b) the water table was not high, (c) the soil along the sliding surface consisted of dense coarse-grained sand and silty sand and (d) laboratory tests on soil samples taken from the bottom of the moved landslide mass showed that the soil was only partially saturated. Certainly, the combination of stratigraphic and topographic amplification played a major role in the triggering stage.

Figure 1.7. View of the Nikawa landslide (after Sassa et al. 1996).

1.1.7 EL SALVADOR EARTHQUAKE (2001)

The earthquake of January 13th (Mw 7.6) triggered many damaging landslides in a broad region of El Salvador. The most significant concentrations of landslides occurred in the slopes of Cordillera Balsamo, around Lake Ilopango and Lake Coatepeque, and on steep flanks of some volcanoes in the southern part of the country (Usulatan Volcano). Landslides concentrations were greatest at the locations of weak pyroclastic deposits and lava rocks. In the former case, landslides tended to be highly disrupted masses of rock and earth that fell and slid into jumbled piles of landslide debris; in the latter, harder lava flows were volumetrically small but very hazardous, as they consisted of boulders as large as several tens of cubic meters. The January earthquake also caused two large and deep landslides. The most damaging was the Las Colinas landslide in Santa Tecla (Figure 1.8), which caused almost 600 deaths, while San Vicente landslide closed the Pan-American Highway and killed 12 people (Jibson & Crone, 2001).

Figure 1.8. a) View of the Las Colinas (Santa Tecla) landslide. ***b)*** Aerial view of the landslide scarp.

1.1.8 THE NIIGATA KEN CHUETSU EARTHQUAKE (2004)

The Niigata Ken Chuetsu earthquake occurred on a blind-thrust fault at a depth of 16 km and produced very high intensities of ground shaking in the epicentral area. Two sites recorded peak horizontal ground accelerations of 1.3–1.8 g. This event triggered a vast number of landslides that were densely concentrated in a mountainous area in central Niigata Prefecture. Landslides severely damaged roads and rail lines, destroyed houses and other structures, and dammed streams and rivers as shown in Figure 1.9. Damage from the landslides was initially estimated at U.S. $8 billion, making this one of the costliest landslide events in history. Several mountain villages became uninhabitable for the foreseeable future and perhaps permanently. The factors which contributed to the extensive landsliding were the steep local topography, the presence of weak, deformed geologic materials, exceptionally high groundwater conditions and very high strong ground motion (Kieffer et al., 2006).

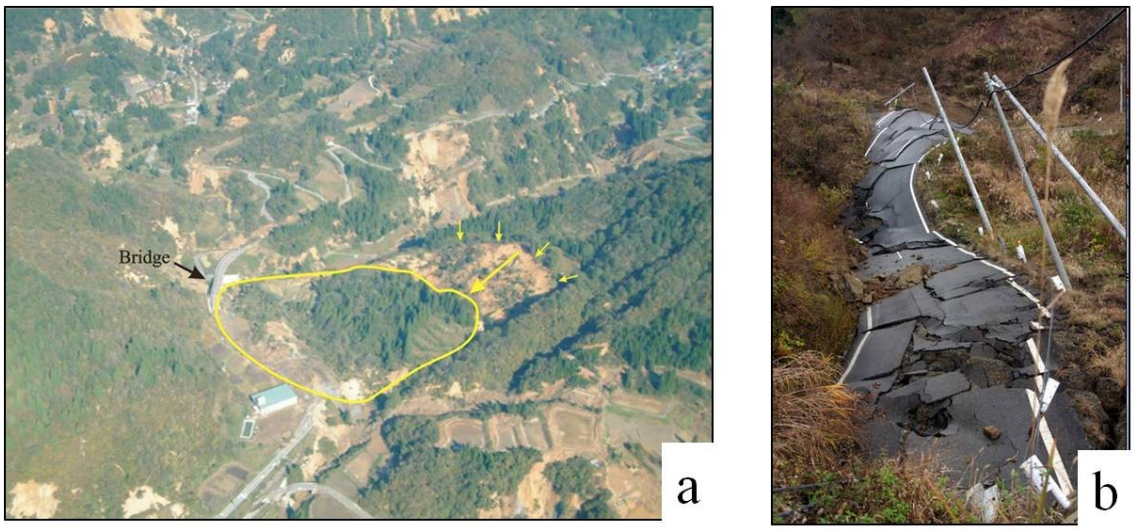

Figure 1.9. a) Aerial view of a landslide dam west of Komatsugura before the reservoir filled. The bridge at left was completely submerged at the time of the reconnaissance, and the reservoir had backed up as far as the village shown in the upper left. ***b)*** Landslide damage to a roadway east of Yamakoshi. Note the backward rotation of the roadway and utility poles in the foreground, together with their forward rotation in the background.

1.1.9 THE WENCHUAN EARTHQUAKE (2008)

The Wenchuan earthquake occurred on May 12, 2008, near the west edge of the Sichuan Basin in China. This earthquake had a magnitude of Mw 7.9 and a focal depth of 19 km. An outstanding characteristic of this earthquake is that it was accompanied by fault ruptures over a distance of 270 km. It induced numerous landslides and killed more than 69,000 people, the worst mountain disaster in the 20th and 21st centuries. The landslides induced by this earthquake created more than 30 dams that threatened both downstream and upstream areas. Landslides triggered by the earthquake include shallow and deep-seated rockslides, rockfalls, debris slides, and debris flows. Shallow landslides were the most common and occurred on convex slopes or ridge tops, where earthquake shaking was amplified (Chigira et al. 2010).

1.2 ITALIAN CASE HISTORIES

In the next section, some of the main Italian earthquakes in the last four decades are briefly described. Further details and references can be found, however, in Tropeano (2010), Pisanò (2011) and Rivieccio (2013).

1.2.1 FRIULI EARTHQUAKE (1976)

The Friuli region (NE Italy) was struck in 1976 by two earthquakes on May 6th (M_L 6.4) and September 15th (M_L 6.1), which caused about 1000 landslides. Most of these, about 90%, were rock falls from steep weathered rock walls (with an estimated rock volume of 100,000 m^3), although some cases of soil falls, debris avalanches and, more rarely, debris slides are documented as well (Civita et al., 1985). One of the most representative events is the Braulins landslide (Figure 1.10) near Gemona town, which is also a national geosite.

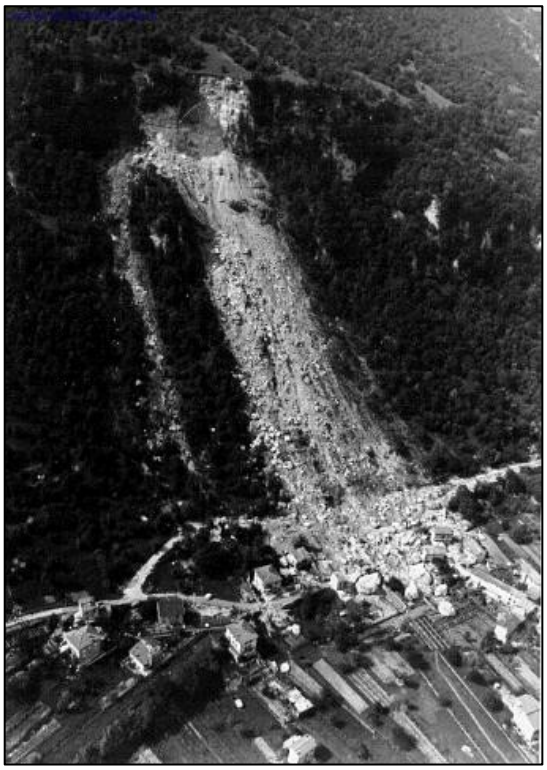

Figure 1.10. The Braulins rock avalanche near Gemona (after www.protezione civile.gov.it).

1.2.2 IRPINIA-LUCANIA EARTHQUAKE (1980)

The Irpinia–Lucania earthquake of 23rd November 1980 (Ms 6.9) was the first event in the Apennines to undergo a systematic field and remote sensing mapping of seismically induced ground effects by independent investigators. The earthquake was a complex event, involving at least three distinct rupture episodes on different fault segments in a time span of approximately 40 s. The focal mechanisms suggest normal slip along NW - SE striking planes, in good agreement with field evidence (Bernard & Zollo, 1989). The earthquake heavily damaged more than 800 localities, mainly in the Campania and Basilicata regions, killing about 3,000 people (Postpischl et al., 1985). Porfido et al. (2002) classified 199 landslides, mainly triggered in overconsolidated clayey soils and structurally complex formations, but also several rock falls and toppling. Several post-earthquake studies identified those landslides as re-activation of dormant or active pre-existing phenomena. The event, which is the most studied among Italian cases, had a very long duration, which was one of the main causes for the large number of landslide, associated with a marked cyclic degradation of shear strength in clays (D'Elia, 1983). Those events moved with some time delay from the main shock and so they have to be interpreted as due to the redistribution of tensions after the excess pore pressure dissipation. It is worth mentioning the landslides of Andretta and Calitri.

The Andretta landslide (Figure 1.11a) was located at 17 km from the epicenter, it is a complex slide, which could be classified in II Category, it was located at the contact between Variegated Clays and regressive succession including clays and silty clays, soft sandstones, sands and conglomerates (Ariano Unit). The sliding surface was estimated at 50 m depth (D'Elia et al., 1986).

The Calitri landslide (Figure 1.11b) was located at 26 km from the epicenter and it was triggered with a 3 hours delay from the main shock, it involved Pliocene clayey soils. It is II

Category rotational slide, with a shear surface located at 100 m depth. Dynamic numerical simulation carried out by Martino & Scarascia-Mugnozza (2005) indicated a diversification of the effects induced by different seismic input frequencies, in terms of propagation and deepening of slope instability, as well as of extent of the displacements. In particular, lower frequencies (0.75 Hz) are more effective in remobilizing large volumes of highly-deformed soil, whereas higher frequencies only induce localized and shallow instabilities with less significant deformations. The lag observed between the onset of gravitational instabilities and seismic events may be attributed to the dissipation time of excess pore pressures. Furthermore the correlation between seismic input frequency and extent of the remobilized soil mass suggests that, in undrained plastic conditions, the dynamic input frequency plays a major role on excess pore water pressures as well.

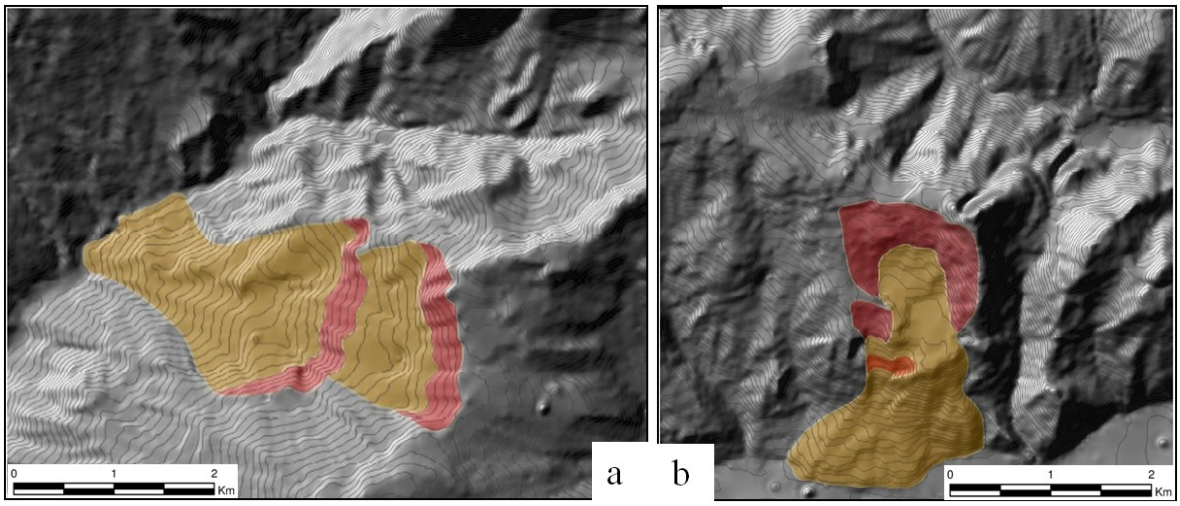

Figure 1.11. The earthquake triggered landslides of Andretta ***(a)*** and Calitri ***(b)*** after Rivieccio (2013).

1.2.3 THE MOLISE EARTHQUAKE (2002)

Between 31st October and 1st November 2002 a Mw 5.7 earthquake occurred in Molise (Central Italy). The focus of the quake was located between accretionary wedge of the ridge and the

foredeep, where the carbonates of the Apulia platform are buried at 4-6 km. The depth of the event was evaluated at more than 10 km, below the carbonate deposits. This event had a poor impact on the regional lifelines as reported in Rasulo et al. (2004), but reactivated a landslide in the municipality of Salcito. This event can be classified as an earthslide (Cat. II), which as reported by local people was triggered 3-4 hours after the 31st October main shock. It was located at 38 km away from the epicenter, which is a remarkably large distance when compared to the plots proposed by Keefer (1984), involved an area of about 1 km^2 and had 2 m of maximum displacement. The displaced material is composed of scaly clay shales interlayered with intensely sheared arenaceous and marly-limestones of Argille Varicolori Formation (Variegated Clays) and involved a 40 m thick layer of calcarenites and marls as shown in Figure 1.12 (Bozzano et al., 2004).

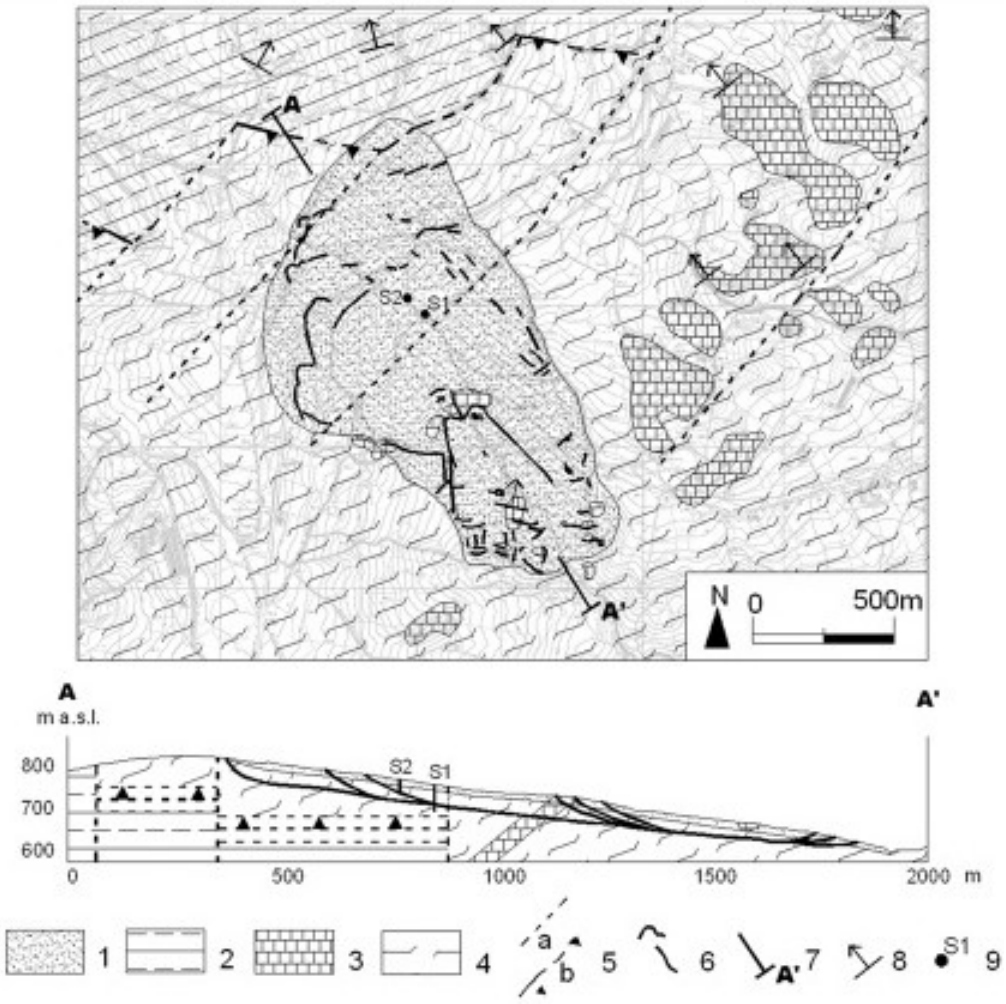

Figure 1.12. Geological sketch of the Salcito landslide area: 1, landslide mass; 2, marls with calcarenites (Tufillo Formation); 3, calcarenites and marls of the Sannio Unit; 4, fissured clay shales (Argille Varicolori Formation of the Molise Unit); 5, tear fault (a), thrust (b); 6, ground crack observed after the Salcito landslide reactivation of 31 October 2002; 7, trace of geological section; 8, attitude of beds; 9, borehole.

The scarp of the landslide is in contact with the Tufillo Formation, which contains an aquifer hydraulically delimited by the Argille Varicolori aquitard, as indicated by the presence of numerous springs. Such an aquifer drains into the top portion of the Argille Varicolori, feeding a superficial aquifer into the landslide mass with a water table located about 1 meter below the ground surface. Bozzano et al. (2008) identified the local seismic site amplification as responsible of the onset of the movement. They conducted numerical stress-strain analysis with FLAC software, analysis of H/V spectral ratios of ambient noise and numerical modeling of both 1-D and 2-D seismic wave propagation using linear and nonlinear solutions. Those data

evidenced: (1) 1 Hz amplification due to 2-D effects within the landslide mass, which presents a basin-like geological structure; (2) a double-peak amplification at about 2 and 3 Hz, respectively, ascribable to 1-D resonance of the landslide mass; (3) 1-D plus lateral wave effects within the landslide mass in the 2.5–3.5 Hz frequency range.

1.2.4 L'AQUILA EARTHQUAKE (2009)

The April 6th earthquake is the most recent strong earthquake in Italy (M_W 6.3, PGA larger than 0.35 g at some locations), which caused enormous losses in terms of both human lives (about 300 casualties) and damaged buildings. However, despite the severe seismic motion, earthquake-induced landslides were not so damaging and mostly concerned falls of sedimentary rocks and small debris avalanches. They were basically induced by considerable inertial solicitations, typical of near fault events.

1.3 SEISMIC SLOPE STABILITY GRADES

Slope stability evaluation is one of the main topics of the hazard assessment and mitigation of the hydrogeological risk, as defined in Italy by De Marchi Commission (1970) and the next DPCM 180/1998. This topic is also an aspect of the seismic risk assessment, as side-effect phenomenon (Gruppo di Lavoro MS, 2008), together with soil liquefaction, surface faulting and seismic settlements. The above mentioned international earthquakes showed that damages due to seismic ground failures can be higher than damages due to shaking. In particular, landslides can affect buildings and population, but also lifelines and distributed infrastructures, which can prevent effective post-earthquake emergency strategies. Hence, adopting planning tools which take in account for possible damage scenarios is fundamental. Those technical tools are represented by the seismic microzonation studies, which can be performed from regional scale to site specific evaluations, passing from the Grade I to Grade II and Grade III/IV (ISSMGE, 1999; Silvestri et al., 2005). Each grade is associated with the enlarging of the map scale, an advance on the analytical methods and the improvement of the detail of the adopted data, as sketched in Table 1.1

Table 1.1. Comparison among the several levels of seismic stability analysis of slope after *Silvestri et al. (2005)*.

Grade	Seismic action	Method of analysis	Damage parameter	Scale
I	M (Magnitude)	Empirical	Maximum Triggering Distance	> 1:100,000
II	PGA_S (Peak Ground Acceleration at surface)	Infinite Slope + Empirical Correlations; Pseudostatic	Yield acceleration (a_c) Displacements (cm)	1:100,000 - 1:10,000
III	a_h (t) (acceleration time-histories)	Definite Slope + Newmark (rigorous)	Displacements (cm)	1:5000 - 1:2000
IV	a_h (t); a_v (t) (acceleration time-histories hz+vert.)	FEM analysis	Stress-strain analysis	< 1:2000

1.3.1 GRADE I

Grade I approaches are the simplest, they consider the seismic-induced landslide hazard expressed as a binary function, which depends from Magnitude (M) and Distance (R). In this way it is possible to assess for different earthquakes the maximum distance at which landslides could occur. The pioneering studies of this topic are due to Keefer (1984); the author collected a database of 40 worldwide earthquakes which triggered landslides between 1811 and 1980. In the same paper a seismic landslides classification is proposed together with Magnitude-Distance curves for the assessment of the triggered landslides hazard. The proposed classification is referenced to Varnes (1978), it identifies three categories, mainly on the involved material and type of movement, which can be easier triggered with increasing earthquake magnitude:

- I Category: disrupted rock and soil slides.
- II Category: coherent rock and soil slides.
- III Category: lateral spreads and flow slides.

These simple empirical correlations pointed out, that the susceptibility to seismically-triggered landslides is related to a Magnitude threshold, below which landslides don't occur. This threshold can be also related to the concept of critical acceleration. In correlations between magnitude of events and epicentral distance, this threshold is at Magnitude IV as shown in Figure 1.13.

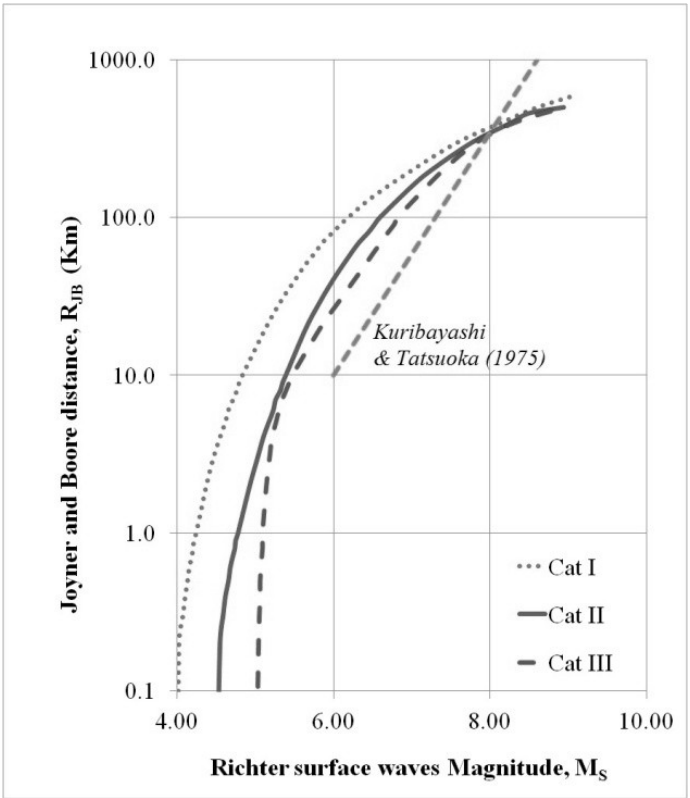

Figure 1.13. Magnitude-Distance curves (modified after Keefer, 1984).

For liquefaction-induced landslides, like lateral spreads, the threshold is magnitude V and it is in accordance with the upper bound liquefaction limit curves identified by Kuribayashi and Tatsuoka (1975) and Youd and Hoose (1977). Moreover, seismically-induced landslides characterized by mass disaggregation (Cat. I) are common to every lithology, while coherent landslides are more frequent in marly-clay deposits (Delgado et al. 2011).

Database analysis has shown that first-time activations are more abundant than reactivations and that an earthquake is a triggering factor for reactivations, whether other concurrent factors are present, such as high values of site amplification or exceeding pore pressures.

Evidences of seismically-induced landslide reactivations have been also collected by Chiodo et al. (1999), who studied the effect of seismic events occurred in Calabria in 1783 and 1905, which caused around 60 landslides, 16 of which were included in the empirical curves compiled by Keefer (1984).

In the end of the 90's Rodriguez et al. (1999) organized a database of 36 earthquakes occurred between 1980 and 1997, thus updating and validating the curves of Keefer (1984) and confirming his correlations. Moreover, data exceeding the threshold of landsliding zones (outliers) have been ascribed to activations caused by seismic sequences. This study also confirms the thresholds related to lateral spreads, in accordance to liquefaction limits in Ambraseys (1988). The most significant differences are in the minimum threshold values accounted as necessary for landslide onset, as shown in Table 1.2.

Table 1.2. Comparison between minimum magnitude thresholds for triggering earthquake-induced landslides.

Landslides (Varnes, 1978)	**Keefer (1984)**	**Rodriguez et al. (1999)**
Rock fall, Rock slides, Soil fall, Disrupted soil slides	M_L 4	M_L 5.5
Soil slumps, Soil block slides	M_L 4.5	M_L 5.5
Rock slumps, Rock block slides, Slow earth flow, Lateral spreads, Rapid soil earth flow	M_L 5	M_L 6.5
Rock avalanches	M_S 6	M_S 6.5
Soil avalanches	M_S 6.5	M_S 6

Furthermore, the same study (Rodriguez et al. 1999) includes a morphometric analysis of landslides, focused on the identification of the depth interval in which the sliding surface is located and on the evaluation of a form factor for both the landslide and the sliding surface. The results of this analysis have led to the estimation of the slope inclination ranges in which the landslides have been triggered, which can be considered a critical slope angle threshold (Table 1.3).

Table 1.3. Critical slope angles for earthquake-triggered landslides.

Landslides (Varnes, 1978)	Critical Slope (Rodriguez et al., 1999)
Falls, Disrupted rock slides	> 35°
Coherent rock slides	> 15°
Soil Slides	> 8°
Lateral spreads	subhorizontal

The first organic study regarding this topic in Italy dates back to the work of Romeo & Delfino (1997), who drew up the first Italian catalogue of soil deformation effects induced by strong historical earthquakes occurred from 1000 to 1992. Due to the long period analyzed, there is a strong uncertainty derived from the unreliability of the historical sources regarding hypocentral distances and magnitude. The catalogue includes 153 earthquakes and about 1800 soil deformation cases. Reported data identifies a greater predisposition of the Italian territory to landslides and fractures during seismic events (see Figure 1.14); indeed, landslides and fractures were observed at higher distances and with lower intensity thresholds (5.5 MCS) compared with liquefaction and subsidence cases (Prestininzi & Romeo, 2000).

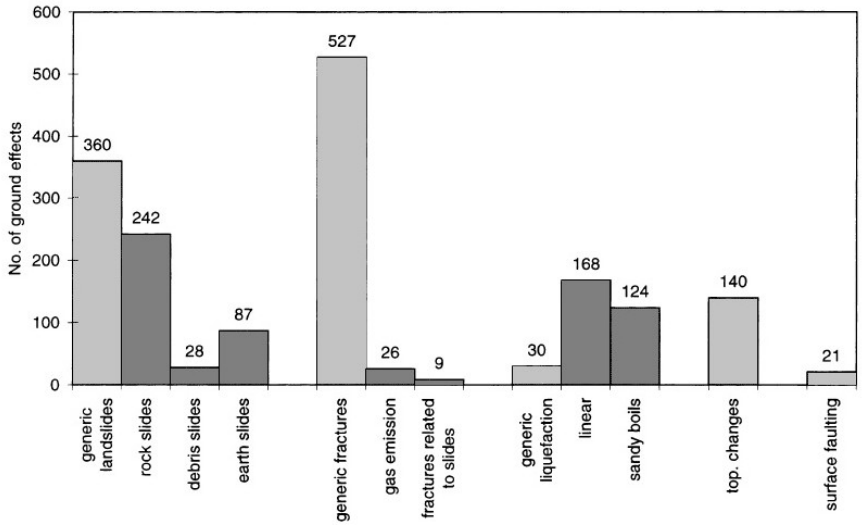

Figure 1.14. Frequency distribution of earthquake-induced ground failures. Landslides are classified on the basis of the prevailing material in which they occurred. Categories labeled as 'generic' refer to ground failure types not better defined (modified after Prestininzi & Romeo, 2000).

The most recent studies on this topic were conducted by Delgado et al. (2011), who focused on the integration of multiple worldwide databases listed in Table 1.4 (Keefer 1984, Mora & Mora 1994, Rodriguez et al. 1999, Papadopoulos & Plessa 2000, Prestininzi & Romeo 2000, Bommer & Rodriguez 2002, Hancox et al. 2002, Keefer 2002, Rodriguez 2006, Delgado et al. 2011).

Table 1.4. List of datasets used by Delgado et al. (2011).

Geographical area	Period	Magnitude	Authors
Global	1811 - 1980	5.2 – 9.2	Keefer (1984)
Costa Rica	1888 - 1993	5.2 – 7.5	Mora & Mora (1994)
Global	1980 - 1997	5.3 – 8.1	Rodriguez et al. (1999)
Greece	1650 - 1995	3.8 – 7.9	Papadopoulos & Plessa (2000)
Italy	461 BC - 1980	4.5 – 7.5	Prestininzi & Romeo (2000)
Central America	1902 - 2001	4.6 – 8.0	Bommer & Rodriguez (2002)
New Zealand	1848 - 1995	4.9 – 8.2	Hancox et al. (2002)
USA	1988 - 1994	4.6 – 5.7	Keefer (2002)
Colombia	1644 - 1999	5.0 – 8.1	Rodriguez (2006)
Spain	1504 - 2005	4.2 – 8.7	Delgado et al. (2011)

The authors considered a dataset of 270 earthquakes reconsidering magnitude-distance curves, focusing more on identifying the causes of the appearance of outlier landslides over the empiric curves. In other words, they paid attention to events triggered by seismic shaking characterized by low magnitude or high distances. Factors determining the appearance of these values are very variable, as Tosatti et al. (2008) pointed out in their study on seismic landsliding in Northern Apennines. Papadopoulos & Plessa (2000) link the high distance of landslides from the epicenter

to the concurrence of earthquake swarms which cause a high degradation of the mechanical properties of materials, resulting in a reduction of the triggering threshold value of landslides. The works by Bommer & Rodriguez (2002) and Rodriguez (2006), based on the study of a dataset representative of Central America, pay special attention to rainfalls preceding the seismic event as a triggering factor, identifying a contributory cause in the meteoric events occurred both before and after the earthquake. Further evidence confirming this thesis is found in both Keefer (1984) and Rodriguez et al. (1999), which analyze landslides mainly located in Central America, where there are particularly critical situations consisting in a complex seismicity pattern (volcanic factor, subduction and transcurrent faults) and abundant rainfalls (tropical climate) on volcanic lithotypes. First level studies by Delgado et al. (2011), regarding the Baetic System, focus on the relationship between macroseismic intensity and the triggering of events on the site, highlighting the role played by local seismic response, as already shown by Del Gaudio & Wasowski (2010). In fact, site response can contribute to the triggering, both in terms of topographic amplification, due to seismic waves reflection, and for the presence of landslide masses, which can influence the signal directivity by amplifying it alongside the sliding surface, due to the contact of rigid and less rigid materials. Therefore they can be responsible for quiescent landslides reactivation.

1.3.2 GRADE II

Several methods have been proposed, in literature, to evaluate, on a regional scale, the seismically-induced landslides hazard, in order to determinate which areas are more vulnerable to landsliding. These approaches, developed through GIS (Geographical Information System), combine topographical, geological and geotechnical data estimating the expected shaking related to a "scenario event" and implement stability models distributed on an indefinite slope (Romeo, 2000). Several authors proposed Grade II methods, Luzi & Pergalani (1996) evaluated seismic slope stability by using the Newmark (1965) method and adopting two recorded accelerograms as seismic input for producing the displacements distribution in an area of the Marche Region, Italy. Miles and Ho (1999) performed a seismic landslide hazard zonation also employing the Newmark (1965) analysis but considering stochastic simulations for the seismic ground motion applied to an area of California. Jibson et al. (1998) calibrated their model of stability on the basis of the Northridge (1994) occurred landslides deriving a probability of slope failures from displacement. Del Gaudio & Wasowski (2004) applied this method to evaluate seismically-induced landslide hazards in Irpinia, southern Italy. Silvestri et al. (2006) carried out a similar approach applying it to an area near the city of Benevento in southern Italy, while d'Onofrio et al. (2013) expanded the model to assess the performance of the gas pipelines after the L'Aquila (2009) earthquake.

In addition to these methods, which couple deterministic procedures to spatial characteristics, there are simpler methods foe evaluating landslide susceptibility based on the attribution of weights and markers, as the method proposed by the Kanagawa Prefecture and Mora & Vahrson (ISSMGE, 1999).

The first identifies seven factors governing slope instability and assigns a given weighting to each of them. The factors considered significant within a mesh square are:

1) the maximum ground acceleration;

2) the length of a contour line at the average elevation;

3) the maximum difference in elevation;

4) the hardness of rock in a typical slope;

5) the total length of faults;

6) the total length of artificial cuts or filled slopes;

7) the topography of typical slopes in a mesh as classified into four morphological categories.

The susceptibility to slope failure in each mesh is obtained in terms of number of slope failures that are likely to occur by the summation of the seven weighted factors.

The second method only considers three factors: relative relief, lithologic conditions and soil moisture as factors influencing the susceptibility. In addition, two factors, seismicity (in terms of MCS intensities) and rainfall intensity are incorporated as triggering factors. The susceptibility, defined as a degree of slope failure hazard (Classes from I to VI), is obtained by combining these five factors. An update of these approaches was reported by Rapolla et al. (2010) and applied for the Island of Ischia (Italy).

A summary of the main scientific papers on this topic is presented in Table 1.5. The several researchers implemented their studies in different geological contexts, adopting different cell sizes and scales. The soil saturation was mainly attributed to two extreme conditions, which are "dry", i.e. groundwater table below the sliding surface, or "sat" in the case of complete saturation, few authors adopted a mean value of the groundwater table depth. The permanent displacements were mainly evaluated through empirical relationships derived from the

resolution of the Newmark (1964) method.

Table 1.5. List of the main literature case studies of II level slope microzonation.

	Andrighetto (1994)	Luzi & Pergalani (1996)	Miles & Ho (1999)	Khazai & Sitar (2000)	Luzi & Pergalani (2001)	Havenith (2002)	Biondi et al. (2004)	Silvestri et al. (2005)	Garcia - Rodriguez et al. (2008)	Jibson & Michael (2009)
Scale	1:5.000-1:50.000	1:25.000-1:50.000	1:50.000	1:25.000-1:100.000	Small scale	Regional scale	1:10.000	1:10.000	1:25.000 - 1:100.000	1:25.000
Cells size	20x20, 40x120 m	30x30 m	n.d.	n.d.	10x10 m	100x100 m	40x40 m	20x20 m	n. d.	n. d.
Seismic Input	PGA = f(M, d) empirical laws; PGA Probabilistic approaches	a(t) recorded	a(t) simulated Boore algorythm; I_a empirical laws and proper formulation	PGA = f(M, d)	I_a & P_d recorded	I_a empirical laws and probabilistic approaches	PGA = f(M, d)	I_a empirical laws	I_a empirical laws	PGA hazard studies
Shear surface depth	Pre – existing landslides	n. d.	n. d.	h = f(α)	Geotechnical tests	h = 10 m pre – existing landslides	n. d.	Pre – existing landslides	n. d.	n. d.
Groundwater	Dry/Sat	Dry/Sat	Dry/Sat	Dry/Sat	Geotechnical tests	z_w = 5 m	n. d.	Stratigraphic features	Dry/Sat	n. d.
PGD	-	Newmark approach	Newmark approach: D = f(a_c, I_a).	D = f(a_c, PGA)	D = f(a_c, I_a); D= f(a_c, P_d).	D = f(a_c, I_a)	D = f(a_c, PGA)	D= f(I_a, a_c)	D= f(I_a, a_c)	D= f(a_c, PGA)

1.3.3 GRADE III

Procedural techniques and evaluation methods of the stability conditions in seismic conditions are well-established in technical and scientific literature (Jibson, 2011). The simplest models are those using pseudo-static analysis, which are based on the principle of limit equilibrium to which a further force simulating shaking is added. This method is definitely one of the most common, due to the simplicity and immediacy of its application. It is based on the hypothesis of the earthquake as a permanent and unidirectional force whose entity depends exclusively on PGA. Obviously, choosing the appropriate value for the seismic coefficient (k) is fundamental for a correct calibration of the model. Stewart et al. (2003) recommend choosing the value of k through a screening procedure based on Bray & Rathje (1998) formula, in which the parameter is calculated as a function of PGA, magnitude, distance and displacement thresholds. A limit of this model is the inapplicability for soils which, due to cyclical loads, are subject to a large pore pressures increase and significant degradation of strength parameters.

More complex and refined methods are total stresses or effective stresses analysis, based on finite element models. These approaches require a large amount of data, which are not always available or obtainable at moderate price, but they can accurately describe ground behavior in seismic conditions. Martino & Scarascia Mugnozza (2005) have thus reproduced, using FLAC software, Calitri landslide triggering mechanism, highlighting the role of interstitial pressures in coseismic and postseismic movements. Marchi et al. (2010) have applied this method to Las Colinas landslide and have observed its applicability limits, with particular regard to boundary value problems and to the definition of Rayleigh damping parameters.

A good compromise between simple pseudo-static models and complex stress-strain models is Newmark's sliding block analysis (§ 4.1). It considers the landslide mass as a block sliding on an inclined plane when a critical acceleration value a_c is exceeded. The critical value is the one

needed to overcome the substrate resistance. In this model, earthquake time histories are double-integrated in order to obtain the cumulative displacement of the block. This value of displacement is an estimation of the performance of the slope subject to seismic shaking; the user must certify the entity of the displacement as acceptable.

This methodology presents some basic assumptions, in fact below the deformation threshold; the "rigid block" is not deformed. Furthermore, dynamic and static resistance is considered as equivalent, upslope resistance is considered infinitely high and critical acceleration is kept constant. This methodology also overlooks pore pressures increase. Another considerable simplification made by this method regards the vertical component, which is considered only directed downslope. This consideration is unrealistic, since seismic motion acts on slopes inducing accelerations of variable entity, both downslope and upslope. Moreover, the relation between acceleration components is conditioned by several parameters such as magnitude, source-to-site distance, fault presence, site conditions and bedrock.

A further aspect to be taken into consideration is the identification of seismic motion descriptive parameter. Several authors state that, instead of using PGA (Peak Ground Acceleration), it is more advisable to rely on Arias Intensity (I_A), since it is a parameter which takes into account event duration in addition to intensity (Kramer, 1996). In this area of interest Tropeano et al. (2007) focus on the identification of relations which are more applicable to natural and artificial slopes, or the definition of simplified methods for estimation of displacements applicable to simplified geotechnical models.

Further refinements of the Newmark method have led to the so-called permanent displacement methods, which can be conducted as coupled or decoupled analysis. These methods are more refined since they also consider seismic site response. Decoupled analysis splits the problem of stability into two steps. First step is the evaluation of local seismic response on the slope, not

considering fracture conditions. This evaluation is obtained through softwares like QUAD4M and SHAKE, which generate time-histories for several points of the slope in order to find a median value. Resulting time-histories are included in a rigid block analysis and permanent displacement is estimated. Main verified results have been obtained for earth-fill dams. Required parameters are the shear waves velocity (Vs), soil thickness and damping. In coupled analyses, seismic response and permanent displacement are modeled together. In these analyses, it is necessary to determine a_c and Vs, both above and under the sliding surface, moving mass thickness and damping (see Tropeano, 2010 and its reference for further details).

2. GEOLOGICAL, GEOMORPHOLOGICAL AND SEISMOLOGICAL SETTING

The pioneering studies on the geological structure of the southern Apennines started in 1880 thanks to consultant geologists working for railways and A. Scacchi and F. Bossani of the Neapolitan geological school. This task was, later, carried out by G. De Lorenzo, who between 1896 and 1904 defined the reference background for the next geological studies, whose validity lasted until the half of the XX century. He considered the Apennine Orogen completely autochthonous, but defining flysch as gravitative deposits related to tectonics. An improvement of this knowledge was due to foreign authors, such as M. Lugeon and E. Argand (1906), who recognized Calabria thrust sheets as allochthonous terrain; N. Tilmann (1912) and M. Limanowski (1913), who identified Calabria granites as the highest tectonic unit together with J. Gryzobowski (1921), S. Franchi (1923), H.W. Quitzow (1935), R.B. Behrman (1936), M. Anelli and R. Signorini (1939). E. Beneo (1950) validated the analogy between the "Argille Scagliose" of northern Apennines with certain shales cropping out in the southern Apennines. Between 1956 and 1957 F. Ippolito , P. Lucini and R. Selli investigated flysch formations and the relationship with the "Miocenic Transgression".

The work of Selli (1962) represents the first important attempt, after De Lorenzo's synthesis, to give an integrated view of the geology of the southern Apennines. In particular, he gives a first coherent paleogeographic reconstruction and identifies several tectonic phases, during Miocene and Pliocene.

In the 1961, the contribution of French geologists Glangeaud and Grandjacquet permitted to localize the boundary between the African and European plate in Calabria, along the "Sangineto line". This tectonic element represents the suture between the autochthonous carbonate Apennines to the North and the Sila, which represent the forefront of the African domain. In

Ogniben (1969) this framework was completed, giving more details on the "Calabria-Lucania border" identifying five periods of orogenesis (Ippolito et al. 1975 and reference therein).

Between the seventies and nineties several authors (D'Argenio et al. 1972; Sgrosso 1986, 1988; Mostardini & Merlini 1986; Sgrosso 1998; Cello & Mazzoli 1999; Scrocca & Tozzi 1999; Di Luzio et al. 1999) defined a modern interpretation of the geological setting of the southern Apennines. According to Patacca & Scandone (2007), four first-order geological elements can be distinguished: the Tyrrhenian area, the Mountain ridge, the Foredeep basin and the Adriatic-Apula Foreland.

- The Tyrrhenian area is characterized by oceanic crust and thinned continental crust, representing a back-arc extensional feature developed at the rear of the Apennine system in late and post-Tortonian.
- The Mountain chain is formed by a deep-seated carbonate duplex system tectonically overlain by a thick pile of NE-verging rootless nappes derived from basin and platform domains. The buried duplex system is composed of shallow water and subordinate deeper-water Mesozoic-Tertiary carbonates stratigraphically covered by Pliocene terrigenous deposits.
- The Foredeep basin corresponds to the youngest (Plio-Pleistocene) flexural depression developed at the front of the thrust belt. The Plio-Pleistocene deposits filling the foredeep basin are mainly constituted by erosional products coming from the chain.
- The Adriatic-Apulia foreland is constituted of Mesozoic-Tertiary carbonates and Triassic evaporites overlying a thick pile of mixed carbonate-siliciclastic Paleozoic deposits, the top of which has been reached at a depth of 6112 m in the Puglia 1 well (Videpi Project). A Precambrian crystalline basement has been hypothesized under the whole Adriatic-Apulia foreland.

During the last decades several palinspastic restoration sketches were proposed. The simplest was elaborated in the last sixties by Ogniben (1969); it consisted in four paleogeographic domains moving from west to the east, Tyrrhenian Basin, Apenninic Platform, Lagonegro-Molise Basin and Apulia Platform. A quite similar scheme, popular among oil geologists, was proposed by Mostardini & Merlini (1986) who recognized six domains. The principal difference between this paleogeographic model and the previous reconstruction consists in the partition of the Apulia domain into two platforms separated by an intermediate basinal domain (Apulia Basin) as shown in Figure 2.1a.

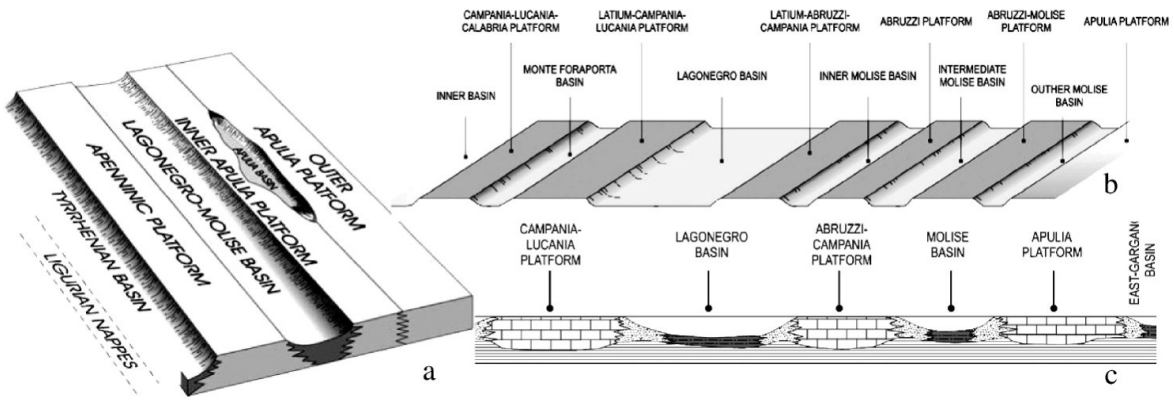

Figure 2.1. a) The Southern Apennine depositional domains during Cretaceous-Paleogene after Mostardini & Merlini (1986). ***b)*** The Southern Apennine platform-and-basin system during Jurassic-Paleogene after Sgrosso (1998). ***c)*** The Southern Apennine platform-and-basin system during Jurassic-Paleogene after D'Argenio et al. (1972).

A more articulated model, popular in the seventies, was proposed by D'Argenio et al. (1972). According to this model (Figure 2.1c), an intermediate platform (the Abruzzi-Campania Platform) separated the Lagonegro Basin from the Molise one. Greater paleogeographic complexities have been subsequently postulated by Sgrosso (1998) who proposed a palinspastic restoration (Figure 2.1b) according to which, five platforms and five basins existed during Mesozoic and Paleogene between the internal oceanic basin and the Apulia Platform.

From the early Miocene to the early Pleistocene, shortening at the collision margin involved progressive folding and thrusting of Mesozoic-Tertiary units and of late Miocene-late Pliocene clastic successions deposited in the eastward-migrating Adriatic foredeep. The timing of eastward migration of shortening is constrained by clastic successions deposited in diachronous, east-younging top-thrust basins (D'Argenio et al. 1972; Sgrosso, 1998; Patacca & Scandone, 2007; Vezzani et al., 2010).

At the beginning of Miocene (Aquitanian, 23.03 Ma), the convergence between the European and African plate started the orogenesis of the southern Apennines. It began with an important transgression of the sea on the internal carbonate platform (Campana-Lucana Platform). Its deposits can be attributed to two phases, represented by concordant and discordant transgressive sedimentary sequences. The first pre-orogenic phase originated concordant calcarenitic deposits passing with the deepening of the sea to arenaceous-turbiditic in flysch facies (i.e. *Cusano Fm*, *Longano Fm* and *Pietraroja Flysch* within the Matese Mts). The second sin-orogenic phase occurred in the Langhian (15.97 Ma), in which two important tectonic events occurred. The flysch was tectonically covered by thrust sheets from the internal domain (Sicilides Unit, Frido Unit) and the Campania-Lucania platform thrusted over the Lagonegro basin. The successions related to the Lagonegro basin can be also retrieved in the North, correlated with the Sannio and Fortore Units. Meanwhile the internal unit nappe continued to move eastward, the formation of a new discordant basin (*piggy-back basin*) called Irpinian Basin occurred; which partly lied on the internal nappe and on the undeformed external Lagonegro basin. *Piggyback basins* generally develop, in the hanging wall, but also in the footwall (i.e. *Gorgoglione Fm*) of active thrusts and are backward limited by inactive ridges. The deposits formed within the Irpinian Basin crop out from *Samnium* to Lucania, where they are addressed with different names, *San Giorgio Fm, San Bartolomeo Flysch, Gorgoglione Flysch, Serra Palazzo Fm, Faeto Flysch* (Pescatore et al.,

1969; Cocco et al., 1972). The last two Formations are mainly calcareous and their source area is located near the eastern flank of the basin.

Between Serravallian (13.82 Ma) and Tortonian (11.62 Ma) the transgression reached the Abruzzese-Campana platform permitting to widen the Irpinian basin and merge it with the Molise basin. This new Basin became the southern Apennines miocenic foreedeep (Pescatore, 1988). Hence the several sheets of the internal units with the Irpinian basin moved eastwards and the Abruzzese-Campana platform thrusted over the Molise basin. Between late Tortonian and early Pliocene several overlied *wedge-top* basins formed on the moving thrusts, they are characterized by strong angular unconformity contacts and are mapped as *Unconformity Bounded Stratigraphic Units* (Salvador, 1994). From bottom upwards it is possible to retrive: *Irpinia Supersynthem* (*Caiazzo Sandstones, Castelvetere Flysch, San Bartolomeo Fm*), *Altavilla Supersynthem* and *Ariano Irpino Supersynthem* (Crostella & Vezzani, 1964; D'Argenio et al. 1972; Pescatore et al., 2000; Boiano, 2000; Di Nocera et al., 2006; Pescatore et al., 2008).

In the middle Pliocene (3.6 Ma) the last translation towards the Apulia platform occurred and the Apulia foreland lowered as graben westward forming a flexural depression which consists in the actual foredeep. The younger deposit, basically represented by the Sub-Apenninic Clay (Grey-Bluish clays), are the upper portion of a thick sequence filling the Bradano Trough, that transgressively covered the outer margin of the mountain chain after the de-activation of the nappe front. The Bradano Trough represents the youngest foredeep basin in the Southern Apennines.

Finally from late Pliocene until early Pleistocene (Calabrian, 1.8 Ma) tectonics mainly showed vertical movements, through normal and strike-slip faults.

Along the Tyrrhenian margin of the Ridge, Pleistocene terrigenous deposits widely developed in the main coastal plains (Sele, Sarno, Volturno and Garigliano), where they reach considerable thicknesses (e.g. more than 3300 m in the Cancello 2 well drilled in the Volturno Plain). The

sudden rapid accumulation of these terrigenous deposits is related to the development of normal faults dissecting the Tyrrhenian margin of the mountain chain and to a major change of tectonic regime that took place around the early Pleistocene/middle Pleistocene (Cinque et al., 1993; Hippolyte et al, 1994).

The extensional regime established in the Tyrrhenian area also permitted the uplift of magmatic bodies, which produced an intensive volcanic activity, which contributed to the aggradation and progradation of the wide coastal depressions.

2.1 GEOLOGICAL SETTING OF THE MOLISE REGION

The synthesis of the geological knowledge of the Molise Region can be mainly retrieved in the official cartographic records. The Region encompasses the following 1:100.000 scale sheets: 148 Vasto, 153 Agnone, 154 Larino, 155 San Severo, 161 Isernia, 162 Campobasso, 163 Lucera. The only three 1:50.000 scale sheets already surveyed and published are: 372 Vasto, 393 Trivento and 405 Campobasso.

(http://193.206.192.231/carta_geologica_italia/centro.htm;

http://www.isprambiente.gov.it/Media/carg/molise.html).

The Molise Region covers a representative portion of the accretionary wedge of the southern Apennines. This area is dominated by low-competence successions of the far-traveled Sicilide thrust sheet (Cretaceous-middle Miocene), thrusted over Mesozoic-Tertiary carbonate units and over late Miocene siliciclastic deposits telescoped with the carbonate substratum of the Adriatic margin. Internal deformation of individual units is heterogeneous, reflecting competence contrasts between sedimentary packages, large-scale rotation of units during tectonic transport, and out-of-sequence propagation of thrust fronts.

The complex paleogeographical setting in which the Region is located will be discussed adopting the palinspastic restoration proposed in Patacca & Scandone (2007) illustrated in Figure 2.2 and the simplified geological setting sketched in Figure 2.3. They permit to identify three paleogeographic domains: Carbonate domains, Flyschs domains, Foredeep - foreland successions as proposed by Cello et al. (1987).

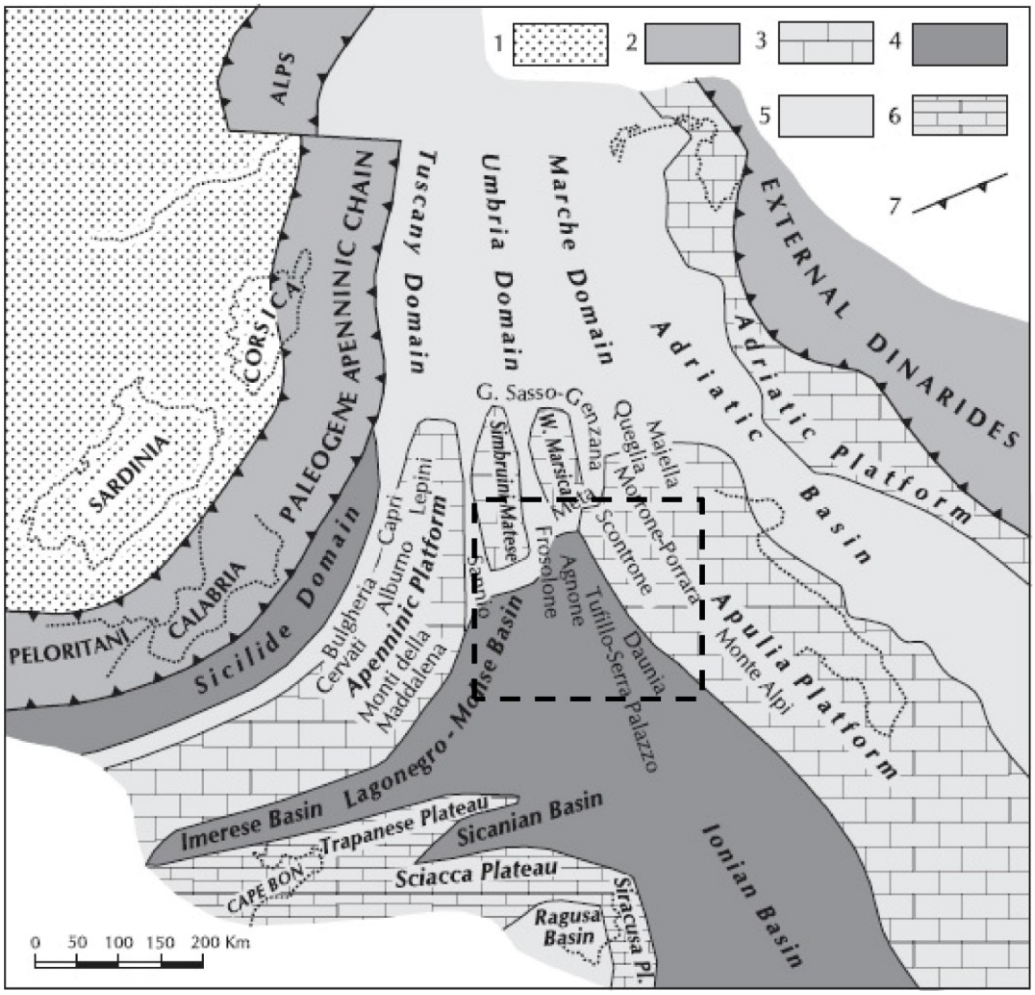

Figure 2.2. Palinspastic restoration of the Central Mediterranean region in the late Oligocene (about 30 Ma) showing the distribution of the Central and Southern Apennine platforms and basins before their incorporation in the mountain chain, modified after Patacca & Scandone (2007). 1) European foreland. 2) Paleogene mountain chains. 3-6) African foreland: 3) shallow-water carbonate platforms; 4) deeper-water basins floored by oceanic or thinned continental crust; 5) basinal areas with isolated structural highs; 6) wide pelagic plateaux. 7) Fronts of the orogenic belts. The dotted box indicates the domains involved in the Molise geological setting.

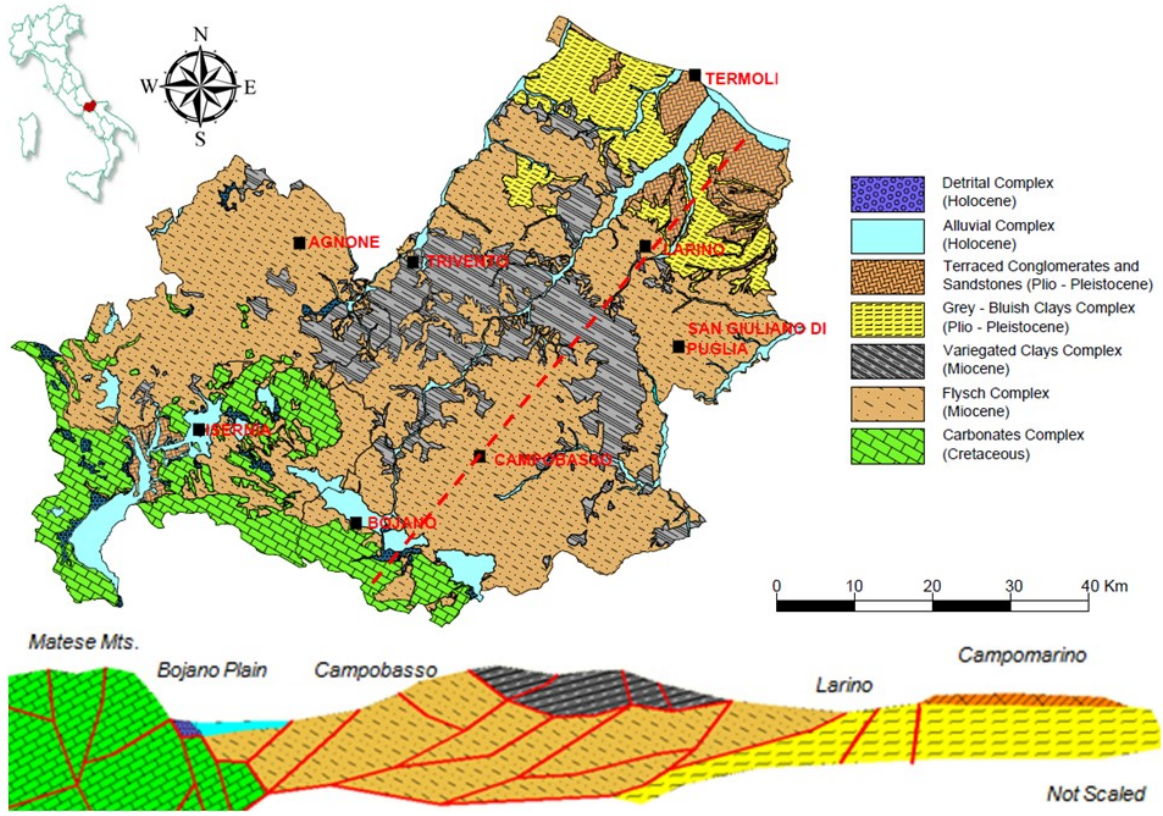

Figure 2.3. Simplified Geological sketch of the Molise Region. The cross-section is traced along the dotted red line.

2.1.1 CARBONATE DOMAINS

The carbonate domain is present in the western part of the Region and it mainly crops out in the Matese, Venafro Mounts and Montagnola di Frosolone (Tozzi et al., 1999 and reference therein). The stratigraphic sequence belongs to the Simbruini-Matese Unit and consists of 2500-3000 meters of Triassic-Cretaceous shallow-platform carbonates disconformably overlain by Miocene inner-ramp shallow-water limestones grading upwards to outer-ramp hemipelagic marls and finally into siliciclastic flysch deposits (*Cusano Fm, Longano Fm* and *Pietraroja Flysch*). The Mesozoic facies are mostly indicative of tidal-flat and platform environments. Upper Cretaceous platform-edge facies crops out in the Eastern sector. Upper Cretaceous-Paleogene slope deposits are widely represented in Western Matese, in the Venafro Mountains and Montagnola di

Frosolone. The latter is part of the Molise Nappe, it is a basinal domain considered very close to the outer margin of the Matese Platform and in contiguity with the Agnone domains. Additional stratigraphic information on the lowest portion of the sequence is provided by the Frosolone 2 well (Videpi Project). It spans from Upper Cretaceous to Messinian and it is composed of silicified fine-grained calciturbidites and subordinate calcirudites with intercalations of shales (50-60 m), gray, greenish and reddish marls passing to calcareous breccias and subordinate calcarenites, followed by hemipelagic limestones and marls rich in planktic foraminifers (which can be correlated to *Cusano Fm* and L*ongano Fm*). The carbonates are overlied by *Frosolone Sandstones* or *Sant'Elena Sandstones* (which can also be correlated to *San Massimo Sandstones*), they are made of clays and silty clays with rare intercalations of fine grained sandstones and coarse-grained sandstones. The contact between the Matese and the Frosolone Unit is represented by a high-angle reverse fault. Some interesting outcrops of the Carbonate Complex are shown in Figure 2.4.

Figure 2.4. a) The transgressive contact in *paraconformity* between the lower Cretaceous limestones and the Upper Miocene limestones (i.e. *Cusano Fm*) within a quarry on Mt. Matese. ***b)*** Rudist bearing limestones of

Santonian-Campanian Age (86-72 Ma) near the village of S. Polo Matese (Di Paola et al., 2011). ***c)*** Fault surface within the *Longano Fm*.

2.1.2 FLYSCH DOMAIN

The flysch domain is the most widespread geological *facies* cropping out in Molise; in the geological scheme of Figure 2.3 it is represented by the Variegated Clays Complex and the Flysch Complex. These complexes encompass the geological formations known in the geological technical literature as Sicilides, Sannio Unit, Fortore Unit, Molise Basin Nappe and Irpinian Basin Nappe. They show the *facies* of *Wild Flysch* (Ogniben, 1963), in which *"the normal flysch sedimentation is associated with sandstones and mudstones intercalations and interposition of huge exotic boulders [...], the latter could be related to the orogenic transport of neighboring nappes"*. In the same paper Ogniben distinguished the Wild flysch from Argille Scagliose (Variegated Clays), *"the latter are made of more or less tectonized deposits, coming from clayey formations and flysch, [...] mixed in twisted sheets; both the clayey component and the competent rock strata experienced an orogenic transport, in which the clays became the dominant part and pieces and shreds of rocks were immersed in them"*. The huge boulders present within these formations are known as Olistoliths and olistostrome (Cocco & Pescatore, 1968).

Sicilides, Fortore and Sannio Units

The Variegated Clays (*Auct.*) are part of the Sicilides Unit and are also correlated to the Fortore Unit and the Lucanian Nappe (Pescatore et al., 2000). The stratigraphic succession, reaching a thickness of 1500-2000 meters, consists of three major intervals:

- *Lower Varicolored Clay*, made up of some hundred meters of gray-greenish and red shales with thin intercalations of siliceous calcilutites. A Cretaceous age has been merely

inferred by the stratigraphic position since no diagnostic fossils have been recovered from this part of the sequence;

- *Corleto Perticara Fm*, which consists of two portions. The lower characterized by white calcilutites containing planktonic foraminifers and siliciclastic calcarenites with sporadic intercalations of red marls and gray calcareous sandstones (*Sant'Arcangelo member*). Its age ranges from late Cretaceous to the late Oligocene. The upper portion corresponds to the *Corleto sandstones* (Oligo-Miocene) and mainly consists of medium to coarse-grained gray calcareous sandstones.
- *Upper Varicolored Clay* and *Tusa Tuffite* are made of red and gray-greenish shales and silty shales with intercalations of calcilutites and siliciclastic calcarenites; fine-grained green quartzarenites occur in the upper portion. The uppermost part contains variable amounts of volcaniclastic sandstones (*Tusa Tuffite*).

In the upper part of the succession are present lenticular intercalations of quartzite sandstones marking the transition in the upper *Numidian Flysch* (Langhian). These deposits are interested by intense colluvial transport and huge and complex landslides that create a thick layer of alteration composed of heterometric and heterogeneous clasts embodied in a clayey matrix, moreover Olistoliths are very frequent, as shown in Figure 2.5. The contact between the Sicilide Unit and the underlying allochthonous sheets is systematically represented by a thrust flat showing low cutoff angles at the footwall and higher angles at the hanging wall.

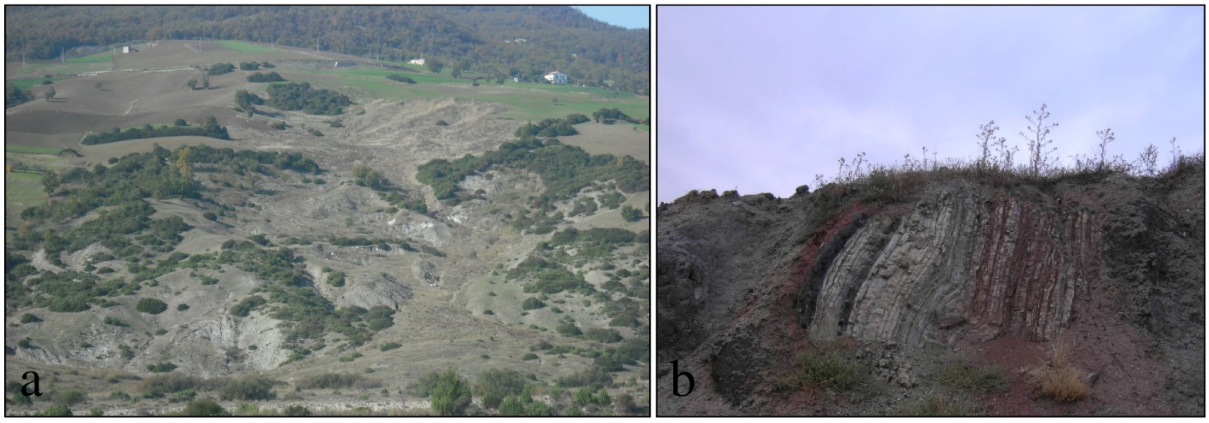

Figure 2.5. a) Complex landslides phenomena within the Fm along the Trigno river, near the village of Trivento. ***b)*** Alternating brick-red and green shales, including olistoliths of the Variegated Clays of the Sicilide Unit in a quarry at the North of Spinete village (Festa et al., 2006).

The Sannio Unit occupies a western position than Sicilides and Fortore Units. It crops out in a restricted sector at the South of Molise in the Mt. Moschiaturo Unit, which could be considered a *klippe* on the Variegated Clays (Festa et al., 2006; Di Nocera et al., 2006 and reference therein).

Molise Basin Nappe

The Molise Basin Nappe is constituted by successions in slope-basin facies (Lias-Messinian). It encompasses the Frosolone, Agnone, Tufillo-Serra Palazzo and Daunia Units.

Frosolone together with Agnone Unit widespread in the Alto Molise Region. It is not yet clear whether the Frosolone and Agnone allochthonous sheets are separated by a major thrust surface or they represent second-order thrust sheets belonging to the same first-order tectonic unit. No doubt exists about the original contiguity of the Frosolone and Agnone depositional domains, which is attested by the gradual transition of facies between stratigraphic sections surely belonging to the Frosolone thrust sheet and stratigraphic sections referable to the Agnone one.

As concerns the Agnone Unit (Figure 2.6a), the flysch deposits are characterized by red and green shales and radiolarian cherts containing sporadic intercalations of calcilutites and graded calcarenites. Some differences exist also in the siliciclastic flysch deposits of the Frosolone and

Agnone sequences. The upper Tortonian clays and silty clays with subordinate intercalations of fine-grained sandstones present at the base of the *Sant'Elena Sandstone* in the Frosolone sequence are lacking in the Agnone sequence, where they are replaced by a few meters of mudstones, in which three members (Verrino, Poggio-Villanelle and Sente) have been distinguished. From bottom upward they are made of grey marly clays with marly limestones, which pass to sandstones and at last to a more clayey *facies* (Di Bucci et al., 1999).

The Tufillo-Serra Palazzo (Langhian–Tortonian) and Daunia units crop out along the outer margin of the Apennines from Abruzzi to Basilicata. They could be correlated with *Gorgoglione Fm* and *Castelvetere Flysch* (Patacca & Scandone, 2007 and reference therein). A type-section of the Tufillo-Serra Palazzo Unit consists of Varicolored shales with subordinate intercalations of calciturbidites, hemipelagic marls and *Numidian sandstones*. Calciturbidites and hemipelagic foraminiferal limestones with thick intercalations of calcareous sandstones (Figure 2.6b). Gray clays and silty clays with intercalations of fine-grained siliciclastic turbidites (*Olmi Fm*). The stratigraphic sequence of the Daunia Unit encompasses the *Serra Funaro Flysch* and upwards the *Faeto Flysch (Crostella & Vezzani, 1964, Lanzafame & Tortorici, 1976)*. These formations differ from the Serra Palazzo for minor content in *Numidian sandstones* and absence of sandstones in the post-Numidian interval, basically constituted of hemipelagic foraminiferal limestones. The latter are associated, mostly in the lower part of the interval, with coarse-grained calciturbidites rich in platform-derived clasts. The uppermost Tortonian?-Messinian fine-grained siliciclastic deposits show a more distal characteristics (*Treste Fm*). In the Molise region, the Daunia Unit is unconformably overlain by Messinian evaporites (*Montecastello Evaporites, Crostella & Vezzani, 1964; Gessopalena Gypsum, Festa et al., 2006*). This unconformity indicates that the first compression deformation of the Tufillo-Daunia depositional domain took place during Messinian times before the salinity crisis. In Molise, the Serra Palazzo and Daunia Units form an imbricate fan in which a gradual transition from the typical Tufillo-Serra Palazzo

lithofacies to the Daunia ones is recognizable moving across the different thrust sheets. The Tufillo-Serra Palazzo and the Daunia Units lie over different thrust sheets on the Apulia Platform.

Figure 2.6. a) Outcrop of sandstones of the middle term of the Agnone Flysch along the road from the village of Pietrabbondante to Verrino (Di Paola et al., 2011). ***b)*** Typical outcrop of the Tufillo-Serra Palazzo Unit along the Trignina expressway, near the village of Trivento.

Irpinian Basin Nappe

The Irpinian Basin represents the foreedeep of the Southern Apennines, during Miocene (Pescatore, 1988). In Molise Region, only the deposits formed near the eastern flank of the basin crop out. In Figure 2.7 the stratigraphic relationships among the several lithostratigraphic Units of the Eastern Irpinia Basin are shown.

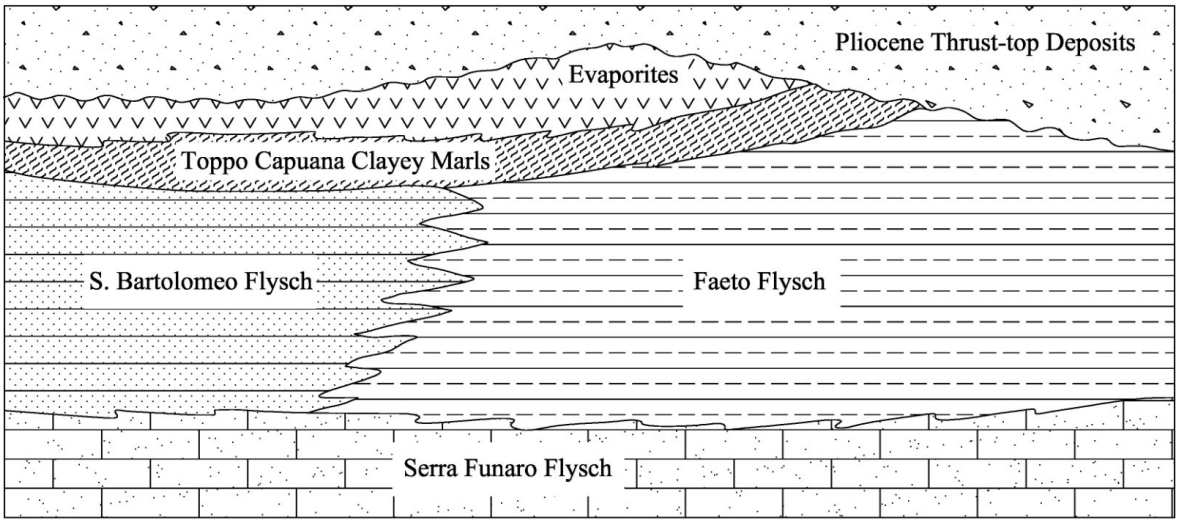

Figure 2.7. Stratigraphic relationships among among the several lithostratigraphic Unit of the Eastern Irpinia Basin, cropping out in the Molise Region, (modified after Crostella & Vezzani, 1964).

Faeto Flysch is mainly constituted by intercalation of marls, calcareous marls and limestones. The strata have a mean thickness spanning from 2 to 20 cm. The marly layers are rich in *orbulina universa*. The mean thickness of the whole formation is about 800 m (Figure 2.8). Upwards it gradually passes to the *Toppo Capuana Clayey Marls Fm* and it is covered through a transgression contact by the Pliocene *Tona Fm.* The *facies* is representative of a proximal deposition basin near the Apulian platform, which passes westwards to axial basin *facies* represented by the *S. Bartolomeo Flysch*.

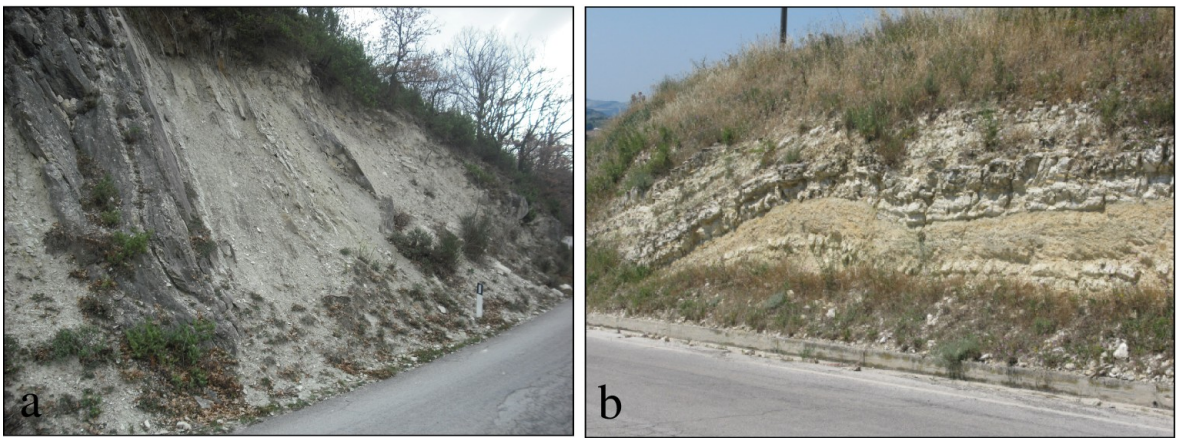

Figure 2.8. Outcrop of the marly limestones and marls of *Faeto Flysch* along the road to the village of ***a)*** Roccavivara. ***b)*** Tavenna.

S. Bartolomeo Flysch is a *wild flysch* sedimented in a top–thrust basin, it can be lithologically divided into two members: *Vallone Castelluccio* and *Valli* (Tortorici, 1975).

- *Vallone Castelluccio member* (Langhian) is a succession of clayey and silty marls, with interbedded well graded arenaceous strata. They present sedimentary structures as *flute cast*, *groove cast* and convolutions. The sandstones are petrographically made of 45% in quartz, 10% in K-feldspars, 15-20% in weathered Plagioclase, 2-3% of Mica, 2-3% of limestones and schists, 20-25% is made of calcite, which is the cement of the rock. It has a mean thickness of 1100 m, in some cases it rests tectonically on the *Variegated Clays* and upwards it passes gradually to the *Valli member*.
- The *Valli Member* (Langhian) is mainly composed of sandstones strata, which spans from competent to poor cemented and nearly loose sands. The latter are characterized by locally cemented ridges parallel to stratification, as shown in Figure 2.9a. At the base conglomerates may be present, made of gneiss, schists, shales, limestones and quartz. It has a mean thickness of 300 m, it can rest stratigraphically on the Vallone Castelluccio member or on the Variegated Complex through tectonic contact (Figure 2.9b). The sandstones are made of 47% in quartz, 17% plagioclase, 3% mica, 2% of shales, limestones and mudstones and 22% of calcitic cement.

The *S. Bartolomeo Flysch* can be correlated with the *San Giorgio Fm, Agnone Flysch, Frosolone Flysch,* and *Gorgoglione Flysch* (Lanzafame & Tortorici, 1976). In the upper part of the succession is present the stratigraphic contact with the *Toppo Capuana Clayey Marls* (Tortonian), which also lies on the *Faeto Flysch*, as shown in Figure 2.7.

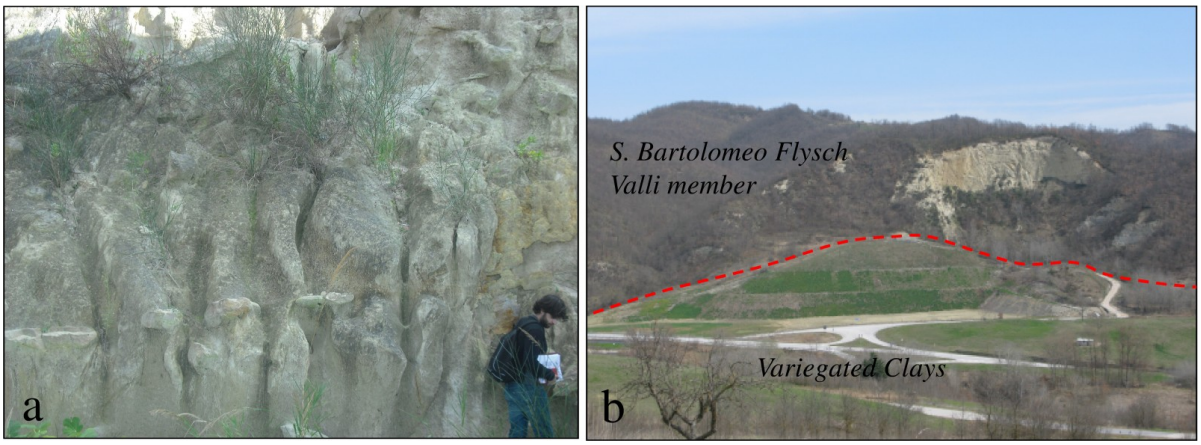

Figure 2.9. a) Detail of the outcrop of the sandstones of the *S. Bartolomeo Flysch* at the South of Casacalenda village. ***b)*** Landscape view of the tectonic contact between the *Valli member* of *S. Bartolomeo Flysch* and the *Variegated Clays*, near the village of Casalciprano (Festa et al., 2006).

Toppo Capuana Clayey Marls, described for the first time by Crostella & Vezzani (1964) in Puglia, are made of grey-bluish marls interbedded with yellow sandstones. It presents a thickness of 300-400 m and it is covered through a transgressive contact by Pliocene *Tona Fm.*

The salinity crisis of Messinian Age is represented in the study area by the *Montecastello Evaporites* they can be correlated to the *Altavilla Supersynthem* (Crostella & Vezzani, 1964, Lanzafame & Tortorici, 1976) and are also known as *Gessopalena Gypsums* (Festa et al., 2006). They are composed of gypsum and carbonate conglomerates in an arenaceous matrix with clay intercalations. They rest on the Faeto Flysch and are transgressively covered by the *Tona Fm,* as shown in Figure 2.10a

The last formation of the Irpinian Basin Unit, the *Tona Fm* (Pliocene) represents a complete sedimentary cycle. It is constituted of a sandy conglomerates at the base, which represent the transgressive facies with a maximum thickness of 50 m, which passes upwards to marly clays with an average thickness of 500-600 m (Figure 2.10d). At last it is closed by sands and conglomerates again (Figure 2.10b and 2.10c).

Figure 2.10. a) Beds of selenitic gypsum with thin pelitic interlayers, discordantly overlain by mudstones and calcarenites of the *Tona Fm* in Colle Gessaro quarry, SSW of Guglionesi village. ***b, c)*** Detail of the outcrop of the Pliocene *Tona Fm.* sandstones-conglomeratic upper member and ***d)*** the grey-bluish marly clayey middle member.

2.1.3 FOREDEEP AND FORELAND SUCCESSIONS

Foredeep-foreland successions crops out in the eastern part of the Molise Region. They include the Grey-bluish complex and the Terraced Plio-Pleistocene Complex. The recent tectonic evolution of this sector has been shown in detail by subsurface studies of deep boreholes and their paleontological content by Casnedi et al., (1981). The pre-Quaternary substratum is made of Sub-Apenninic Clays (Grey-Bluish clays), correlated with the infill of the Bradano Trough. It lies on Miocene deposits, Messinian Evaporites and the buried carbonates of the Apulia Platform (Campomarino 1 borehole, Videpi Project). This sector was characterized by a Middle Pliocene phase of tectonic subsidence, due to foredeep activity, followed by a phase of tectonic uplift at

the Gelasian-Calabrian transition (1.8 Ma), in response to the last important phase of NE migration of the foredeep. This tectonic phase led to the replacement of marine sedimentation with nearshore to non-marine deposits (Lanzafame & Tortorici, 1976; Bracone et al., 2012a and reference therein).

The succession corresponds to the *Ofanto Fm.* (Crostella & Vezzani, 1964), it starts with the *Montesecco Clays Fm.* described for the first time by Boni et al., (1969), composed of grey-bluish marly and silty clays (Figure 2.11a), which passes upwards to *Serracapriola Sands* (Bracone et al., 2012b). They are made of Calabrian yellow coarse sands and sandstones (Figure 2.11b), the contact with the underlying Clays is concordant and the upward passage to the *Campomarino Conglomerates* is through interbedding. The latter represents the closure of the regressive cycle, mainly composed of conglomerates and sandstones.

Figure 2.11. a) Landscape through badland of *the Montesecco Clays*, near the village of Guglionesi (Di Paola et al., 2011). ***b).*** A particular of the paleo-seacliff within the *Serracapriola Sands* cropping out in the town of Termoli.

In the simplified geological map of Figure 2.3 the Holocene deposits are grouped within the Alluvial Complex and the Detrital Complex. The first is made of gravels sands and also clays

deposited at the bottom of the flood plains. The latter is mainly composed of loose gravels related to *talus* deposition.

A summary of the outcropping geological formations and the relative Complexes in which were grouped for this study is shown in Table 2.1.

Table 2.1. Summary of the Geological Formations and the relative Geological Complex.

Geodynamic domain	Geological Complex		Geological Formation	Age	
-	Alluvial Complex		*Alluvial, lacustrine and marsh deposits*	Holocene	
	Detrital Complex		*Talus deposits*		
Foredeep-Foreland Successions	Terraced Plio-Pleistocene Complex		*Campomarino conglomerates*	Post-Calabrian	
			Serracapriola Sands	Calabrian?	
	Grey-Bluish Clays Complex		*Montesecco Clays Fm*	Pliocene–Calabrian	
Flysch Domains	Terraced Plio-Pleistocene Complex	Irpinian Basin Nappe	*Tona Fm*	Miocene	Pliocene
	Flysch Complex		*Monte Castello Evaporites*		Messinian
			Toppo Capuana Clayey Marls Fm		Tortonian
			S. Bartolomeo Flysch; Faeto Flysch		Tortonian Langhian
		Molise Basin Nappe	*Frosolone (S.Elena; Pietraroja; San Massimo); Agnone; Tufillo-Serra Palazzo; Daunia*		
	Variegated Clays Complex		*Sicilides; Fortore Unit; Sannio Unit*	Miocene Cretaceous	
Carbonate Domains	Carbonate Complex		*Frosolone Unit, Cusano Fm, Longano Fm*	Miocene	
			Simbruini-Matese Unit	Cretaceous-Trias	

2.2. GEOMORPHOLOGICAL SETTING OF THE MOLISE REGION

Molise Region presents a typical mountainous-hilly landscape with few area of plain located within inner basin or in flood and coastal area, as shown in Figure 2.12. The highest peaks are associated with the most competent Carbonate Complex on Matese Mts. (Miletto Mt., 2050 m a.s.l.) in the SW. Eastward, passing through *flysch*, the topography gently declines toward the Adriatic sea.

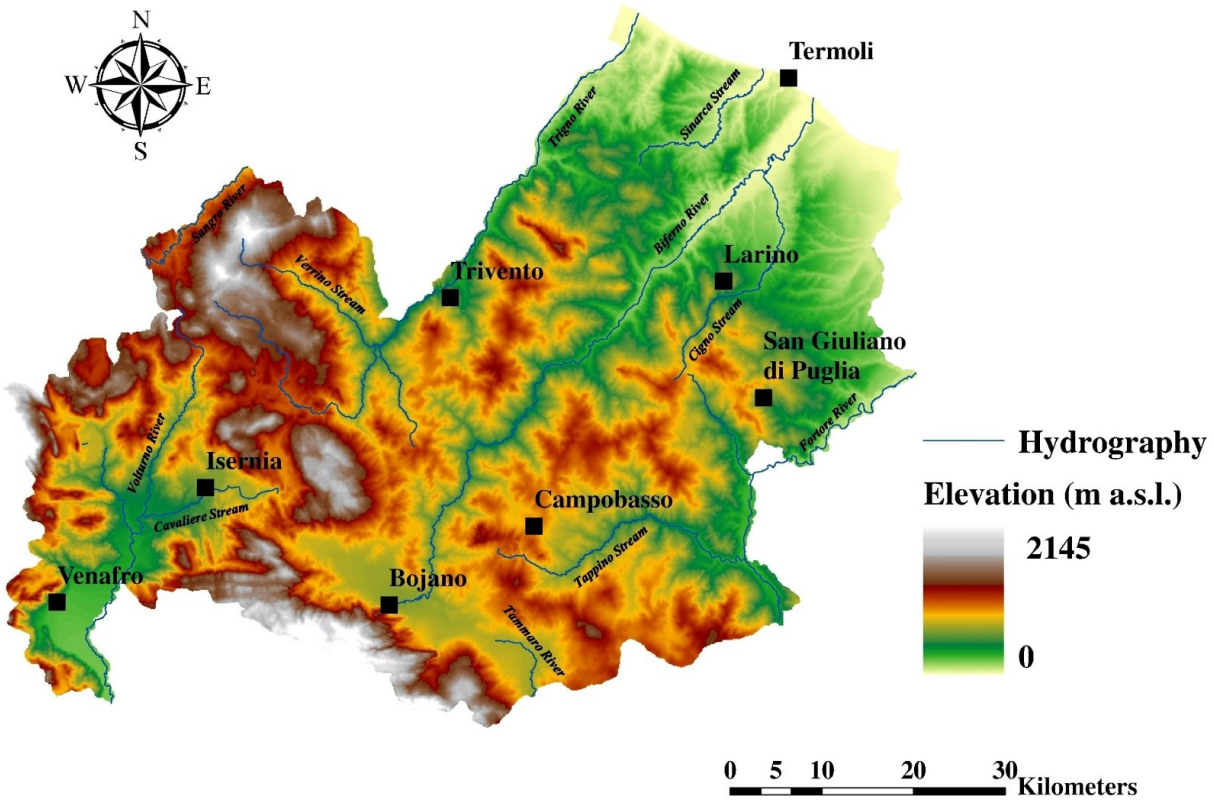

Figure 2.12. Digital terrain model (DTM) 200 x 200 m cell of the Molise Region.

The geological and tectonic setting is the main factor in controlling the geomorphological evolution of this area. The influence of geological structures on landscape is easier to detect where limestones crops out, hence fault-related scarps are present, which are hill slopes related to a basal fault plane. Furthermore, due to the alternation of weak and resistant lithologies, stream dissection allowed the development of homoclinal ridges and structure-controlled slopes along gently to steeply dipping strata. The landscape dominated by *flysch* presents more gentle

slopes and consists of hills. These deposits can be classified as *structurally complex formations,* namely these materials are formed by competent rocks and hard shales with disarranged or chaotic silty and marly clays. They are also characterized by strong heterogeneity and anisotropy, which is due to stratification, nodules, inclusions, joints and fractures. The source of complexities can be found either at the sample scale than at the scale of engineering problems (Croce, 1977). In fact, those features define strongly landslides-prone deposits. The striking coincidence between Complex Formations and the occurrence of landslides worldwide is also remarked by Esu (1977) and will better be discussed in the next section.

The low permeability and high erodibility lithologies cropping out in the study area are marked by peculiar landforms, as badlands, rills and gullies. Longitudinal and cross profiles of the main valleys show low relief landscapes named Hanging Valley Side Glacis (typically 3° to 8° inclined). These features may be related to phases of base level stability during the Quaternary, which deepened the drainage network, as also testified by local occurrence of fluvial deposits (Aucelli et al., 2010). Surface water run-off differently shapes the landscape as function to materials erodibility and resistance. Low competent lithologies mainly experience sheet erosion forming gentle slopes, but also rills and badlands landscapes. Meanwhile, the more competent rocks mainly present embedded valleys, with steep slopes, linear pattern and gullies. Most of the river valleys show an asymmetric shape, with a steeper flank coinciding with the rocky layers and a more gentle flank on soils (Frazzetta & Lanzafame, 1977). Several hydrographic basins can be identified, namely, Volturno R., Sangro R., Fortore R., Saccione R., Trigno R. and Biferno R. They flow out eastward into the Adriatic sea, only the Volturno River has its mouth in the Tyrrhenian sea at West.

The Trigno and Biferno Rivers are the most important ones (Figure 2.12), they both flow along an anti-Apenninic direction (i.e. SW-NE), their hydrographic network is strongly controlled by tectonic trends and they meet their tributaries, which flow in Apenninic direction (i.e. NW-SE) at

an angle of 90°, forming an angulated pattern. Trigno River marks the Northern boundary with Abruzzo Region and has its spring at Capo Trigno Spring on Mt. Capraro (1200 m a.s.l.); Biferno River completely flows within the regional territory with its springs at the foothill of Matese Mt. at 500 m a.s.l. within the village of Boiano. Their flow paths remained unchanged during historical times as shown in the historical topographic maps (Figure 2.13a) by Rizzi Zannoni (1809). Downstream of Ponte Liscione dam, the river presents a meandering pattern and the geomorphological features of its flanks are quite different from each other. The left flank is quite steep and high, while the right side of the valley is more gently sloping to a large plateau, where regressive and continental deposits crop out, (i.e. Larino Plateau). According to Galeandro et al. (2013) this feature is controlled by a huge deep seated landslide, testified by the presence of the great scarp at the toe (where stream Cigno is located), the lowering of the large Larino Plateau and the pattern of the horizontal and vertical alignment of river Biferno (Figure 2.13b). However the presence of deep seated landslides and Deep Seated Gravitational Slope Deformations (DSGSD) is also remarked by Corniello & Santo (1994) and Aucelli et al., (2013).

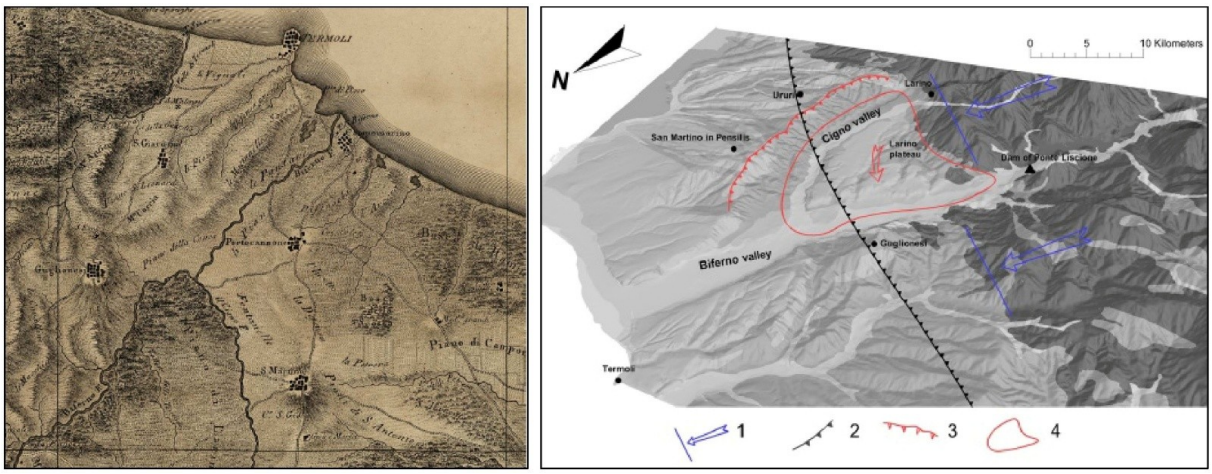

Figure 2.13. a) historical map of Molise by Rizzi Zannoni (1809), It shows the pattern of the river Biferno quite similar to nowadays. ***b).*** 3-D view of the large landslide of the low Biferno Valley. after Galeandro et al. (2013) 1 – differential stretching-out of outcropping Apennine front with a major advancing left side bank of Biferno Valley (dark-grey zones represent the allochthonous masses); 2 – buried front of the Apennine; 3 – main scarp of the landslide; 4 – schematic landslide body.

Landforms originated and reshaped by mass movements are very widespread in the study area. A large percentage of the landslides are the result of a combination of various movements (e.g. both rotational and/or translational slides coupled with flows), which either occurred in sequence (a complex landslide), or simultaneously, in different sectors of the displaced mass (a composite landslide). The geomorphological evolution of the area also encloses sectors characterized by widespread shallow landslides with soil creep and solifluction. The analysis of landslides phenomena in the Region was carried out by Ispra (2005), the authors evaluated a landslide index of 12.5 %, namely the ratio between the landslides area and the mountainous-hilly area, with the first equal to 494.33 km². Following the Varnes (1978) landslides classification, the phenomena occurring in Molise are Translational and Rotational Slides, Flows, Falls and Complex Landslides. Most of the area in which clayey formations crop out is also interested by shallow areal landslides and badland landscapes. A map reporting the distribution of the existing landslides from the IFFI database (Italian Inventory of Landslides) is shown in Figure 2.14 for the various states of activity.

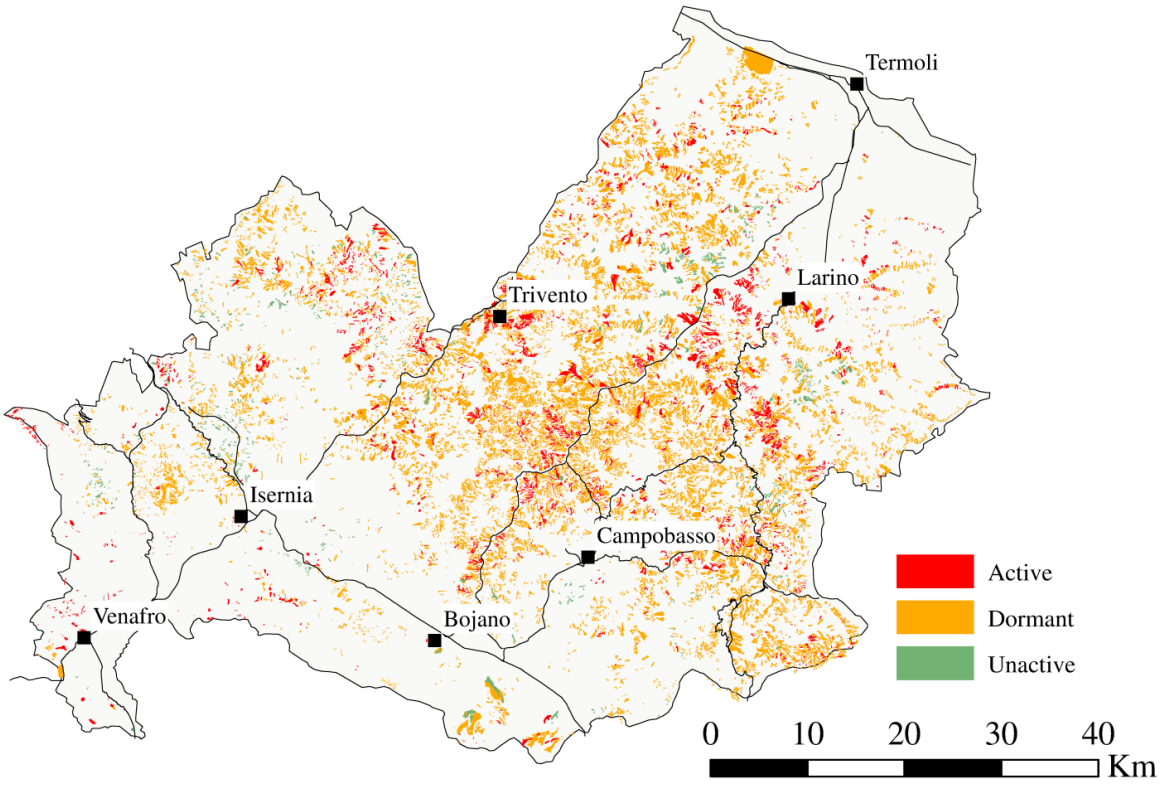

Figure 2.14. Distribution of the Landslides with their states of activity from the IFFI database (http://www.isprambiente.gov.it/it/progetti/iffi-inventario-dei-fenomeni-franosi-in-italia).

The most infamous landslide of the Region is the Covatta landslide (Figure 2.15), which on 12th April 1996 struck a portion of the Biferno expressway (e.g. Corbi et al., 1999).

Figure 2.15. Main body of the 12th April 1996 Covatta Landslides.

This event completely destroyed the Pozzillo II bridge and the river was dammed, the landslide movements continued with high velocities the next year. The onset of the movement has to be related to the activation of a complex landslide system. The lenght of the phenomenon was 1200 - 1400 m, involving more than $2*10^6$ m^3 of mobilized material and a shear surface located at 8-12 m in the middle portion (more details can be found in Comegna, 2005).

The landscape is also dominated by remnants of paleosurfaces; most of them have an erosional origin, either on carbonate or terrigenous rocks, while those originated by deposition are genetically related to Quaternary continental deposits, present at lower altitudes within the main fluvial valleys and the major tectonic depressions. Aucelli et al. (2011) recognized four orders of paleosurfaces, between 1100 and 720 m a.s.l., identified in the Matese and Montagnola di Frosolone massifs, in the upper portion of the Biferno and Trigno valleys and in the sector

including the Sessano and Carpino Basins. Other relicts of erosional and depositional surfaces are present in the Region below 500 m a.s.l. They were ascribed to the Middle Pleistocene by Brancaccio et al. (2000). Such surfaces generally represent stripped fluvial terraces hanging a few tens of meters over the valley floors; they are mainly located in the upper part of the Volturno River catchment area. In this sector, near the town of Isernia, four orders of alluvial terraces was recognized, constituted by a sequence of 150 m of fluvial and lacustrine deposits rich in pyroclasts coming from Roccamonfina volcano. This area is distinguished from the southern Venafro plain through a left strike-slip fault, where only three order of terraces can be detected (Brancaccio et al., 1997).

2.3. SEISMOLOGICAL SETTING OF THE MOLISE REGION

The Molise region falls between the Apennine axial zone, the Abruzzo-Molise corridor and the Apulia-Gargano foreland corresponding to the well-identified 927, 923 and 924 SSZs (seismogenic source zone) by ZS9 shown in Figure 2.16 (Meletti et al., 2008).

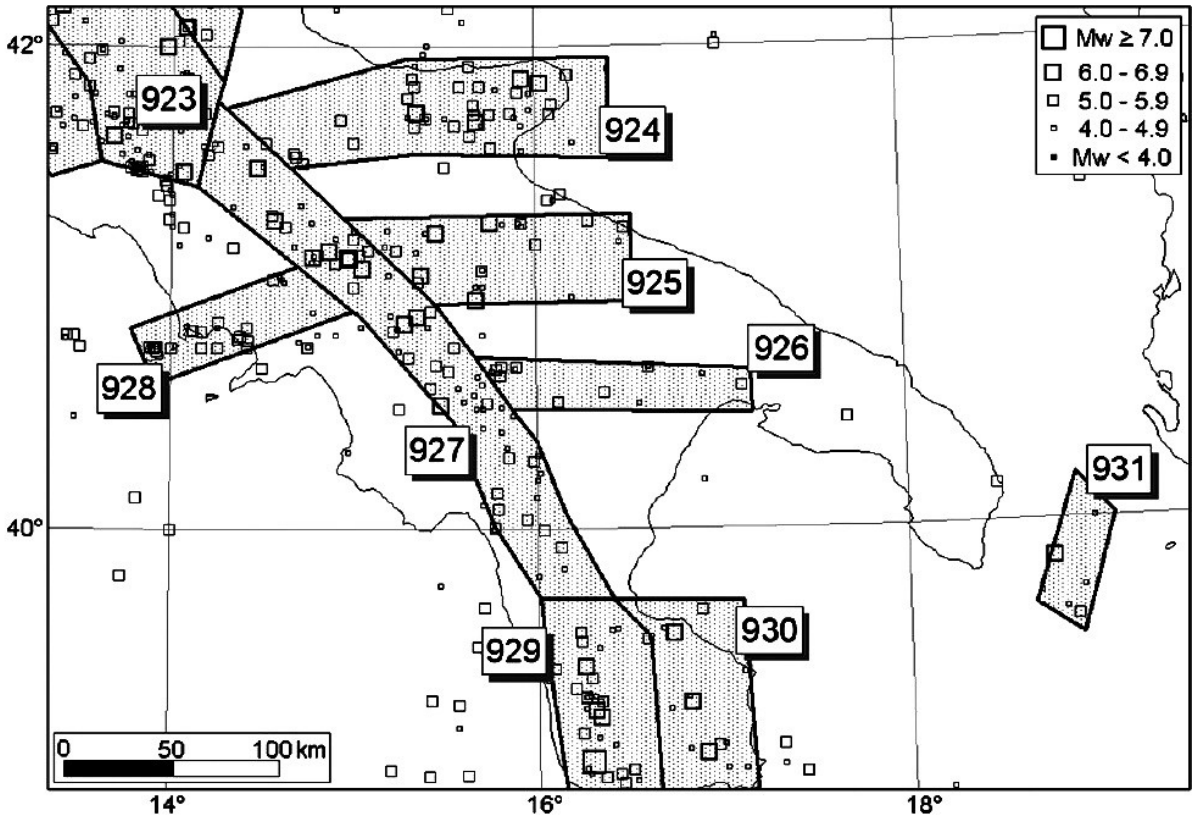

Figure 2.16. SSZs (Seismogenic Source Zones) of the Southern Italy after Meletti et al., (2008) DISS 3.0.

The 927 SSZ the axis of Apennine chain, which is characterized by a post-orogenic extensional regime, it is the focus of some of the largest earthquake in italian history. It results from the merging of several former ZS4 zones which span from Maiella Massif in Abruzzo to Pollino Massif in Northern Calabria, an effective focal depth of 10 km was assigned to this zone on the basis of mode and shape of earthquake distribution with depth.

The Abruzzo-Molise 923 SSZ includes the highest seismicity areas of central Italy, both in terms of frequency and severity of earthquakes. This zone is mainly characterized by normal faults and

contains the source zones of 1349 and 1654 earthquakes, with an assigned effective focal depth of 9 km.

The 924 SSZ of the Apulian foredeep-foreland was strongly improved after the new knowledge on seismotectonics coming from the post Molise 2002 earthquake studies (Di Bucci & Mazzoli, 2003, Valensise et al. 2004). This sector is E-W elongated and mainly present strike-slip faults. It includes all the seismicity of the whole Northern Apulia-Southern Molise (e.g. 30 July 1627 M_w 6.7 earthquake) and encompasses the Mattinata fault zone within the Gargano promontory; the assigned focal depth is 13 km.

Those seismogenic structures in the past generated several destructive earthquakes with felt intensities up to IX MCS in Molise. All these faults have generated earthquakes of high magnitude (M_w 6.5-7) and have strongly damaged the Molise. The strongest earthquakes recorded in the area are shown in Figure 2.17 and listed in Table 2.2.

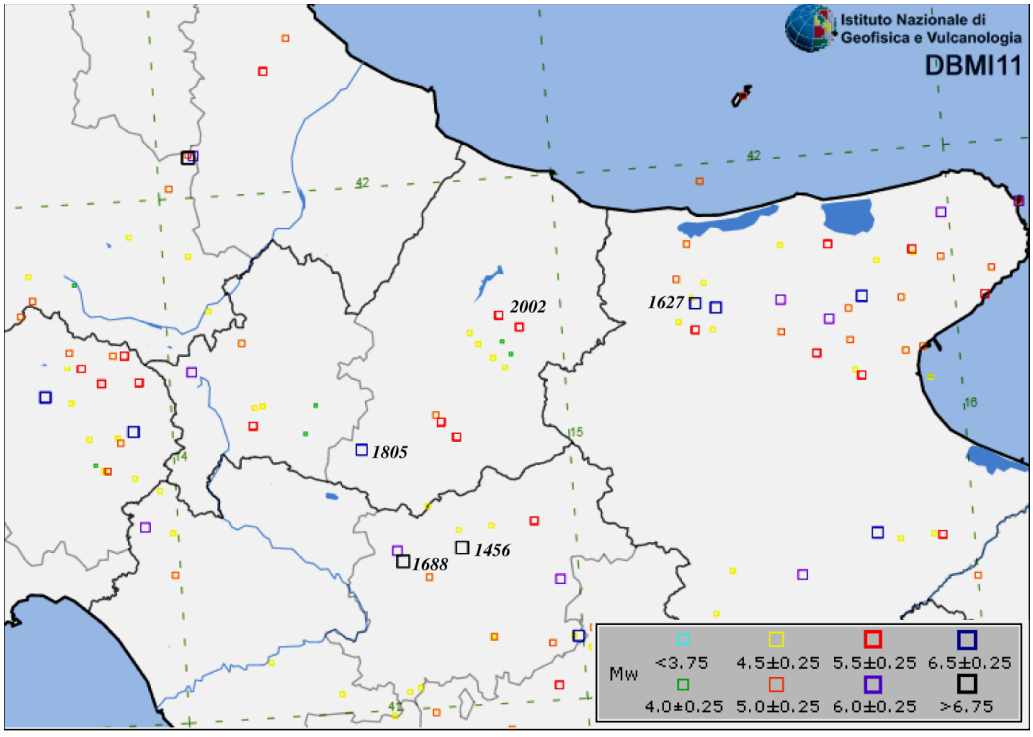

Figure 2.17. Strongest earthquakes which struck Molise region between 1000 AD and 2006 after CPTI11(Rovida et al., 2011).

Table 2.2. Main Historical Earthquakes which struck the Molise Region

Seismogenic Area	Date			Epicenter Coordinates		I_0	M_w
	Year	Month	Day	Lat. N	Lon. E		
Boiano	1456	12	5	41.54	14.72	XI	7.0
Gargano	1627	7	30	41.76	15.37	X-XI	6.9
Sannio	1688	6	5	41.24	14.70	X-XI	6.8
Boiano	1805	7	26	41.50	14.47	X	6.6
S. Giuliano di Puglia	2002	10	31	41.69	14.94	VIII-IX	5.74

2.3.1 THE APENNINE SEISMIC SEQUENCE OF 1456

The 1456 seismic crisis consisted of at least two large mainshocks, the first on 5 December and the second on 30 December. In the absence of positively identified earthquake sources, seismotectonic models of the southern Apennines generally assumed that the 1456 earthquake had ruptured several ~NW-SE trending normal fault segments. The maximum damage was reported in historical references (i.e., letters, official statements, reports of property damage) dated from 5 to 10 December, and must hence be attributed to the first mainshock. The sequence continued up to early 1457, causing further damage. Less frequent aftershocks of decreasing intensity continued from March to the end of May 1457. Historical reports assess two intensity XI MCS data points at Boiano and Isernia, several intensity X data points extending from Acquaviva d'Isernia (northwest) to Santo Stefano (northeast) to Cercemaggiore (southeast). High intensities are also recognized from Isernia to the upper Sangro River valley (Pescocostanzo, VIII); Castellino del Biferno, Campobasso, towards Santo Stefano and northeast of the Matese massif, with X and XI MCS. The unusual extent of the damage was also explained through a depth of the sources consistently below 10 km (Fracassi & Valensise, 2007 and reference therein).

2.3.2 THE GARGANO SEISMIC SEQUENCE OF 1627

On 30 July 1627 a severe earthquake struck in Southern Italy the Basso Molise, Western Gargano and Northern Capitanata regions producing widespread destruction and causing more than 5000 victims. The seismic event was also responsible for a tsunami whose effects was particularly significant along the northern coast of the Gargano Promontory and strongly affected the town of Termoli and Campomarino, in Molise. The source of the disastrous event has been recognised as NNW-SSE Apricena Fault (Patacca & Scandone, 2004 and reference therein).

2.3.3 THE SANNIO EARTHQUAKE OF 1688

This earthquake (Mw 7.1) struck the SW area of the Matese massif; it produced a wide damage area, especially in the town of Benevento, with several ground effects too. Most of these effects are follows a NW-SE direction along the Calore River valley (Di Bucci et al., 2005 and reference therein).

2.3.4 THE ST. ANNA EARTHQUAKE OF 1805

On July 26 1805 (Mw 6.7-6.8), an infamous earthquake struck Molise Region and Campania as well. The maximum intensity was experienced in the village of Frosolone, claiming more than 5000 lives. The earthquake also produced many side effects, as hydrogeological anomalies of spring discharges, ground displacements, only one liquefaction case in Cantalupo del Sannio and several landslides, mainly rockfalls and earth slumps (Esposito et al., 1987; Romeo & Delfino, 1997; Porfido et al., 2007; Serva et al., 2007).

2.3.5 THE 2002 MOLISE EARTHQUAKE

The 2002 earthquake was the last disastrous event occurred in Molise, when between 31st October and 1st November a moderate earthquake (Mw 5.7) hit the village of San Giuliano di Puglia, causing the collapse of a primary school and the death of 27 pupils and a teacher. The focus of the quake was located between accretionary wedge of the ridge and the foredeep, where the carbonates of the apulian platform are buried at 4-6 km. The depth of the event was evaluated at more than 10 km, below the carbonate deposits. This event was strongly unexpected, because it reactivated the E-W striking right-lateral faults, which cross the mesoseismal area of the 1627 Gargano earthquake and are linked to the Mattinata fault and the Gondola line (Morasca et al. 2008; Valensise et al. 2004).

The small village of San Giuliano di Puglia experienced VIII–IX MCS intensity. The detected damage pattern resulted strongly conditioned by the phenomenon of the seismic amplification (Puglia, 2008 and reference therein)

This event represented a turning point for the Earthquake Engineering practice in Italy, since it pushed towards a quick introduction of new seismic codes, due to the pressure of the public opinion.

An emergency procedure supported by the Prime Minister issued the ordinance n. 3274, on 20 March 2003, which established a new seismic code similar to the Eurocode 8 (EC8; 2003). The new seismic classification map is shown in Figure 2.18a. The number of municipalities classified as high (Zone 1), medium (Zone 2) and low seismicity (Zone 3) is now equal to 4.674; 3.424 municipalities are in Zone 4, with a seismicity lower than that for Zone 3. In 2005 the building code assigned seismic actions to several values of peak ground acceleration (PGA) on bedrock as function of the different seismic zones. Finally, the OPCM 3519/2006 issued a Seismic Hazard Map based on the reference input motion as horizontal acceleration (a_g or PGA), and spectral ordinates for several Return Periods (30-2475 years); in Figure 2.18b the Seismic Hazard Map for a Return Period of 475 years is shown.

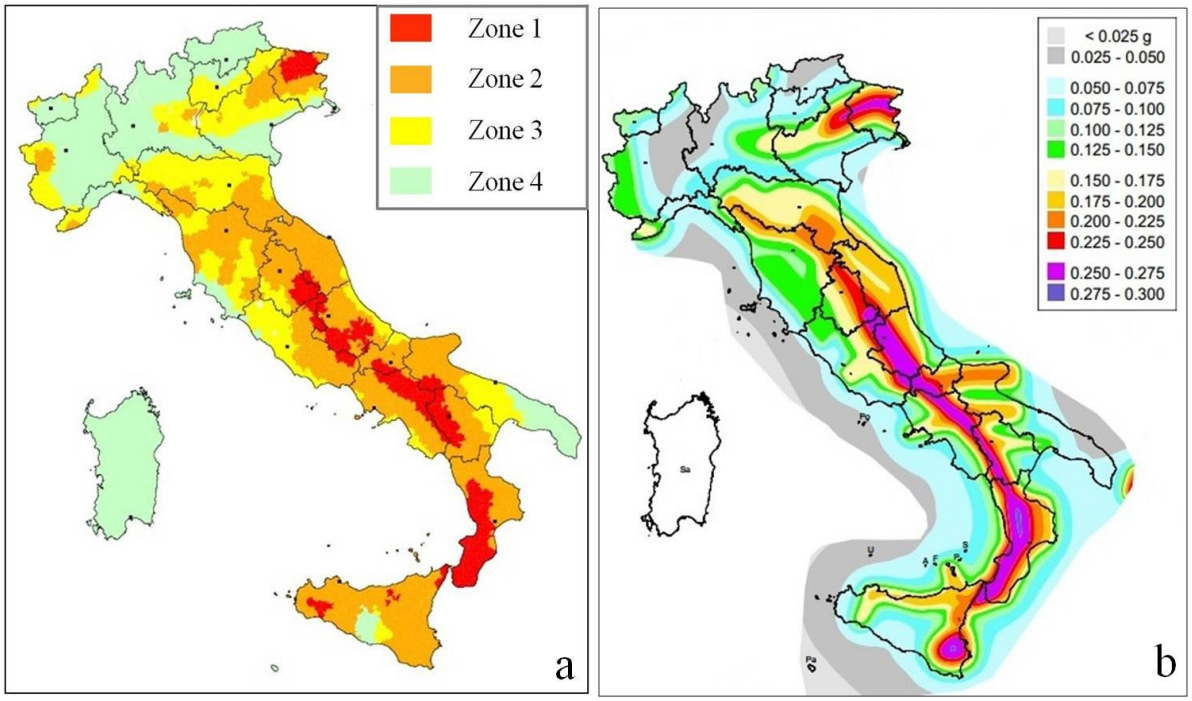

Figure 2.18 a) Seismic Classification Map in 2003 (OPCM 3274/2003). ***b)***Seismic Hazard Map for a Return Period of 475 years (OPCM 3519/2006).

At last, DM 14/01/2008 unified the Italian Building Code and established four limit states verifications, namely, SLO (Operative Limit State), SLD (Damage Limit State), SLV (Life safeguard Limit State) and SLC (Collapse Limit State) associated with the exceeding probability of 81; 63, 10 and 5 %.

3. DATABASE OF GEOLOGICAL AND GEOTECHNICAL INVESTIGATIONS

The planning and management of lifelines systems (highways, pipelines and distributed infrastructures) in seismic conditions requires the knowledge of the geologic and geotechnical conditions, either at territorial scale than at detailed scale. This knowledge usually requires the acquisition of a certain amount of data, such as geometrical size and shape of the construction, material properties, intensity measures of natural events and so on.

In the field of structural engineering, the mechanical properties of common construction materials like steel and concrete are quite easy to obtain. In fact they are usually prescribed and checked or measured by destructive and non-destructive tests (Fabbrocino et al., 2005).

In the case of engineering geology and geotechnical engineering, the access to the information is more complex and time consuming. In fact, the part of the soil that interacts with the construction and/or area of interest needs to be characterized in terms of geometric, hydraulic and physical-mechanical properties, generally all a-priori unknown and affected by large uncertainties (EC7-1, 2004). To this end, a series of specific investigations need to be planned and correctly executed (EC7-2, 2007) in order to outline the complex natural situation and set a rational model for engineering, namely the subsoil model.

As stated in Kulhawy & Mayne (1990) "*design engineer must either measure the properties under controlled conditions in the laboratory or field or estimate the properties from other test data. These estimates are made most often from laboratory index tests and in-situ test results, which are correlated to the soil properties either by calibration studies or by back calculation from full-scale load test data obtained*

The collection and organization of the pre-existing knowledge through the constitution of a database of geological and geotechnical investigations represent the backbone of every large scale project aimed at territorial analysis. Hence an essential part of this work was devoted to this task. The retrived information was organized through GIS (Geographical Information Systems) technology adopting the *ESRI ArcGis 9.3* software. A great amount of data was due to the post-Molise 2002 earthquake reconstruction activities.

In fact the study of seismic microzonation of all the municipalities belonging to the district of Campobasso (Regione Molise, 2003), is constituted by a large amount of in-situ and laboratory investigations, which encompasses the available pre existing studies (E) and investigations specifically performed for the seismic microzonation (M), that are made available through the website: http://www3.regione.molise.it. This database constitutes the main part of the geotechnical investigations available as shown in Figure 3.1. Minor part of data came from a regional program, aimed at evaluating the seismic vulnerability of strategic buildings, road infrastructures and major bridges (ANAS) (Di Carluccio et al. 2009, Evangelista et al. 2011). Finally, other data were retrieved from Public Agencies and Privates, for the construction of the 3D subsoil model implemented for the seismic assessment of the critical infrastructures (Fabbrocino et al. 2014), located in the Pantano area, which is in the easternmost and coastal part of the investigated Region and from the geotechnical characterization of the San Giuliano di Puglia village (d'Onofrio et al. 2009), severly hit by the 2002 earthquake (A).

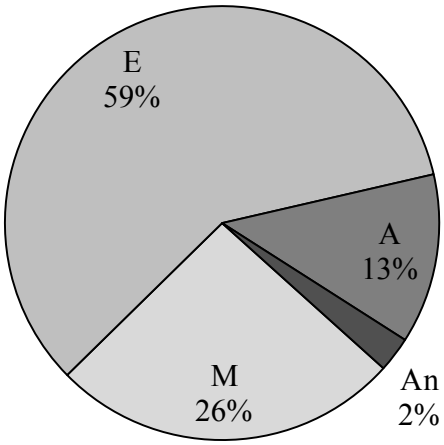

Figure 3. 1. Distribution of the available tests

The available investigations distribution in Figure 3.2 shows an higher density for the area of the Campobasso district, as the target of the microzonation, but it is also due to the fact, that Isernia district is less prone to landslides for the presence of less erodible geological formations, as reported in the IFFI landslide inventory project, whose some of the results are synthetically shown in Figure 3.3 (ISPRA, 2005).

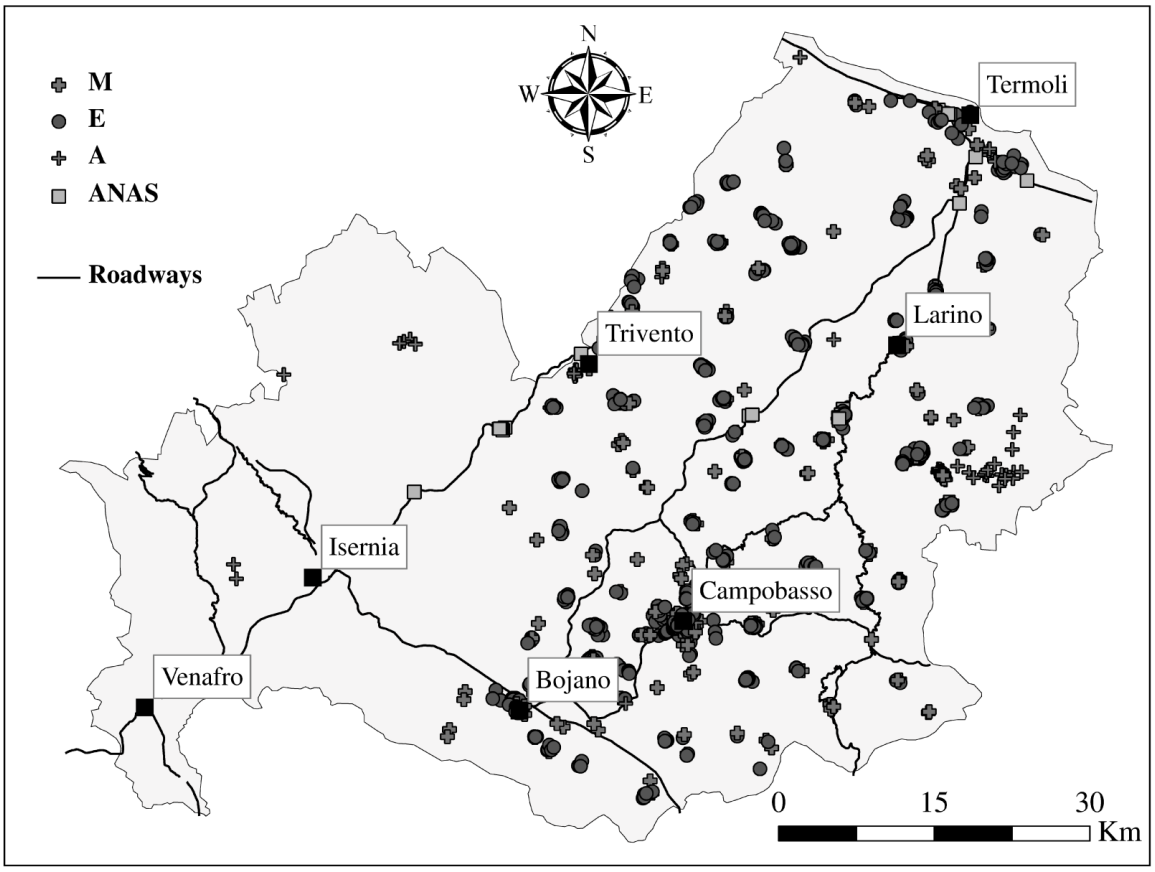

Figure 3.2. Spatial distribution of the available geological and geotechnical investigations; M) Tests performed for the Microzonation Study; E) Existing Tests also adopted for the Microzonatio Study; A) Data coming from several sources and Public Agencies and Privates; ANAS) Investigations for the seismic vulnerability assessment of the ANAS national bridges in the Region.

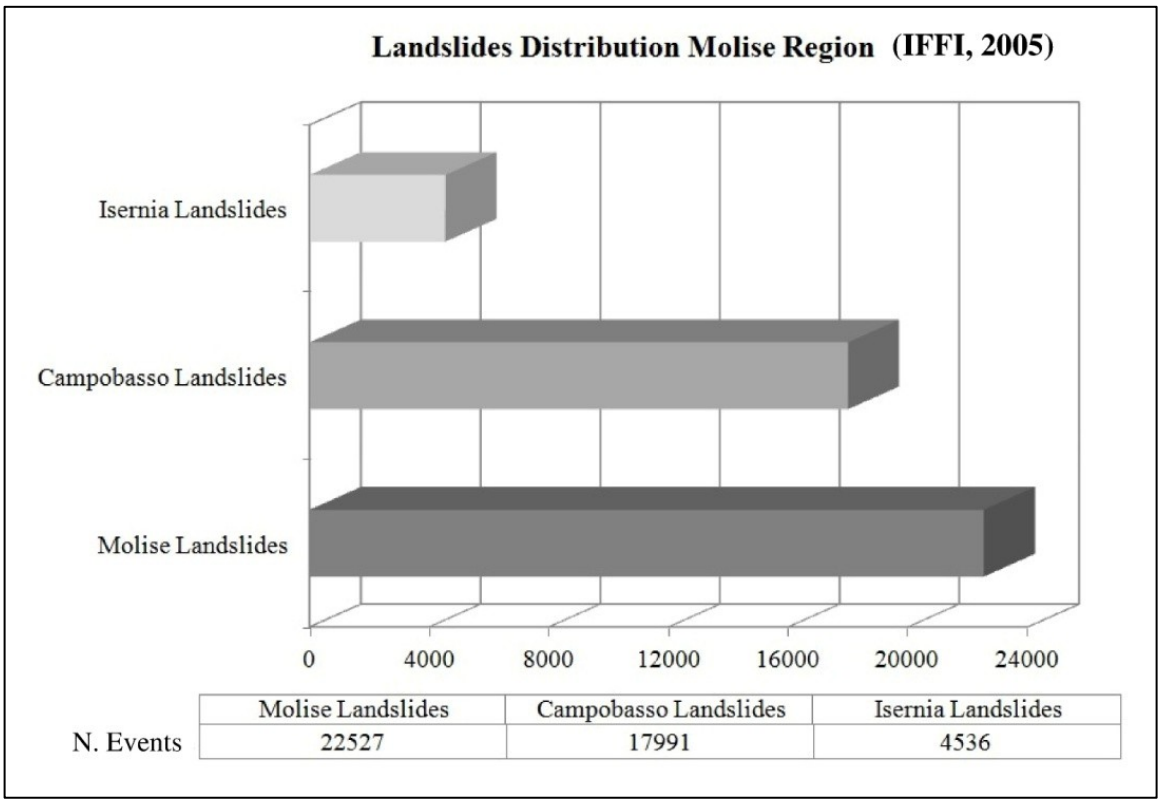

Figure 3. 3. Landslides distribution in the Molise Region (after ISPRA, 2005).

In the investigations performed for the microzonation of Campobasso municipalities a standard protocol was followed, i.e. in the same borehole, together with the downhole geophysical investigation, an accompanying stratigraphic log and several standard penetration tests (SPT) were available. Moreover, in each vertical, some undisturbed soil samples were taken in order to obtain physical and mechanical properties by laboratory investigations. The test was generally performed until 30 m depth, to obtain the equivalent shear wave velocity of V_{S30} used for seismic site classification, according to EC8 (EN1998-1 2006) and to Italian building Code (NTC 2008) prescriptions, as:

$$V_{S30} = \frac{30}{\sum_{i=1,N} \frac{h_i}{V_{S,i}}} \quad (3.1)$$

where h_i is the thickness of the i-th layer and V_S its mean shear waves velocity.

In Figure 3.4, a typical result of the investigation in a test site is reported.

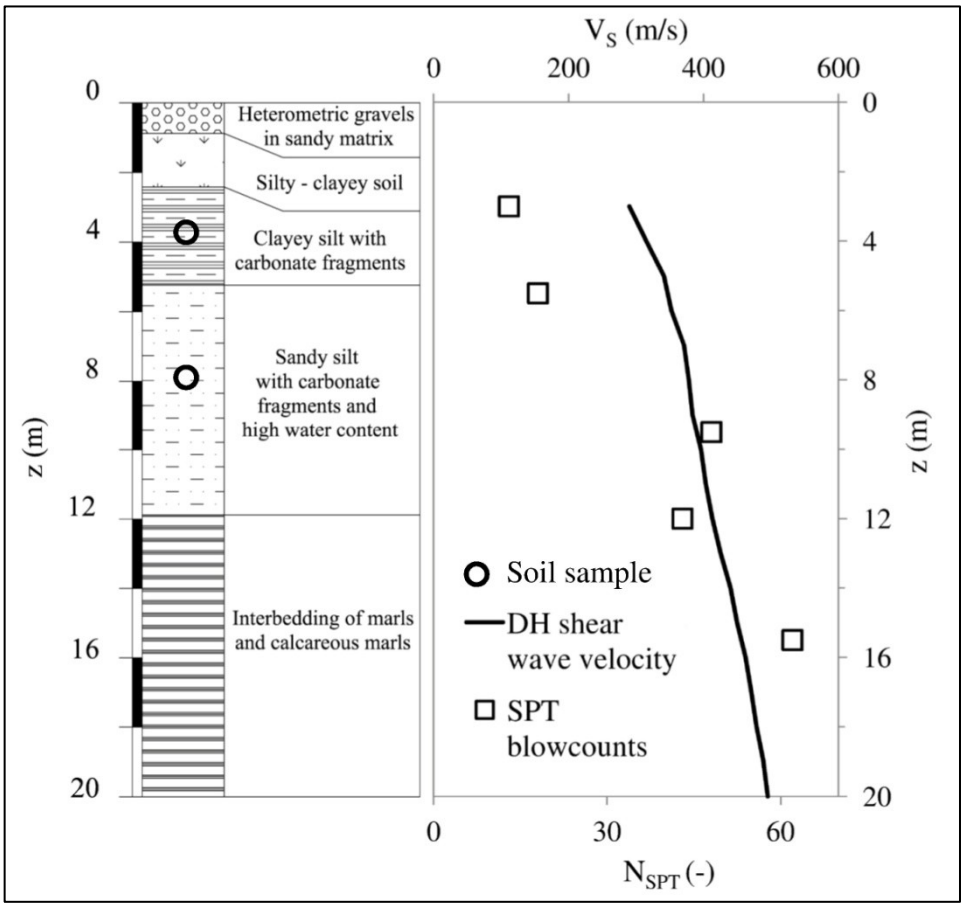

Figure 3. 4. Main results of integrated borehole microzonation data (stratigraphic log, shear wave velocity profile SPT profile, soil samples depth).

Finally the implemented database of geological and geotechnical investigations encompass the following test results (Figure 3.5):

a) Stratigraphic logs;

b) Standard Penetration tests (SPT);

c) Cone Penetration tests (CPT);

d) Down-hole tests (DH);

f) Samples for laboratory tests (Physical-mechanical characterizations, grain size curves, triaxial UU and SS tests);

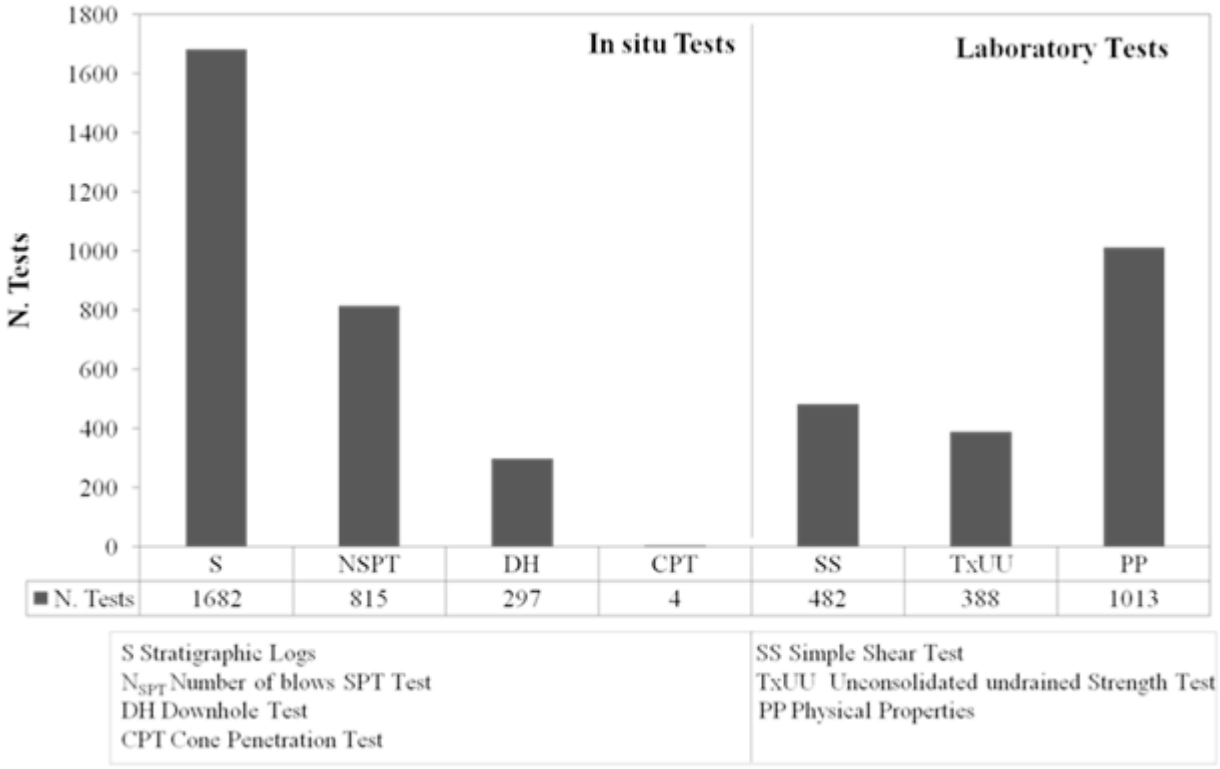

Figure 3.5. Histogram reporting the amount of investigations collected in the Database.

These investigations were georeferenced adopting two different coordinates systems, geographic coordinates WGS84, in order to permit comparisons with worldwide data and Italian projected coordinates Monte Mario (Rome), to easily manage Italian data. Each test was firstly grouped as function of the municipality in which it lies and the source of information (Table 3.1), .then the sample features are highlighted (Table 3.2), together with the main physical-mechanical characterization properties and strength parameters (Table 3.3). Finally the in-situ tests results and a summary of all the performed tests is reported (Table 3.4).

Table 3.1. Database example showing Municipality, Source and Coordinates of the investigation.

Comune_ID	Source	Coordinate N	Coordinate E
Lupara (CB)	M	41.762	14.733
Lupara (CB)	M	41.762	14.734

Monacilioni (CB)	E	41.610	14.807
Monacilioni (CB)	E	41.606	14.811

Table 3.2. Database exemple showing ID,Groundwater Table depth (z_g), Geological formations at different scales, Grain size content (C= clay; M= mud/silt; S= sand; G= gravel).

ID	z_g (m)	z_t (m)	Geo 5,000	Geo 50,000	Geo 100,000	C (%)	M (%)	S (%)	G (%)
S1	n.a.	6.5	San 2b	n.a	PMc	43.3	32.6	22	2.1
S1-C2	n.a.	13.3	San 2b	n.a.	PMc	40.4	44.6	15	0
S13	n.a.	8.0	San 2b	n.a.	M^4am	22	58	20	0
S14-C1	n.a.	3.0	San 1b	n.a.	ms	44	33	23	0

Table 3.3. Database exemple showing Atterberg limits, Strength parameters, Unit weights, Saturation conditions.

LL (%)	LP (%)	IP (%)	φ' (°)	φ_r (°)	c' (kPa)	s_u (kPa)	e (-)	γ_{nat} (Kg/m^3)	γ_{sat} (Kg/m^3)	w (%)	Sr (%)
50.6	32.8	17.8	n.a.	n.a.	n.a.	29	0.951	18.2	18.5	32.7	93.6
42.5	28.4	14.1	n.a.	n.a.	n.a.	266	0.5311	20.3	20.9	16	82.3
38.8	18.9	19.9	19.8	n.a.	15.69	n.a.	0.44	21.1	22.8	n.a.	n.a.
40.9	19.6	21.3	21.6	n.a.	15.7	n.a.	0.66	20	10.4	20.4	n.a.

Table 3.4. Database exemple showing the results of the in-situ tests and a summary of all the performed tests.

V_{S30} (m/s)	N_{SPT}	Grain Size	Phys. Prop.	SS	TxUU	SPT	DH
501	43	x	x		x	x	x
501	n.a.	x	x		x		x
n.a.	n.a.	x	x	x			
n.a.	n.a.	x	x	x	x		

As a result, a large database of soil investigations was organized. It shows a considerable potential in the geological and geotechnical characterization of the materials cropping out in the study area.

In the following sections it will be discussed four main topics will be discussed:

- The engineering geology classification;
- The geotechnical characterization;

- The elaboration of an original seismic soil map based on the results of downhole tests (DH)
- The developments of empirical relationships between SPT blowcount (N_{SPT}) and the shear wave velocity (V_S).

3.1 ENGINEERING GEOLOGY CLASSIFICATION

For the purpose of this study, the geolithological complexes, showed in the simplified geological map in Figure 2.3, were refined and enhanced in order to identify more homogeneous groupings, based on their main *lithofacies*. The new 1:100,000 scale map shown in Figure 3.6 was built through a multi-scale geological map joining. Namely, the merged information came from 1:100,000 scale official geological maps by http://www.isprambiente.gov.it/it/cartografia (sheets: 161 Isernia; 162 Campobasso; 163 Lucera; 153 Agnone; 154 Larino; 155 San Severo;), the only two available official 1:50,000 geological maps (sheets: 393 Trivento; 405 Campobasso), the 1:5,000 geological map coming from seismic microzonation studies and the geological surveys carried out for seismic vulnerability assessment of existing bridges (Di Carluccio et al., 2009). A greater weight was attributed to bigger scale ratio maps and surveyed evidences.

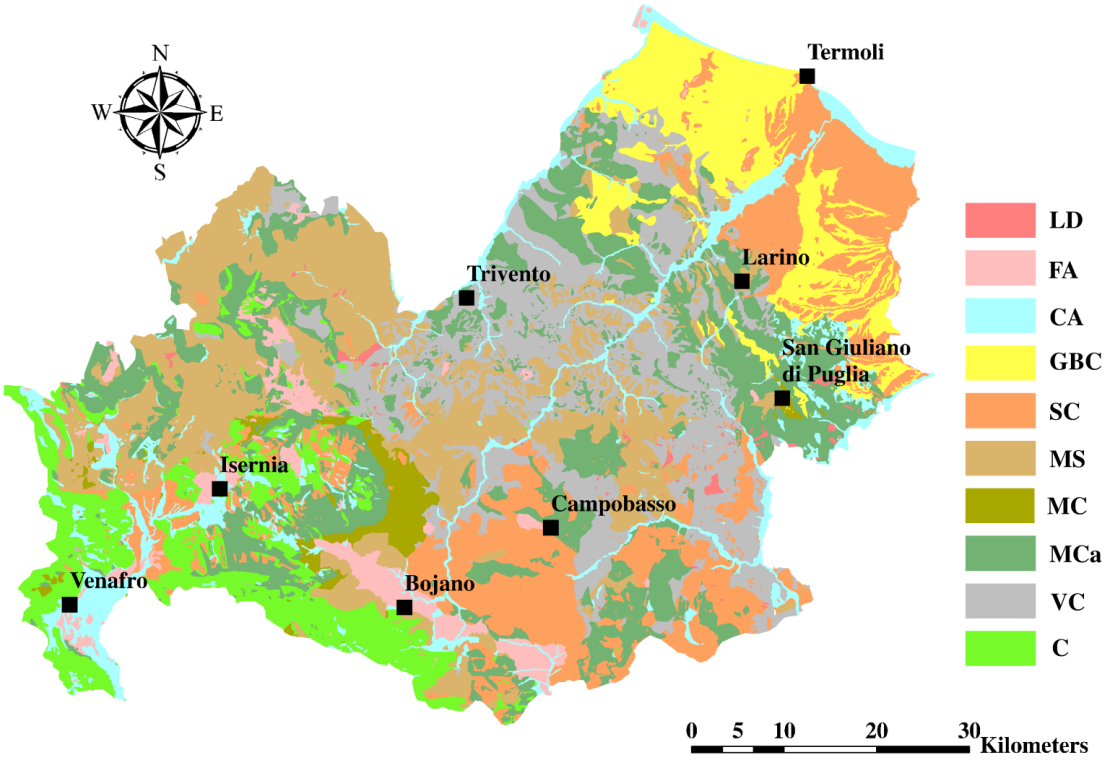

Figure 3.6. Geolithological map LD) Landslide Complex; FA) Fine Alluvial Complex; CA) Coarse Alluvial Complex; GBC) Grey-Bluish Clays Complex; SC) Sandstones and Conglomerates Complex; MS) Marly Sandstones

Complex; MC) Marly Clayey Complex; MCa) Marly Carbonate Complex; VC) Variegated Clays Complex; C) Carbonate Complex.

The Alluvial Complex (Holocene) was split into a Coarse Alluvial (CA) and a Fine Alluvial (FA), in order to distinguish sand and gravel rich *facies* related to fan and alluvial environments from clay and silt rich *facies*.

Following the classification of Crostella & Vezzani (1964) and Lanzafame & Tortorici (1976), the Flysch complex, which is characterized by highly heterogeneous *lithofacies* can be distinguished into several complexes, as function of the prevailing grain size sorting.

The coarser Flysch *lithofacies*, which include the upper arenaceous beds of San Bartolomeo Flysch Formation (Langhian-Tortonian) and the Messinian Evaporites deposits, constitute the Sandstones and Conglomerate Complex (SC), in which the Tona Formation (Pliocene) and the Plio-Pleistocene terraced deposits outcropping along the coast (Serracapriola Sands, Campomarino Conglomerates) are also inserted due to their lithological affinity, although different for geologic age and depositional environment.

The lower and finer *facies* of the San Bartolomeo Formation (Langhian-Tortonian) together with Molise Flysch formations (Frosolone, S.Elena; Pietraroja; San Massimo, Agnone), as addressed in the official 1:50,000 geological map, are attributed to a Marly Sandstones Complex (MS), as it reflects their feature of distal turbiditic deposits.

Eastwards the lithological composition of these deposits assumes a more calcareous rich *facies* through heteropic contacts, as nearer to the carbonate foreland domain. The latter are extensively represented by the Faeto and Tufillo Formations (Langhian-Tortonian), which are the Marly Carbonate Complex (MCa).

Finally a Marly Clayey Complex (MC), mainly constitued by the Toppo Capuana Formation (Early Tortonian) is identified.

The clayey complexes consist of the Variegated Clays (Oligo-Miocene), made of marls and overconsolidated clays, strongly fissured and tectonized, and the Plio-Pleistocene Grey-Bluish Clays (Subapennine Clays), constituted by silty clays with higher plasticity.

The geological setting is completed by a Carbonate (C) Complex (Trias-Cretaceous), made of limestones and dolostones, and a Landslides Complex (LD), only delimited when it was present in 1:100,000 official maps.

Most of these deposits can be classified as S*tructurally Complex Formations,* namely, they are a middle term between soils and rocks and show an *en masse* behavior strongly depending on the scale of heterogeneities and discontinuities, but also on the scale of the problem. Similar materials extensively crop out in Italy, but also in many other Countries (Carpathian Flysch; Franciscan Tectonic Melange of California coastal ridge, Great Plains of Central America and Canada). They are characterized by high landslide density, as pictured in Figure 3.7, but they are poorly documented in the international literature (D'Elia et al., 1998).

Figure 3.7. Landslides distribution in Structurally Complex Formations of Italy (after Esu, 1977).

In Geology those materials are usually referred with the term *flysch,* which was assigned by the Swiss geologist Bernhard Studer in 1827. The name comes from the German word *fliessen*, which means to flow, probably denoting the frequent landslides in areas consisting of these formations. Flysch consists of varying alternations of clastic sediments that are associated with orogenesis. It closes the cycle of sedimentation of a basin before the "arrival" of the paroxysmal folding process. The clastic material derived from erosion of the previously formed neighboring mountain ridge. Flysch is characterized by rhythmic alternations of sandstone and fine grained (pelitic) layers. The sandstone may also include conglomerate beds. The fine grained layers

contain siltstones, silty shales and clayey shales. Rarely and close to its margins, limestone beds or ophiolitic masses can be found. The thickness of the sandstone beds range from centimeters to meters. The siltstones and schists form layers of the same order but bedding discontinuities may be more frequent, depending upon the fissility of the sediments. The overall thickness of the flysch is often very large (hundreds to a few thousand meters) albeit it may have been reduced considerably by erosion or by thrusting. The formation may contain different types of alterations and is often affected by faults and thrusts. This results in a degradation of the geotechnical quality of the flysch rock mass. Thus, sheared or even chaotic rock masses can be found at the scale of a typical engineering design. A typical outcrop of those materials is sketched in Figure 3.8.

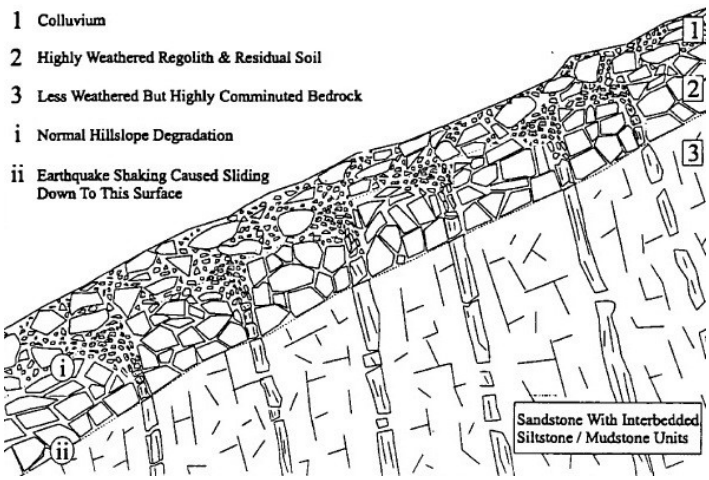

Figure 3.8. Typical outcropping conditions of materials as Flysch. (after Mankelow & Murphy, 1998).

Their features can be represented by the following characteristics:

- Heterogeneity: alterations of competent and incompetent members,
- The bedrock is usually covered by a weathered layer,
- Presence of clay minerals,
- Tectonic fatigue and sheared discontinuities, often resulting in a soil-like material,
- Permeability generally low, because of the presence of clay minerals.

Marinos & Hoek (2001) propose a modified GSI (Geological Strength Index) classification to account for the behavior of these materials mainly in tunneling projects (see Figure 3.9).

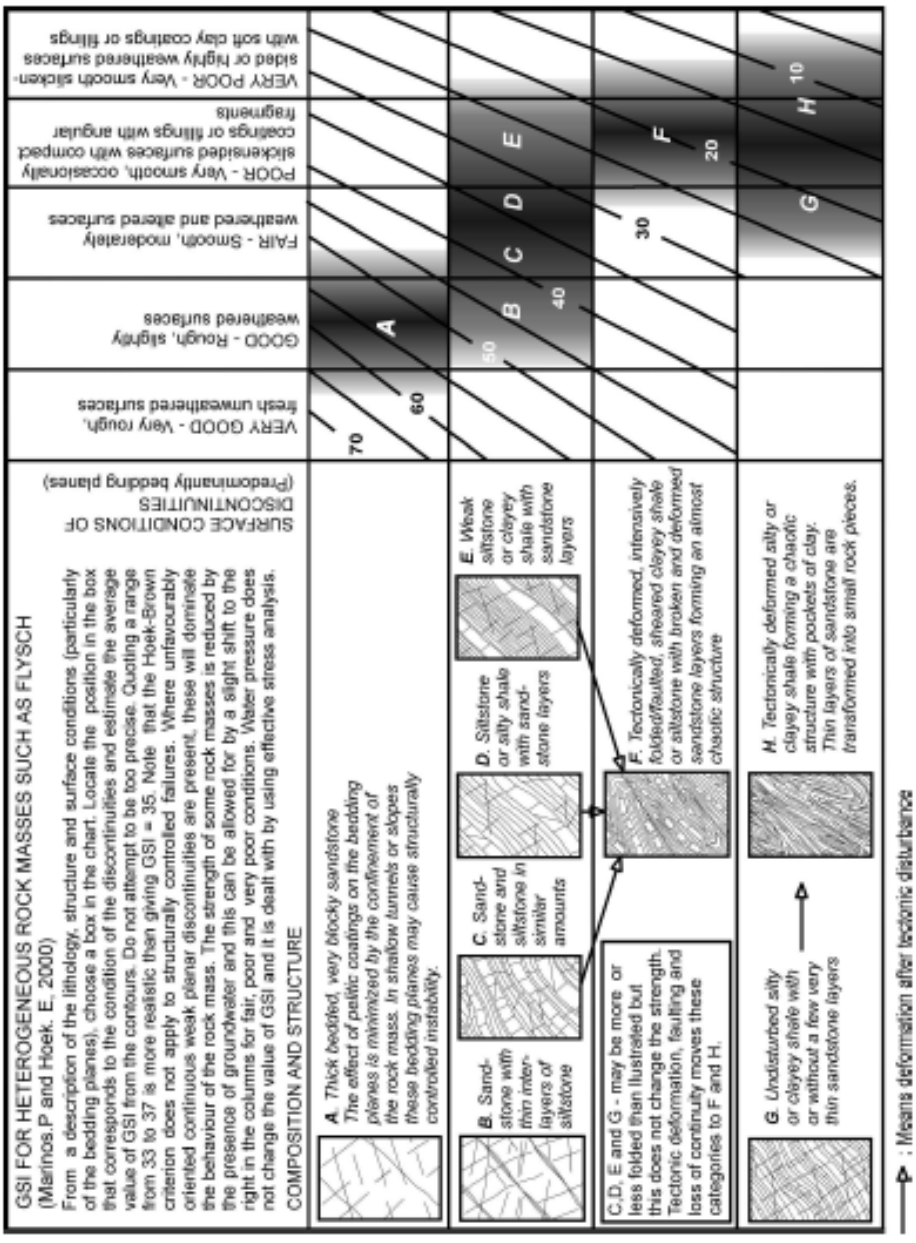

Figure 3. 9. GSI estimates for heterogeneous rock masses such as Flysch. (after Marinos & Hoek, 2001).

The most relevant contribution to the classification of those complex materials was proposed by Esu (1977), who mainly distinguished two groups:

a) lithologically homogeneous materials having singenetic or superimposed structures;

b) materials formed by at least two constituents (usually clay and a rock) with marked differences in their mechanical properties, characterized by an ordered or randomly assembled arrangement (Figure 3.10).

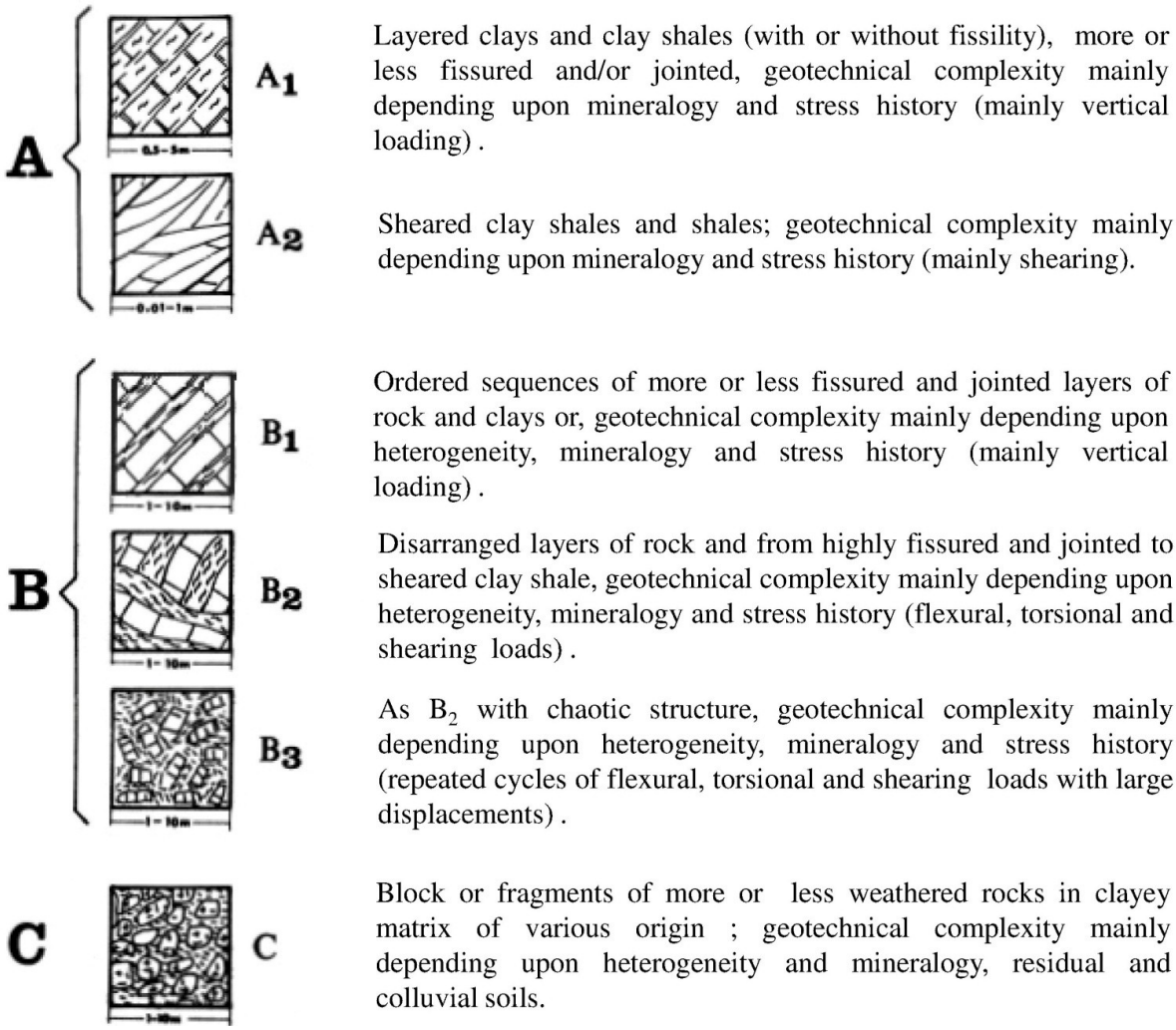

Figure 3.10. Esu (1977) Structurally Complex Formations Classification

Adopting this classification, the Coarse (CA) and Fine alluvial Complexes (FA) are respectively attributed to C and A_1 class, while Landslides (LD) is C and B_3. The Clayey Complexes GBC and MC are in A_1 class, while the Variegated Clays (VC) are more differentiated and can present outcropping *facies* representative of A_2, B_2, B_3. Flysch (SC, SM, MCa) can be found with all the

outcropping feature of B class, except SC, which could also present the C class. In Table 3.5 a summary of the identified complexes with their *engineering geological classification* is reported.

Table 3.5. Summary of the identified Complexes and their Engineering Geology Classification.

Geological Complex	Geolithological Complex	Age	ID	Esu (1977)
Alluvial Complex	*Landslides Complex*	Holocene	LD	B_3; C
	Fine Alluvial Complex		FA	A_1
Detrital Complex	*Coarse Alluvial Complex*		CA	C
Terraced Plio-Pleistocene Complex	*Conglomerates and Sandstones Complex*	Post-Calabrian Calabrian (?)	SC	B_1; C
Grey-Bluish Clays Complex	*Grey-Bluish Clays Complex*	Pliocene-Calabrian	GBC	A_1
Terraced Plio-Pleistocene Complex	*Conglomerates and Sandstones Complex*	Pliocene-Miocene	SC	B_1; C
Flysch Complex	*Marly Sandstones Complex*		MS	B_1; B_2
	Marly Carbonate Complex		MCa	B_1; B_2; B_3
	Marly Clayey Complex		MC	A_1
Variegated Clays Complex	*Variegated Clays Complex*	Miocene Cretaceous	VC	A_2, B_2; B_3
Carbonate Complex	Carbonate Complex	Miocene-Trias	C	-

3.2 GEOTECHNICAL CHARACTERIZATION

In this section the geotechnical characterization of the identified geolithological complexes is reported. It is mainly based on the elaboration of the laboratory test and it is mainly aimed at characterizing the shear strength.

In the previous section the materials which constitute the geological formations were addressed as *Structurally Complex Formations,* as interbedding of soils and rocks. The laboratory samples available in the database collected for this study are taken from the finer part of each geolithological complex, as it is portion which most contribute to the localization of the sliding surface as it is the least resistant. This feature was also reported in the technical-scientific literature by Pellegrino et al. (1985), which analyzed the slope behavior in the Variegated Clays (VC) cropping out in the Trigno River valley (Molise), where the stability conditions were dependent on the shear strength of the clayey layers. After it follows a geotechnical characterization, strongly aimed at studying the failure conditions and the landslide triggering susceptibility.

3.2.1 SOIL CLASSIFICATION

The grain size sorting curves for the main geolithological complexes are shown in Figures 3.to 3.14. Figure 3.14 also presents a triangular plot of the USDA (United States Department of Agriculture) Soil Classification, which summarizes the mean values for each geolithological complex of the particle size distribution, in terms of percentage of clay, silt and sand plus gravel.

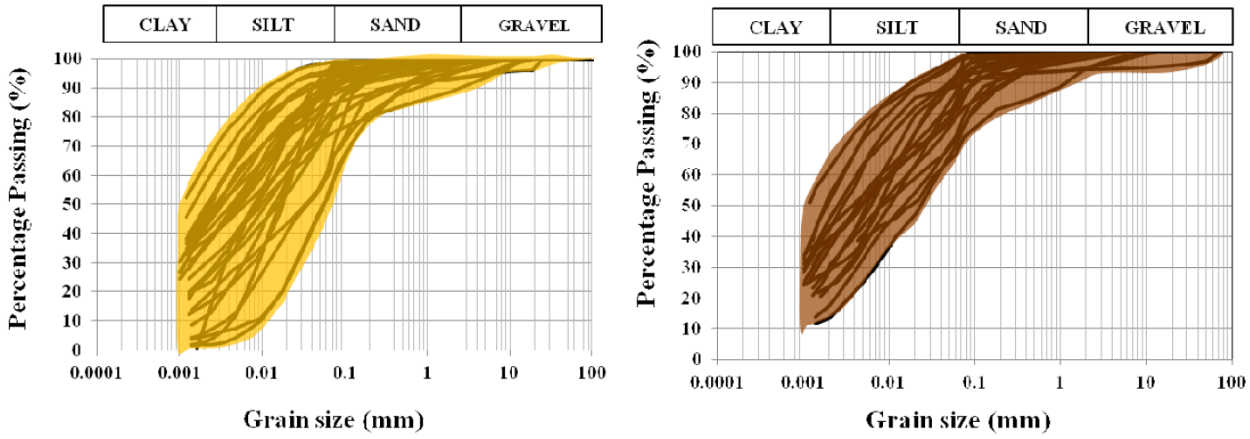

Figure 3.11. Grain Size Sorting Curves for the - SC - Sandstones and Conglomerates Complex ***(left)*** and - MS - Marly Sandstones Complex ***(right)***.

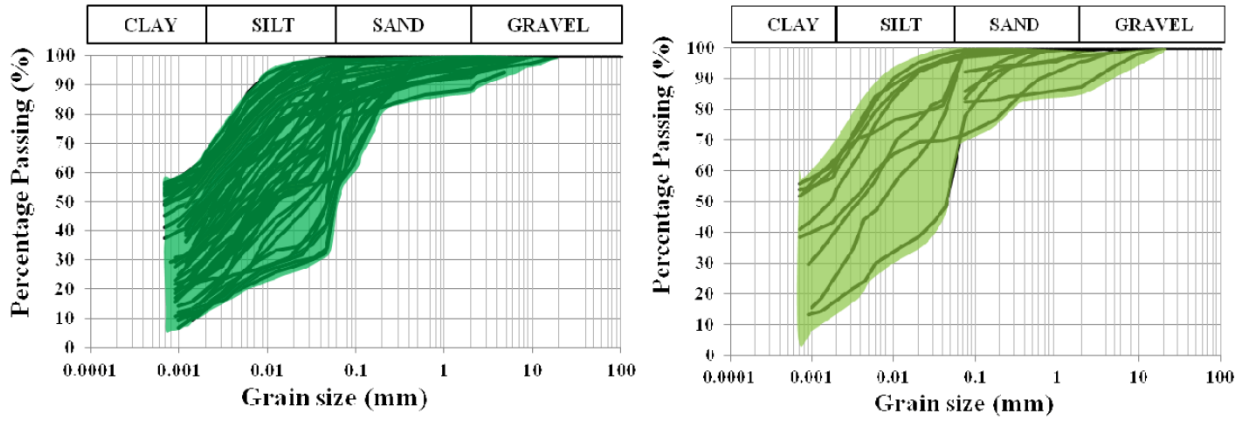

Figure 3.12. Grain Size Sorting Curves for the - MCa - Marly Carbonate Complex ***(left)*** and - MC - Marly Clayey Complex ***(right)***.

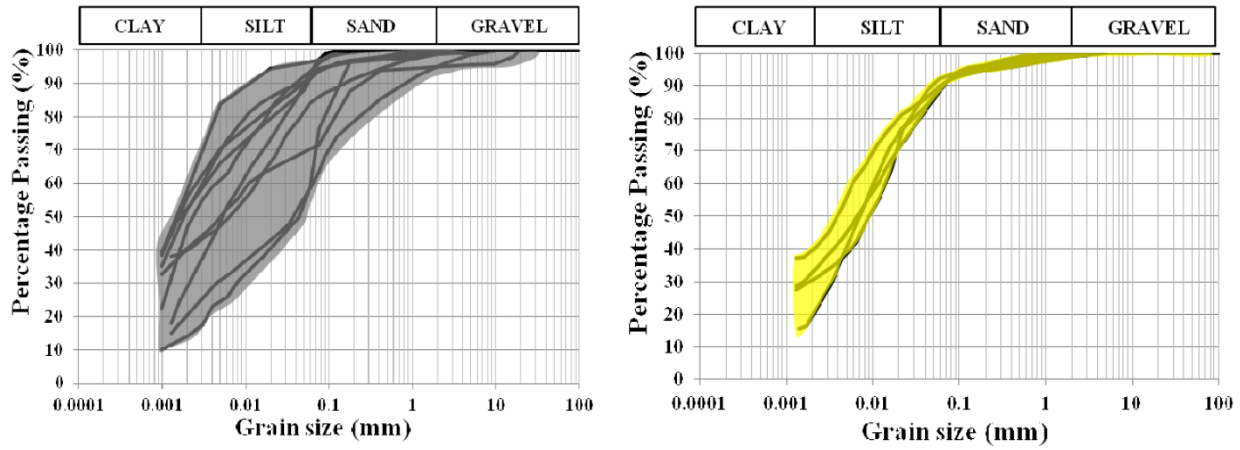

Figure 3.13. Grain Size Sorting Curves for the - VC - Variegated Clays Complex ***(left)*** and - GBC - Grey-Bluish Clays Complex ***(right)***.

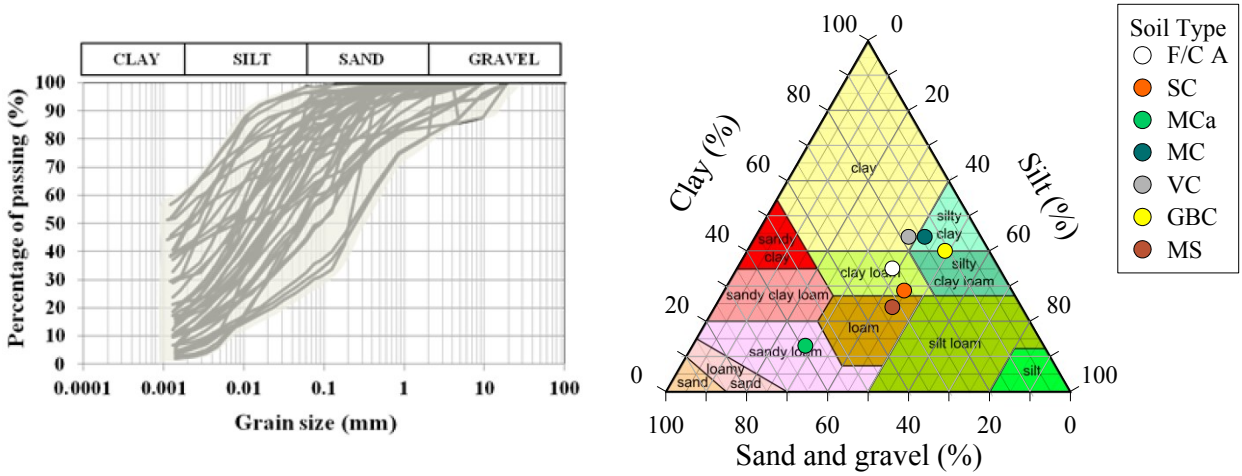

Figure 3.14. Grain Size Sorting Curves for the - FA and CA - Fine alluvial and Coarse alluvial Complexes ***(left)***.USDA (United States Department of Agriculture) Soil Classification for all Geolithological Complexes ***(right)***.

All the sampled materials are constitued by fine particle sizes. The matrix of the Clayey Complexes, as expected, is mainly constituted by clays and silty clays; the samples within the Alluvial Complexes presented a poor difference between fine and coarse alluvial soil, so they were analyzed together and are constituted by clay loam. The matrix of the Arenaceous Complexes present a higher heterogeneity and is classified as loam, as made of clays, silts but also of an important sand content. Finally the coarser matrix is the one of the Marly Carbonate Complex (MCa), which is classified as a sandy loam.

The characterization of fine soils through the Casagrande plasticity charts shown in Figures 3.15 - 3.16 mainly identifies clays and silts of middle and high plasticity. The higher amount of low plasticity soil is in the flysch formations, i.e. the Marly Carbonate Complex (MCa), the Arenaceous Sandstones and Conglomerate Complex (SC) and Marly Sandstones Complex (MS).

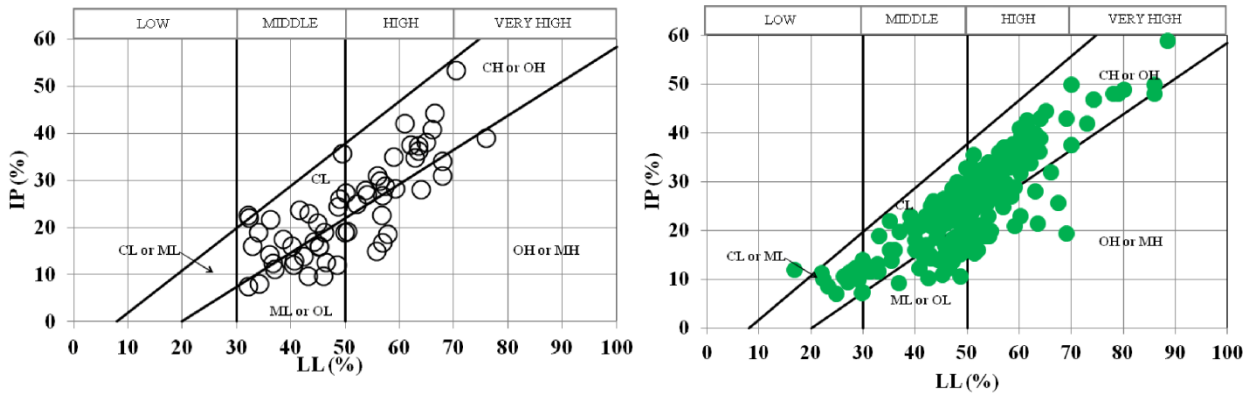

Figure 3.15. Casagrande Plasticity Chart for the - FA and CA - Fine alluvial and Coarse alluvial Complexes ***(left)*** *and* - MCa - Marly Carbonate Complex ***(right)***.

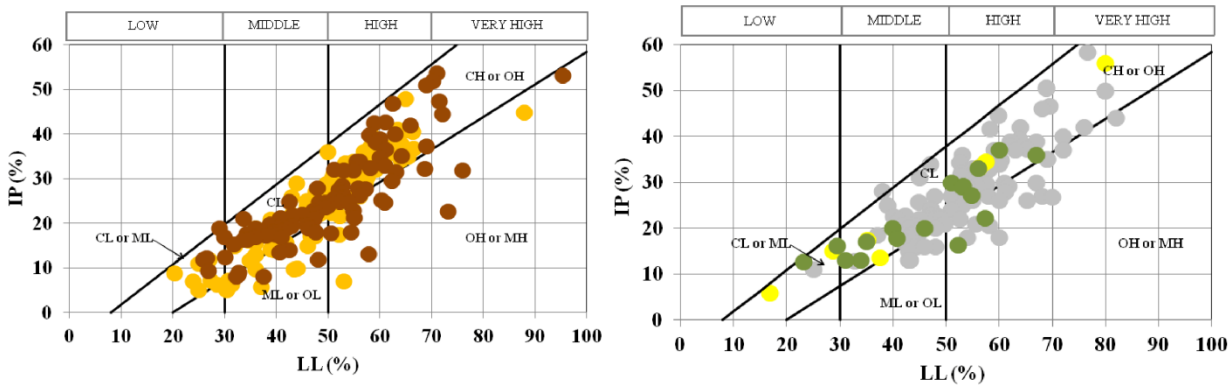

Figure 3.16. Casagrande Plasticity Chart for the - SC and MS - Sandstones and Conglomerates and Marly Sandstones Complexes ***(left)*** *and* - MC, VC; GBC - Marly Clayey, Variegated Clays and Grey-Bluish Clays Complexes ***(right)***.

Similar results were also reported in the studies on analogues geological formations carried out on Variegated Clays in Basilicata by Guerriero (1995) and Di Rosario (2008); Santaloia et al. (2001) in Ofanto River Valley; Cherubini et al. (1989) on Grey-Bluish Clays near Matera and Grana (2007) on Marly Carbonate formations of Umbria, some of them are reported in Figures 3.17 - 3.18.

It is interesting to note how the lowest plasticity values can be found in Grana (2007) for the Marly Carbonate Complex (Figure 3.18 right); the author explains that the analyzed soils were

sampled from the weathered cover of the bedrock, mainly constituted of coarse grains (sandy clays).

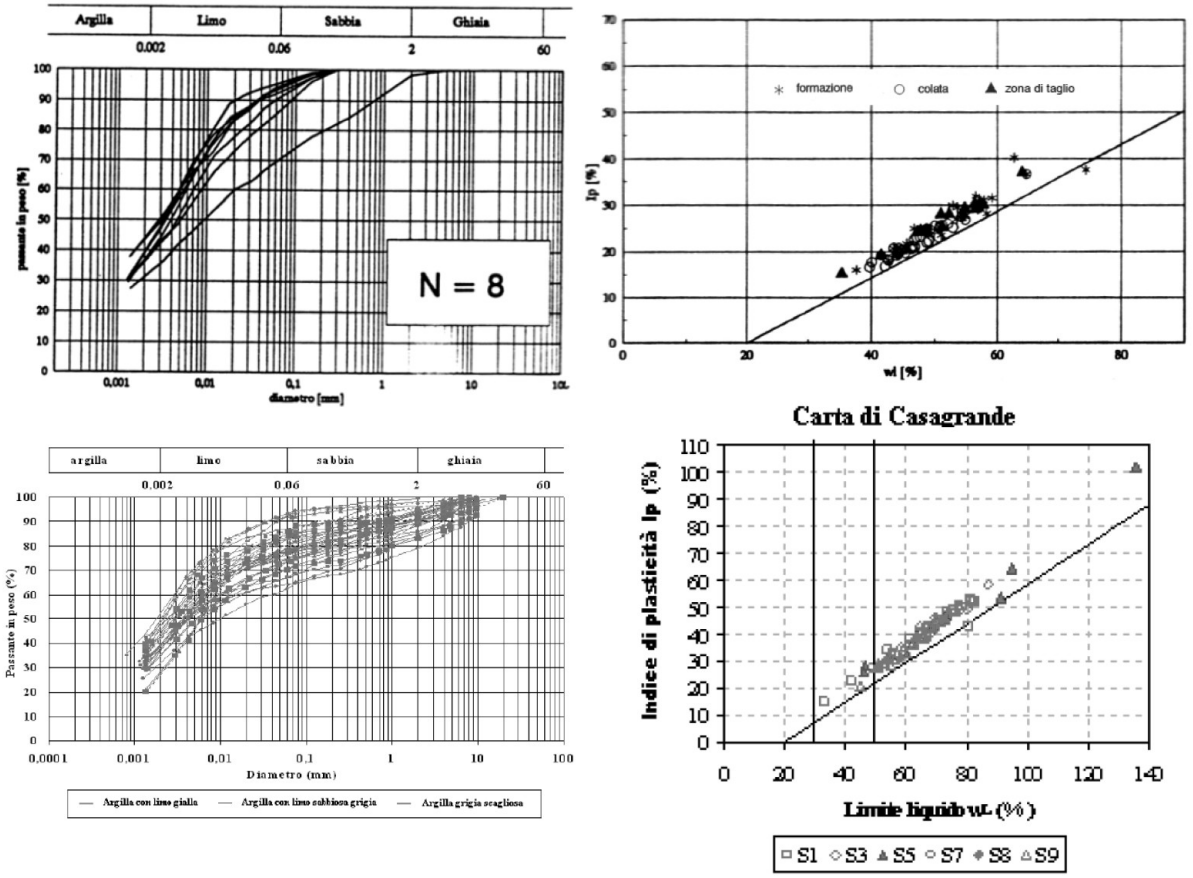

Figure 3.17. Grain Size Sorting Curves and Casagrande Plasticity Chart for the - VC - Variegated Clays Complex ***(Up)*** Masseria Marino Landslide (PZ) after Guerriero (1995) and ***(Down)*** Costa della Gaveta Landslide (PZ) after Di Rosario (2008).

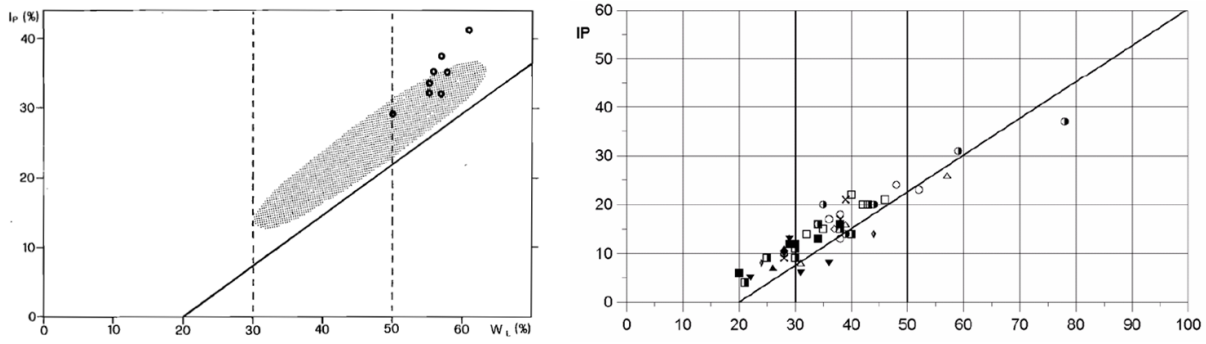

Figure 3.18. Casagrande Plasticity Chart for the - GBC - Grey-Bluish Clays Complex after Cherubini et al. (1989) ***(left)*** and - MCa - Marly Carbonate Complex after Grana (2007) ***(Right)***.

The index properties profiles of the identified geolithological complexes, shown in Figures 3.19 to 3.21 evidence a significant consistency of those materials, which seems to increase around 10 - 15 m b.g.l., identifying the limit between the altered eluvial cover and the bedrock. The most heterogeneous soils, such a SC and MS are characterized by a strong interbedding of clay and rock. High plasticity clayey samples can be also found at deeper depths; this evidence also suggests that those layers could be ancient shear bands, as also evidenced by Cotecchia et al. (2011), which will contribute to the formation of a sliding surface and triggering of a landslide.

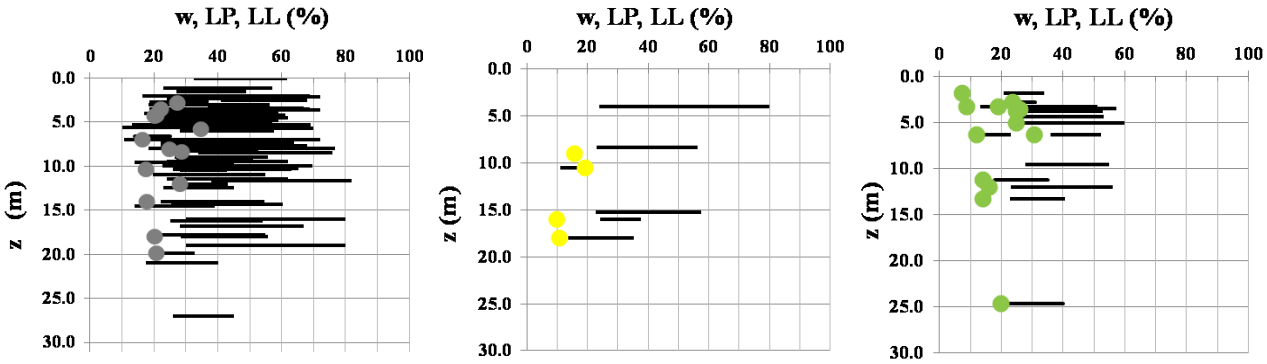

Figure 3.19. Natural water content and Attemberg limits profile Vs. Depth for Variegated Clays Complex (VC), Grey-Bluish Clays Complex (GBC) and Marly Clayey Complex (MC).

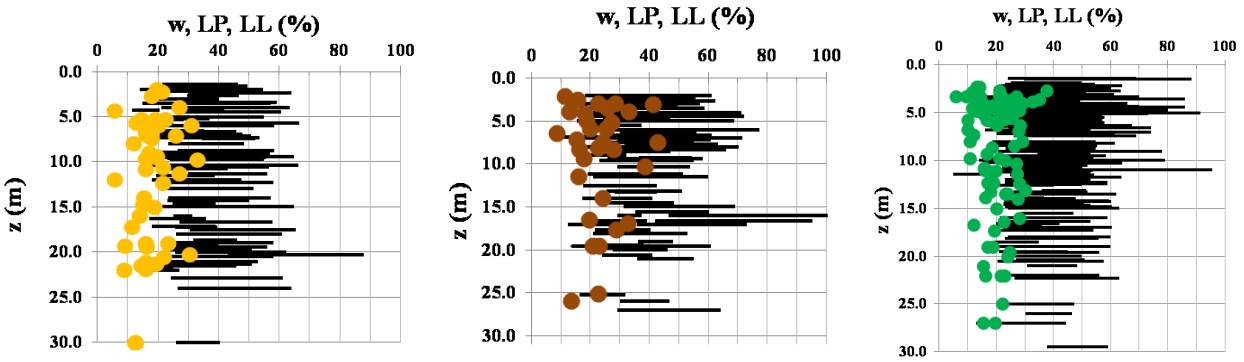

Figure 3.20. Water content and Attemberg limits profile Vs. Depth for Sandstones and Conglomerates Complex (SC), Marly Sandstones Complex (MS) and Marly Carbonate Complex (MCa).

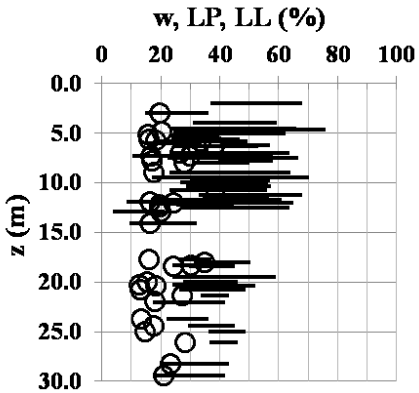

Figure 3.21. Water content and Attemberg limits profile Vs. Depth for Coarse (CA) and Fine Alluvial Complexes (FA).

The shrink-swell capacity was analyzed through the Activity Charts shown in Figures 3.22-3.23, in which at regional scale, the clayey content of these materials is characterized by moderate activity and a mineralogic composition between the illite and kaolinite clays groups. Vitone & Cotecchia (2011) show similar results of activity (A) are shown in Table 3.6 for the Variegated Clays of the Daunia Apennine (Senerchia and Santa Croce di Magliano), even though a bentonitic composition was found for some layers of the Santa Croce di Magliano outcrop.

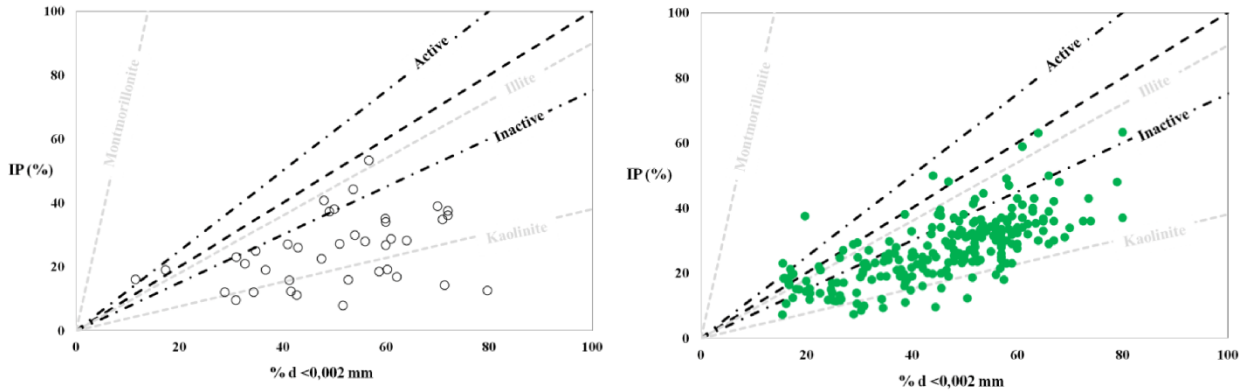

Figure 3.22. Activity chart of clay for - FA-CA -Alluvial Complexes (***left***) and - MCa - Marly Carbonate Complex (***right***). The boundary lines for inactive (***act***<0.75), normal (0.75<***act***<1.25) and active (***act***>1.25) clay are from Skempton (1953). The lines for montmorillonite, illite and kaolinite are from Lambe & Whitman (1969).

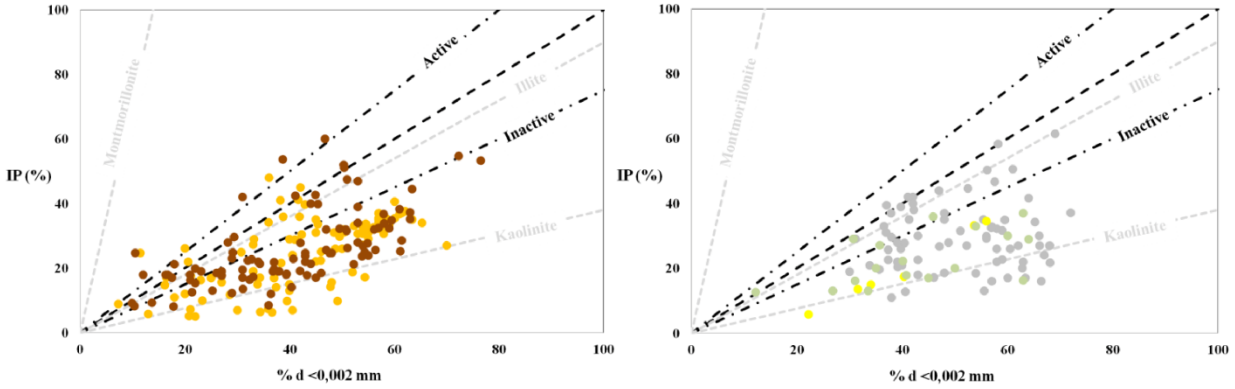

Figure 3.23. Activity chart of clay for - SC;MS - Sandstones and Conglomerates, Marly Sanstones Complexes (***left***) and - VC; GBC; MC - Variegated Clays, Grey-Bluish Clays and Marly Clayey Complexes (***right***). The boundary lines for inactive (***act***<0.75), normal (0.75<***act***<1.25) and active (***act***>1.25) clay are from Skempton (1953). The lines for montmorillonite, illite and kaolinite are from Lambe & Whitman (1969).

Table 3.6. Index properties of fissured clays (after Vitone & Cotecchia, 2011)

Clays	Sampling	z: m (from g.l.)	CF: %	w_L: %	PI: %	S_r: %	γ_s: kN/m^3	γ: kN/m^3	A	e_0
SCM scaly clay	Block	3·00	91·0	81	52	77	27·20	20·80	0·57	0·880
SE scaly clay borehole samples	I6/1	16·70	61·0†	57†	33†	94†	27·40†	22·08†	0·54†	0·420†
	I6/3	16·00	55·0†	66†	41†	100†	27·40†	22·16†	0·75†	0·449†
	P5/1	19·70	54·8†	50†	23†	100†	27·40†	22·22†	0·42†	0·430†
	P5/3	52·35	63·0†	83†	54†	93†	27·40†	21·86†	0·86†	0·429†
	P8/5	20·75	57·3†	57†	36†	92†	27·18†	20·75†	0·63†	0·572†
	P8/9	26·30	53·1†	67†	37†	93†	27·47†	21·71†	0·69†	0·464†
	P8/11	31·40	77·5†	67	37	93†	27·56†	21·70†	0·48	0·586
	P8/12	31·70	68·0	77	43	88	27·56	21·40	0·63	0·526
SCM bentonite clay	Block	18·00	66·2	139‡	86‡	90	26·50	16·50	1·30	1·670

† Values from Cotecchia & Santaloia (2003).
‡ Values from Cotecchia *et al.* (2003).
nd = not determined.

3.2.2 SHEAR STRENGTH

The mechanical behavior of the complex materials is highly variable, as it depends on index properties, stress history, state parameters and structural features. Some of the main national scientific papers dealing with the characterization of the mechanical behavior of *structurally complex formations*, mainly concerning the slope stability topic are reported in Table 3.7 together with the shear strength parameters. The main findings also summarized in D'Elia et al. (1998) are reported here:

- The intact clayey materials typically express the behavior of overconsolidated clays, i.e. a

significant shear strength followed by a strong decrease in the post-rupture stage; instead the jointed clays present smaller peaks, with a slight reduction in strength due to the fissures, along which rigid displacements develop before the mobilization of the peak strength (Guerriero 1995; Olivares 1996).

- The shear strength envelope is characterized by the same friction angle in jointed and intact material, instead the cohesion can strongly vary, as it depends on the roughness of the joint surface, which usually is smooth, slickensided and exhibits very low shear strength.
- The shear strength along faults is at residual value, and the residual strength of the intact and jointed material is the same.
- Fissures can be oriented and exhibit mechanical anisotropy, which affects the values of cohesion.
- At low stress rate, the failure is preceded by dilatancy, due to the irregularities between the sliding fragments, while at high stress rate those irregularity are severed (Pellegrino & Picarelli, 1982; Pellegrino et al. 1985).

Table 3.7. Summary of the shear strength parameters retrieved in some of the most relevant scientific papers for analogous materials.

ID	Location	φ' (°)	c' (kPa)	φ_R' (°)	s_u (kPa)	TxCD	TxCU	TxUU	UCS	SS	RS	Reference
GBC	Vasto (CH)	26	30				X			X		Esu & Martinetti (1965)
	Numana (AN)	11	10		23÷22		X	X				Colleselli & Colosimo (1977)
	Petacciato (CB)	23.5 ÷ 22	22 ÷ 5	16.5 ÷ 12						X	X	Guerricchio et al. (1996)
		27 ÷21	160 ÷ 27	16		X	X					Cotecchia & Melidoro (2002)
		25 ÷ 17.5	50 ÷19	12 ÷ 17						X		
		17.4	16		130 ÷ 600			X			X	Fiorillo (2003)
	Amendolara (CS)	26 ÷ 24	71 ÷14	26 ÷ 16	200 ÷ 390	X	X	X	X	X	X	Fruzzetti et al. (2013)
SC	Benevento	35.7 ÷ 21.14	14 ÷ 0							X		Silvestri et al. (2006)
MS	Agnone (IS)	22.6	60	9.4 ÷ 8.2						X		Guadagno et al. (1987)
		23.23 ÷ 19.3	60 ÷ 20	21.9 ÷ 17.2						X		Calcaterra et al. (2006)
MC	S.Giuliano di Puglia (CB)	20 ÷ 18	170 ÷ 40	21 ÷ 20			X					d'Onofrio et al. (2009)
	Volturino (FG)	20 ÷ 18	50 ÷ 0	9.6						X		Cotecchia et al. (2011)
MCa	Spoleto (PG)			28 ÷ 10							X	Grana (2006)
	Volturino (FG)	25	40							X		Cotecchia et al. (2011)
VC	Valle del Trigno (CB)	20	29.4	11						X		Federico & Tancredi (1980)
	Torrente Fiumarella (AV)	23 ÷ 11	20 ÷ 13	6						X		Fenelli et al. (1982)
		20 ÷ 15	27 ÷ 18				X					

	Laviano (SA)	29 ÷ 22	11 ÷ 10	11						X		
		14 ÷ 7	58 ÷ 26				X					
	Brindisi di Montagna (PT)	25 ÷ 16	22 ÷ 8				X			X		Cotecchia et al. (1986)
	Valle del Basento (PT)	22 - 20	16 ÷ 0.15			X				X		Guerriero (1995)
	Covatta (CB)	24 ÷ 17	12.3 ÷ 4.6	19 ÷ 11			X			X		Comegna (2005)
	Lama del Gallo (CB)	20	21.8	24.5			X			X		

The shear strength was characterized through the collection and analysis of 482 simple shear tests and 388 unconsolidated undrained triaxial strength tests. The available data were not homogeneous and frequently was not possible to define the stress-strain path (σ; τ); only the friction angle (φ'), the true cohesion (c') and the undrained shear strength (s_u) were available.

The collected tests were grouped as function of the geolithological complex in which they were sampled and for each one the Mohr-Coulomb failure envelope was plotted as grey lines forming a fuse and shown in Figures 3.24 to 3.29 left.

The maximum and minimum failure conditions were evidenced with dotted lines and the mean failure envelope was marked with a bold continuous line. In order to validate the obtained results, the samples in which were available the stress-strain distribution were regressed through a linear Ordinary Least Squares (OLS) technique, shown in the same Figures on the right. This analysis was carried out for the assessment of the materials peak strength, as only in few cases the evaluation of the residual strength was permitted. The results evidence for each material an agreement between the friction angle (φ') retrieved from the OLS analysis and the mean value coming from the whole dataset; instead the values of the true cohesion result more dispersed, this feature may be related to the different outcropping conditions of the soil samples and to the random orientation of the pre-existing fissures, as previously evidenced. In the case of Figure 3.26, the Marly Carbonate Complex (MCa), in which the most of the database samples are located, presents a perfect fitting of both analyses.

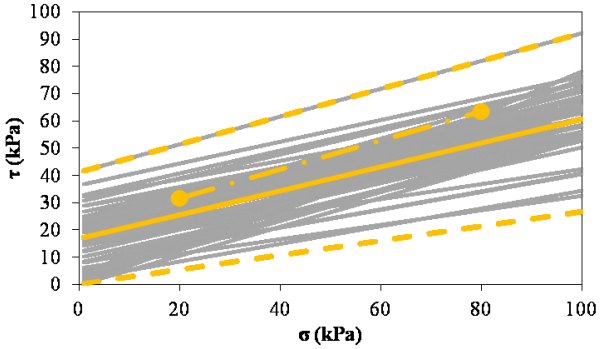

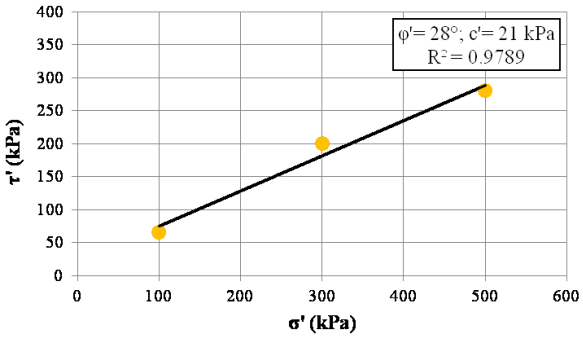

Figure 3.24. Mohr-Coulomb failures envelopes for the Sandstones and Conglomerates Complex (SC) (***left***) and the result of the ordinary least squares (OLS) analysis (***right***).

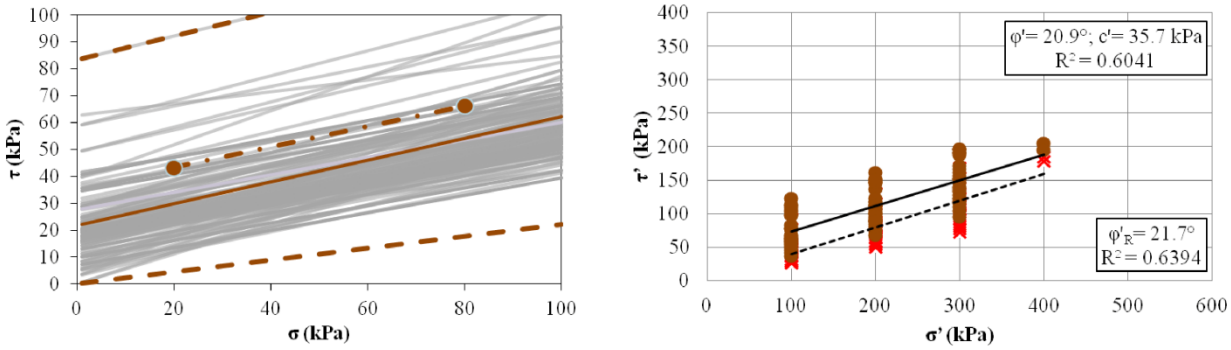

Figure 3.25. Mohr-Coulomb failures envelopes for the Marly Sandstones Complex (SC) (***left***) and the result of the ordinary least squares (OLS) analysis (***right***).

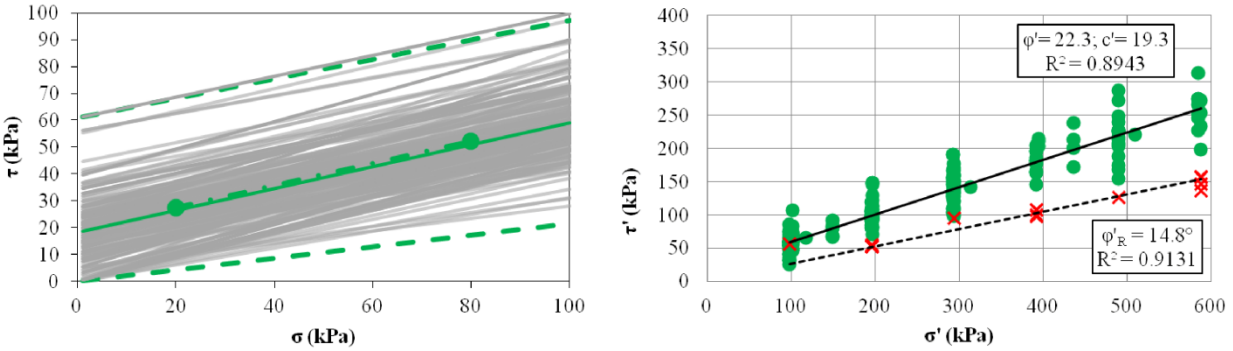

Figure 3.26. Mohr-Coulomb failures envelopes for the Marly Carbonate Complex (MCa) (***left***) and the result of the ordinary least squares (OLS) analysis (***right***).

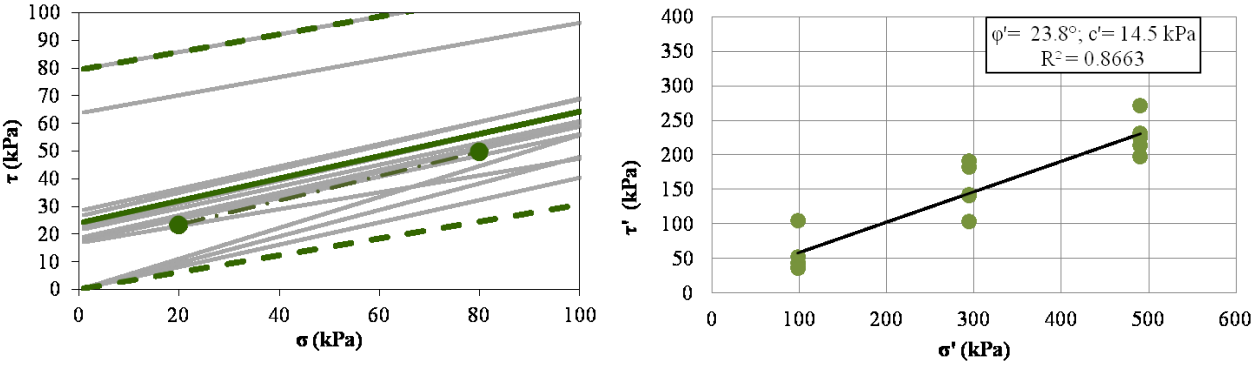

Figure 3.27. Mohr-Coulomb failures envelopes for the Marly Clayey Complex (MC) (***left***) and the result of the ordinary least squares (OLS) analysis (***right***).

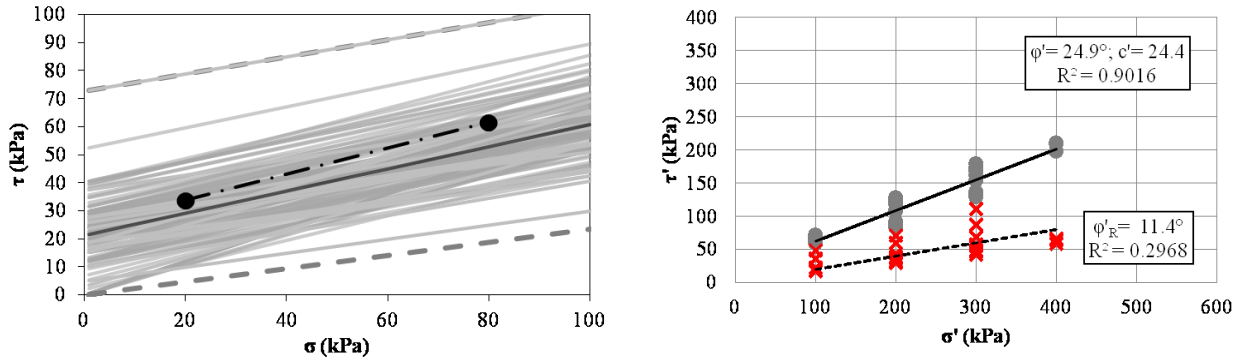

Figure 3.28. Mohr-Coulomb failures envelopes for the Variegated Clays Complex (VC) (***left***) and the result of the ordinary least squares (OLS) analysis (***right***).

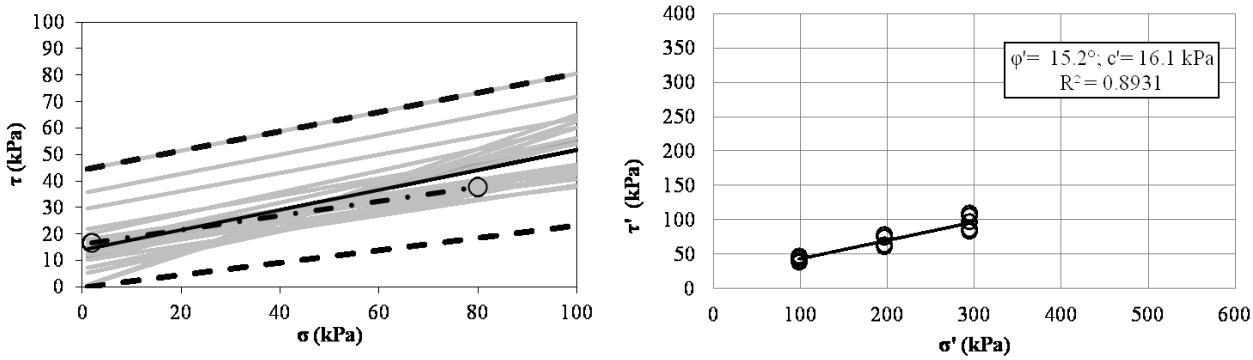

Figure 3.29. Mohr-Coulomb failures envelopes for the Coarse and Fine Alluvial Complex (CA/FA) (***left***) and the result of the ordinary least squares (OLS) analysis (***right***).

The s_u evaluation was simply based on the mean value coming from the whole dataset of Unconsolidated Undrained Triaxial strength tests (TxUU), for the maximum depth of 15 m b.g.l.

In Tables 3.8 - 3.9 - 3.10 a summary of the effective shear strength values and the one of the undrained shear strength characterization for the structurally complex formations at issue is reported.

Table 3.8. Shear strength characterization from the database (DB) values.

Geolithological Complexes	φ'DB (°)						c'DB (kPa)					
	Max	Min	Mean	σ	CV	N. Tests	Max	Min	Mean	σ	CV	N. Tests
Landslides Deposits (LD)	-	-	-	-	-	-	-	-	-	-	-	-
Alluvial Complexes (CA-FA)	33.0	13.0	20.6	5.7	27%	30.0	44.1	4.9	14.2	9.5	67%	26.0
Grey-Bluish Clays Complex (GBC)	-	-	-	-	-	-	-	-	-	-	-	-
Sandstones and Conglomerates Complex (SC)	38.0	15.0	23.7	5.0	21%	52.0	41.2	1.0	16.7	9.6	57%	48.0
Marly Sandstones Complex (MS)	36.0	12.4	22.1	4.2	19%	126.0	83.4	2.9	21.6	14.2	66%	122.0
Marly Clayey Complex (MC)	29.2	17.0	21.9	3.2	15%	13.0	79.4	16.7	24.1	21.9	91%	10.0
Marly Carbonate Complex (MCa)	35.5	12.1	22.2	3.8	17%	180.0	64.7	1.0	18.4	11.4	62%	159.0
Variegated Clays Complex (VC)	31.0	13.2	21.5	3.9	18%	112.0	72.6	2.0	21.3	10.3	48%	105.0
Carbonate Complex (C)	-	-	-	-	-	-	-	-	-	-	-	-

Table 3.9. Shear strength characterization from ordinary least squares(OLS) regression analysis.

Geolithological Complexes	ID	φ'OLS (°)	c'OLS (kPa)	N. Tests	φR OLS	N. Tests
Landslides Deposits	LD	-	-	-	-	-
Alluvial Complexes	CA-FA	15.2	16.1	5	-	-
Grey-Bluish Clays Complex	GBC	-	-	-	-	-
Sandstones and Conglomerates Complex	SC	28.0	21.0	1	-	-
Marly Sandstones Complex	MS	20.9	35.7	30	21.7	20.0
Marly Clayey Complex	MC	23.8	14.5	5	-	-
Marly Carbonate Complex	MCa	22.3	19.3	68	14.8	9.0
Variegated Clays Complex	VC	24.9	24.4	11	11.4	8.0
Carbonate Complex	C	-	-	-	-	-

Table 3.10. Undrained shear strength characterization from the TxUU tests of the database (DB).

Geolithological Complexes	ID	$s_{u\ DB}$ (kPa)					
		Max	Min	Mean	σ	CV	N. Tests
Landslides Deposits	LD	-	-	-	-	-	-
Alluvial Complexes	CA-FA	380	24	144	85	59%	17
Grey-Bluish Clays Complex	GBC	74	30	54	22	41%	3
Sandstones and Conglomerates Complex	SC	350	40	157	96	62%	27
Marly Sandstones Complex	MS	293	11	109	58	54%	81
Marly Clayey Complex	MC	141	40	90	41	46%	7
Marly Carbonate Complex	MCa	378	36	136	78	57%	75
Variegated Clays Complex	VC	359	25	117	67	57%	62
Carbonate Complex	C	-	-	-	-	-	-

The above Tables also list the main statistical indexes, i.e. the maximum (Max) and minimum (Min) value of each subset, the mean value with its standard deviation (σ), the number of tests and the coefficient of variation (CV). The latter is a normalized measure of dispersion of a probability distribution, which is defined as the ratio of the standard deviation (σ) to the mean (μ):

$$CV = \frac{\sigma}{\mu} \tag{3.2}$$

It is usually expressed in percentage and it is a useful statistic for comparing the degree of variation of data series, which can also present very different order of magnitude. In Table 3.11 a collection of some coefficients of variation for the most common parameters in geotechnical engineering is reported, compared with the results of this study.

Table 3.11. Representative values of the variability in common geotechnical engineering parameters, expressed as coefficient of variation in percent from the main technical scientific literature.

Geotechnical Parameter	in Harr (1987)	Lee et al. (1983)	Lacasse & Nadim (1996)	Lumb (1974)	Phoon & Kulhawy (1999)	Phoon & Kulhawy (1999)	This study	
					Range	Mean		
γ	3% (Hammit 1966)	-	-	-	3-20%	9%	6%	
γ_d	-	-	-	-	2-13%	7%	-	
φ (Gravels)	7% (Schultze 1975)	-	-	-	-	-	All Soils	20%
φ (Sands)	12% (Schultze 1975)	5-15%	2-5%	-	5-11%	9%		20%
φ (Clays)	-	12-56%	-	-	10-50%	21%		20%
c (Clays)	40% (Fredlund & Dahlaman 1972)	20-50%	-	-	-	-		57%
c (Sands)	40% (Fredlund & Dahlaman 1972)	25-30%	-	-	-	-		57%
LL	-	2-48%	3-20%	-	7-39%	18%	24%	
LP	-	9-29%	3-20%	-	6-34%	16%	29%	
IP	-	-	-	-	9-57%	29%	40%	
Void ratio	-	13-42%	7-30%	15-30%	-	-	26%	
s_u (TxUU)	-	5-20%	-	20-50%	11-49%	22%	62%	
s_u (not reported)	-	-	-	-	6-80%	32%	-	

The reported values clearly show the high variability of the soil properties and the related geotechnical parameters, nevertheless the quantification of this variability, even with simple indexes as the coefficient of variation (CV) is indeed a relevant step in developing reliability-based approaches. The result of this study, in term of mean value of the variation coefficient, is comparable with some of the main existing scientific contributions; in particular the unit weight (γ) and the friction angles (φ) are in the range of variability reported by Phoon & Kulhawy (1999) and Lee et al. (1983) for the clayey materials. The cohesion (c) together with the undrained shear strength (s_u) presents the highest values of CV, as also evidenced in the material characterization.

The collected dataset permitted the characterization of the physical properties and shear strength of the finer portions, which were resulted in agreement with the value retrieved in the scientific literature. The obtained results, in terms of φ', c', s_u and γ were attributed to homogeneous geolithological complexes and not to the single geological formation, in order to give the

opportunity of adopting these values in similar geological contexts, even if in different geographical areas.

3.3 SEISMIC SOIL CLASS CLASSIFICATION

3.3.1 THE METHOD OF WALD AND ALLEN (2007)

The prediction of reliable ground-motions is a key topic for the USGS National Earthquake Information Centre within the Prompt Assessment of Global Earthquakes for Response (PAGER) (Wald et al., 2006). The fulfilment of this aim needs an average evaluation of materials stiffness for shaking amplification along the shallower soil layers. On the basis of DH in situ tests, the $V_{S,30}$ (m/s) experimental values and topographic slope (m/m) were correlated at each measurement point. Wald & Allen (2007) collected 1629 V_{S30} measurements mainly coming from California (767). In Table 3.12, the spatial density of DH tests for California, calculated as the ratio between the number of surveys and the investigated area, has been compared to the values obtained for their study in Italy and with the amount of data in this research.

Table 3.12. Density of in-situ test

Reference	Area (km^2)	N° tests	Density (n° tests/km^2)
California (Wald & Allen, 2007)	423970	767	1.81×10^{-3}
Italy (Wald & Allen, 2007)	301340	43	1.43×10^{-4}
Molise Region (This study)	4438	294	4.15×10^{-2}

The test density in California and in Molise context differ by one order of magnitude, confirming the higher number of experimental evidences for this small territory.

The method implemented by U.S.G.S. was globally applied and was provided online (http://earthquake.usgs.gov/hazards/apps/vs30/), on the basis of topographic data derived from the Shuttle Radar Topography Mission 30-sec (SRTM30) global topographic data set (Farr & Kobrick, 2000). These data are considered as an upgrade of the commonly-used USGS 30-sec

topographic data (GTOPO30). The choice of adopting 30-sec data is related to the global availability of this DEM at global scale; it corresponds nearly to 1 km x 1 km cell.

Table 3.13 shows the identified topographic slopes and V_{S30} ranges for site Classification into EC8 and NEHRP (National Earthquake Hazard Reduction Program) categories (BSSC, 2001). The slope range for each soil class has been updated and divided by Wald & Allen (2007) between *active tectonic* and *stable continental* areas. The Molise region belongs to *Active tectonic* areas, as most of the Italian Territory.

Table 3.13. Slope ranges adopted in site classification by USGS

V_{S30} ranges (m/s)	EC8 classes	Similar NEHRP classes	Slope ranges (m/m)	
			Active tectonic Wald and Allen (2009)	Stable continental Wald and Allen (2007)
> 800	A	A/B	> 0.14	> 0.025
360 – 800	B	C	0.018 – 0.14	0.0072 – 0.025
180 – 360	C	D	0.0003 – 0.018	$2 * 10^{-5}$ - 0.0072
< 180	D	E	< 0.0003	$< 2 * 10^{-5}$

Based on Wald & Allen (2007) approach, Lemoine et al. (2012) obtained the V_{S30} map for Mediterranean Europe and compared their result with a large database of 702 in situ geophysical investigations. The main findings of this study might be listed as follows:

a) it was found a general overestimation of the $V_{S,30}$ by the USGS approach compared to the in-situ measurements;

b) the results are dependent by the size of the DEM basic cell, which was quite large (1 km^2) in USGS.

However, the authors observed that this approach could be considered reliable for a first stage estimation, also because the differences is attenuated when the site class are considered (according the existing codes), instead of absolute value of V_{S30}.

Concerning, in particular, the Italian territory, a similar trend was also recognized by the authors of the original approach (Wald & Allen 2007), but it was based on very few data (43), mainly located in the areas in which the strongest Italian earthquakes occurred until 2002. The spatial density of data has been also calculated in Table 3.12, and was strongly lower compared to our case study. In any case, following the U.S.G.S. approach, the $V_{S,30}$ maps for Molise Region was adopted, as shown in Figure 3.30.

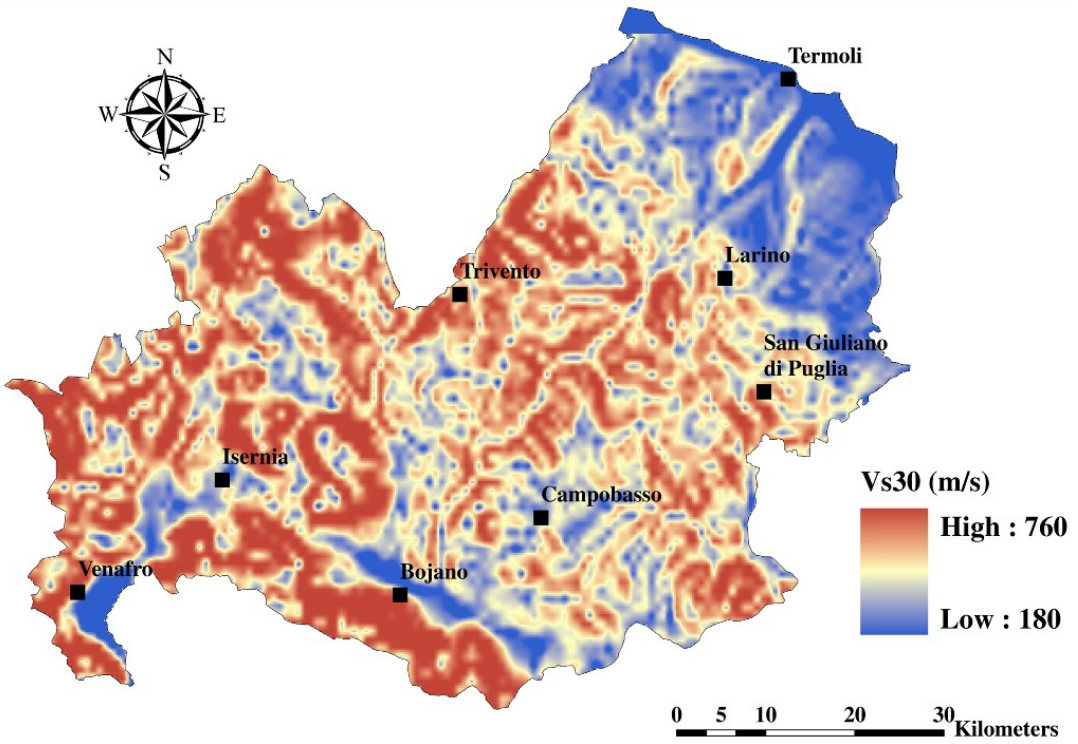

Figure 3.30. V_{S30} map obtained from USGS for Molise region (http://earthquake.usgs.gov/hazards/apps/vs30/)

The slope-based estimation of V_{S30} was then compared to the measured values obtained from DH tests available for the geologic classes of Table 3.14 and illustrated in Figure 3.31.

Table 3.14. Geolithological Complex of Molise Region

Acronym	Description	Age	N° tests
LD	Landslides deposits Complex	Holocene	-
FA	Fine Alluvial Complex	Holocene	18
CA	Coarse Alluvial Complex	Holocene	15
GBC	Grey Bluish Clays Complex	Plio-Pleistocene	8
SC	Sandstones and Conglomerates Complex	Laghian – Pleistocene	62
MS	Marly Sandstones Complex	Langhian – Tortonian	52
MC	Marly Clays Complex	Tortonian	4
MCa	Marly Carbonates Complex	Langhian – Tortonian	103
VC	Variegated Clays Complex	Oligocene – Miocene	31
C	Carbonates Complex	Cretaceous Miocene	1
	Total		294

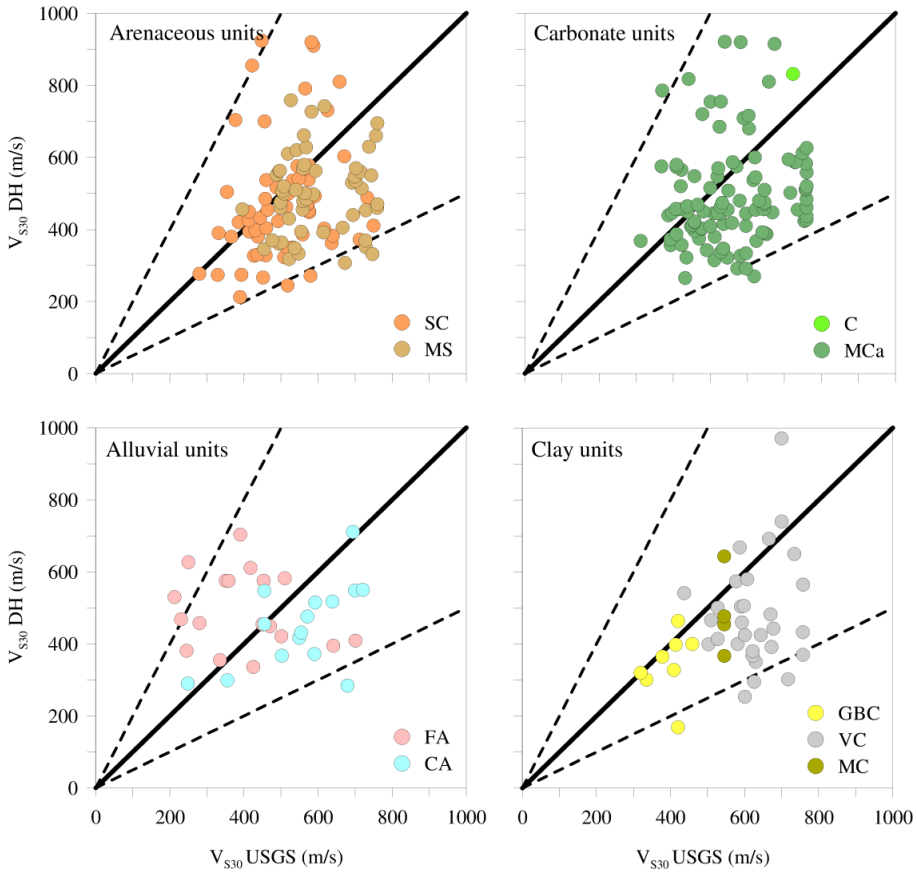

Figure 3.31. V_{S30} estimated from USGS vs. V_{S30} DH measurements for different geological groupings.

For most of the groupings, the V_{S30} values obtained from U.S.G.S. map overestimates the measured ones, except for the case of Fine Alluvial soils (FA), in which the shear wave

velocities are slightly understimated. No significant difference could be observed among the Arenaceous and Carbonatic soils, for which the range of the measured values is larger than those estimated; for Clayey soil, the average values of shear wave velocity for Variegated Clays (VC) are correspondigly higher than the Grey Bluish Clays (GBC), because of the higher overconsolidation of VC soils.

In order to provide a quantitative validation in $V_{S,30}$ estimation, Figure 3.32 presents the histogram of the logarithm of the ratio between the measured value and the corresponding value obtained from USGS maps. The results obtained from this analysis are compared in Table 3.15 with Wald & Allen (2007) and Lemoine et al. (2012). It shows, for this case study, a bigger mean error (μ) but a lesser dispersion (σ) than the other studies.

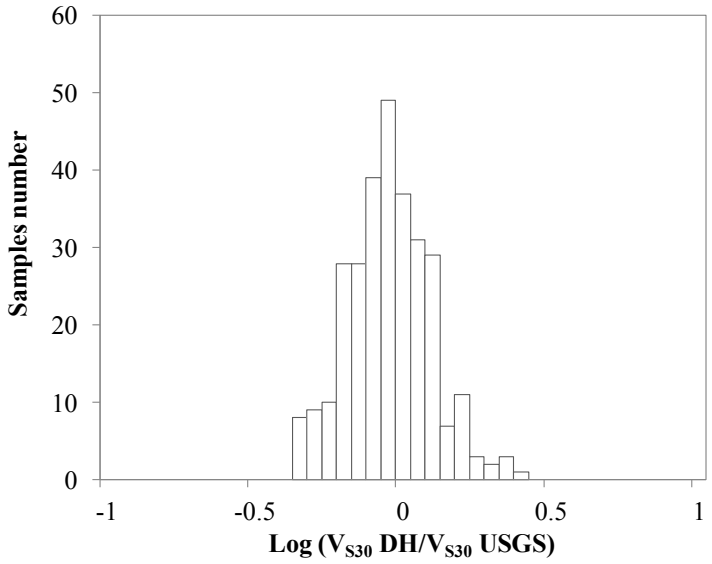

Figure 3.32. Logarithmic difference of measured VS30 and estimated by U.S.G.S.

Table 3.15 Statistical parameters of error slope-based estimation

Reference study	μ	σ	N
California (Wald & Allen, 2007)	-0.02	0.15	767
Italy (Wald & Allen, 2007)	0.00	0.19	43
Med. Europe (Lemoine et al. 2012)	-0.02	0.22	702
Molise Region (This study)	-0.07	0.14	296

Similar comparison has been carried out in terms of EC8 ground type. Following the identification of ground types specified by Eurocode 8, the site class has been assigned for each in situ DH investigation; the number of data samples, belonging to each seismic site class, is plotted in the histogram in Figure 3.33.

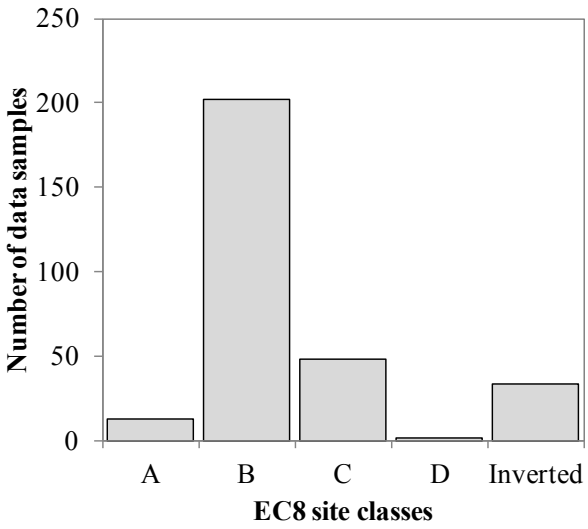

Figure 3.33. Number of data samples per each EC8 site class

In most of the cases, the assigned class is B; a consistent amount of data is also relevant to C class, few data are in A class, also because no test was performed in rock sites. Finally, only one data is relative to D class, no E class was found and many V_S profile presented inversions of velocities with depth. The latter were not considered for this study.

Following Lemoine et al. (2012), in Table 3.16 and Figure 3.34a, a correlation matrix is presented; the percentage of site correctly classified and/or misclassified is shown.

Table 3.16. EC8 Class Correlation matrix: Slope-based estimation from USGS vs. measured V_{S30} from DH investigations

		Slope-based USGS			
	(%)	A	B	C	D
Measured DH	A	**0**	4.4	0	0
	B	0	**76**	1.3	0
	C	0	15.5	**2.3**	0
	D	0	0.3	0	**0**

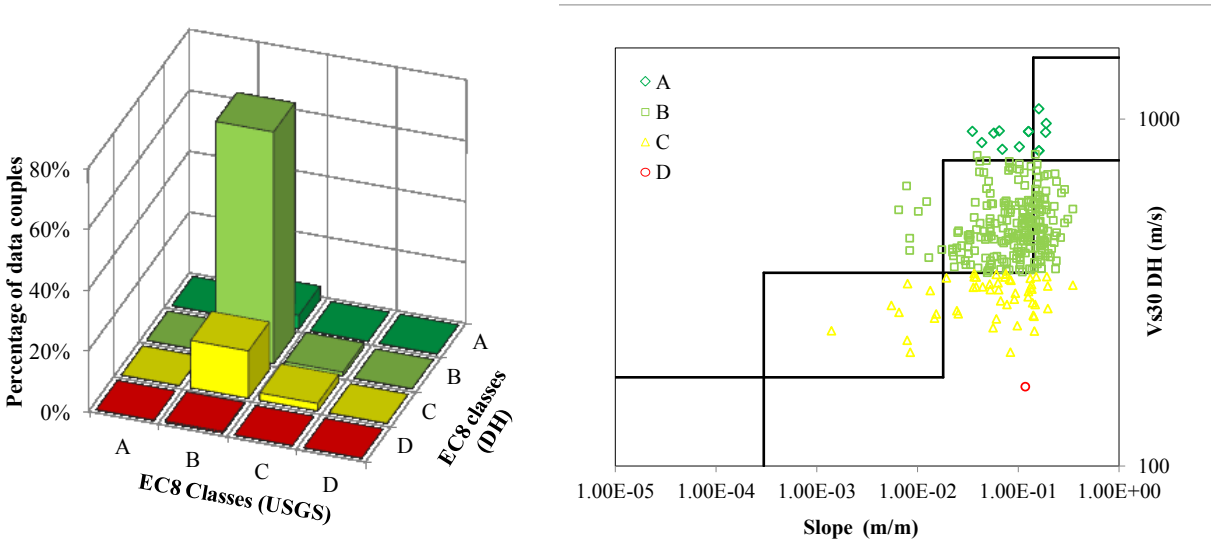

(a) (b)

Figure 3.34*; *a) histogram of correlation matrix between predicted and measured EC8 classes; ***b)*** experimental V_{S30} values (m/s) plotted vs. slope (m/m).

In Figure 3.34b, the measured V_{S30} (m/s) in Molise has been plotted against the topographic slope obtained through ArcGis 9.3 "slope tool" on a DEM 200 x 200 m cell. Furthermore, the same Figure also displays the limit values of V_{S30} and slope, which are consistent to Wald & Allen (2007) method of Table 3.13 for Active Tectonics regions.

The 76% of V_{S30} values are adequately estimated by U.S.G.S. method and correctly attributed to B class. In the 15.5% of the cases, the C class is wrongly assigned to B class, underestimating the soil amplification. The A and D class are, instead, completely mistreated. These

inconsistencies in class attribution occur because most of the slope values of the measured data fall into the range of B class, according to Table 3.16 (Figure 3.34b).

In order to obtain a better fit between predicted and observed data, in the next section the reliability of a geology-based approach has been investigated.

3.3.2 SURFACE GEOLOGY PROXY APPROACH

Italian Institute of Geophysics and Volcanology (I.N.G.V.) fulfills the similar role of U.S.G.S. in the implementation of the ShakeMaps in Italy. For this purpose, Michelini et al. (2008) considered a site classification map, based only on a rough geotechnical division in three soil classes: a) rock: class A (V_{s30} 1000 m/s); b) stiff soil: class B (V_{s30} 700 m/s); c) soft soil: class C (V_{s30} 350 m/s). Afterwards, this approach was enhanced in order to better suit EC8 and Italian Building Codes provisions (NTC 2008). The updated map is composed of five site classes (A, B, C, D, E), that were identified following lithological and age criteria. The identified classes are characterized by the following values of V_{s30}:

A) 1000 m/s;

B) 600 m/s;

C) 300 m/s;

D) 150 m/s;

E) 250 m/s, with soil layer thickness lower than 20 m.

Adopting the INGV V_{S30} map, the distribution of the estimated error, computed with the same procedure used by USGS (Figure 3.32), is shown in Figure 3.35.

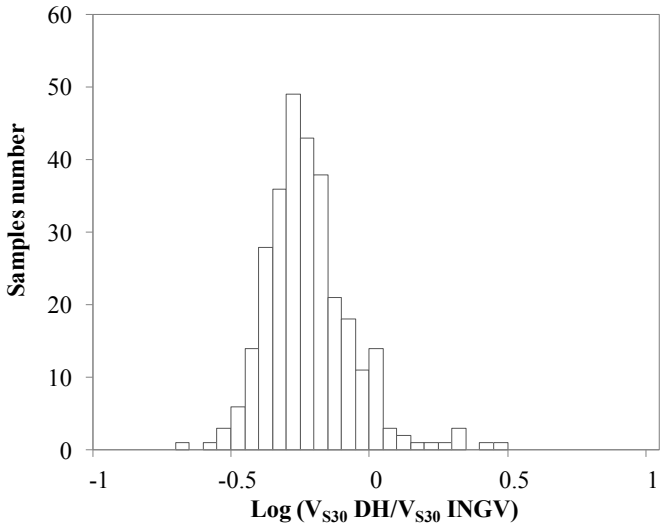

Figure 3.35. Logarithmic difference of measured V_{S30} and estimated by I.N.G.V.

In Table 3.17, the bias μ and the standard deviation σ of the distribution of Figure 3.35 has been given. The $V_{S,30}$ maps based on geological classification were also used by Wald & Allen (2007) to validate the slope-based method, with very good results for California, in which the same authors mark the striking agreement between material stiffness and topographic slope. Conversely, the same comparison between the italian slope-based map with the geology-based map by Michelini et al. (2008) showed a higher bias value (Table 3.17).

Table 3.17. Statistical parameters of error on geology-based estimation

Reference study	μ	σ	N
California (Wald & Allen, 2007)	-0.05	0.16	767
Italy (Wald & Allen, 2007)	-0.18	0.16	43
Molise Region (This study)	-0.26	0.15	296

3.3.3 UPDATED GEOLOGY-BASED CLASSIFICATION

On the basis of geological classification of Table 3.14, the $V_{S,30}$ data population for each Complex has been statistically treated. In Figure 3.36, the first, second (median) and third

quartile values of the V_{S30} distribution has been showed in a box plot. Moreover, the adjacent upper - lower range and the outliers values are given. In order to show the limits of the EC8 classes, a grid was drawn in the graph.

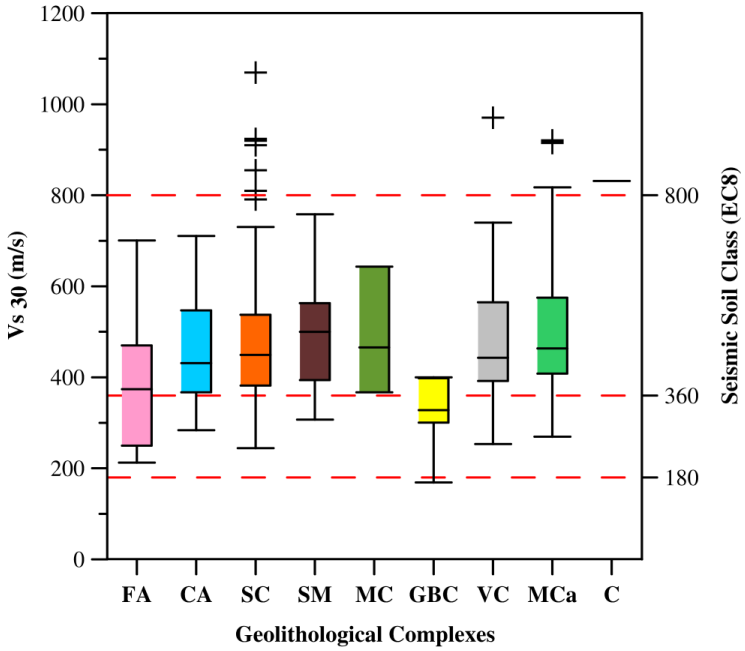

Figure 3.36. Box plot for DH V_{S30} values of the geolithological complexes as listed in Table 3.14.

Most of the median values fall in the range of class B, except the case of GBA Complex, which clearly belongs to C class. However, the min/max range of each class in some cases is very large (SC and MCa) and the value of VS30 varies from Class A to Class C. In other significant cases, the data population is very few (GBC and MC) and the values of extreme quartiles and adjacent range limits coincide. In the case of Carbonate unit (C), only one data sample is available.

Simply based on the average value of V_{S30}, the same graph of Figure 3.32 and 3.35 has been again plotted in Figure 3.37.

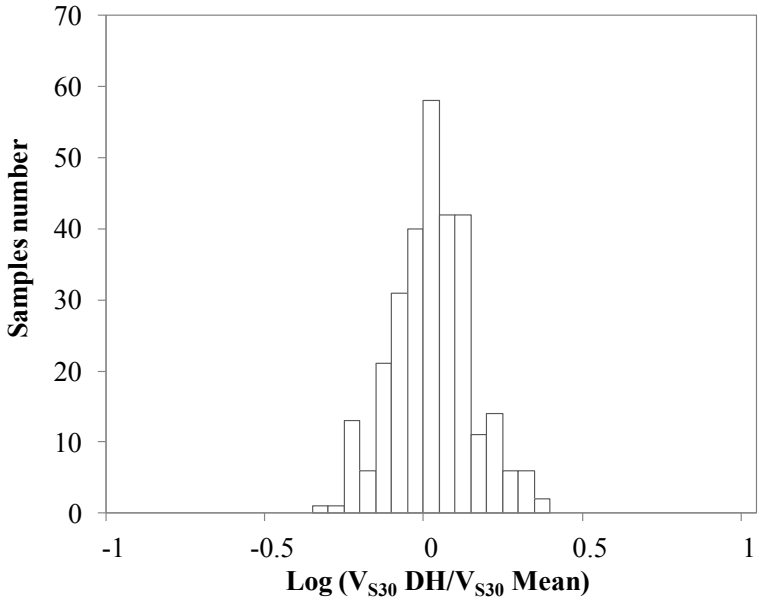

Figure 3.37. Logarithmic difference of measured VS30 and mean value for each complex

In this case, the bias μ is -0.014 and the standard deviation σ is about 0.12; as expected, the statistical parameters are the lowest compared to above discussed approaches. In order to correctly assign the soil amplification class to each geological complex, the main statistical moments were evaluated and summarized in Table 3.18. For each group, the amount of data, the average value of $V_{S,30}$, the standard deviation and the first quartile were estimated.

Table 3.18. Statistical parameters of the selected geologic complexes for the purpose of EC8 soil classification.

ID	N° samples	μ (m/s)	σ	1st Quartile (m/s)	EC8 class assignment
LD	-	-	-		D
CA	15	442.5	124	367	B
FA	18	385	130	272.5	C
GBC	8	325.8	79	310	C
SC	62	498.2	191	384	B
SM	52	492.6	113	394	B
MC	4	485.5	115	433	B
MCa	103	502.5	144	409	B
VC	31	482	152	392	B
C	1	-	-		A
	294				

Accordingly to Figure 3.36, most of the identified complexes fall into EC8 B class. Despite of this evidence, the EC8 class assignment was carried out adopting the 1st quartile of the data distribution, for safety advantage criterion. The Carbonate Unit (C), in which one only Vs(z) profile is available, was considered A class, since it is made of rock and can be considered the outcropping seismic bedrock.

Another dataset analysis was carried out also for the DH profiles of shear wave velocity with depth, $V_S(z)$, which are plotted in Figure 3.38. For each geologic complex, all the $V_S(z)$ profiles have been plotted as a grey line; the average profile as a colored line. The V_{S30} value of the average profile has been also given in each graph.

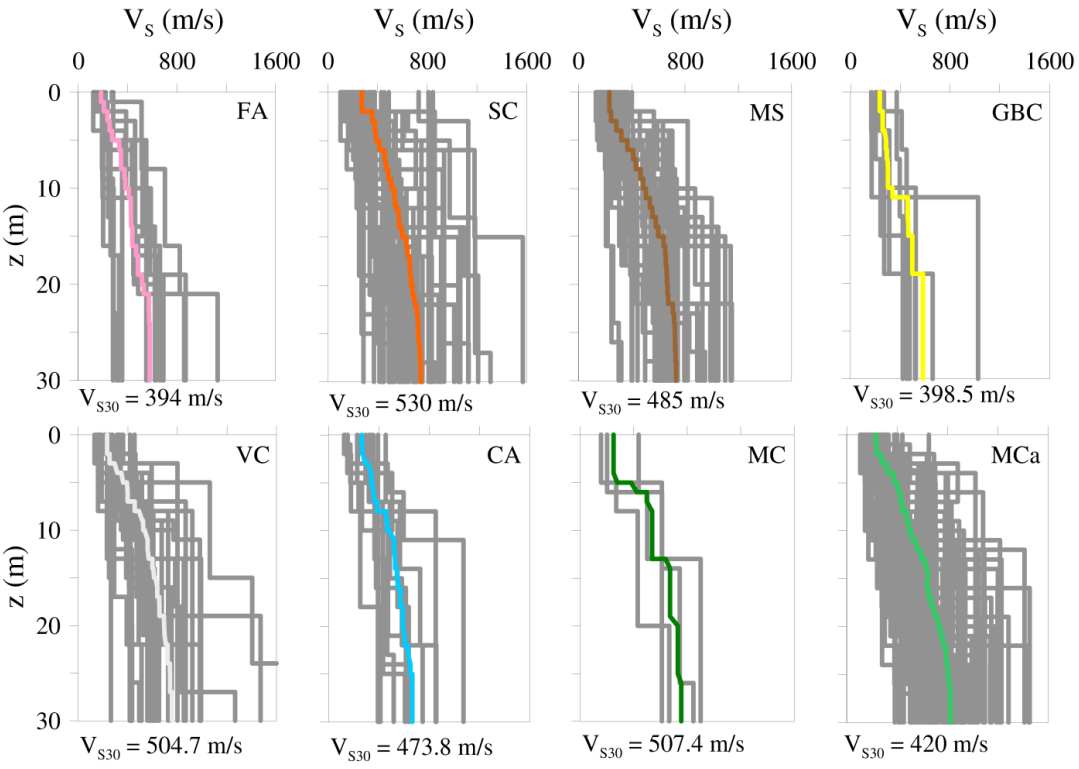

Figure 3.38. V_S (z) profiles for the identified geological complexes

The information, retrieved by Figure 3.38, is mainly consistent to Table 3.18 and Figure 3.36. A new map of soil amplification class has been finally given in Figure 3.39, according to assignments in Table 3.18. The DH data was also plotted and colored according to its soil class.

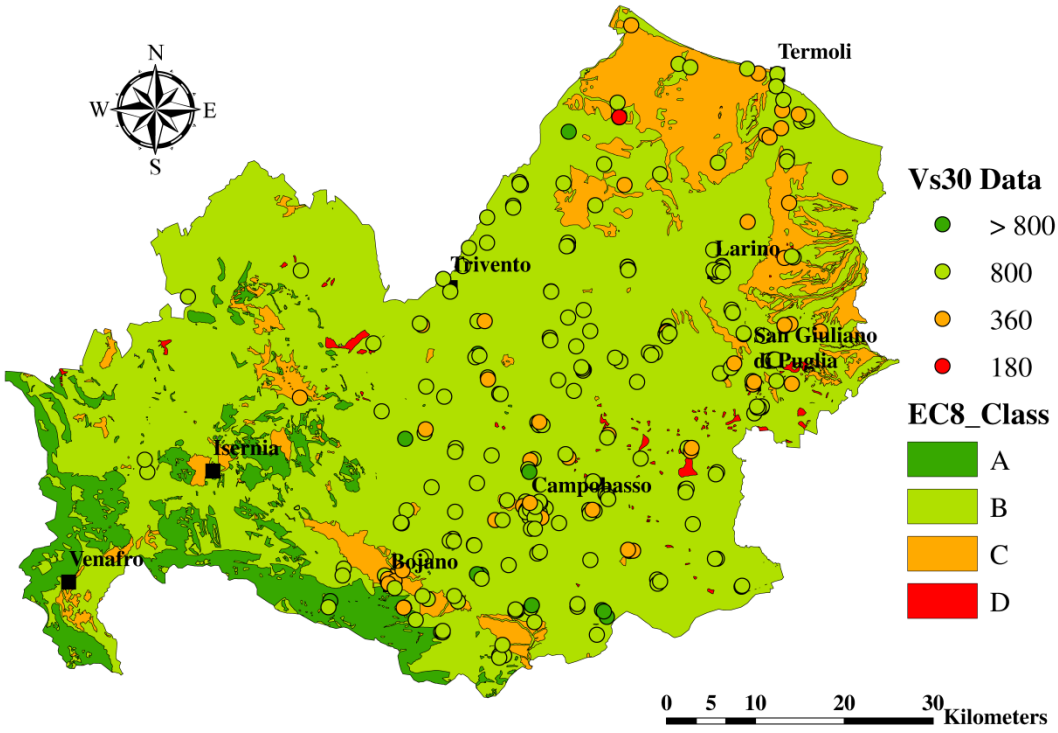

Figure 3.39. New proposed geology-based maps for EC8 classes in Molise Region

At this scale (1:100,000), it can be observed a reasonable agreement between measured DH data and the soil class assigned, can be observed. Finally, on the basis of the new map of EC8 class, the correlation matrix is again given in Table 3.19; furthermore, same data are plotted in Figure 3.40 as histogram graph.

Table 3.19. EC8 Class Correlation matrix: new geology-based map vs. measured V_{S30} from DH investigations

		Geology-based map			
	(%)	A	B	C	D
Measured	A	**0.3**	3.4	0	0
	B	0.3	**72.8**	4.8	0
	C	0	13.9	**3.7**	0
	D	0	0	0.3	**0**

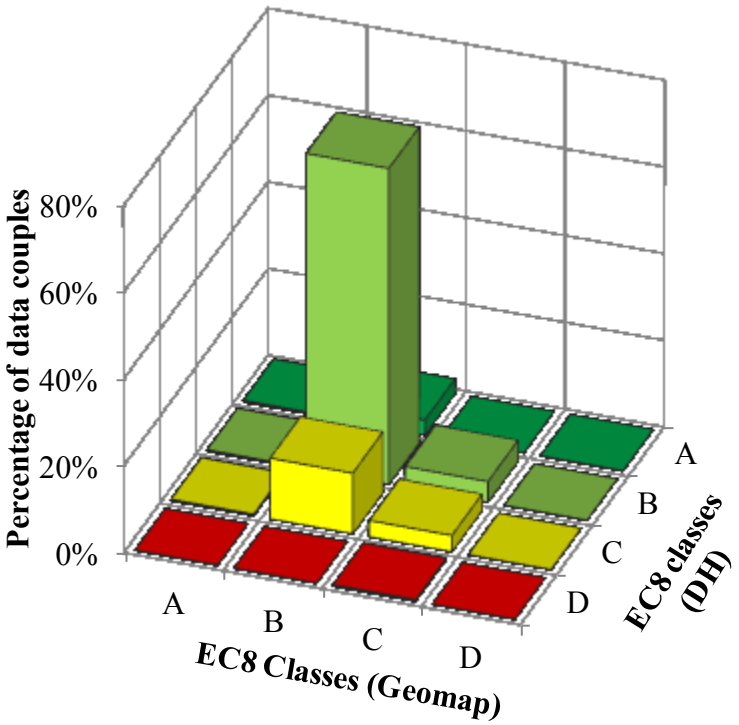

Figure 3.40. Histogram of correlation matrix between geology-based predicted and measured EC8 classes

A better comparison is also observed in terms of correlation matrix is observed: the geology-based map still correctly predicts most of the measured B class profiles. Moreover, the prediction for A and C class improves compared to slope-based map.

3.4 EMPIRICAL N_{SPT}-V_S CORRELATIONS

The correlation between the shear wave velocity, V_S, and the number of blows, N_{SPT}, obtained by the Standard Penetration Tests (SPT), was largely investigated in the last decades. A large number of Authors already proposed correlation for soils with different features on empirical bases. This is possible since, as the parameters correlated (Vs and N_{SPT}), have different mechanical meanings. The shear wave velocity V_S is a measure of the initial soil shear stiffness. The number of blows N_{SPT}, instead, is not directly a measurement of a soil property, but using empirical correlation could be related to soil strength parameters, both for cohesive soil (undrained shear strength s_u) and granular materials (friction angle φ' and true cohesion c'). Hence, the two parameters V_S and N_{SPT} are representative of the soil behaviour far and close to the failure. It is commonly understand that for geomaterials initial stiffness and strength are dependent by the same intrinsic and state parameter, including their lithological nature and void ratio, effective confining stress and stress-history.

Other relevant aspects related to the significance of these empirical formulations are listed below:

1. according to the standard for the execution of the SPT, N_{SPT} is the total number of blows needed to obtain a sample tube penetration of the last 30 cm out of the total 45 cm in each test step. The penetration of the sampler is obtained from the hammering of a 63.5 kg weight form a constant free falling height (76 cm) onto an anvil mounted on top of the drill rods. Despite of this standardization of the test, the results were influenced by some features of the equipment and the procedures to perform the in situ test, as diameter of the borehole, the length of the shafts and the energy content of the hammer. A way to avoid these false responses of the test is to correct, and eventually normalize; the number of blows according to the procedures mainly established for liquefaction analyses procedures (see for instance, Idriss & Boulanger, 2004). Nevertheless, as it

is found in the literature, the use of the corrected number of blows almost never represents an improvement in terms of best-fitting of experimental data (Sykora, 1987);

2. N_{SPT} blowcount could give a false response under given geotechnical conditions. In saturated silty sands, the dynamic loading conditions induce instantaneous undrained behaviour, giving a higher value of the blow number for empirical correlations. Usually N_{SPT} could be corrected according to Terzaghi & Peck (1948);

3. the N_{SPT}-V_S correlations were generally site dependent: the empirical correlations should be obtained in a homogeneous geologic context and used only in that considered environment. This is why the most recent correlations were obtained for specific and limited areas.

In turn, Anbazhagan et al. (2012) tried to correlate the results of SPT test with G_0 in any regional context, performing a combination of the database employed to obtain the previous published correlation, using data mostly obtained in Japan (as for example those by Ohta et al., 1972).

An intermediate solution between these two outermost approaches could be the setting of empirical N_{SP}T-Vs correlation for specific geologic context in combination with the widening of the results to similar areas, in order to extend and validate the equations.

3.4.1 EMPIRICAL N_{SPT}-V_S CORRELATIONS BY GRAIN SIZE APPROACH

Based on the outcomes of the literature review reported in Fabbrocino et al. (2014), the first step of the analysis consisted of the superposition of the available dataset and particularly of the N_{SPT}–V_S pairs with the most common and applicable available empirical correlation laws for "all soils" (Ohta & Goto, 1978; Yokota et al., 1991; Kalteziotis et al., 1992; Iyisan, 1996; Jafari et al., 1997; Hasançebi & Ulusay, 2007; Dikmen, 2009; Akin et al., 2010), as shown in Figure 3.41. It

is clear the large dispersion of the experimental data and the inability of any earlier correlation laws to characterize the examined terrain.

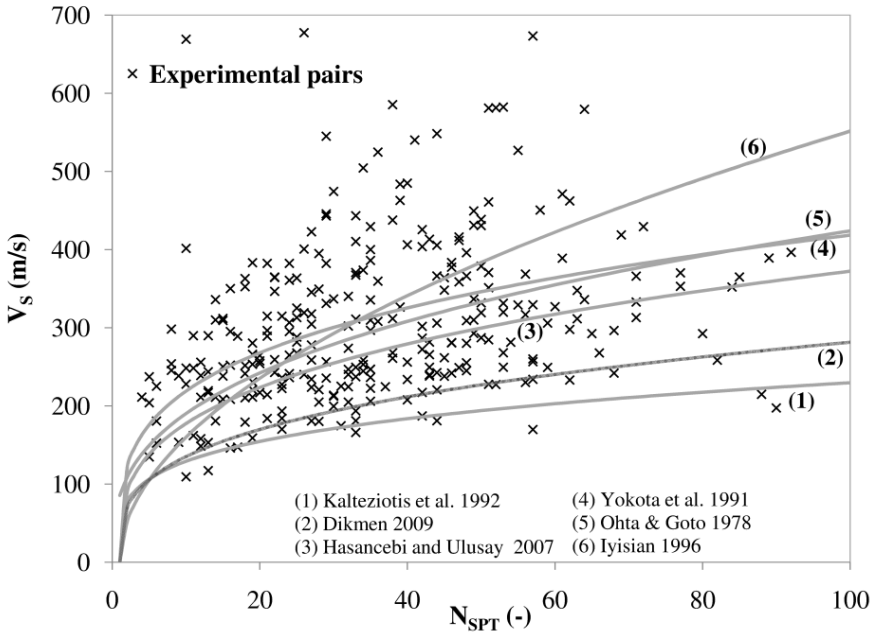

Figure 3.41. Comparison between experimental values and the most common empirical N_{SPT}-V_S correlations for "all soils".

Several N_{SPT}-V_S regression equations, available in the technical literature, were, instead, referred to the different "soil types". Hence, the integrated borehole experimental data were analysed in order to better define the soil grain size classes in the dataset. The available stratigraphic log descriptions and laboratory findings were compared in order to validate the results.

In this way, the database was divided according to the main component of the grading curves: the larger amount of data (58%) was relative to clayey soil samples, followed by silty (23%) and sandy ones (11%). A very few pairs of measures (8%) referred to gravelly soils, and so they were neglected. Then, for each grain size class the correlations were developed for uncorrected N_{SPT} blowcount.

As shown in Figure 3.42, statistical correlations, between uncorrected number of blows N_{SPT} and relating V_S measurements, and their coefficients of determination, R^2, were evaluated by a

simple power law, for sandy (Figure 3.42a), silty (Figure 3.42b) and clayey soils (Figure 3.42c) respectively. Despite the Standard Penetration Test is more appropriate for coarse-graded soil rather than for fine-graded material, it seems that there is no correlation between N_{SPT} and V_S for the sandy materials, while two relationships can be derived for silty and clayey soils. This is probably due to the limited amount of sand data available for the empirical correlation (32 pairs).

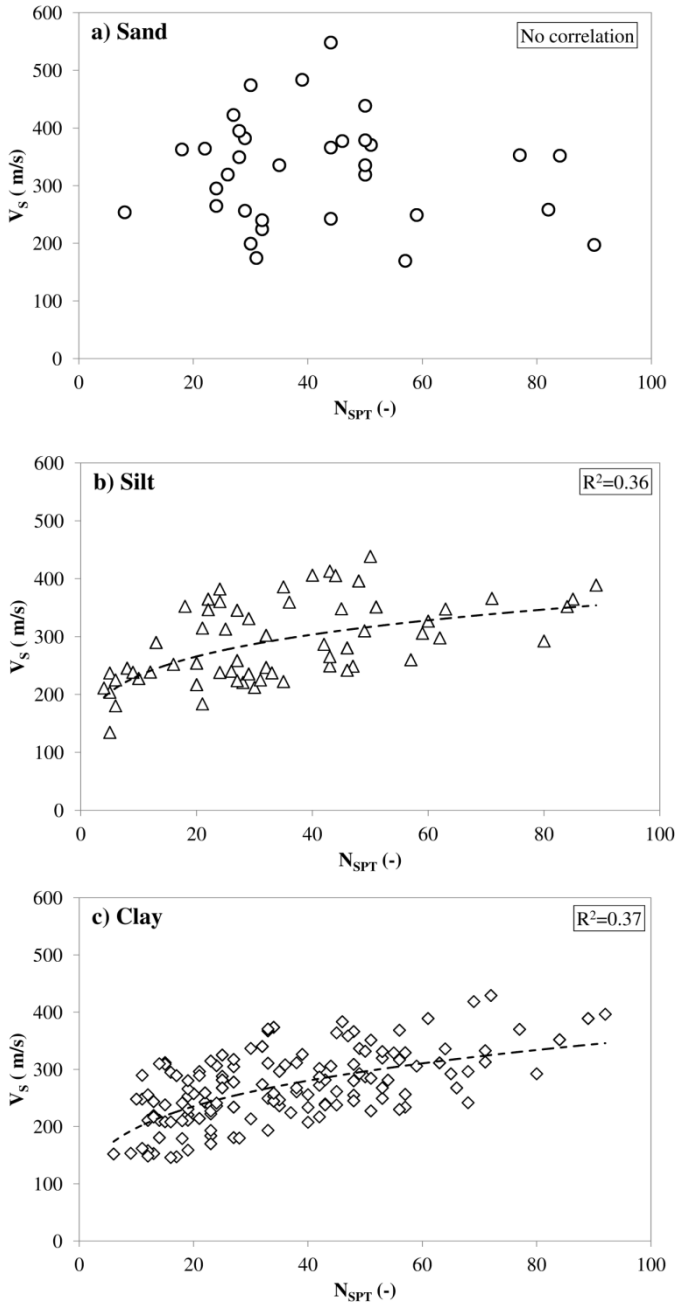

Figure 3.42 V_s – N_{SPT} empirical correlations based on grain size approach: ***a)*** sandy, ***b)*** silty and ***c)*** clayey soils.

For medium and fine graded soils the shear wave velocity (m/s) could be obtained from the following relationship:

$$V_S = 149.3 N_{SPT}^{0.192} \qquad (R^2=0.362 - r=0.571) \qquad (3.3)$$

based on the non-linear regression of 62 V_S-N_{SPT} pairs. For clayey soils, the resulting relationship (178 pairs) is:

$$V_S = 110.5 N_{SPT}^{0.252} \qquad (R^2=0.369 - r=0.604) \qquad (3.4)$$

It is worth noting that a quite large dispersion of data is observed, and confirmed by low values of R^2; thus these analytical functions are not representative of the data best fitting. This circumstance suggests that the soil type have only a slight effect on the investigated correlations.

Hence, this approach seems to be not reliable to characterize the structurally complex formations of the Molise, where, many complex geological and morphological factors control and mark the mechanical behaviour of soils.

With reference to the features of the geolithological complexes previously described, in the following sections a composite analysis of the same correlation data is proposed.

3.4.2 EMPIRICAL N_{SPT}-V_S CORRELATIONS ACCORDING TO A LITHOSTRATIGRAPHIC APPROACH

As already explained, the same geolithological complex can be characterized by a high variability of geotechnical properties as well as the grain size classification of soils; hence in order to improve the empirical correlations between N_{SPT} and V_S an important role may be rather ascribed to the lithostratigraphic features of the examined geolithological complexes.

Particular attention was paid to local conditions of outcropping sedimentary deposits, such as weathering processes, tectonic setting, hydrodynamic models, human impact, which can modify intrinsic properties of recognized layers and influence the geotechnical characteristics of the same horizon. For instance, the integrated boreholes derived from the investigations in the Mafalda, Santa Croce di Magliano and Casacalenda villages, were correlated with the succession of the Faeto Flysch (Figure 3.43), i.e. a formation of the Marly Carbonate Complex (MCa).

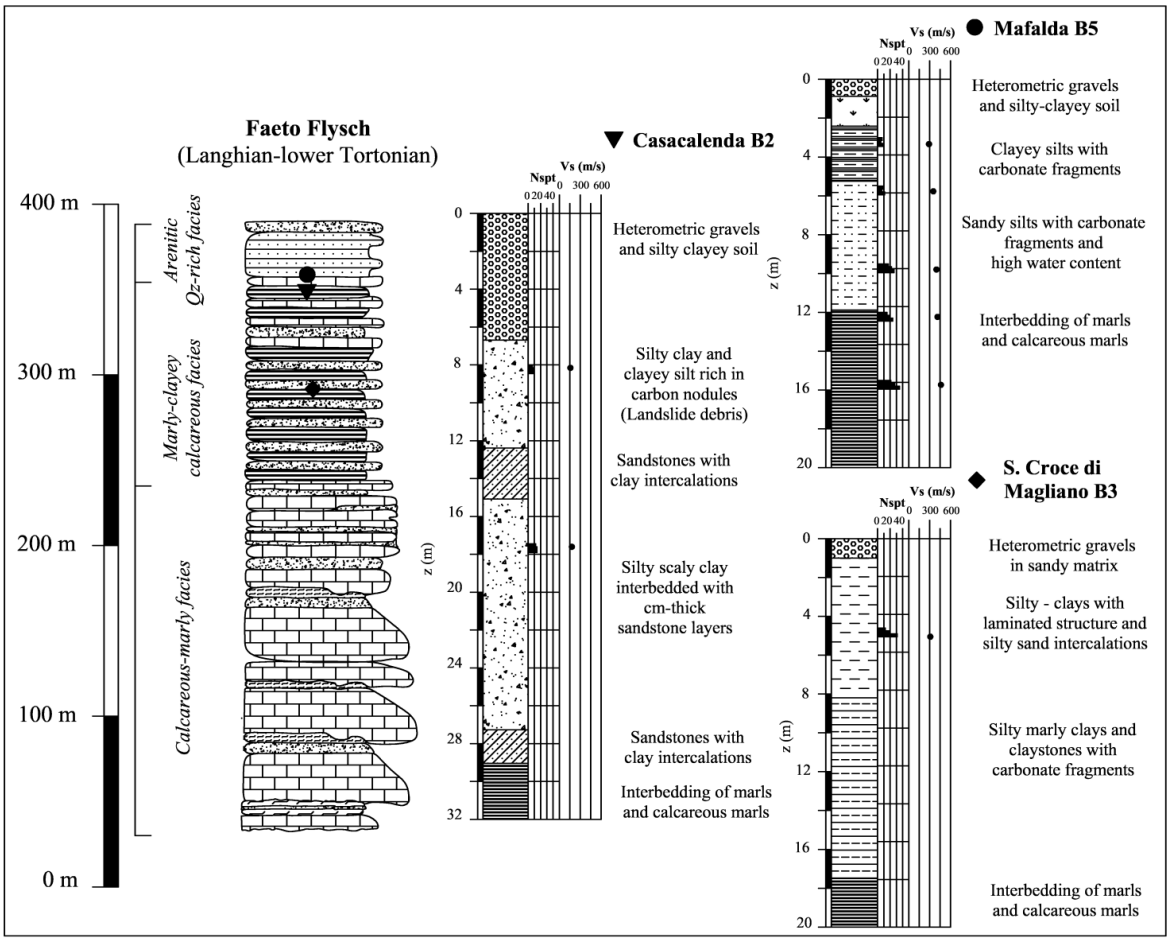

Figure 3.43. Correlation between integrated borehole data and lithofacies. An example for the Faeto Flysch, MCa Complex.

The Faeto Flysch consists of a calcareous marly turbiditic succession. The lower part was characterized by a calcareous-marly facies; the upper part acquired a marly-clayey-calcareous facies. The top layer, on the contrary, was characterized by an arenitic Qz-rich *facies* (i.e. Pertusati & Buonanno, 2009).

All experimental N_{SPT}-V_S data pairs shown in Figure 3.43 were correlated to the upper member of the Faeto Flysch formation, but the data from Mafalda village B5 described the arenitic Qz-rich turbidites interbedded with massive marls and marly limestones. The data of Santa Croce di Magliano B3 and Casacalenda B2 identified the marly-clayey-calcareous facies, composed of regular alternations of massive marls, marly limestones, calcilutites and white and grey clays. In particular the corresponding N_{SPT}-V_S value pairs were evaluated for the clayey layers. The location of the Casacalenda investigation in displaced materials of landslide is also noteworthy.

This approach pointed out that the evident dispersion of experimental N_{SPT}-V_S data pairs recorded in Figure 3.41 could be reasonably related to the different lithofacies observed in the study area.

In particular, three main lithofacies could be distinguished and related to the geotechnical behaviour of the examined structurally complex formations in view of the optimization of the empirical N_{SPT}-V_S correlation formulas (Figure 3.45):

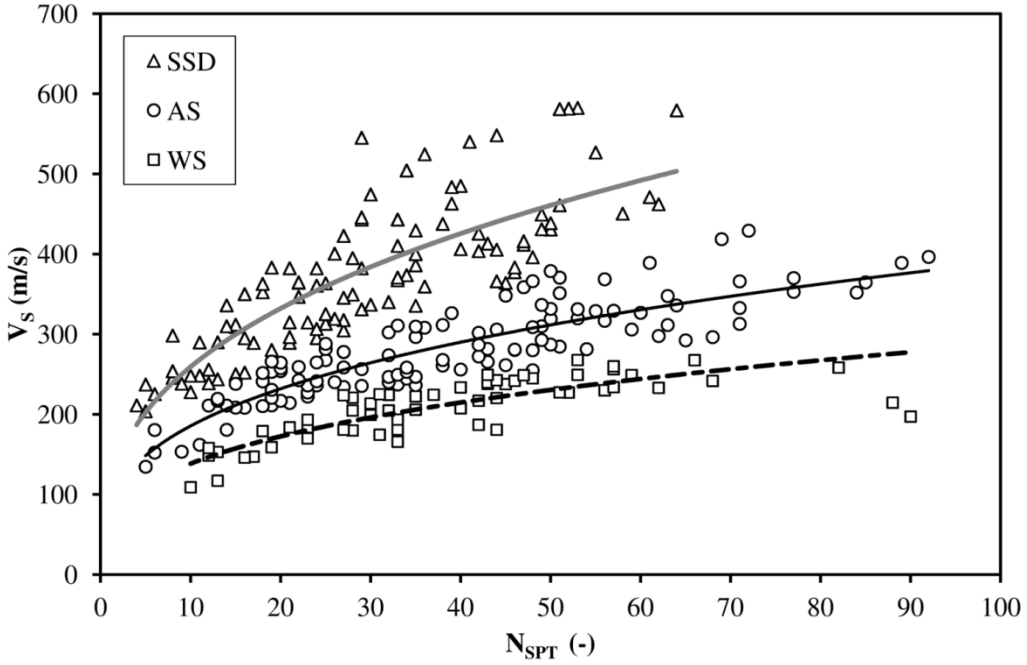

Figure 3.45. Novel V_s – N_{SPT} empirical correlations based on lithostratigraphic approach.

- Structured soils deposit (SSD): this facies is typical of complexes and formations (or only of some horizons of them) in which the rock interebeddings are not negligible and highly affect the soil behaviour (Figure 3.43 – Mafalda B5);
- All soils (AS): this facies involves complexes and formations (or only some horizons of them) in which the argillaceous fraction is dominant. Its behaviour could be considered similar to the sensu-strictu soils, because it encompasses the frictional and cohesive materials (Figure 3.43 – S. Croce di Magliano B3);
- Weathered soils (WS): this facies includes the same complexes and formations of the so-called "All soils", but the geotechnical properties are affected by both natural and anthropic factors (Figure 3.43 – Casacalenda B2). This group is mostly composed of very shallow measurements, composed by eluvium, colluvium or talus deposits.

As a result, a non-linear regression analysis was able to define the three following novel empirical functions between the NSPT and Vs, controlled by the lithostratigraphic features of outcropping geological formations (Figure 3.45):

SSD) $V_S = 104.55\ N_{SPT}^{0.385}$ (R^2=0.681 – r=0.825) (3.5)

AS) $V_S = 90.35\ N_{SPT}^{0.317}$ (R^2=0.748 – r=0.865) (3.6)

WS) $V_S = 78.59\ N_{SPT}^{0.272}$ (R^2=0.607 – r 0.774) (3.7)

In all the cases, the developed analytical functions represent a better fit of data, as marked by the higher correlation coefficients.

Some remarks can be proposed based on the comparison between the updated and the available empirical correlation formulas (Figure 3.46):

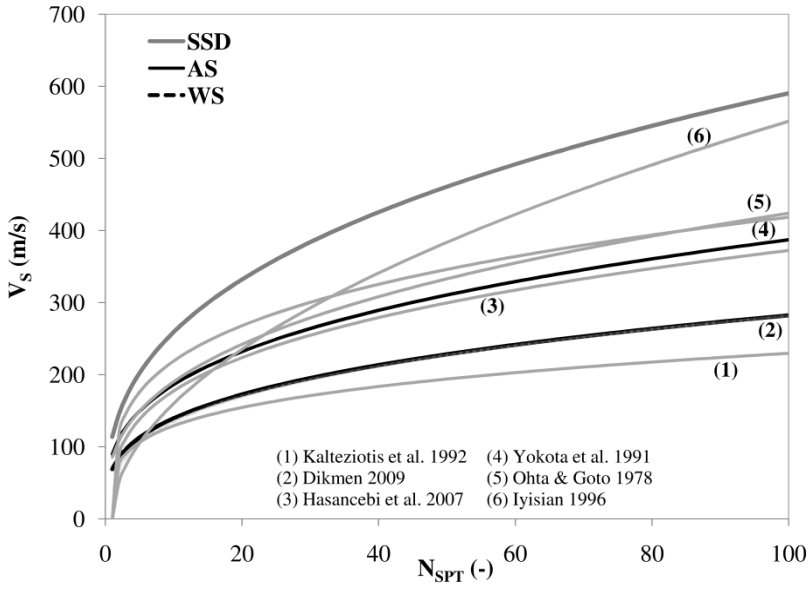

Figure 3.46. Comparison between the lithostratigraphic-based empirical relationships and the existing ones.

The SSD relationship shows higher values of V_S compared to other existing expressions; this is probably due to the prominent contribute of the rock component of the deposit.

For the case of AS, the empirical correlation is quite similar to Otha & Goto (1978) relationship, because the soils investigated by the Authors are mainly composed of clays and silty clays successions, with sandy intercalations.

The correlation for WS is similar to the expression of Dikmen (2009); this empirical evidence was probably due to similar lithofacies in which the analyses were done.

In order to validate the results, a statistical analysis of the datasets was carried out and discussed in the next section.

3.4.3 STATISTICAL VALIDATION

A simple statistical treatment of data was carried out to assess the reliability and significance of the updated relationships.

The lithostratigraphic analysis of geolithological complexes documented in the Molise provided an improvement of the investigated mathematical relations. It was marked by higher values of correlation coefficients, such as already mentioned in the previous section.

In order to check the capability of the three novel empirical correlations for shear wave velocity prediction, the relative percentage error, Er was evaluated as follows:

$$E_r = 100 \cdot \frac{V_{s,c} - V_{s,m}}{V_{s,c}} \qquad (3.8)$$

where Vs,c is the shear wave velocity calculated by eqs. (5) to (7) and Vs,m is the experimental measured value. As shown in Figure 3.47, eq. (5) for SSD provides about 90% of the predicted values within a 20% error margin; eq. (6) for AS gives about 97% of predicted values within a 19% error margin; finally, eq. (7) for WS leads to about 90% of values predicted within a 20% error margin. It is thus confirmed that the three proposed correlations offer a good estimation of the investigated parameter.

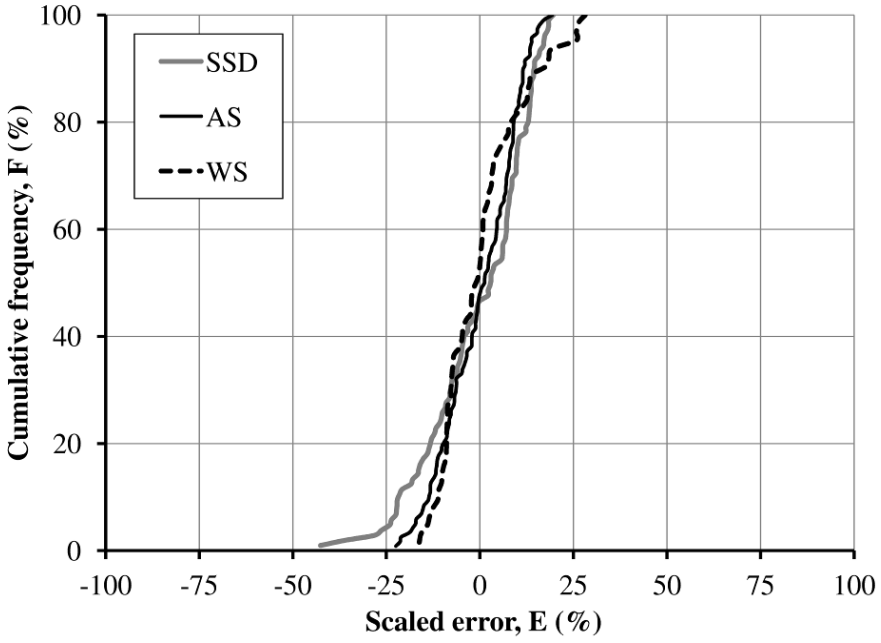

Figure 3.47. Scaled relative errors of V_S for the novel correlations based on the lithostratigraphic approach.

The comparison between Vs,c and Vs,m derived from the normalized consistency ratio C_d strengthen such remark (Figure 3.48). The normalized consistency ratio was evaluated as:

$$C_d = \frac{V_{s,c} - V_{s,m}}{N_{SPT}} \tag{3.9}$$

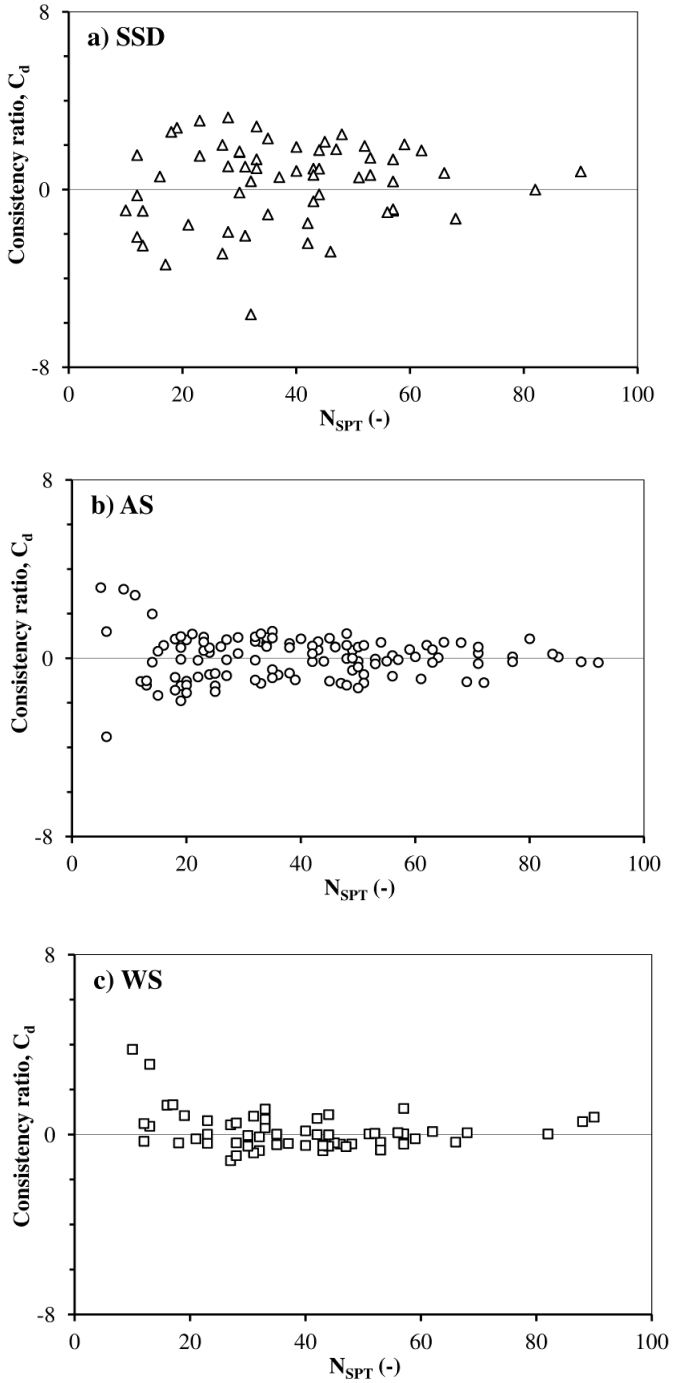

Figure 3.48. Normalized consistency ratio C_d for ***(a)*** Structured Soil Deposit (SSD), ***(b)*** All Soils (AS) and ***(c)*** Weathered Soils (WS).

A reliable estimation of V_S values is observed in the case of the AS and WS correlations: the Cd values are generally close to zero, except for small N_{SPT} values (generally lower than 15).

However, the lower values were measured under particular local conditions, such as weathered or fully saturated soils, which affect the results. As expected, a larger variability was observed for SSD, even if the predictive capability of the relative mathematical relation may be considered reliable.

It is worth underlying that the proposed approach and the related results can be justify also thinking at the experimental procedures employed to obtain the two values N_{SPT} and V_S that are here correlated. The first data is a local measurement that is well-affected by the site specific soil characteristics where the measurement is performed; the second is a global information. This means that the SPT blowcount in structured soil deposits usually detect the strength of the weaker part of the material, as the testing device is not able to penetrate into the lithoid part of the soil, and, as usually, N_{SPT} larger than 100 is not considered. On the other hand, the shear wave velocity, even obtained at a given depth, is a more global measurement accounting for both the stiffer and the softer part of the soil formation. Then, the SSD correlation law is located in the upper part of the V_S-N_{SPT} plane. Conversely, the WS correlation lies in the lower part of the plane, because the local SPT blowcount is mostly influenced by the remoulded and the fully saturated nature of the soil belonging to the formation.

Even if only a sector of the Apennine chain is concerned, the proposed correlation could reasonably be applied in different sector of the same chain, or in similar geological terrain, whenever the uncertainties and the features of this simplified tool fit the aim of the analysis and the scale of the engineering problem of interest.

4. GRADE II SEISMIC SLOPE STABILITY ASSESSMENT

4.1 METHODOLOGICAL APPROACH

The prediction of the order of magnitude of the slope displacements induced by earthquakes is a relevant tool, which can be adopted for the assessment of the hazard due to seismic-triggered landslides at regional scale and in designing slopes to withstand earthquake shaking.

As reported in the chapter I, the seismic performance of a slope can be evaluated in several ways. The simplest is pseudostatic analysis, in which an earthquake acceleration acting on the mass of a potential landslide is treated as a permanent static body force in a limit-equilibrium analysis, simply based on the calculation of a factor of safety (FS). Different earthquake accelerations are applied iteratively until the factor of safety is reduced to 1.0. This procedure is quite simple and requires no more information than is needed for an analysis in static conditions. The utility of pseudo-static analysis is thus limited, because it provides only a single numerical threshold above which "failure" is predicted. Conversely, 2D finite element modeling (FEM) permits to accurately assess slope deformation, but its implementation requires high quality and density data, which make the common use expensive and time-consuming.

Newmark (1965) proposed a method of analysis intermediate between the pseudostatic and FEM analysis. Newmark's method models a landslide as a rigid-plastic friction block having a known yield or critical acceleration (a_c), which is the acceleration required for overcoming frictional resistance and initiating sliding on an inclined plane (Figure 4.1). The analysis calculates the cumulative permanent displacement of the block as it is subjected to the effects of an earthquake acceleration time history.

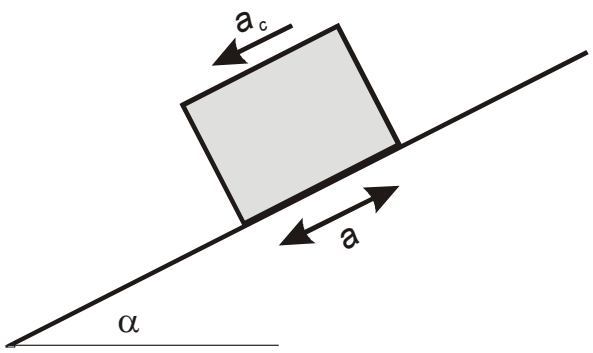

Figure 4.1. Sliding-block model, where ***α)*** is the slope from the horizontal, ***a_c)*** is the yield acceleration, ***a)*** is the earthquake acceleration. (after Jibson et al. 1998).

Newmark's method is relatively simple to apply and provides a quantitative prediction of the inertial landslide displacement that will result from a given level of earthquake shaking; the slope geometry and soil properties. The validity of its results permitted to implement this approach into Grade II of seismic microzonation of slopes at small scale, as reported in chapter I (§ 1.4.2).

The basic assumptions of this approach are the following:

- The landslide is treated as a rigid-plastic body, specifically, the mass does not deform internally and experiences no permanent displacement at accelerations below the critical (or yield) level; it deforms plastically along a discrete shear surface when the critical acceleration (a_c) is exceeded. Thus, the Newmark's method is best applied to coherent landslides such as translational block slides and rotational slumps.
- The static and dynamic shear strength of the soil is assumed to be the same, as the soil cyclic degradation is not accounted.
- The effects of dynamic pore pressure are also neglected.
- The critical acceleration does not depend on the strain and thus remains constant throughout the analysis.

- Upslope displacements are also prohibited.

4.1.1 THE YIELD ACCELERATION

The first step of the analysis is the evaluation of the critical acceleration (a_c) of the potential landslide. This parameter is considered representative of the seismic triggering susceptibility and it is expressed as:

$$a_c = (FS - 1)gsin\alpha \quad (4.1)$$

where

a_c is the critical acceleration in terms of g,

FS is the static factor of safety;

g is the gravity acceleration;

α is the slope angle.

Thus, determining the critical acceleration by this method requires the assessment of the stability performance in static condition (safety factor) and its geometrical features (slope angle).

4.1.2 LIMIT EQUILIBRIUM OF THE INFINITE SLOPE

In grade II studies, extended to a large territory, the factor of safety, FS, can be calculated with the limit equilibrium analysis of an infinite slope. In which the FS is expressed as a function of the soil shear strength as the ratio between the available shear (s) strength and the equilibrium shear stress (τ):

$$FS = \frac{s}{\tau} \quad (4.2)$$

In the infinite slope procedure, the slope is assumed to extend infinitely in all directions and sliding is assumed to occur along a plane parallel to the face of the slope. Because the slope is infinite, the stresses will be the same on any two planes that are perpendicular to the slope, such as the planes A-A and B-B in Figure 4.2. Equilibrium equations are derived by considering a rectangular block like that shown in Figure 4.2.

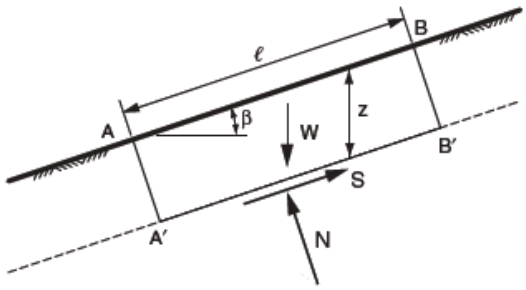

Figure 4.2. Infinite slope and plane slip surface (after Duncan & Wright, 2005)

For an infinite slope, the forces on the two ends of the block will be identical in magnitude, opposite in direction, and collinear. Thus, the forces on the ends of the block exactly balance each other and can be ignored in the equilibrium equations. The sum of forces in directions perpendicular and parallel to the slip plane gives the following expressions for the shear force, S, and normal force, N, on the plane:

$$S = W sin\beta \tag{4.3}$$

$$N = W cos\beta \tag{4.4}$$

where β is the angle of inclination of the slope and slip plane, measured from the horizontal, and W is the weight of the block. For a block of unit thickness in the direction perpendicular to the plane of the cross section in Figure 4.2, the weight is expressed as:

$$W = \gamma l z cos\beta \tag{4.5}$$

where γ is the total unit weight of the soil, l the distance between the two ends of the block, measured parallel to the slope, and z the vertical depth to the slip plane. The shear and normal

stresses on the shear plane are constant for an infinite slope and are obtained by substituting the Eq. (4.5) into Eqs. (4.3-4.4) and dividing by the area of the plane (l*1), to give:

$$\tau = \gamma z cos\beta sin\beta \tag{4.6}$$

$$\sigma = \gamma z cos^2\beta \tag{4.7}$$

Substituting these expressions for the stresses into Eq. (4.2) and considering the shear strength (s) expressed by the Mohr-Coulomb criterion, the factor of safety expression becomes:

$$FS = \frac{c' + (\gamma z cos^2\beta - u) tan\varphi'}{\gamma z cos\beta sin\beta} \tag{4.8}$$

where u is the pore water pressure contribution, which can be written as:

$$u = \gamma_w z_w = m\gamma_w z \tag{4.9}$$

where

$$m = \frac{z_w}{z} \tag{4.10}$$

being z_w is the height of the groundwater table above the slip surface.

Making the appropriate substitutions, the relationship of the factor of safety can be expressed as:

$$FS = \frac{c'}{\gamma z sin\beta} + \frac{tan\varphi'}{tan\beta} - \frac{m\gamma_w tan\varphi'}{\gamma tan\beta} \tag{4.11}$$

in which the first term accounts for the cohesion contribution, the second for the friction angle and the last is a reducing factor which is dependent on the position of the groundwater table.

4.1.3 THE SEISMIC INPUT

A very important aspect of conducting a Newmark analysis is selecting an appropriate input ground motion. Common design or hazard-assessment criteria identify two possible solutions. The first is a probabilistic approach, which considers a specified level of ground shaking, relative to the most likely earthquake of specified magnitude and location, mainly coming from the seismic disaggregation study; the second is to select deterministically a scenario earthquake, which usually is the strongest earthquake experienced by the analyzed site. In small scale

approaches (grade II), it is common practice to consider this second way and implement an historical earthquake through Shakemaps or with ground motion prediction equations (GMPEs). The choice of suitable GMPE for the estimation of the seismic parameters is also an important decision and should be carefully weighted, depending on the parameter of the seismic motion, the complexity of the formulation, but mainly, on the database on which it was calibrated. The latter, in fact, directly influences the reliability of the results. This choice is made even more complex due to the large amount of existing relationships, for instance Douglas (2004) gathers 165 relationships for the estimate of the peak ground acceleration (PGA) and 100 for the Response Spectra (S_a).

At European level, one of the most commonly adopted relationship was obtained by Ambraseys (1995) from a strong motion database of Europe, including the Italian events of Friuli (1976), the Nera Valley (1979), Irpinia (1980) and Gubbio (1984). The formal relationship is:

$$logY = C_1' + C_2 M + C_4 logr + C_A S_A + C_S S_s \tag{4.12}$$

$$r = \sqrt{d^2 + h_0^2} \tag{4.13}$$

where Y is PGA in g; C'_1 = -1.48 ,C_2 = 0.266, C_4 = -0.922, C_A = 0.117, C_S = 0.124, h_0 is the focal depth equal to 3.5, σ is the standard deviation of 0.25. S_A and S_S are correction parameters dependent on the class of subsoil and the velocity of shear wave (Vs). The lower bound of validity for this formulation is set at Ms= 4.

In Italy, the most widespread GMPE was derived by Sabetta & Pugliese (1996) from a database of 95 accelerograms of 17 Italian earthquakes with magnitude between 4.6 and 6.8:

$$logY = a + bM - \log\left(R^2 + h^2\right)^{1/2} + eS \tag{4.14}$$

where Y is PGA in g, a = -1562, b = 0.306, e = 0.169, h is the focal depth of 5.8, σ is the standard deviation of 0.173 and S is a correction factor for site condition.

The latter was substituted by the most recent GMPE relationship shown in Eq. (4.15) proposed by Bindi et al. (2011), based on a dataset, including the last strong motion events occurred in Italy, i.e. Umbria-Marche (1997), Molise (2002) and L'Aquila (2009):

$$logY = e_1 + F_D(R, M) + F_M(M) + F_S + F_{sof} \quad (4.15)$$

where: Y is the PGA in cm/s^2; e1 is a constant, R is the Joyner-Boore distance, M is the moment magnitude, F_S is the correction for site conditions; F_{SOF} is the correction for the style of faulting. Furthermore, the value of PGA at bedrock accounted in Newmark analysis could be corrected for different site conditions, in terms of stratigraphic (S_S) and topographic amplification (S_T) factors. Following several codes such as the Italian building code NTC (2008), S_S is dependent on the PGA at bedrock and subsoil classification.

The selected seismic input modified to account for stratigraphic and topographic amplifications can be adopted for the calculation of the Newmark displacements. The analysis can be carried out by a rigorous approach or by a simplified dynamic analysis, which are discussed in the next section.

4.1.4 CALCULATING NEWMARK DISPLACEMENT-RIGOROUS ANALYSIS

Once the critical acceleration (a_c) of the landslide has been determined and the acceleration-time histories are selected, the Newmark displacements can be calculated. They are obtained by double integrating those parts of the strong-motion record that lie above the critical acceleration. In Figure 4.3a a strong-motion record is superimposed to a hypothetical a_c of 0.2 g. Before time X, accelerations are less than a_c, and no displacement occurs. After time X, those parts of the strong-motion record lying above a_c are integrated over time to derive a velocity profile of the block. Integration begins at point X (Figure 4.3a - 4.3b), and the velocity increases to point Y. Past point Y, the ground acceleration drops below a_c, but the block continues to move because of

its inertia. Friction and ground motion in the opposite direction cause the block to decelerate until it stops at point Z. All pulses of ground motion exceeding a_c are integrated to yield a velocity profile (Figure 4.3b), which, in turn, is integrated to yield a cumulative displacement profile of the landslide block (Figure 4.3c).

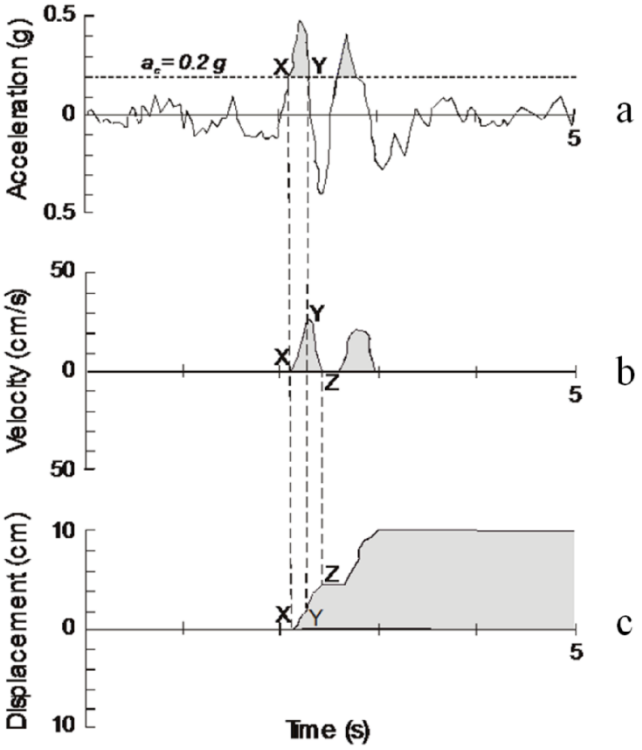

Figure 4.3. Illustration of the Newmark algorithm, modified from Wilson & Keefer (1983). ***a)***, earthquake acceleration-time history with critical acceleration (dashed line) of 0.2 g superimposed; ***b)***, velocity of the landslide versus time; ***c)*** displacement of landslide versus time.

4.1.5 CALCULATING NEWMARK DISPLACEMENT: SIMPLIFIED DYNAMIC ANALYSIS

The previous section described how to rigorously conduct a Newmark analysis, although this approach is straightforward for a single site, it is far more complex when the analysis requires the evaluation of the permanent displacements on a regional basis. In those cases, simplified

dynamic approaches for estimating Newmark displacements are more suitable and many researchers developed simple tools to assess them.

Those studies are based on empirical relationships between Newmark displacements and some normalized parameter(s) of critical acceleration (a_c). Most of them depends directly on PGA, which is a measure of shaking intensity widely used and simply to find. Other relationships adopt different seismic parameters as the Arias intensity, introduced by Arias (1970), which is the integral over time of the square of the acceleration, expressed as:

$$I_a = \frac{\pi}{2g}\int_0^T [a(t)]^2 dt \tag{4.16}$$

where I_a is Arias intensity in velocity units, g is the gravity, a(t) is the ground acceleration as a function of time, and T is the total duration of the strong motion.

Knowing the yield acceleration (a_c) and the distribution of a given seismic parameter through Shakemap or GMPE permits to apply empirical correlations to estimate the Newmark displacement. Table 4.1 reports some of the main national and international empirical relationships proposed in literature.

Table 4.1. Comparison among some of the main national and international empirical relationships for the assessment of Newmark displacements

Reference	Accelerogramms	Soil Class	Expressions	Statistics
Ambraseys & Menu (1988)	48 records *near field* (M_S = 6.4 ÷ 7.7)	-	$\log D = 0.90 + \log [(1-\eta)^{2.53}(\eta)^{-1.09}] +0.3\ t$	(*)
Ambraseys & Srbulov (1995)	76 records (M_S = 5.5 ÷ 7.7)	-	$\log D = -2.41+0.47\ M_s - 0.010\ r + \log [(1-\eta)^{2.64}(\eta)^{-1.02}]+ 0.58\ t$	(*)
Simonelli & Fortunato (1996)	Friuli, 1976	Rock-	$\log D = 1.95 - 2.254 \cdot \eta \quad (0.1 \le \eta \le 0.5)$	upper bound
		Soil	$\log D = 3.118 - 4.62 \cdot \eta \quad (0.5 < \eta \le 0.9)$	
	Irpinia, 1980	Rock	$\log D = 2.652 - 3.333\ \eta$	
		Soil		
Rampello et al. (2006)	Italian records M_L = 4 ÷ 6.6 (database: http://sisma.dsg.uniroma1.it/) scaled at 0.35g	Rock	$\log D = 1.32 - 3.26 \cdot \eta + 0.62 \cdot t$	(*)
		Stiff Soil	$\log D = 1.51 - 3.43 \cdot \eta + 0.41 \cdot t$	
		Soft Soil	$\log D = 1.25 - 3.50 \cdot \eta + 0.55 \cdot t$	
Ausilio et al. (2007)	Italian records M_L = 4 ÷ 6.6 (database: http://sisma.dsg.uniroma1.it/) Not Scaled	Rock	$\log D = 2.769 - 3.637 \cdot \eta$	upper bound
		Soil	$\log D = 1.669 - 4.058 \cdot \eta + 0.54 \cdot t$	(*)
			$\log [D/(a_{max} \cdot d_{5-95})] = 1.543 - 3.869 \cdot \eta + 0.31 \cdot T$	(*)

Tropeano et al. (2009)	Italian records $M_L = 4 \div 6.6$ (database: http://sisma.dsg.uniroma1.it/) Not scaled	Rock Soil	$\log [D/(a_{max} \cdot d_{5-95} \cdot T_m)] = -1.349 - 3.410 \cdot \eta + 0.35 \cdot t$ $\log [D/(a_{max} \cdot E[d_{5-95}] \cdot E[T_m])] = -1.349 - 3.410 + 0.45 \cdot t$ $a_{max} = a_g$ Rigid Block $a_{max} = \alpha_F \cdot S \cdot a_g$ Deformable Block	(*)
Jibson et al. (1998)	13 California records $M_L = 5.1 \div 7.5$	-	$\log D = 1.521 \cdot \log I_a - 1.9931. \log a_c - 1.546$	Mean
Miles & Ho (1999)	11 Records $I_a = 0.2 \div 10$ m/s	Dry or Sat Soil	$\log D = 1.46 \cdot \log I_a - 6.642. \log a_c + 1.546$	Mean

η = a_c/a_{max} or $k_c/k_{max.}$ (*) t = cumulative distribution function for a standard normal inverse fixed percentile: t = 0 → median; t = 1.282 → 90° percentile.

4.1.6 VULNERABILITY ASSESSMENT

The usefulness of Newmark displacements is to provide an index of correlation with the field performance of slope in seismic conditions. Wieczorek et al. (1985) used 5 cm as the critical displacement leading to macroscopic ground cracking and general failure of landslides in San Mateo County (California).; Keefer & Wilson (1989) used 10 cm as the critical displacement for coherent landslides in southern California; and Jibson & Keefer (1993) used this 5-10 cm range as the critical displacement for landslides in the Mississippi Valley. In most soils, displacements in this range cause ground cracking and previously undeformed soils can lose some of their peak shear strength and end up in a weakened or residual strength condition. In such a case of strength loss, a static stability analysis in residual strength conditions can be performed to determine the slope stability after earthquake shaking ceases.

Other researchers tried to combine the displacements experienced by slopes with the damage, which could affect an infrastructure located in the neighboring of the failed slope, for instance roadway networks, adopting in this case the Newmark displacements as deterministic tool to assess the performance of the involved infrastructure. Some of those are reported in Table 4.2.

Table 4.2. Comparison among some displacements range for the assessment of the vulnerability of the structures.

Structures			**Highways**		
Damage State	**Legg & Slosson (1984)**	**Idriss (1985)**	**Silvestri et al. (2006)**		
	PGD (cm)		Damage State	PGD (cm)	DS
Poor	< 0.5	< 3	Poor	< 2	DS2
Modest	0.5 – 5	15	Restorable	2 - 10	DS3
Strong/Modest	5 – 50	30	Interruption	10 - 50	
Severe/High	50 – 500	90	Collapse	> 50	DS4
Catastrophic	> 500	300			

Conversely, the semi-probabilistically evaluation of the performances of a structural component is based on vulnerability functions, also known as fragility curves for the different elements. Several researchers dedicated to this task, for instance Eidinger (1998) retrieved functions for lifelines, ALA (2001) dealt with water systems, Argyroudis & Pitilakis (2012) with shallow

tunnels, Lanzano et al. (2013) focused on gas and liquid buried pipelines and Panico et al. (2013) on wastewater treatment plants.

Furthermore, several authors also adopted these tools to assess the seismic vulnerability of structural components, Pitilakis et al. (2006) made a vulnerability analysis in the urban environment of Thessaloniki, Mavrouli et al. (2014) adopted fragilities for reinforced concrete buildings exposed to landslides and Forte et al. (2014) for highways affected by landslides.

Fragility functions express by log-normal distributions the probability of exceeding different damage states (DS) for a level of ground deformation. This latter is represented through the median (μ) of a seismic input parameter and the standard deviation (β).

The Hazus methodology (NIBS, 2004) accounts for a total of three damage states, which are defined for highway system components. These are slight/minor (ds2), moderate (ds3), extensive and complete (ds4).

For roadways, ds2 is defined by slight settlement (few inches) or offset of the ground; ds3 is defined by moderate settlement (several inches) or offset of the ground and ds4 is defined by major settlement of the ground (few feet).

Fragility curves for four-lane and two-lane roads are shown in Figures 4.4 and 4.5, respectively. The medians (μ) and dispersions (σ) of these curves are presented in Table 4.3.

In the next sections the II Grade slope microzonation methodology was applied for the case study of Molise (Italy) following two approaches; a simplified geomorphologic approach, which does not rely upon the database of geotechnical test collected and a more rigorous dataset-based approach.

Table 4.3. Damage Statistics for Roadways (Hazus, 2003)

Permanent Ground Deformation			
Components	Damage State	μ (in)	σ
Four-lane Roads	slight/minor (DS2)	12	0.7
	moderate (DS3)	24	0.7
	extensive/complete (DS4)	60	0.7
Two-lane Roads	slight/minor (DS2)	6	0.7
	moderate (DS3)	12	0.7
	extensive/complete (DS4)	24	0.7

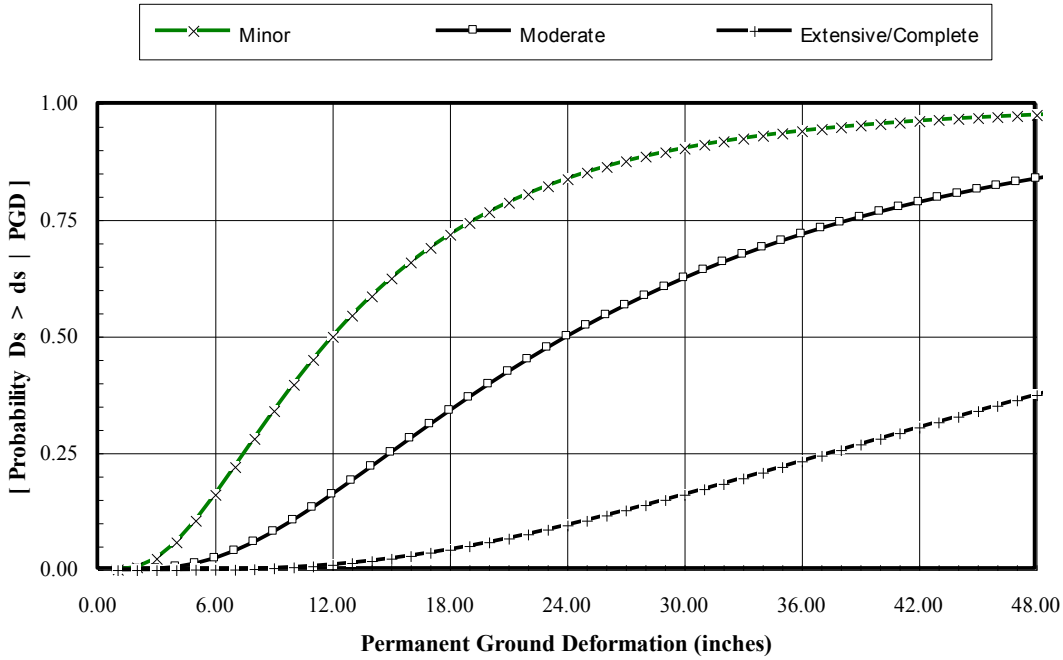

Figure 4.4. Fragility curves at various damage states (DS) for four-lane Highways after HAZUS.

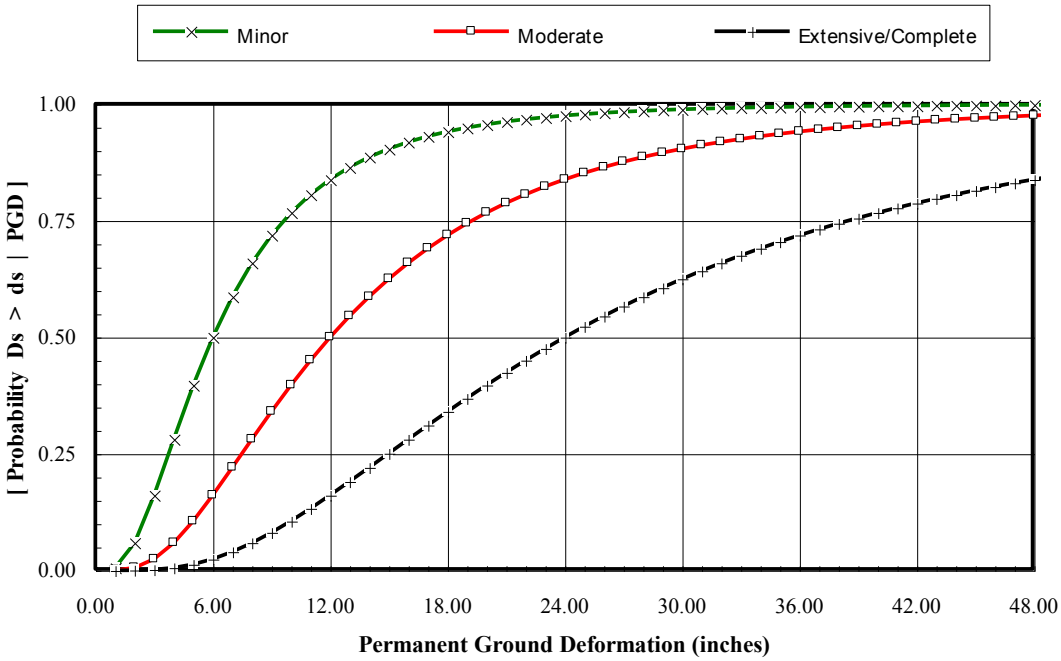

Figure .4.5. Fragility curves at various damage states for two-lane roads (after HAZUS).

4.2 GEOMORPHOLOGIC APPROACH TO THE SEISMIC SLOPE STABILITY

The Grade II developed in this work deals with the elaboration of thematic maps that picture the vulnerability of physical environment microzonation on regional scale. In this context the natural slope instability due to seismic events and their impact on the roadway network are accounted.

Roadway networks, as lifelines, are spatially distributed systems made of several components, which could experience different ground effects due to the same earthquake event. The evaluation of the vulnerability of these systems needs tools for information storage, overlay, integration and display. The Geographic Information Systems are suitable to this task, thus the arcGIS 9.3 software was adopted for this study.

The area selected to apply the method is located in the Campobasso district (Molise Region, Italy), within the Southern Apennines, which is a landslides-prone area, also characterized by medium-high seismicity, as discussed in section 2. In particular the most of the landslides of the Region are mainly II category (Keefer, 1984), as shown in the graph of Figure 4.6, modified after ISPRA (2005). It shows a high amount of slumps and slides, but also complex landslides, which can be included in Category II, because they are usually triggered as slides and later evolve into flows.

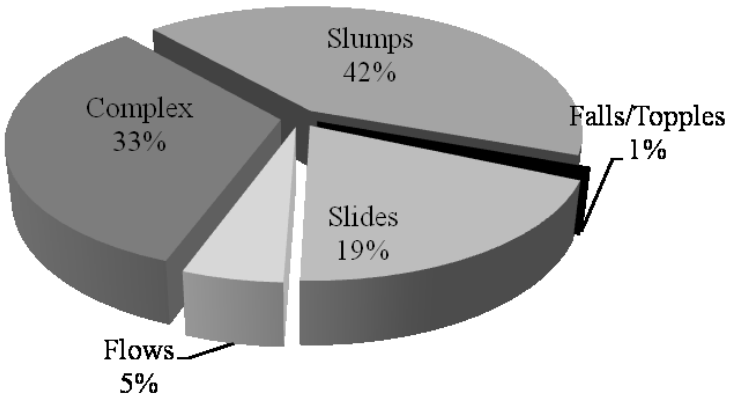

Figure .4.6. Percentage of the kind of landslides in the Molise Region modified after Ispra (2005).

4.2.1 SEISMIC SUSCEPTIBILITY MAPS

In this approach, also reported by Forte et al. (2013), a simplified assessment of the slope stability in static conditions has been dealt considering cohesionless soils and two extreme conditions, i.e. groundwater table below the slip plane (dry) and at field level (sat). Consequently, the factor of safety (Eq. 4.11) for the "dry" and "sat" conditions respectively becomes:

$$FS = \frac{tan\varphi'}{tan\beta} \tag{4.17}$$

$$FS = \frac{\gamma'}{\gamma_{sat}} \frac{tan\varphi'}{tan\beta} \tag{4.18}$$

where φ' is the effective friction angle, γ' and γ_{sat} are the buoyant and the saturated unit weight, respectively. The slope angle (β) was mapped from the reconstruction of a 1:100,000 digital elevation model (DEM, 200x200 m cell) shown in Figure 4.7.

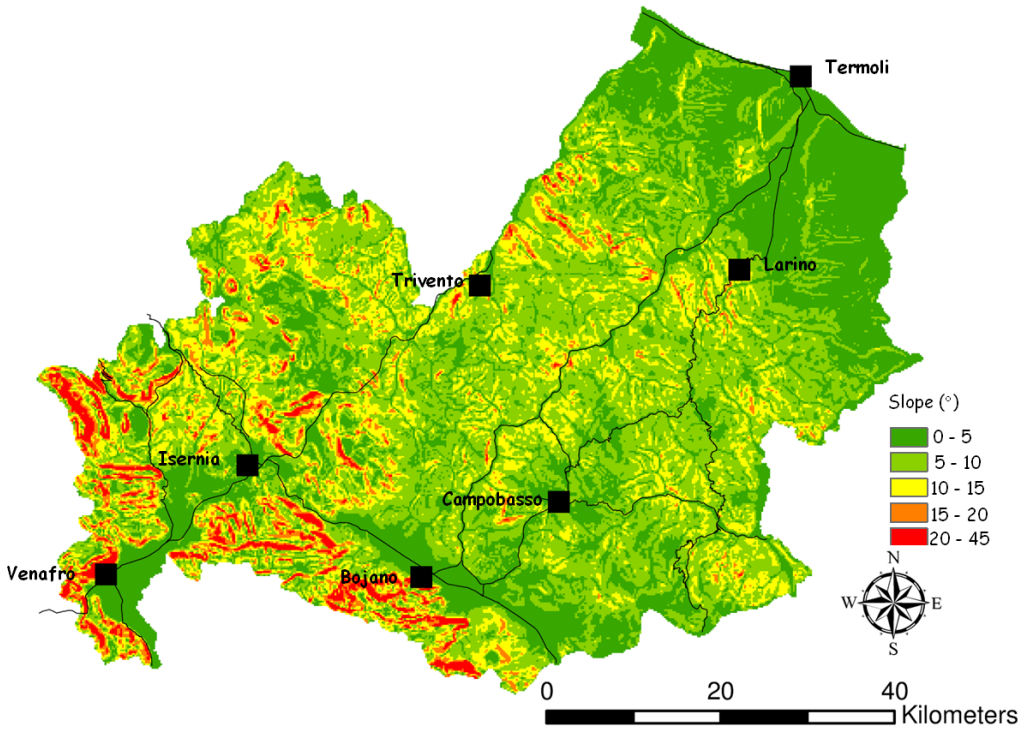

Figure .4.7. Slope angle (β) map from the DEM (200 x 200 m cell) of the area.

The strength parametes were attributed to the simplified geolithological complexes shown in the map of Figure 4.8.

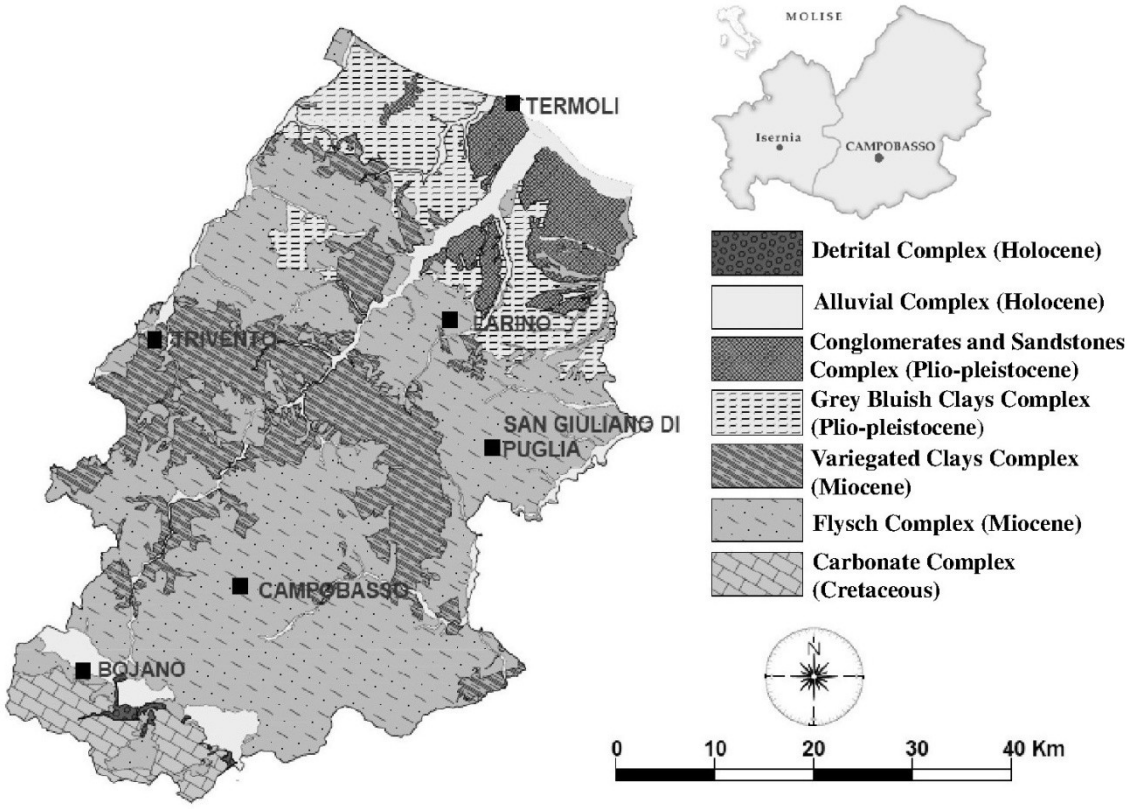

Figure .4.8. Geolithological Map of the study area (Molise Apennines - Campobasso district).

The strength values were attributed following a geomorphological approach. The Italian Inventory of Landslides (IFFI project) for the Molise Region was acquired and the landslides plotted on the Geolithological Map of Figure 4.7; then for each complex the total landslide area was normalized to the whole area. The results in terms of percentage are reported in the histogram of Figure 4.9.

Those results evidence a sort of ranking of "the susceptibility to be eroded", hence for each complex an "erodibility" class was assigned together with a representative parameter of the soil

strength; the higher the erodibility the lesser the value of the assigned friction angle (φ'), as reported in Table 4.4.

Those results are in agreement with the regional geomorphological analysis carried out by ISPRA (2005) and Regione Molise (2001).

The saturation conditions (sat), were attributed only to those complexes, in which such conditions could be observed (see again Table 4.4).

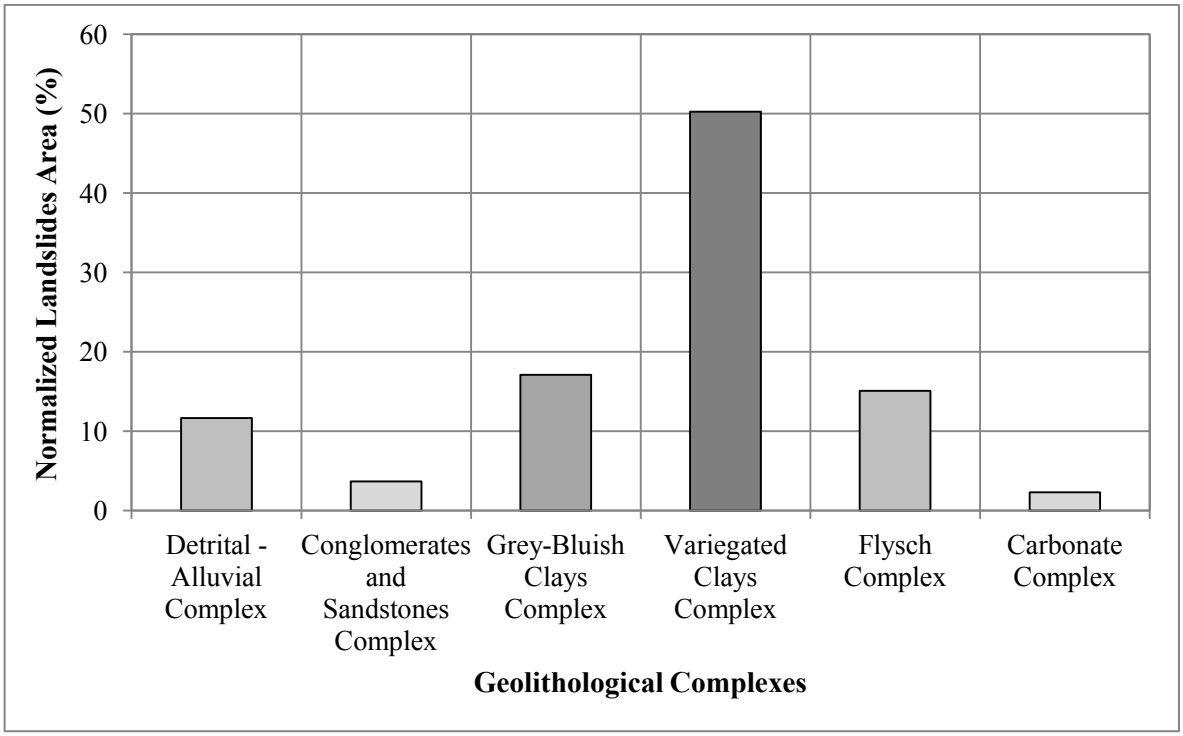

Figure 4.9. Histogram of the percentage of Normalized Landslides Area for each complex.

Table 4.4. Geolithologic Complexes with their erodibility rank and assigned friction angle.

Geolithological Complex	Erodibility	Saturation	Friction Angle	Hazus Class
Carbonate Complex	Low	No	45°	A
Conglomerates and Sandstones Complex	Medium/Low	No	35°	B
Detrital Complex	Medium	No	30°	B
Flysch Complex	Medium	Yes	30°	B
Blue-Grayish Clays Complex	Medium/High	Yes	25°	C
Variegated Clays Complex	High	Yes	18°	C

The factor of safety (FS) showed in Figure 4.10 for the "dry" and "sat" conditions was respectively calculated according to Eqs. (4.17) and (4.18). Conversely, the critical acceleration (a_c) was calculated with Eq. (4.1) and it is reported in Figures 4.11. The obtained results are compared with the widespread approach of the HAZUS methodology (NIBS, 2004), which characterizes the landslide susceptibility in static condition by assigning a geologic group, considering the slope angle and groundwater conditions. It is measured on a scale of I to X, with I being the least susceptible. The site condition is identified using three geologic classes (rock, stiff and soft soil) and two groundwater levels. The description for each geologic group and its associated susceptibility is given in Table 4.5. The connection between the Campobasso district geolithological complexes and the HAZUS classes is reported in Table 4.4.

Table 4.5. Landslide susceptibility of geologic groups according HAZUS.

Geologic Group		Slope Angle, degrees					
		0-10	10-15	15-20	20-30	30-40	>40
(a) DRY (groundwater below level of sliding)							
A	Strongly Cemented Rocks (crystalline rocks and well-cemented sandstone, $c' = 300$ psf, $\phi' = 35^o$)	None	None	I	II	IV	VI
B	Weakly Cemented Rocks and Soils (sandy soils and poorly cemented sandstone, $c' = 0$, $\phi' = 35^o$)	None	III	IV	V	VI	VII
C	Argillaceous Rocks (shales, clayey soil, existing landslides, poorly compacted fills, $c' = 0$ $\phi' = 20^o$)	V	VI	VII	IX	IX	IX
(b) WET (groundwater level at ground surface)							
A	Strongly Cemented Rocks (crystalline rocks and well-cemented sandstone, $c' = 300$ psf, $\phi' = 35^o$)	None	III	VI	VII	VIII	VIII
B	Weakly Cemented Rocks and Soils (sandy soils and poorly cemented sandstone, $c' = 0$, $\phi' = 35^o$)	V	VIII	IX	IX	IX	X
C	Argillaceous Rocks (shales, clayey soil, existing landslides, poorly compacted fills, $c' = 0$ $\phi' = 20^o$)	VII	IX	X	X	X	X

The groundwater regime can be set into either dry (groundwater below level of the sliding) or wet (groundwater level at ground surface) condition. The critical acceleration is then estimated for the corresponding geological class, groundwater conditions and slope angle. To avoid calculating the occurrence of landsliding for very low or zero slope angles and critical accelerations, lower bounds for those parameters are established.

Finally, at each susceptibility class a value of the critical acceleration (a_c) is assigned, as shown in Table 4.6.

Those maps represent the landslide susceptibility in seismic condition.

Table 4.6. Critical accelerations (a_c) for susceptibility categories according Hazus.

Susceptibility Category	None	I	II	III	IV	V	VI	VII	VIII	IX	X
Critical Accelerations (g)	None	0.60	0.50	0.40	0.35	0.30	0.25	0.20	0.15	0.10	0.05

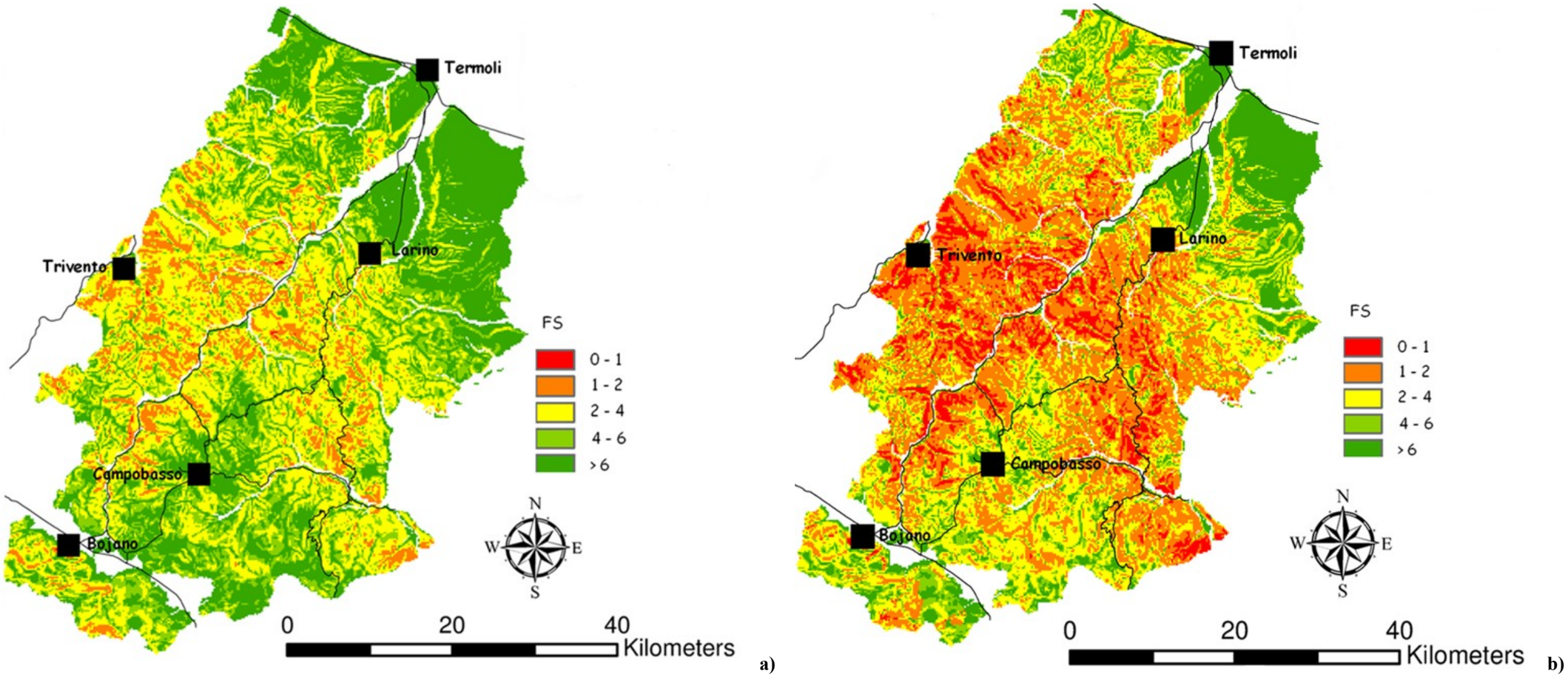

Figure 4.10. Factor of safety map for ***a)*** dry condition and ***b)*** sat condition (200 x 200 m cell).

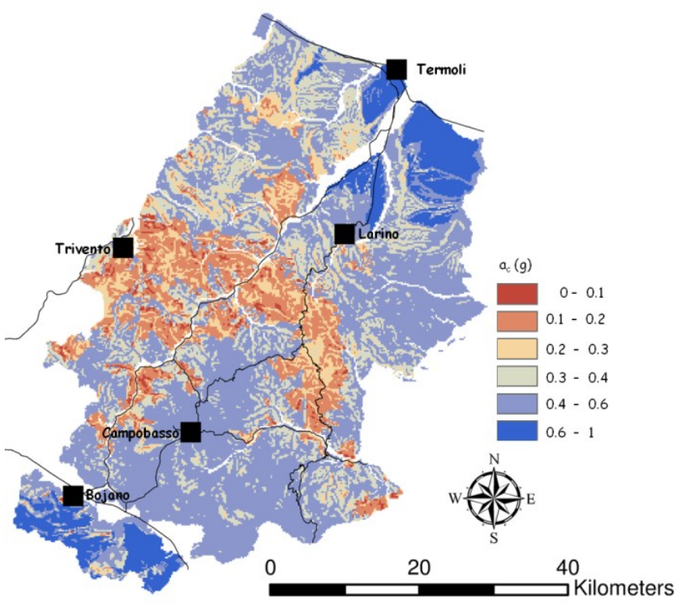

a)

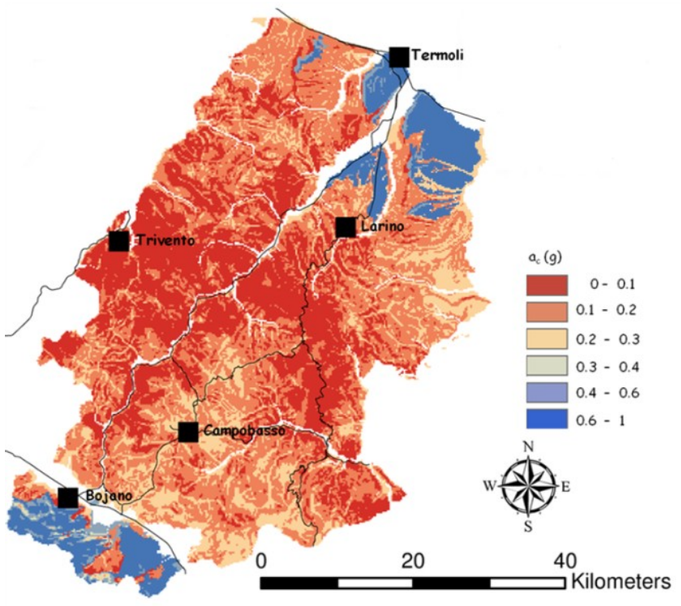

b)

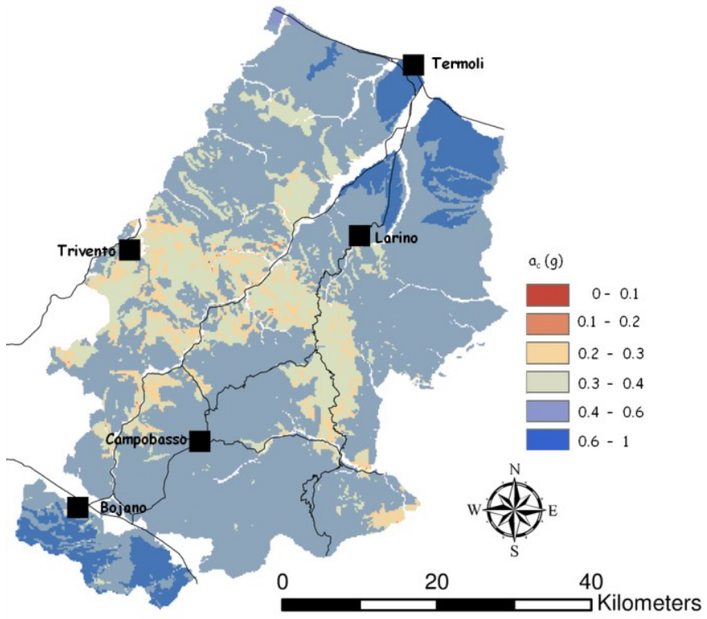

c)

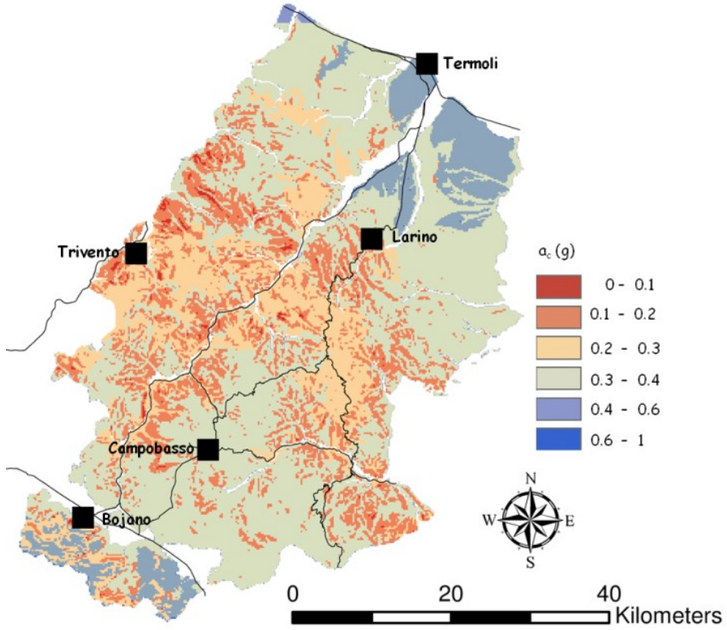

d)

Figure 4.11. Landslides susceptibility maps in seismic condition from the geomorphological approach in a) "dry" and b) "sat" condition and from the Hazus methodology for c) "dry" and d) "wet" conditions (200 x 200 m cell).

The results of both approaches are also shown in Figure 4.12, where the relationship between yield acceleration (a_c) and the slope angle (α) is plotted for the several HAZUS classes.

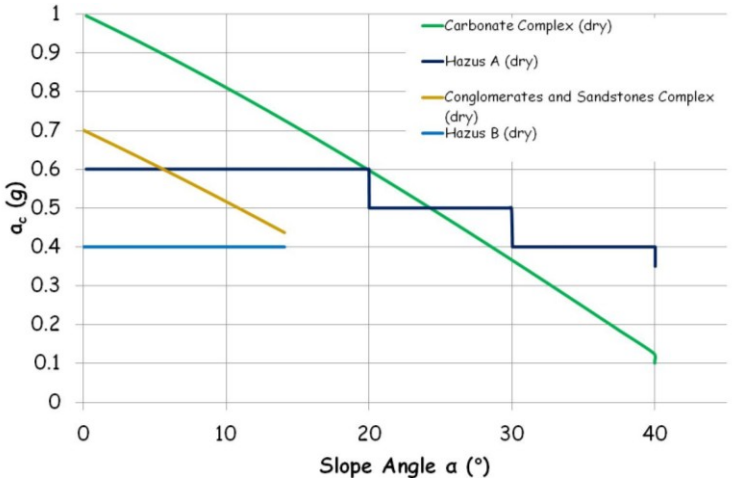

a)

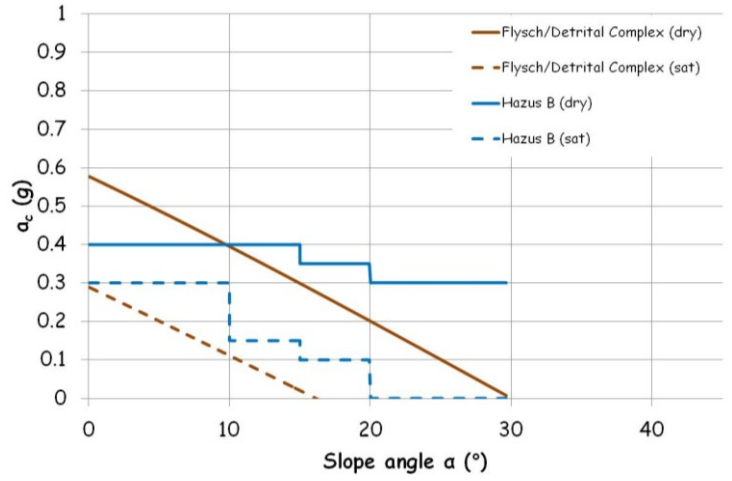

b)

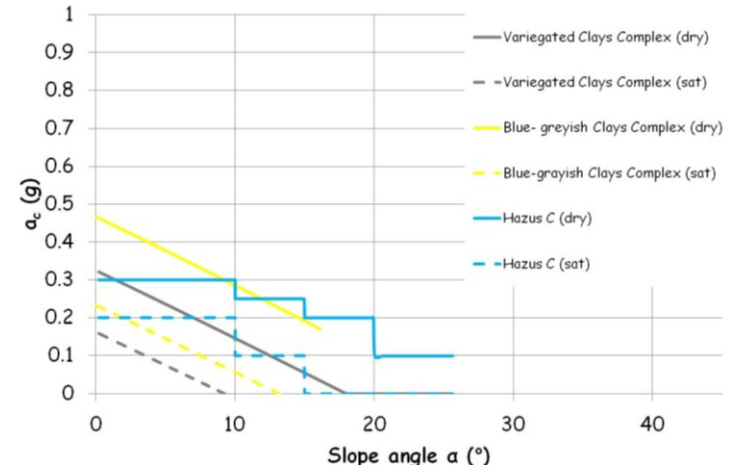

c)

Figure 4.12. Comparison between a_c:. α relationships obtained in this study and those resulting from the application of the HAZUS approach for ***a)*** A class soils and dry B class; ***b)*** dry and wet B class; ***c)*** dry and wet C class.

Figures 4.11 and 4.12 generally evidence lower yield acceleration values in the results of this study than in those produced by the HAZUS method. In particular, the geomorphological approach evidences a linear decreasing trend of the critical acceleration with the slope, while HAZUS presents a stepwise trend. Furthermore for the dry A, B and C class (Figure 4.12a, 4.12b and 4.12c) at very low slope angles the geomorphological approach gives higher yield acceleration values, but at the slope threshold respectively of 25° and 10°, the results are more conservative than those of HAZUS. In all the classes, the saturated conditions give the lowest values in this study.

4.2.2 NEWMARK DISPLACEMENTS

As discussed in § 4.1.5, in the evaluation of the permanent displacements, the appropriate selection of the seismic input is relevant. In this study, a deterministic scenario analysis simulating the infamous July 26, 1805 St. Anna Earthquake (M_w 6.62 ± 0.11) was adopted. This event was the strongest earthquake, which affected the Molise Region, after the 1456 Earthquake. It was selected because records of the location of the triggered landslides are available from the papers by Romeo & Delfino (1997) and Porfido et al. (2007). The reference ground motion distribution predicted through the GMPE by Sabetta & Pugliese (1996) is shown in Figure 4.13.

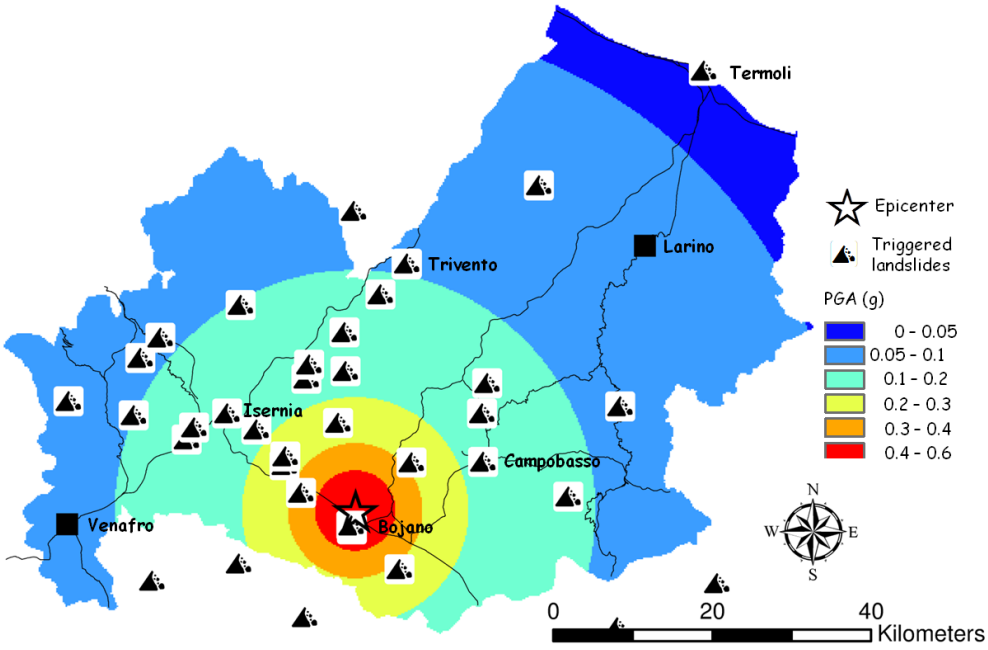

Figure 4.13. Shaking map at bedrock of the 1805 Earthquake Scenario predicted through the GMPE by Sabetta & Pugliese (1996).

The peak ground acceleration (PGA) at bedrock can be corrected to account for different site conditions, in terms of stratigraphic (S_S) and topographic amplification (S_T) factors. Following several codes indications such as NTC (2008), S_S is dependent on the PGA at bedrock and the subsoil classification. At small scale, it is difficult to have a detailed distribution of the stiffness of the different formations to classify sites. Hence in this preliminary approach, the V_{S30} map obtained by USGS according to Wald & Allen (2007) criterion shown in Figure 3.30 was imported. The stratigraphic factors were quantified through the relationships proposed by Landolfi et al. (2011) for the different soil classes and PGA values. These relationships shown in Figure 4.14 were calibrated on the Italian seismicity and account for the non-linear and dissipative soil behavior.

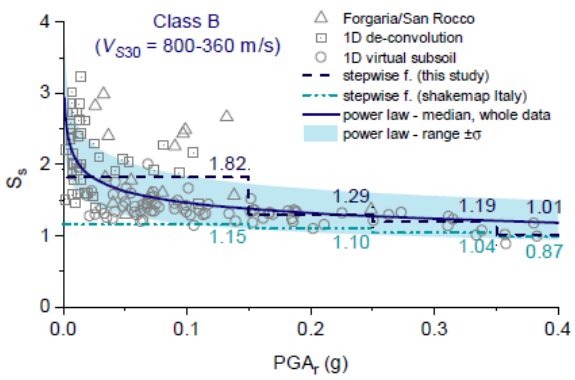

$$S_S = 1.028 * PGA_r{}^{-0.15}; \sigma = \pm 0.099$$

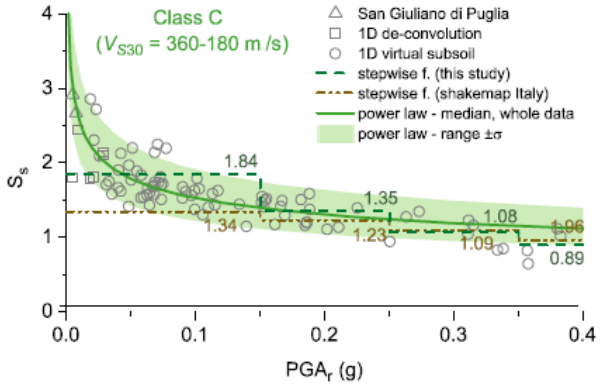

$$S_S = 0.904 * PGA_r{}^{-0.23}; \sigma = \pm 0.098$$

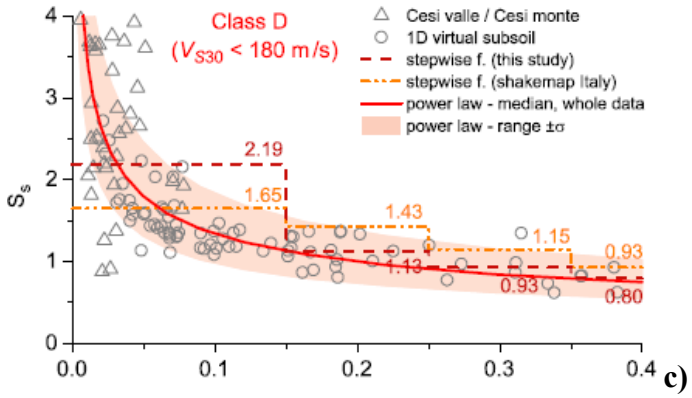

$$S_S = 0.508 * PGA_r{}^{-0.42}; \sigma = \pm 0.136$$

Figure 4.14. Non-linear amplification factors for subsoil classes B ***(a)***, C ***(b)***, D ***(c)*** after Landolfi et al. (2011).

The topographic amplification factor (S_T), depends on the shape of slopes, because irregular surface geometry affects the focusing, defocusing, diffraction and scattering of seismic waves, which could change amplitude, frequency and duration of ground motion compared to flat ground conditions (Sanchez-Sesma, 1990; Paolucci, 2002, Pagliaroli, 2006).

Following Garcìa–Rodriguéz et al. (2002), a geometrical parameter more suitable for small scale studies seemed to be the slope curvature, which can be obtained from the DEM of the area. It is defined as "*the second derivative of a surface, or the slope of the slope*" (www.esri.com) and permits to mark the concave and the convex features of a landscape, with negative and positive

values respectively. Garcìa–Rodriguéz et al. (2002) associated topographic amplification factors (S_T) to a certain range of slope curvature, accounting for attenuation in valleys and the seismic waves focusing on ridges. The effectiveness of this parameter was also validated by the numerical study of Torgoev et al. (2013), who directly corrrelated the curvature and the topographic amplifications for several slope geometries. Torgoev et al. (2013) results are shown in Figure 4.15, together with an average fitting curve. The same Figure also reports the range of factors (0.5 ÷ 1.4) adopted in this study which result from merging the seismic code with those suggested by Garcìa–Rodriguéz et al. (2002), which, in turn, are shown in Table 4.7. In particular, the upper bound adopted in this study follows the upper bound of 1.4 for S_T specified in the Italian Building Code (NTC, 2008).

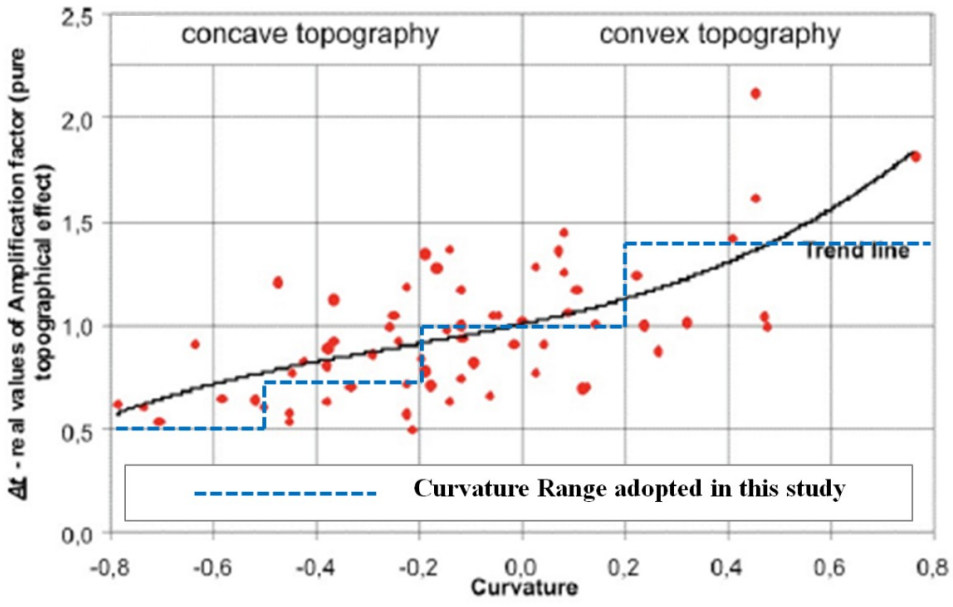

Figure 4.15. Plot of amplification factors vs. curvature; the blue dashed line is the range of values adopted in this study.

Table 4.7. Comparison between S_T amplification factors.

Curvature	S_T (Garcìa–Rodriguéz et al. 2002)	Curvature	S_T (This Study)
-10 ÷ -0.9	0.5	< -0.5	0.5
-0.9 ÷ -0.2	0.7	-0.5 ÷ -0.2	0.7
-0.2 ÷ 0.2	1	-0.2 ÷ 0.2	1
0.2 ÷ 0.9	1.5	> 0.2	1.4
0.9 ÷ 10	2	-	-

The PGA map for the Campobasso district corrected to account for the stratigraphic and topographic amplification factors is pictured in Figure 4.16.

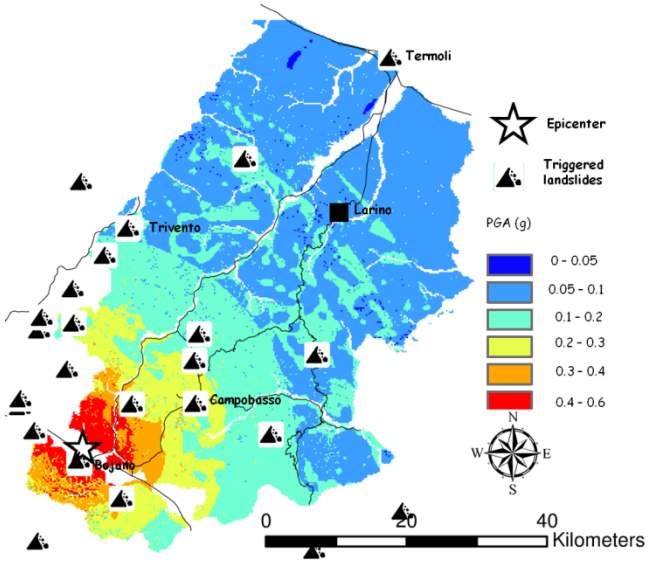

Figure 4.16. Shaking map at surface of the 1805 Earthquake Scenario predicted through the GMPE by Sabetta & Pugliese (1996) for the Campobasso district.

The permanent ground deformations (PGD) were estimated selecting among the existing empirical correlations (see Table 4.1), the upper bound relationship proposed by Ausilio et al. (2007). The most critical areas are evidenced by displacement values as high as 587 cm. The risk can be significant in the areas in proximity of a strategic expressway (SS 647 Biferno). The results of the method were checked against the effective distribution of the 1805 earthquake landslides shown in Figure 4.17.

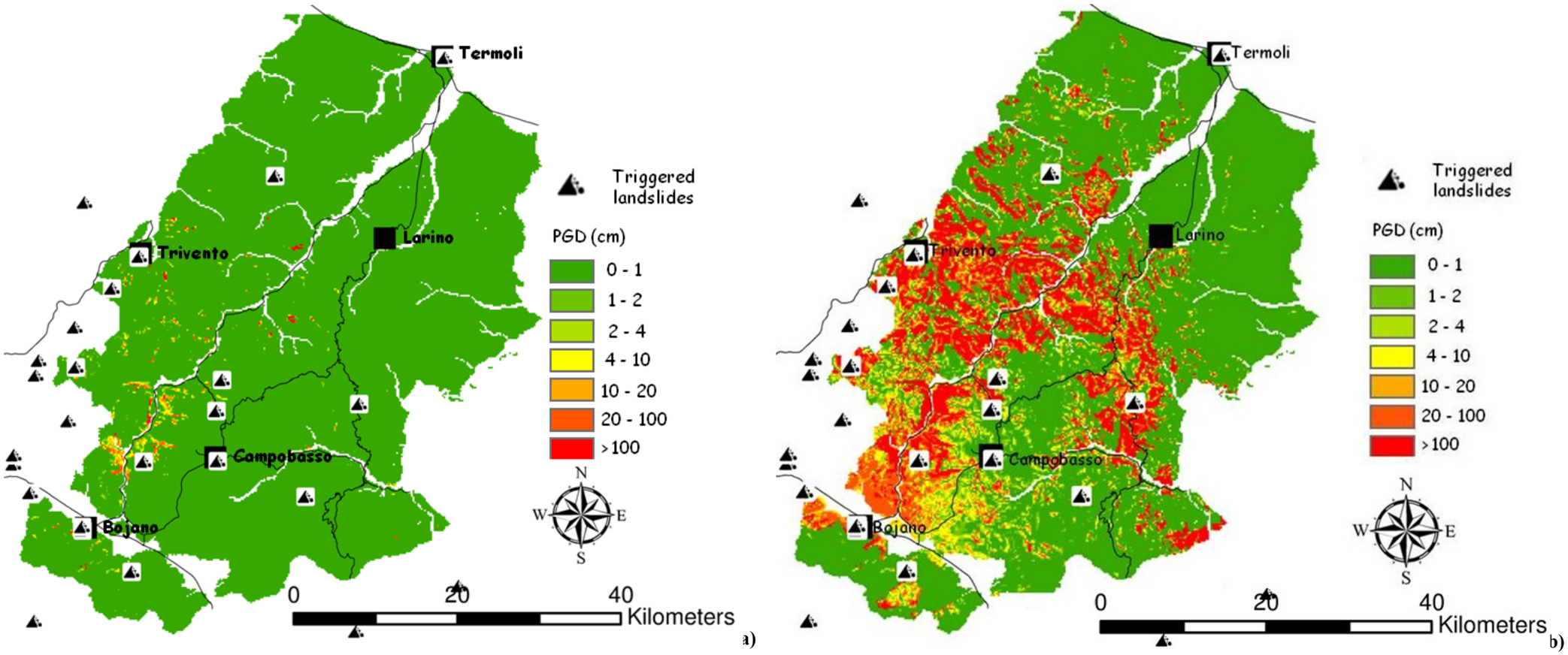

Figure 4.17. Permanent Ground Deformation Maps (PGD) of the study area ***a)*** dry conditions and ***b)*** sat conditions (200 x 200 m cell).

The vulnerability of the road network was assessed through the fragility functions proposed by Hazus (NIBS, 2004) for two-lanes roads, by expressing the probability that the expected damage exceeds the minor P(ds > DS2), the moderate P(ds >DS3) and the extensive P(ds >DS4) reference damage states of Table 4.3. Some exemples for the "dry" case are shown in Figure 4.18. The results give a preliminary picture of the areas that can be most likely affected by each damage state in a similar shaking scenario in a performance-based approach; it is clear that the higher the damage state, the less the probability to be exceeded.

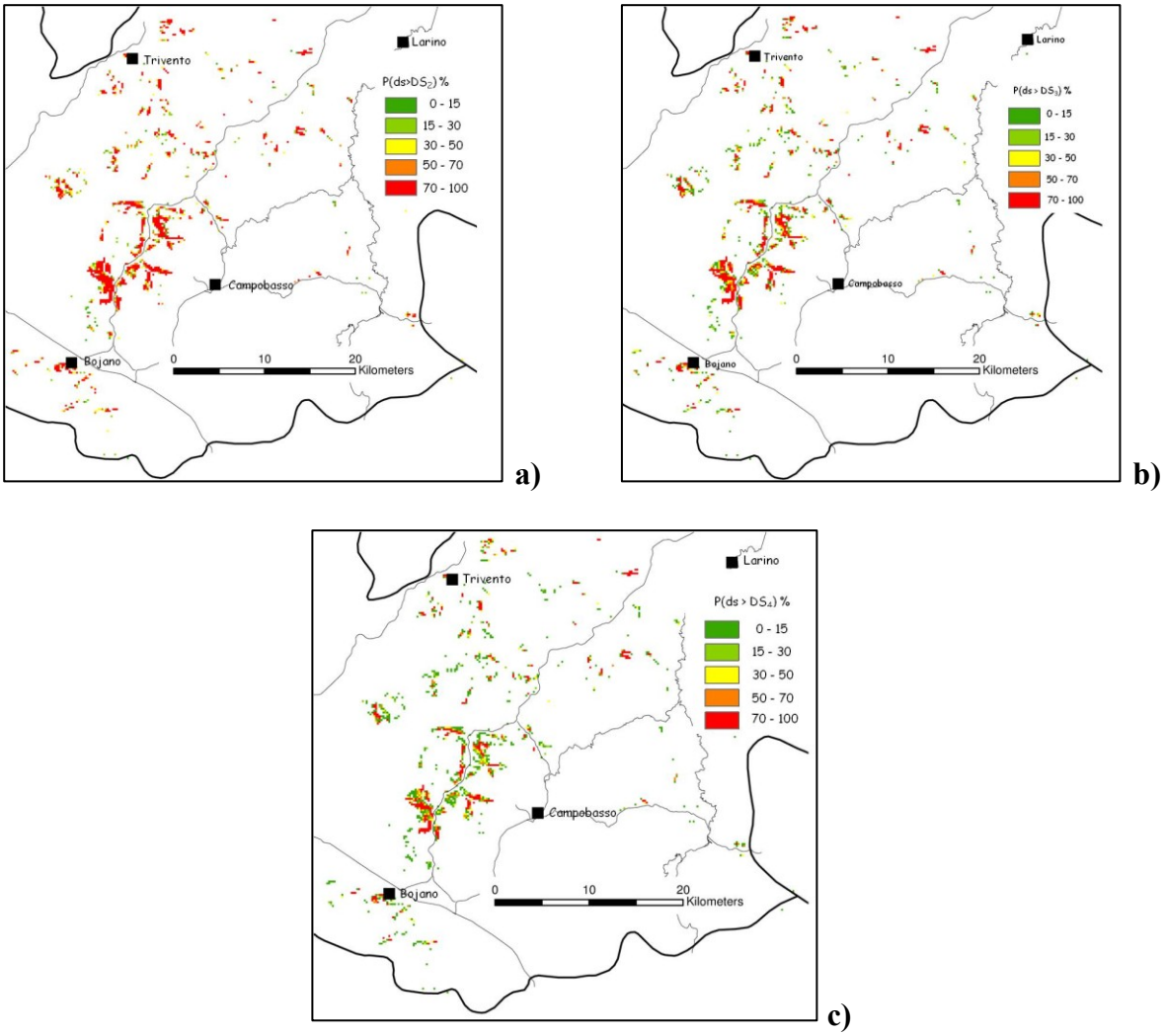

Figure 4.18. Probabilities of exceedance of ***a)*** the DS2, ***b)*** DS3; ***c)*** DS4 for the dry conditions (200 x 200 m cell).

4.3 ENGINEERING GEOLOGY APPROACH TO THE SEISMIC SLOPE STABILITY

4.3.1 LANDSLIDES SUSCEPTIBILITY MAPS

In this section it is reported an approach to the seismic slope stability which updates the results of the geomorphologic approach and relies on the data gathered in the geological and geotechnical database reported in Chapter 3.

In this method the stability analysis was extended also to the district of Isernia, in order to envelope the whole Region, while the roadways vulnerability was still evaluated only for the Campobasso district.

The factor of safety was calculated according to its complete formulations as shown in Eq. (4.11), differentiating the several geolithological complexes on the basis of the map showed in Figure 3.6. The Carbonate Complex was completely excluded from this analysis, since the Newmark method, as discussed in § 4.1, is suitable to model seismic triggering of category II landslides according to Keefer (1984) classification. Landslides of that kind are the most typical for the geological context of Molise Region, as also discussed in § 2.2 and ISPRA (2005), except for the Carbonate Complex which is not prone to these landslides. Furthermore the cells characterized by slope values lesser than 5° were also discarded, to reduce the computation time, because a more detailed digital elevation model (DEM) was adopted. It was downloaded from the ISPRA web site at http://www.sinanet.isprambiente.it/it/sia-ispra/download-mais/dem20/view and is a 20 m resolution DEM, which permitted to obtain cells 50 x 50 m, nearly one order of magnitude more detailed than the previous one, which had cells of 200 x 200 m.

The slope angle map for the 50 x 50 m cell is shown in Figure 4.19.

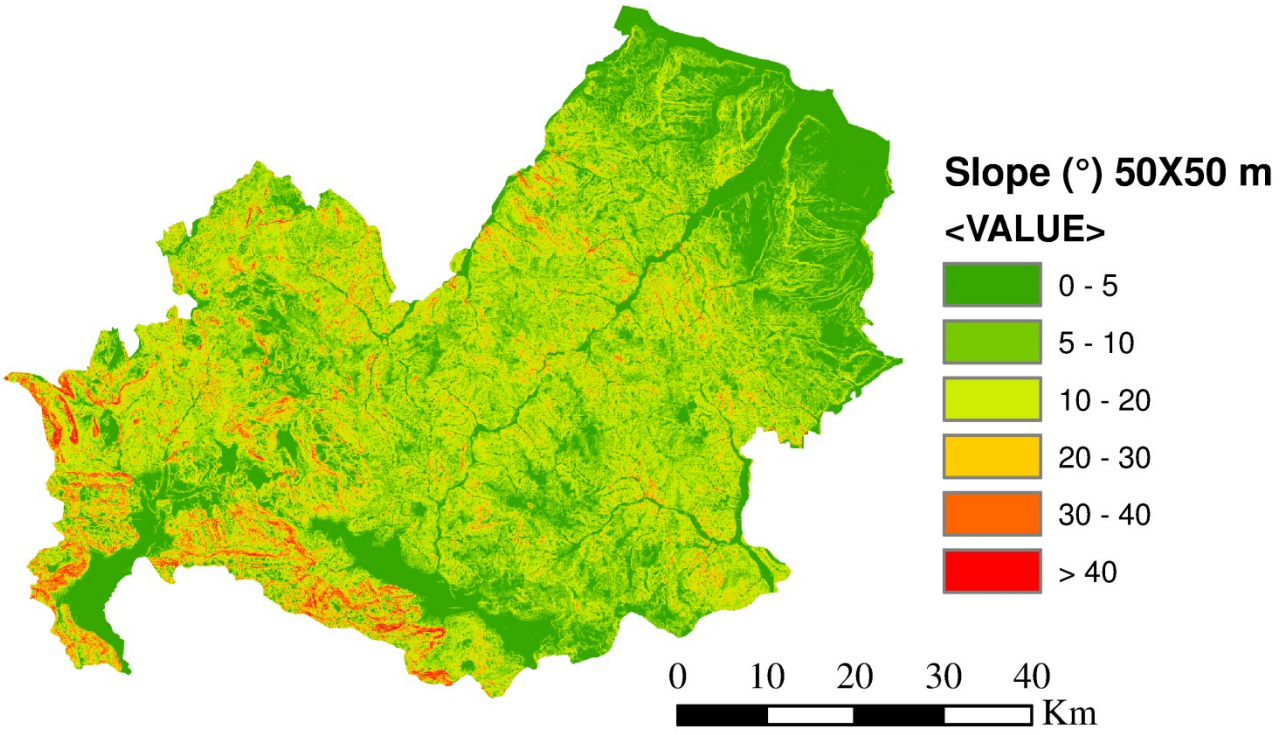

Figure .4.19. Slope angle (β) map from the DEM (50 x 50 m cell) of the area.

The adopted strength parameters (φ' and c') were obtained from the mean values of the collected dataset, summarized in Table 3.8. For the clayey complexes, the undrained shear strength (s_u) was preferred over to the effective shear strength. The groundwater conditions were accounted through the attribution of a mean *m* value, as reported in Eq. (4.10), for each geolithological complex. Clayey formations were attributed to m = 1, (which identifies saturation conditions), as those soils usually represent the aquiclude of the main springs of the Region. The input parameters adopted for the stability analyses are summarized in Table 4.8.

Table 4.8. Strength parameters adopted in the stability analysis with Engineering Geology approach.

Geolithological Complex	**γ (kN/m^3)**	**φ' (°)**	**c' (kPa)**	**s_u (kPa)**	**m (-)**
LD	19.5	18	-	-	1
FA-CA	20.76	21	14	-	0.8
GBC	20.82	-	-	54	1
SC	19.78	23.74	16.7	-	0.5
MS	20.4	22.09	21.6	-	0.5
MC	20.9	-	-	90	0.8
MCa	19.94	22.16	18.39	-	0.5
VC	20.37	-	-	117	1

The stability analysis accounted for a sliding surface located at the mean depth of 15 m b.g.l., in fact from the analysis of the water content is evident in Figures 3.19 to 3.21, at this depth a significant increase in consistency, which could define the stratigraphic passage from the weathered cover to the intact soil mass.

Figure 4.20 shows the static susceptibility map through the evaluation of the factor of safety (FS) and the seismic susceptibility map with the a_c distribution.

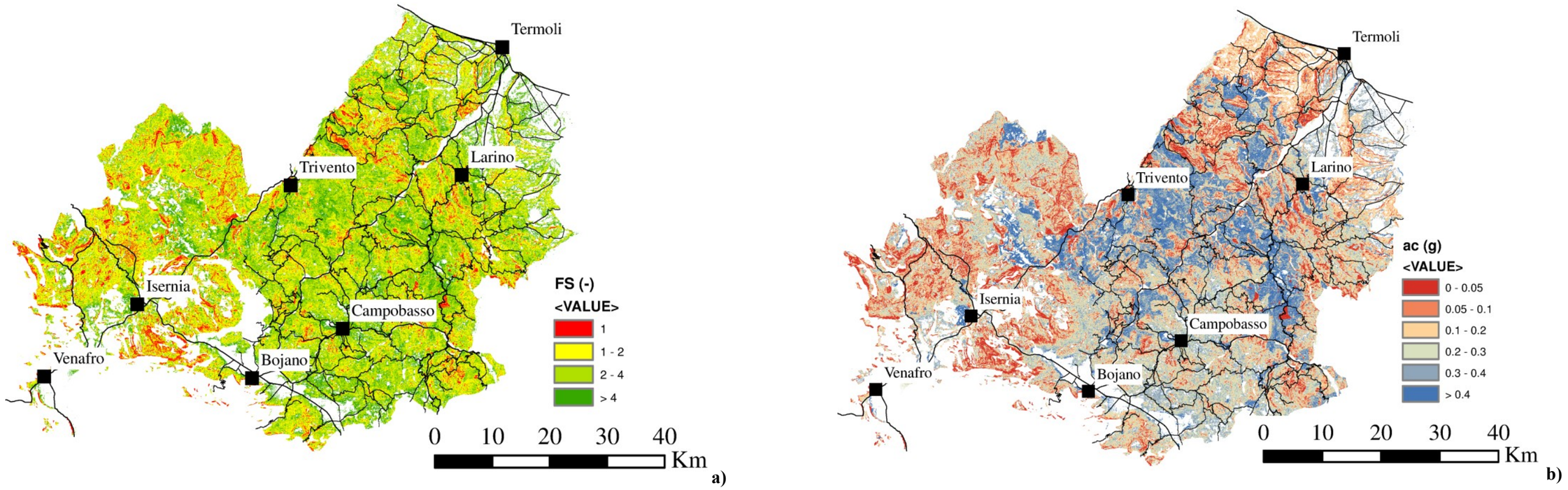

Figure .4.20. Landslides susceptibility maps ***a)*** in static condition and ***b)*** seismic condition from the engineering geological approach (50 x 50 m cell).

4.3.2 DAMAGE SCENARIO

The St. Anna 1805 Earthquake was again adopted as seismic input motion. The ground motion prediction equation was updated with the more recent GMPE by Bindi et al. (2011), which accounts for the distance from the strike of the seismogenic fault. The comparison in Figure 4.21 shows that this GMPE predicts higher acceleration values than that by Sabetta & Pugliese (1996).

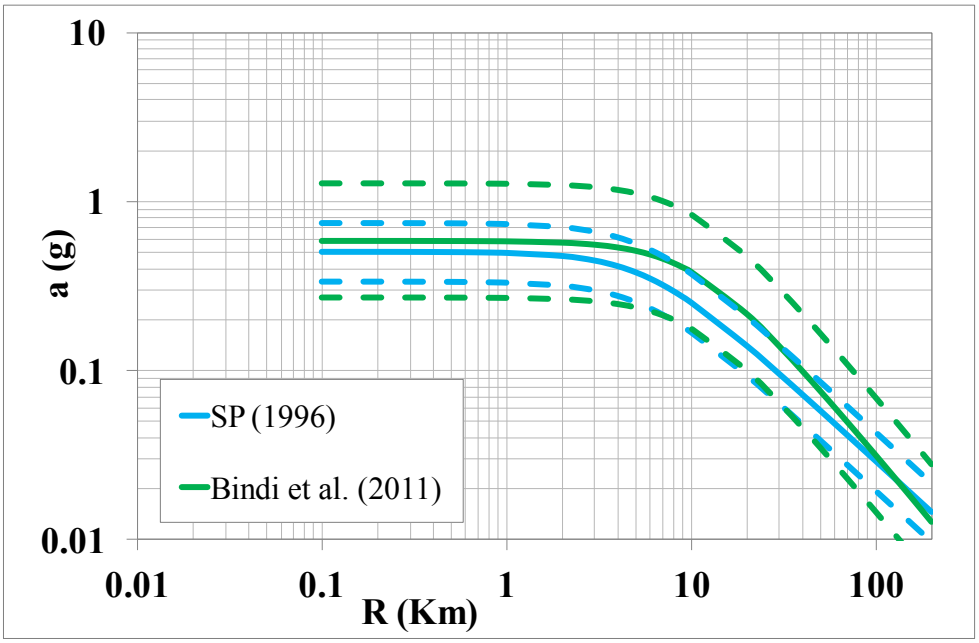

Figure .4.21. Comparison between the accelerations attenuation predicted by the GMPE of Sabetta & Pugliese (1996) and Bindi et al. (2011).

The Shake map at bedrock was amplified for the topographic conditions, as already discussed in the previous section, adopting the ranges of the slope curvature as proxy to assign topographic amplification factors (S_T). The stratigraphic amplification was again calculated with the Landolfi et al. (2011) relationships for the soil classes, which in this case were derived by the map shown in Figure 3.39. The amplified shakemap adopted in this approach is shown in Figure 4.22,

together with the location of the landslides triggered, which appear accordingly oriented along the fault strike.

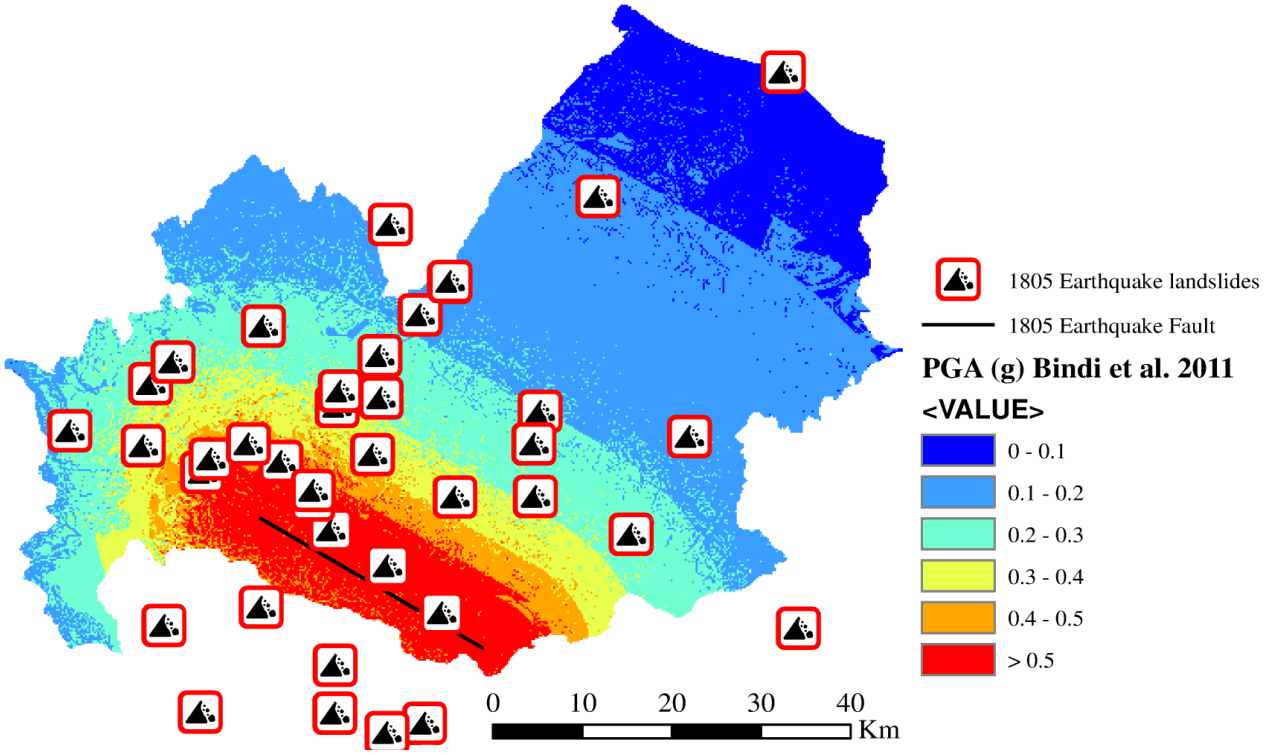

Figure 4.22. Shaking map at surface of the 1805 Earthquake Scenario predicted through the GMPE by Bindi et al. (2011) for the Molise Region, with the location of the triggered landslides.

by combining the simplified shakemap with the susceptibility maps (§ 4.3.1), the Newmark displacements were again estimated with the upper bound relationship by Ausilio et al. (2007). The displacement map (Figure 4.23a) lead to a damage map (Figure 4.23b) following the damage criterion proposed by Silvestri et al. (2006).

Those results more accurately permit to quantify critical areas and to identify intervention priorities in view of emergency management, in which to increase the degree of knowledge and analysis. A Grade III analysis was also performed in one of the most critical areas (see next section) in order to validate the results of the above Grade II study.

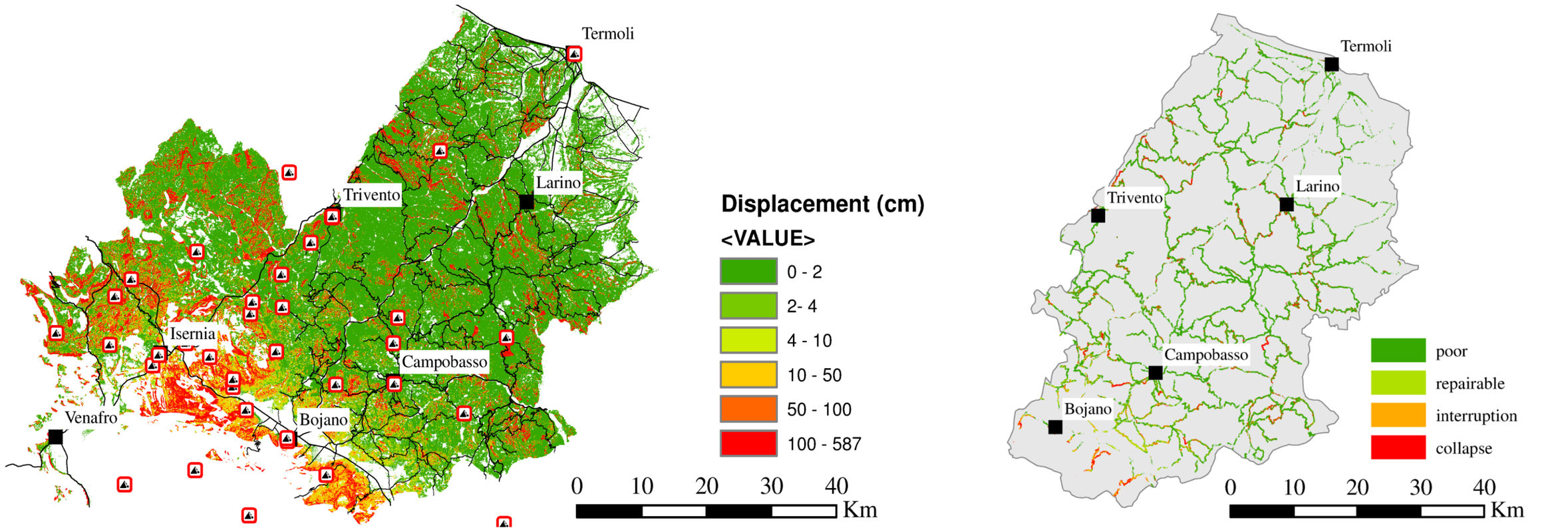

a) **b)**

Figure .4.23. a) Permanent Ground Deformation Maps (PGD) of the Molise Region (50 x 50 m) ***b)*** Vulnerability analysis of the roadway network of Campobasso district with Silvestri et al. (2006) approach.

5. GRADE III SEISMIC SLOPE STABILITY: THE CASE STUDY OF ROCCAVIVARA EARTHSLIDE

A grade III analysis of microzonation for slope stability was carried out in a small area in order to compare and validate the results obtained in the II grade engineering geological approach.

The studied landslide is located in the municipality of Roccavivara village (CB) and can be classified as *earthslide*, according to the Cruden & Varnes (1996) classification. In Figure 5.1, the main features of the landslide are reported, namely the main scarp, the landslide body which affected a roadway and the pond located at the toe of the slope.

Figure 5.1. Main features of Roccavivara earthslide: ***a)*** and ***b)*** main scarp; ***c)*** body of the landslide, which affected the roadway; ***d)*** artificial pond located at the toe of the slide.

The case study was chosen as typical of the very widespread instability phenomena, which seasonally occur in Molise Region and also because it was possible to directly follow the whole investigation phase. The slide involved nearly 36.600 m^3 of material, which affected and displaced the regional neighboring roadway.

5.1 GEOLOGICAL SETTING

The site is located in the Northern sector of Molise Region, along the right shore of the Trigno River, at the border with the Abruzzo Region. Its position can be seen in the sheet 154 LARINO of the official 1:100,000 Geological Map of Italy reported in Figure 5.2.

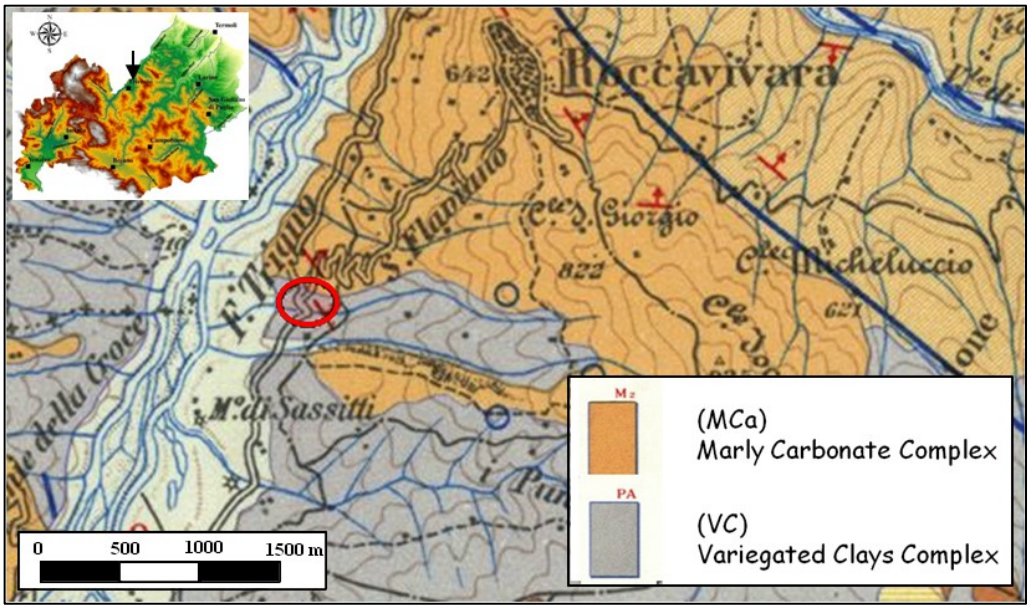

Figure 5.2. Location of the earthslide mapped on the excerpt from the 1:100,000 Geological Map of Italy # 154 LARINO.

The geological setting is quite similar to the one of the Salcito landslide, which was triggered by the 2002 Molise Earthquake. It is made of Variegated Clays Complex (Cretaceous-Miocene),

which lithologically consists of clays and silty-marly clays, in tectonic contact with the Marly Carbonate Complex (MCa), made of Tufillo Formation (Langhian-Tortonian) and represented by blocks of cherty calcarenites with thick gray marls intercalations. The landslide is located at the topographic heights of 220-240 m a.s.l. upstream of a river terrace, which consists primarily of alluvial deposits of loose gravels and sands of the Trigno River, representative of an ancient flooding surface, separated from the main flooding bed by a natural embankment, whose height is lower than 5 m. The topographic gradient of the area reflects the contrast of competence between the geolithological complexes, i.e higher slope angles are for the MCa Complex and lower ones for the VC Complex.

Regarding to hydrogeological setting, the Marly Carbonate Complex (MCa) presents higher permeability due to fracturing and secondary porosity, while the Variegated Clays Complex (VC) is poorly permeable for porosity. The former can be classified as *aquifer*, while the latter represents the *aquiclude*. Along this contact, the permeability contrast permitted the outflow of several springs, both seasonal and perennials, the nearest of which to the earthslide is the S. Fabiano Spring located at 435 m a.s.l. and characterized by a mean discharge of 2.46 l/s (www.regione.molise.it).

The groundwater flow from the MCa aquifer is drained by the shallower layers of weathered clayey deposits (VC), feeding a sub-surface flow in the very first meters buffered at various altitudes by less permeable lenses. The groundwater flow feeds an artificial pond dug at the toe of the landslide, while the main flow direction is towards the Trigno River.

This hydrogeological setting contributed to the morphoevolution of this landscape through runoff and slope instability.

For the purposes of the III grade analysis, the investigation campaign was supported by a detailed 1:5,000 scale geological and geomorphological survey around the area of the landslide. Those surveys permitted to verify the geometric relationships between the outcropping

formations and to identify the main geomorphological features of the area. The results are summarized in the following geolithological and geomorphological maps shown respectively in Figures 5.3 and 5.4.

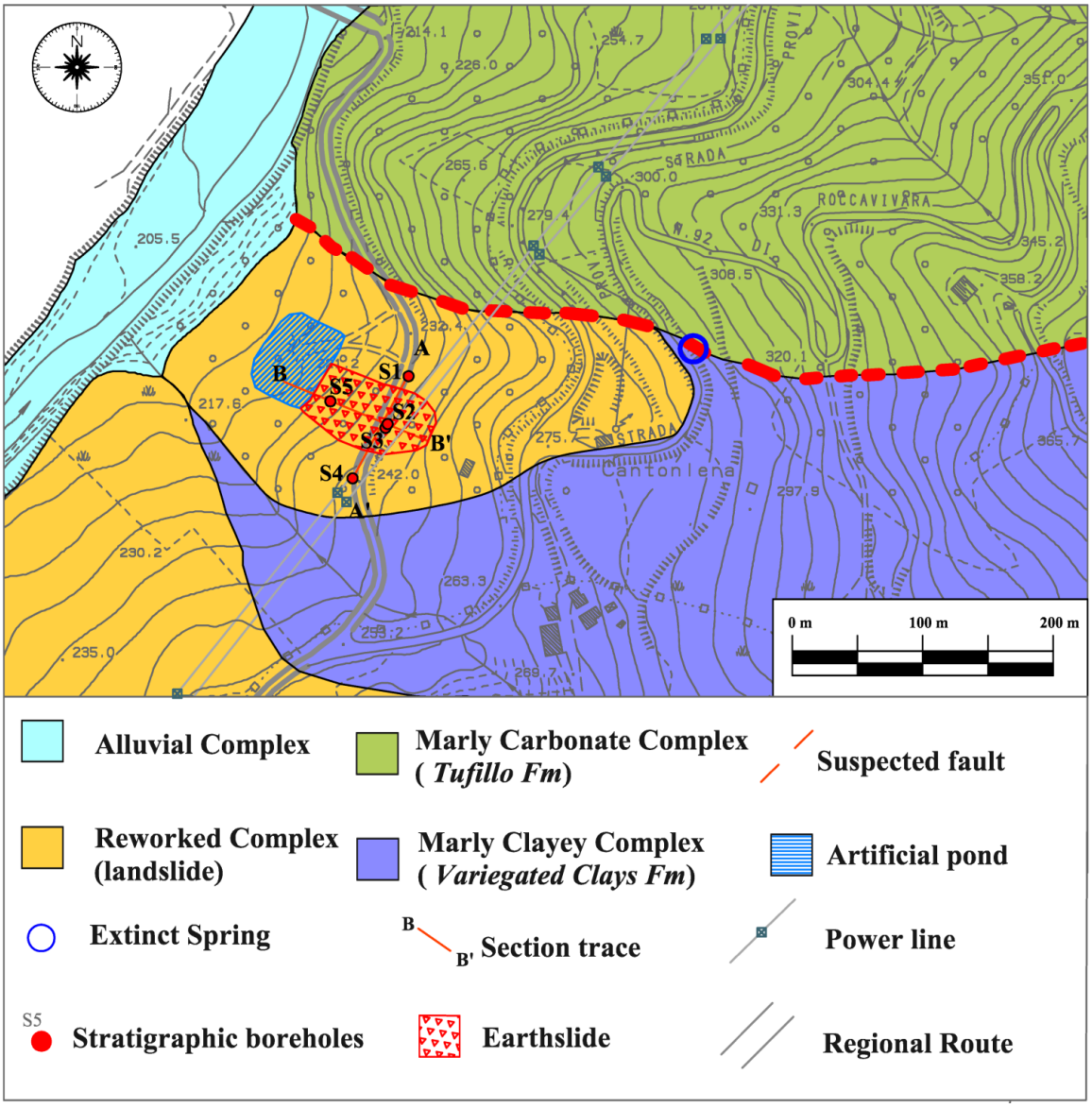

Figure 5.3. Geolithological Map of the area involved by the Roccavivara Earthslide.

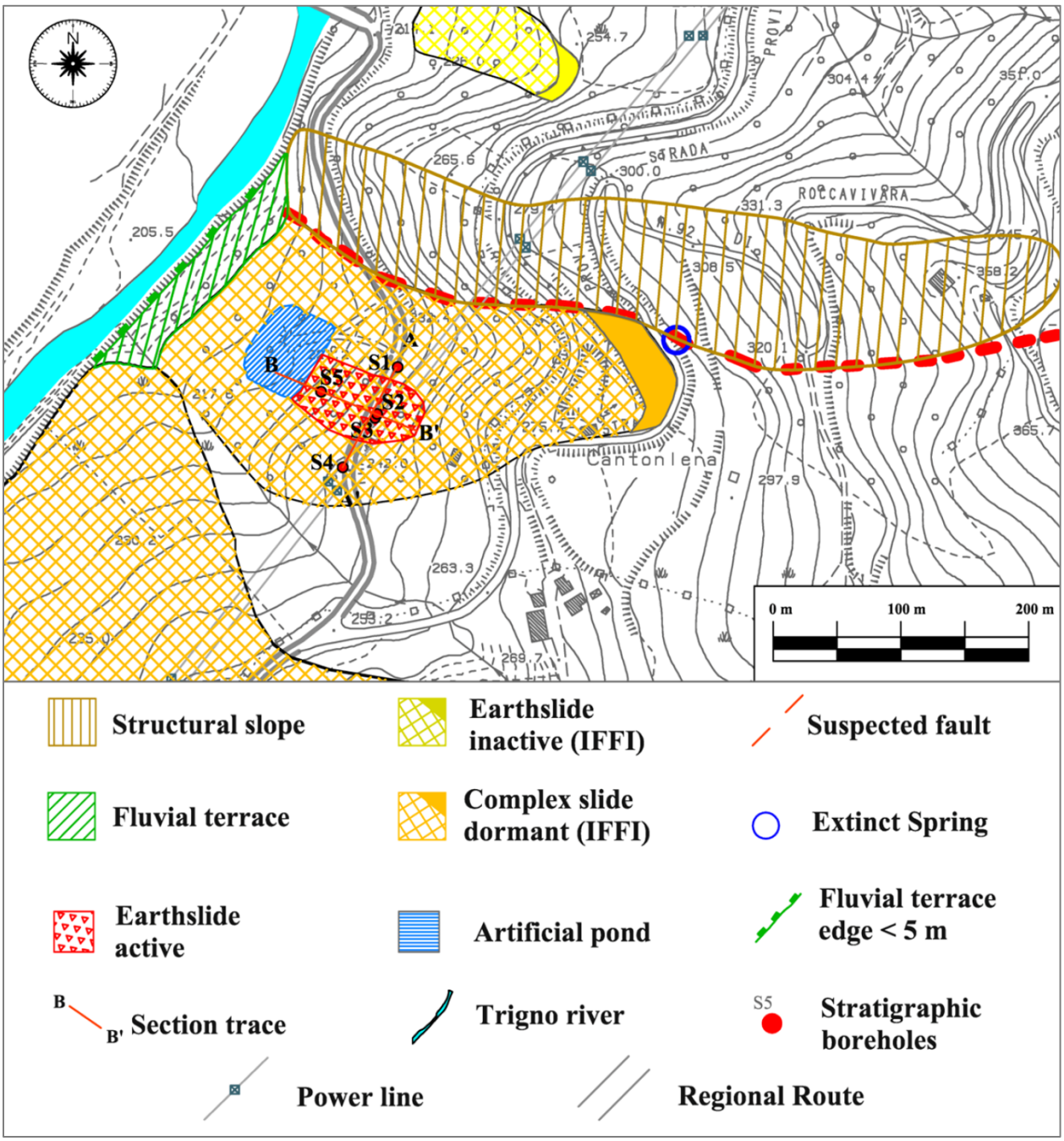

Figure 5.4. Geomorphological Map of the area involved by the Roccavivara Earthslide.

The local geological model of the landslide is pictured in the geological cross-sections shown in Figure 5.5 and is constituted of three main layers, which are bottom upward the intact bedrock, the weathered cover and shallower eluvium/colluvium. The bedrock is made of grey stiff clayey marls with scaly structure, which is overlied by a weathered cover of about 3-4 m thick of marly clays with a high water content, which, in turn is capped by a reddish-brown reworked

colluvium. The latter crops out with two main *facies*, a finer made of silty clays and a coarser made of sharp carbonate gravels in abundant clayey matrix. On the surface of the landslide numerous traction cracks are found, which also constitute preferential pathways of infiltration for the rainwater into the ground.

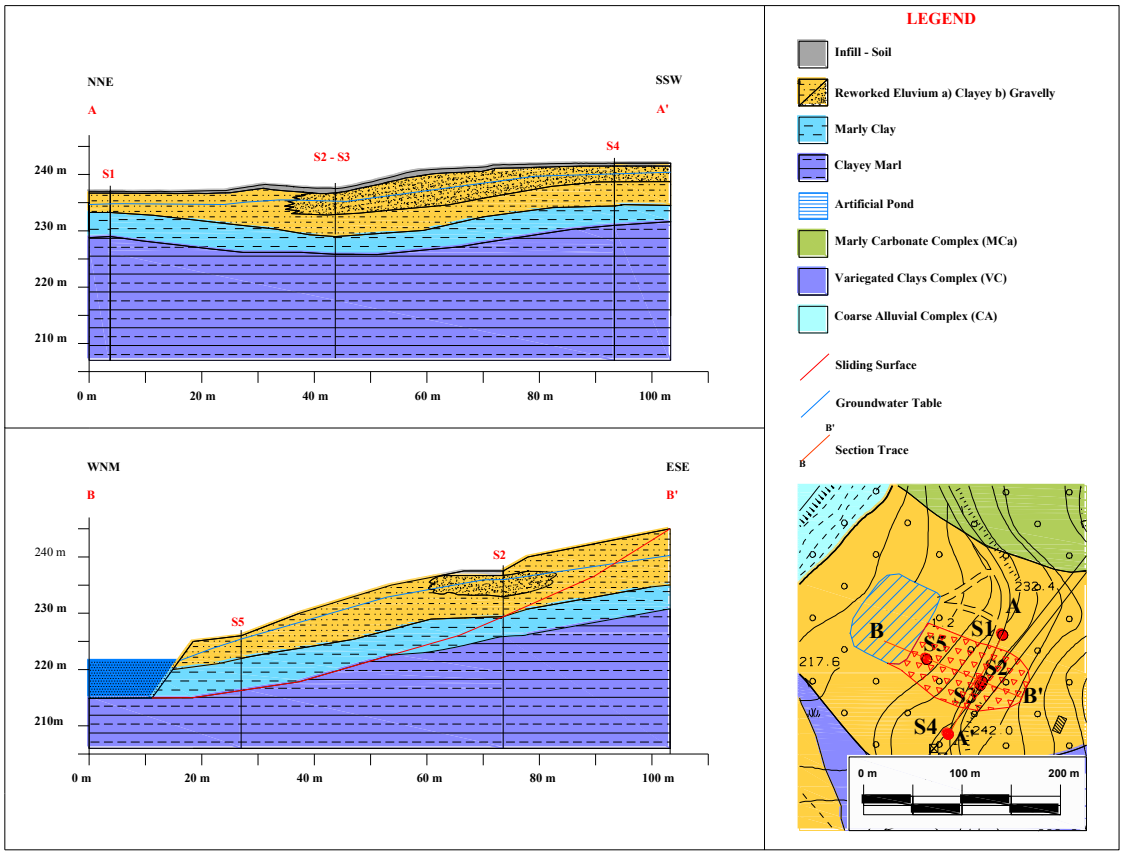

Figure 5.5. Geological cross-sections along the Roccavivara Earthslide. Section B-B' was employed in the following stability analyses.

5.2 GEOTECHNICAL CHARACTERIZATION

The investigation plan designed by Provincia di Campobasso consisted in three continuous stratigraphic boreholes and two destruction boreholes, one of which was adopted as piezometer (S5). In the other two (S2 - S3) a seismic cross - hole test was performed (CH). A total of six undisturbed soil samples for the physical properties and shear strength assessment were collected until the depths of 20.5 m; three were taken in the intact bedrock, two in the weathered cover and only one in the landslide mass (Figure 5.6). The testing program consisted of standard classification tests, unconfined compression strength tests and direct shear tests.

The grain size distributions of the three layers recognized within the Variegated Clays Complex (VC) are shown in Figure 5.7.

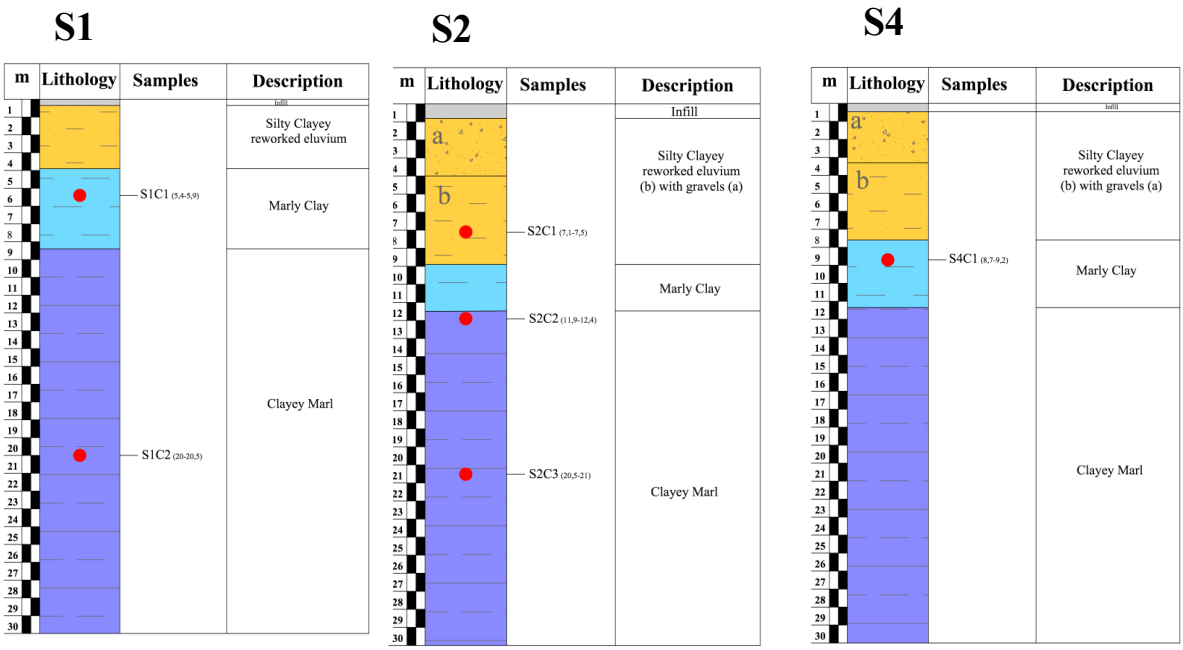

Figure 5.6. Stratigraphic logs and position of the undisturbed soil samples.

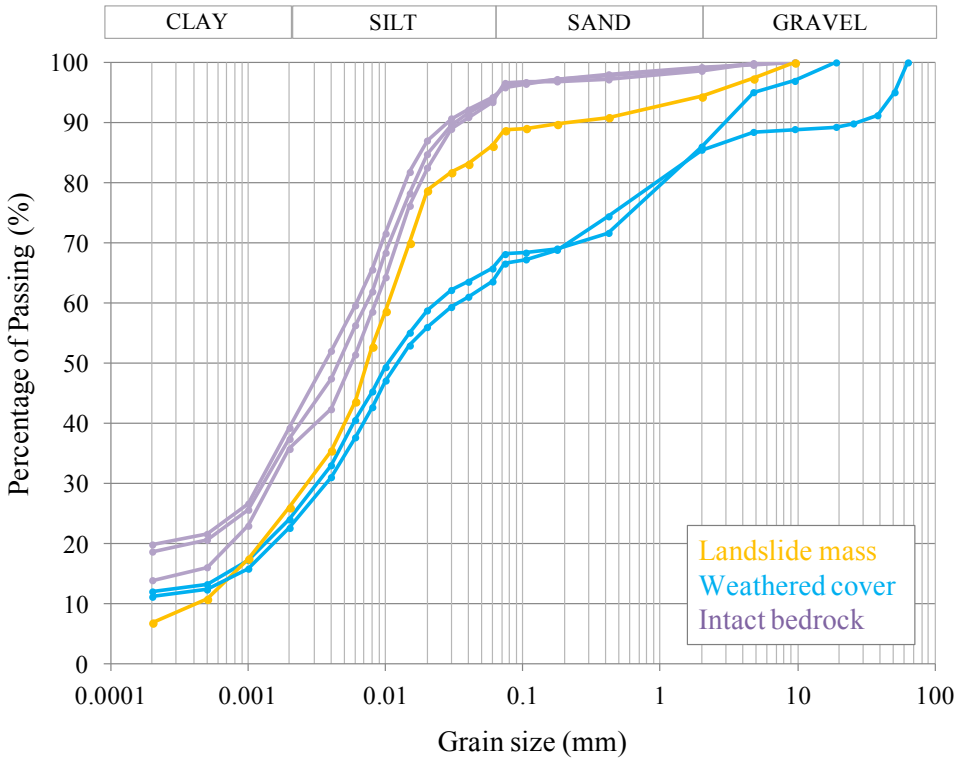

Figure 5.7. Particle size distributions of the three layer of Variegated Clays Complex (VC).

The overall values of the main physical properties and the values of the undrained shear strength (s_u) resulting from the unconfined compression strength test (UCS) are summarized in Table 5.1.

Table 5.1. Physical properties and UCS test.

Sample		S2 (C1)		S1 (C1)	S4 (C1)		S1 (C2)	S2 (C2)	S2 (C3)
γ_n (kN/m^3)	CLAYEY SILT	19.2	CLAYEY SILT WITH SAND	20.1	20.5	CLAYEY SILT	21.7	21.3	21.5
Sr (%)		96		76	85		82	99.6	80.2
Cu (kPa)		48		115	167		321	195	336

According to Figure 5.7 and Table 5.1, very little differences exist among the particle size distributions of the bedrock and landslide mass, which are very rich in silts, while the weathered cover presents a higher sandy content. The undrained shear strength (s_u) evidences a very low value for the landslide mass. The Figure 5.8 shows the variations of the Atterberg limits with depth, together with the average water content measured on each undisturbed sample. The values of plastic and liquid limits for the intact and weathered bedrock do not vary significantly with depth and they are characterized by middle plasticity, while the landslide mass is characterized by a higher plasticity as also shown in the plasticity chart of Figure 5.9. In all the layers, the natural water content is always below the plastic limit and the consistency index being always above unity. The results of the tests are in agreement and confirm the identification of a subsoil model constituted by three materials.

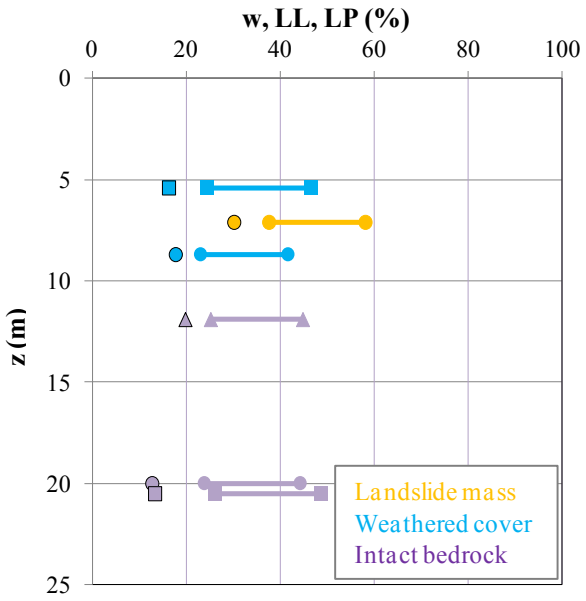

Figure 5.8. Vertical profile of Attemberg limits and natural water content.

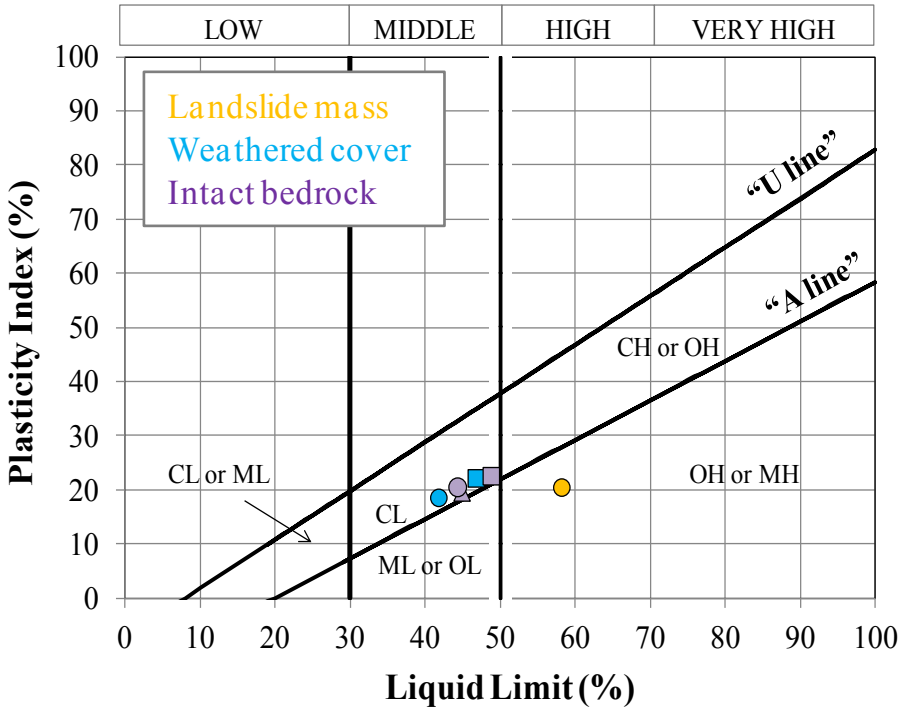

Figure 5.9. Casagrande plasticity chart

In Figure 5.10 the strength envelope of the three layers recognized in the Roccavivara landslide as coming from the direct shear tests are regressed through a linear ordinary least squares (OLS) technique, the resulting peak and residual strength values are also shown.

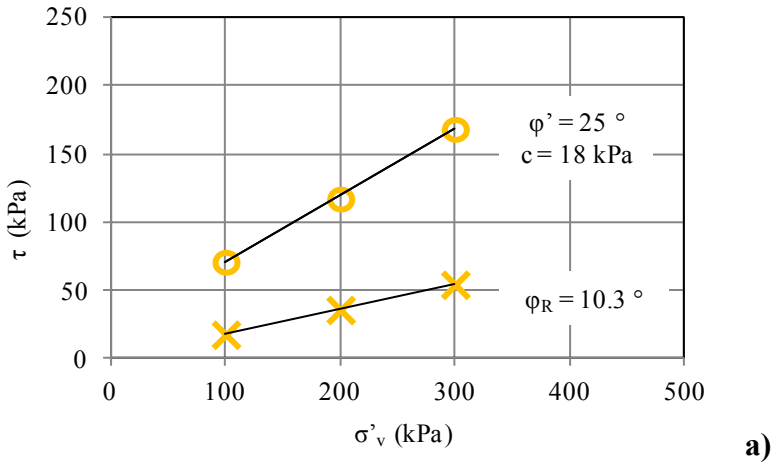

a)

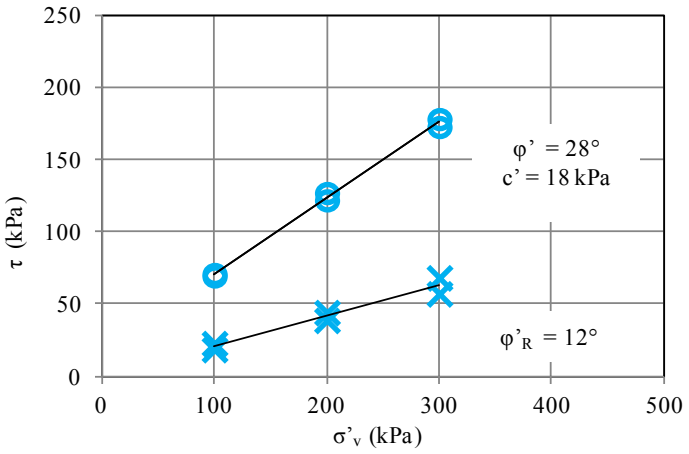

b)

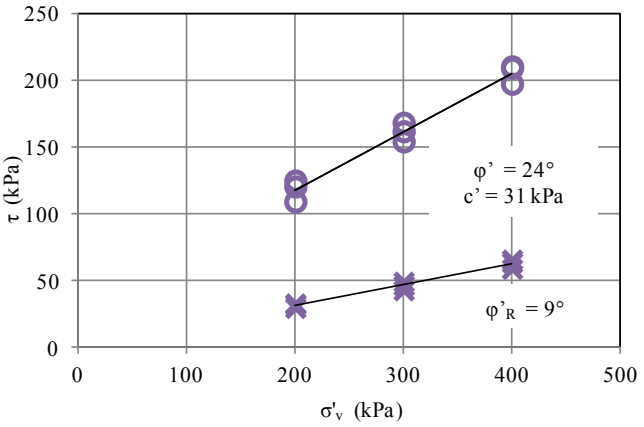

c)

Figure 5.10. Shear strength envelopes for the three layers: ***a)*** the landslide mass; ***b)*** weathered bedrock ***c)*** intact bedrock.

The seismic cross - hole test (CH) permitted to assess the soil stiffness and to evaluate the parameter V_{S30}, necessary for the identification of the seismic soil class as required by the seismic regulation in force (NTC, 2008). The results correlated with the stratigraphy of the S2 log are shown in Figure 5.11, the V_{S30} is 500 m/s, and hence the site can be classified as B class, according to the V_{S30} ranges also reported in Table 3.13.

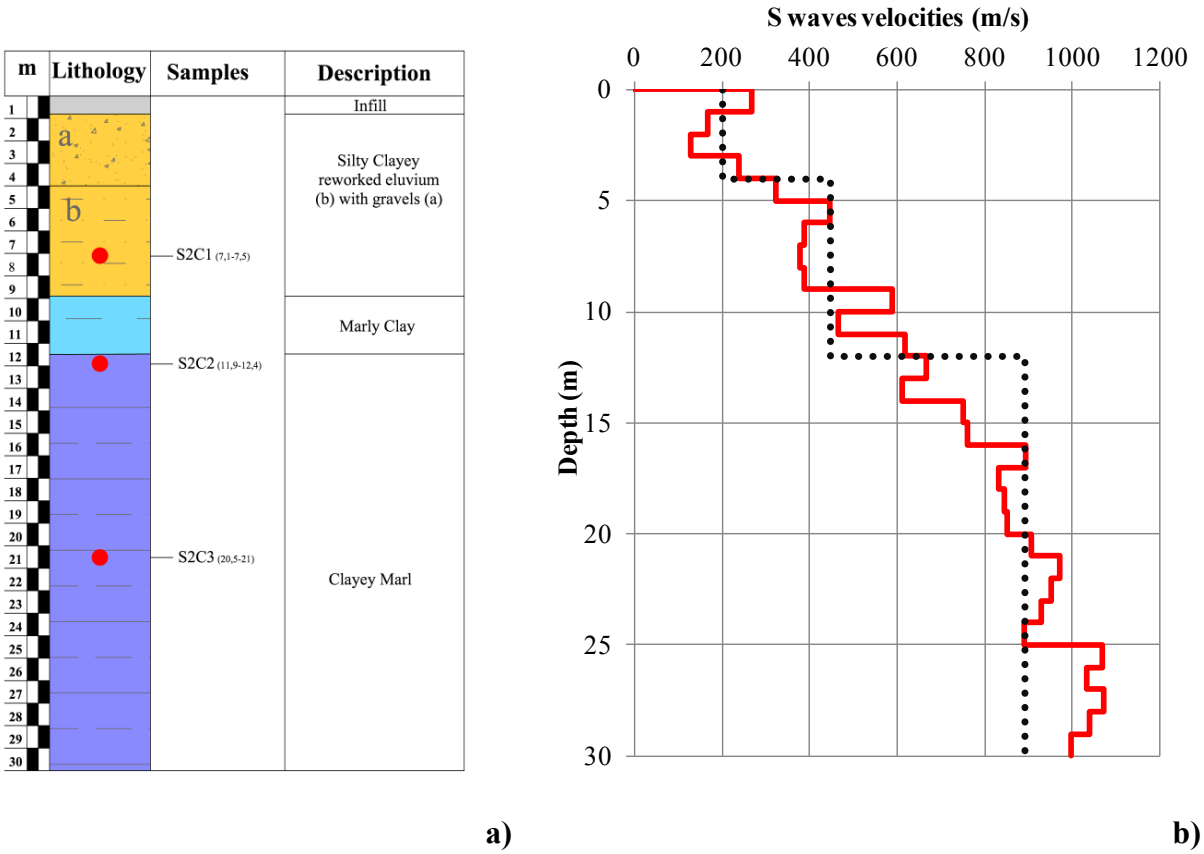

Figure 5.11. a) Stratigraphic log in the S2 borehole. ***b)*** Shear waves profile derived from the cross - hole test in S2 - S3 boreholes.

5.3 STABILITY ANALYSIS

The detailed analysis of the Roccavivara earthslide was aimed at evaluating the seismic behavior of the slope through the calculation of the permanent ground deformations and verifying the results coming from the II grade.

Two reference scenarios were considered; case I in which an earthquake occurred while the slope was in pre-failure setting, which is also the one referred into the II grade analysis and the case II of incipient failure. Those two conditions are regulated by variation of the depth of the groundwater table, coinciding with the two settings shown in Figure 5.12.

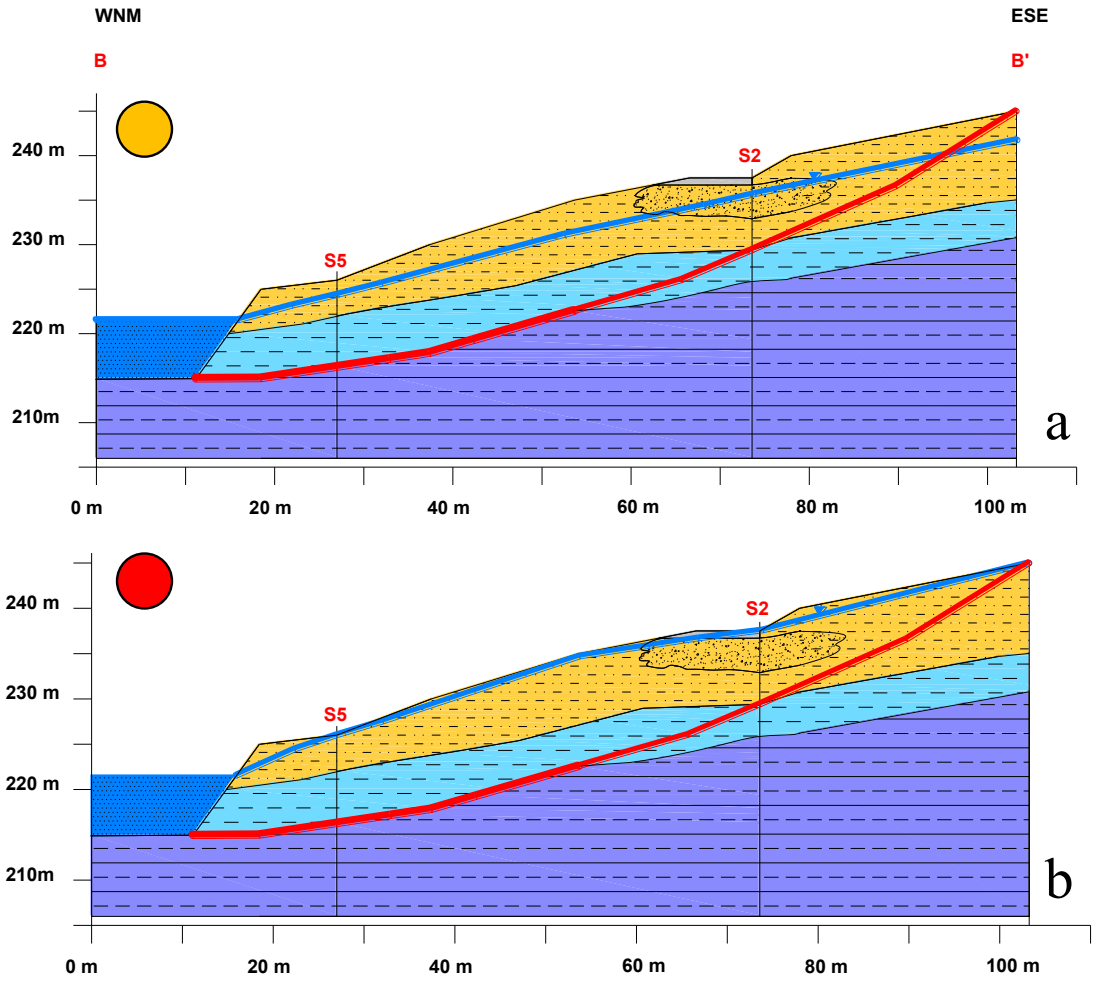

Figure 5.12. a) Groundwater table position in pre-failure conditions. ***b)*** Groundwater table position in incipient failure conditions.

The approach is the same as the one adopted for the small scale study reported in § 4.1, but the static stability analyses were carried out with the slices method, in particular the Fellenius (1936), Janbu (1954) and Bishop (1955) approaches were assumed.

The Fellenius method or Ordinary method together with Bishop satisfy only the moment equilibrium, but the former ignore all interslice forces, while the latter considers only normal interslice forces, neglecting the interslice shear force. Janbu method is quite similar to Bishop, but satisfies only horizontal force equilibrium, as opposed to moment equilibrium. The parameters adopted for the stability analysis are the peak strength values summarized in Table 5.2.

Table 5.2. Parameters adopted in the slope stability analysis

Material	γ' (kN/m^3)	φ' (°)	c' (kPa)
Landslide Mass	19.2	25	18
Weathered Cover	20.2	27.8	18
Intact Bedrock	Impenetrable		

The factor of safety (FS) was chosen as the mean value of the results of those three methods. In Figure 5.13 is shown the variation of the FS with the position of the groundwater table, which was considered as the height of water column above the slip surface (d_w) measured in the S2 boreholes of Figure 5.4 B-B', in which it represents the pre-failure height (6.6 m). The condition of limit equilibrium (FS = 1) is reached with an height of 8.1 m above the slip surface, which represents a condition of complete saturation with groundwater table located at field level. This setting is very likely, as confirmed by field investigation and interview with local people. In fact

upstream from the landslide there was a natural spring (see Figures 5.3 -5.4), which became extinct due to the construction of the roadway. The consequence was the depression of the spring outflow altitude and the groundwater feeding of the artificial pond located downstream.

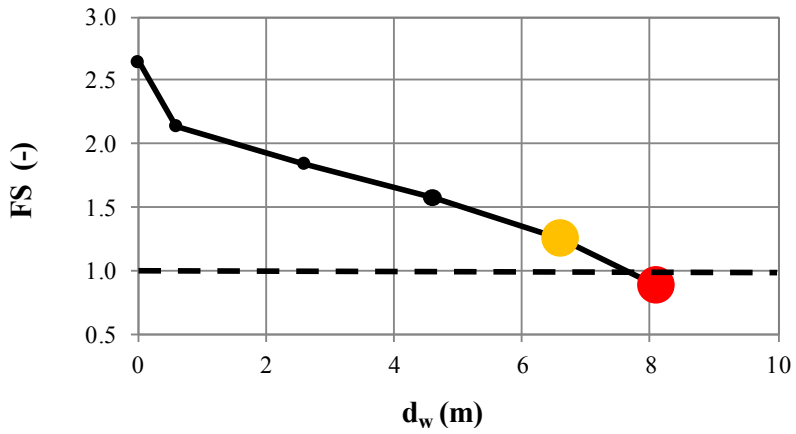

Figure 5.13. Variation of the Factor of safety (FS) with the height of the groundwater table (d_w) measured above the slip surface in S2 borehole; the yellow dot is representative of the pre-failure condition, while the red one is for failure condition.

The assessment of the slope stability in seismic condition was performed through the rigorous Newmark analysis as discussed in § 4.1.4, considering yield acceleration (a_c) calculated with the Eq. (4.1). The trend of a_c with the variation of the factor of safety in static conditions (FS) can be observed in Figure 5.14. For pre-failure condition the a_c is 0.07g, while for incipient failure conditions a very low value of 0.01g was attributed.

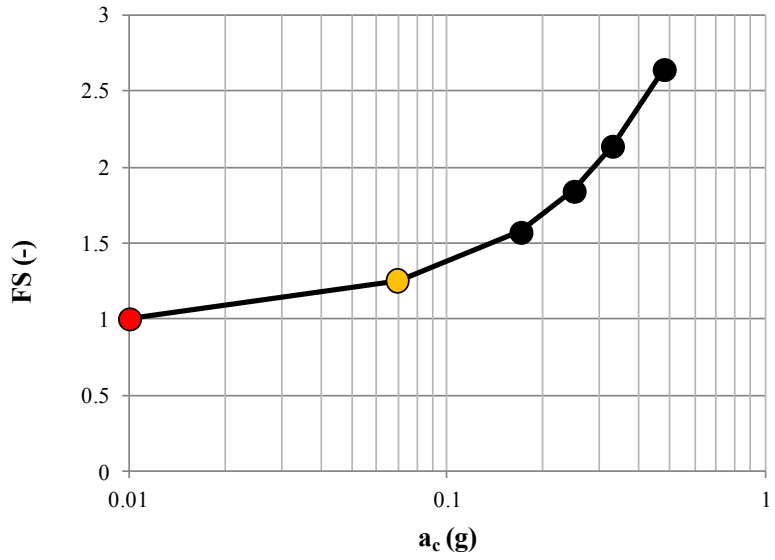

Figure 5.14. Variation of the yield acceleration (a_c) with the factor of safety (FS), the yellow dot is representative of the pre-failure condition, while the red one is for failure condition.

The seismic input for the analysis consisted in a set of 8 recorded accelerograms selected through the REXEL software (Iervolino et al., 2010). This tool permits to choose recorded time-histories of acceleration, whose average spectrum is compatible in broad period ranges, with the reference spectra of both the new Italian building code (NTC, 2008) and EC8 (2003). It ensures that individual records in the returned combinations have a spectral shape as much similar as possible to that of the target spectrum. This is the one employed in seismic design of above ground structures.

The target spectrum was built considering the value of peak ground acceleration (PGA) at Roccavivara site. Furthermore, it was considered the verification at "Collapse Limit State" for the interested infrastructure, that is the roadway, which possesses a nominal life of 50 years and is functional type III. REXEL also permitted to account for the site amplification of B class and the T1 topographic category, as resulted from the CH test and the mean slope value of 13°. The research of the dataset was guided by the most likely M - R (Magnitude and Distance) pairs given by the INGV disaggregation study (http://esse1-gis.mi.ingv.it/s1_en.php), which give the

pairs that mostly contribute to the seismic hazard of the area, which in this case are Magnitude (M) 4 ÷ 7 and Distance (R) 0 - 40 km.

Eight recorded accelerograms were selected from both the Italian Accelerometric Archive and the European Strong-Motion Database for normal fault earthquakes, in order to be coherent with the scenario selected for the II grade analysis. The selected records are summarized in Table 5.2 and Figure 5.15.

Table 5.2. Selected acceleration time-histories for the rigorous Newmark analysis.

EVENT	Station	PGA [g]	Mw	$D_{(5\text{-}95\%)}$ [s]	T_m [s]	R [km]	DATA
Kalamata 413ya	ST164	0.297	5.9	7	0.57	9	13.09.1986
Kalamata 414xa	ST163	0.24	5.9	5.2	0.6	11	13.09.1986
Umbria-Marche 594xa	ST60	0.524	6	5	0.21	11	26.09.1997
Irpinia 171ya	CLT	0.169	6.9	46.9	0.8	18.85	23.11.1980
Irpinia 178xa	RNR	0.094	6.9	49.6	0.57	35.58	23.11.1980
Irpinia 181xa	STR	0.225	6.9	39.5	0.67	33.26	23.11.1980
Irpinia 190xa	CTL	0.021	5	15	0.58	6.84	24.11.1980
Gran Sasso 928xa	AQA	0.056	5.4	5.4	0.44	12.05	-

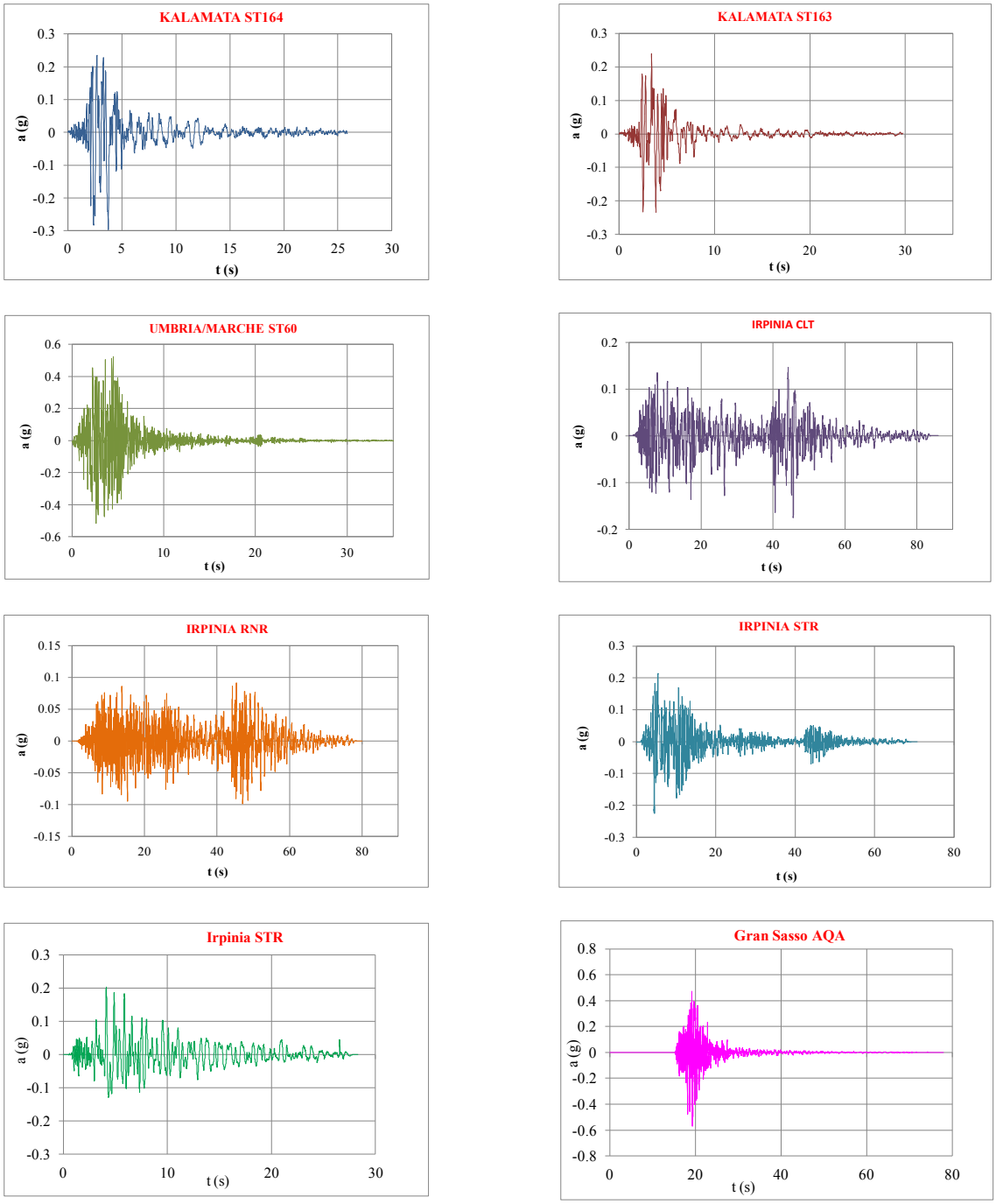

Figure 5.15. Acceleration time histories selected through the REXEL software adopted for the Newmark rigorous analysis.

The Newmark displacements were calculated for both the pre-failure and incipient failure scenarios and the results are shown in Figure 5.16 and 5.17.

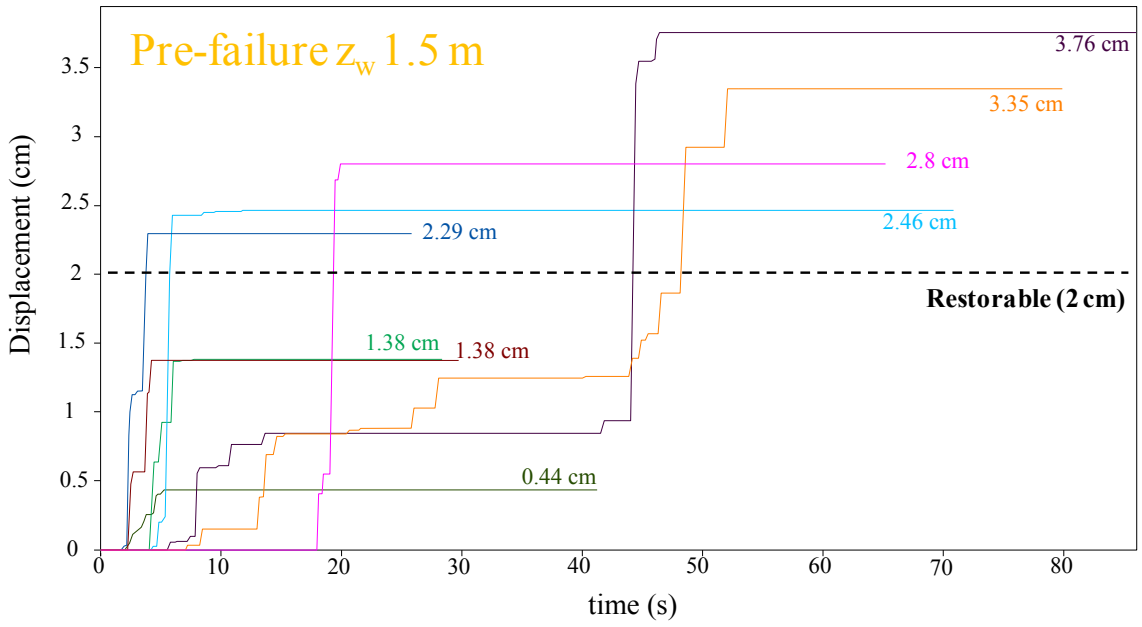

Figure 5.16. Cumulative displacements in pre-failure condition, with depth of the groundwater table (z_w) at 1.5 m b.g.l.

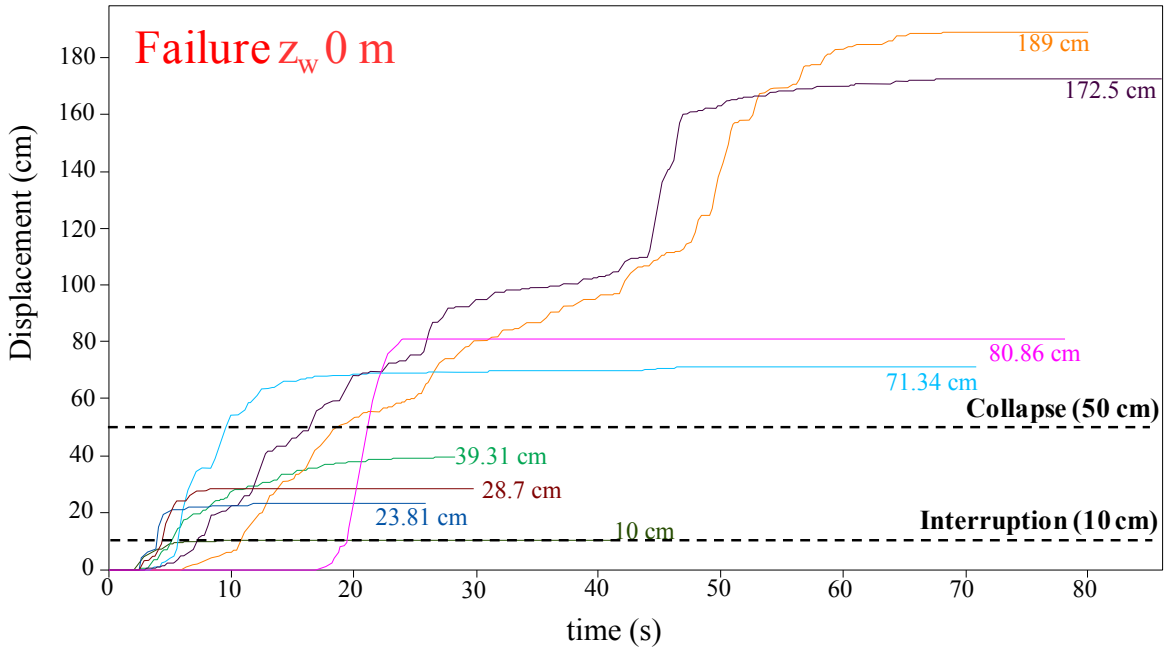

Figure 5.17. Cumulative displacements in failure condition, with depth of the groundwater table (z_w) at ground level.

The incipient failure condition reported as maximum displacements the value of 189 cm, furthermore in this condition all the selected records bypassed the "interruption" stage of the roadway vulnerability values reported in Table 4.2 by Silvestri et al. (2006). Half of them also exceed the "collapse stage". For the pre-failure conditions five accelerograms are in the field of "recoverable" damage.

In Figure 5.18 the obtained displacements values were compared with some of the main italian and international existing empirical relationships for the displacement assessment.

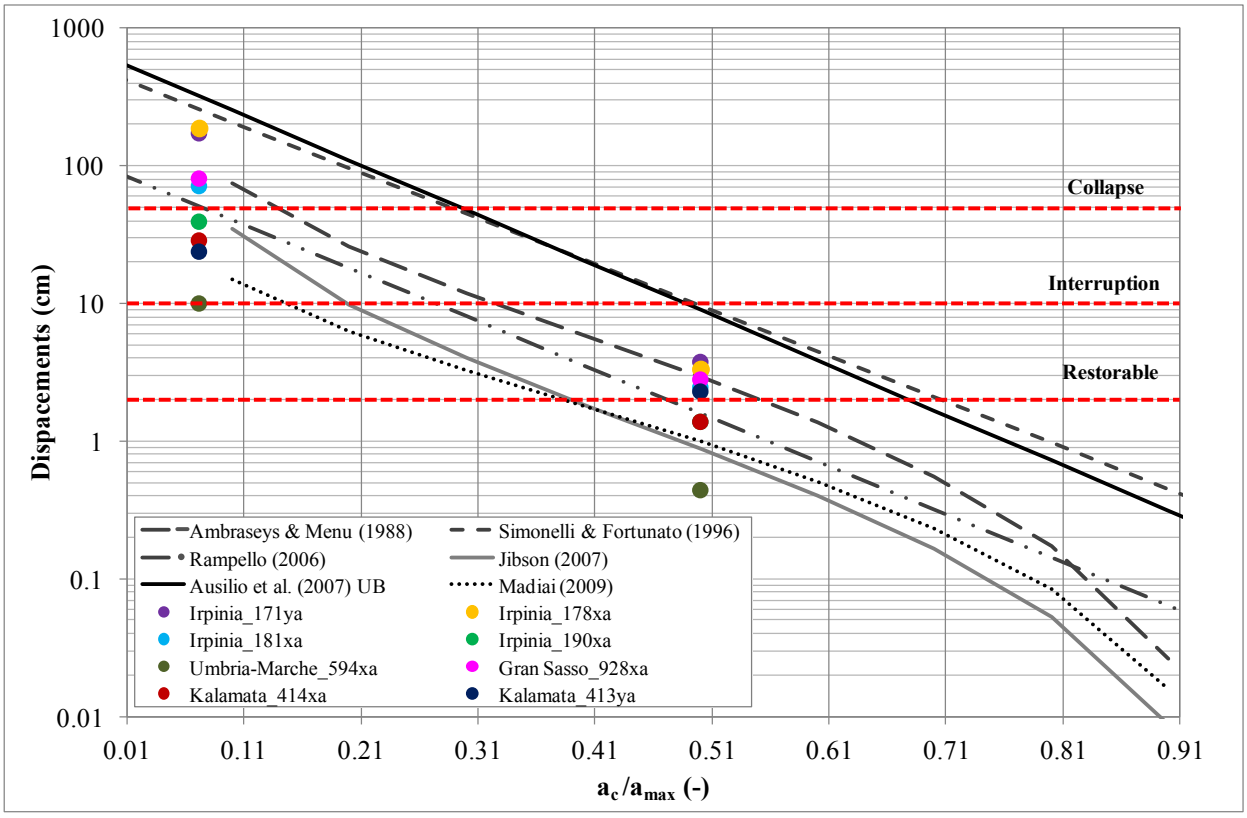

Figure 5.18. Comparisons of the cumulative displacements calculated with the rigorous Newmark method in pre-failure and failure conditions, with the main italian and international empirical relationships based on the acceleration ratio.

The comparison evidences that all the values are within the upper bound relationship of Ausilio et al. (2007), which confirms the trend already identified by Simonelli & Fortunato (1996). The

other relationships based on the mean value of the displacements differently match the several displacements calculated by the rigorous Newmark approach. Hence the choice to adopt in the II grade analysis an upper bound relationship appears well suited in the view of safety advantage.

Furthermore, the maximum value of 3.76 cm resulted from the double integration of the accelerations time-histories was compared with the results of the II grade displacements for the site of the Roccavivara earthslide. In this case the landslide perimeter occupies four pixels (see Figure 5.19), whose mean, weighted for the area of each pixel, resulted in a total value of 4.75 cm, which is well matched with the value obtained from the rigorous analysis. This evidence validates the results of both approaches.

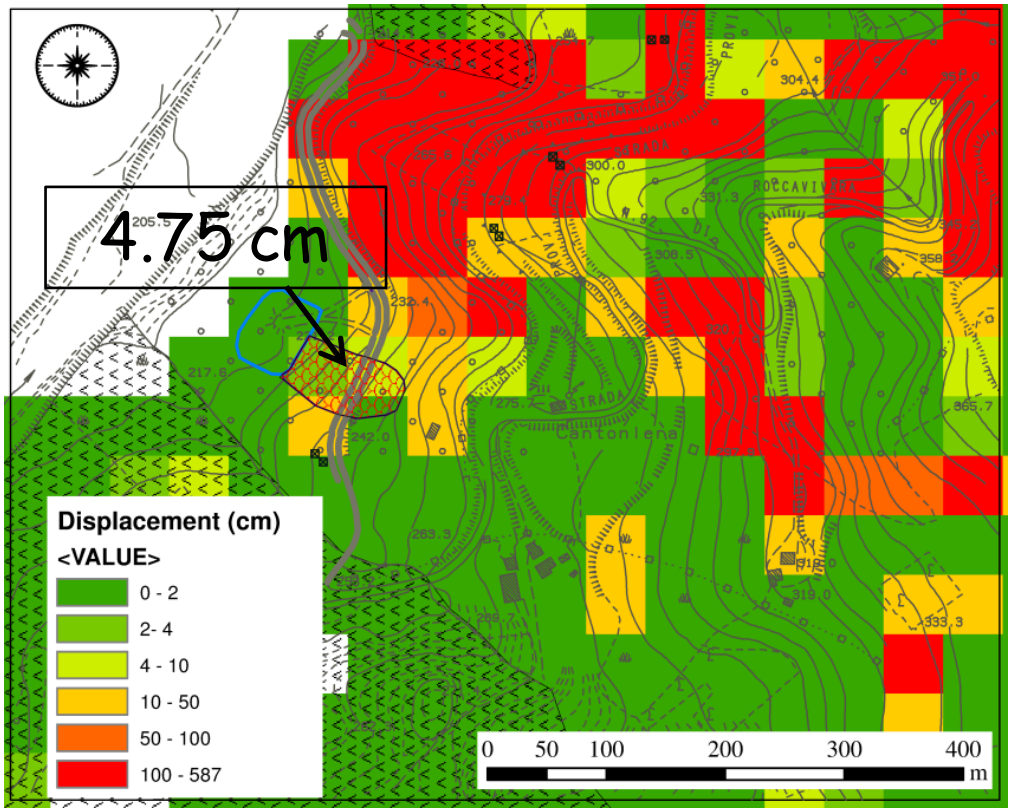

Figure 5.19. Results of the permanent ground deformations map (50x50 m) produced with the II grade approach for the Roccavivara Earthslide, with the value of the mean displacements weighted for the area of the occupied pixel.

Finally the vulnerability of the roadway is calculated adopting the fragility curves shown in Figure 4.5, for the pre-failure, incipient failure and also for an intervention scenario, in which the groundwater level is drained and lowered of 2 m. A synthesis of the results is presented in Table 5.3.

Table 5.3. Results of the vulnerability analysis for the pre-failure, failure and intervention scenario

	d_w (m)	F	a_c (g)	Max Displacement (cm)	P (d>DS4) %	P (d>DS3) %	P (d>DS2) %
Pre-failure	6.6	1.25	**0.07**	**3.8**	**0**	**0.14**	**2.36**
Failure	8.1	1.00	**0.01**	**189.0**	**94**	**99**	**99**
Intervention	4.6	1.578	**0.17**	**0.0**	**0**	**0**	**0**

The results point out very high probabilities of overcoming the three damage states for the failure conditions, very low probabilities for the pre-failure and no probabilities after the intervention.

This unfavorable condition, derived by the analytical approach here reported, well matched the real described scenario, where a landslide is present at Roccavivara site, with no seismic condition.

SUMMARY AND CONCLUSIONS

This thesis dealt with one of the main side-phenomena, which can occur during or after a seismic event, namely earthquake-triggered landslides. These phenomena involve both natural and man-made slopes, whose occurrence is very common and widespread as testified by several recent earthquakes. Their consequences can be dramatic, as they can strongly contribute to the death toll, since they often affect buildings and infrastructures, preventing effective post-emergency strategies. Hence it appears relevant to consider earthquake-induced landslides into the framework of seismic risk, which can also be carried out from regional to the scale of the single slope.

The area selected for this thesis is the Molise Region, (Central-Southern Italy) within the Southern Apennines, which is one of the Italian areas struck by earthquakes in the last decade, suffering damages both in building heritage and physical environment. It is characterized by medium-high seismicity and high landslide susceptibility. In particular, the most abundant landslides are represented by *coherent landslides*, i.e. rotational and translative slides, on which this dissertation focused.

The main issues concerned with the prediction of permanent displacements, as an index with the field performance of slope in seismic conditions.

An essential part of this work was devoted to the collection and organization of the pre-existing information on the geological and mechanical features of the outcropping terrains. A database of geological and geotechnical investigations was organized, since every territorial analysis requires a background knowledge. It dealt with *structurally complex formations*, which are defined as middle term between soils and rocks and show an *en masse* behavior strongly depending on the scale of heterogeneities and discontinuities, but also on the scale of the problem. Such materials

extensively crop out not only in Molise, but also along the whole Apennine chain and in many other Countries. They are characterized by high density of slope instabilities, which are dependent on the shear strength of the clayey layers. The collected dataset permitted the characterization of the physical and mechanical properties of those finer portions, which were resulted in agreement with the value retrieved in the scientific literature. As expected by literature the obtained results, in terms of φ', c', s_u and γ were attributed to homogeneous geolithological complexes and not to the single geological formation, in order to give the opportunity of adopting these values in analog geological contexts even if in different geographical areas. The reliability of each parameter was assessed through the adoption of a coefficient of variation (CV), which permitted to compare data series, which can also present very different order of magnitude. The most variable parameters resulted in the true cohesion (c') and the undrained shear strength (s_u).

The collected downhole tests (DH) permitted to focus on the validation of some of the main seismic soil classification approaches at regional scale. In particular the methods proposed by USGS based on the slope angle and INGV based on simplified surface geology were tested. The main result is a, slight but steady,V_{S30} overestimation of slope-based method (USGS), which becomes even larger for the INGV method. This evidence in terms of site amplification means underestimation of the likely seismic shaking. Hence, a new geology-based map for seismic soil class was built up on the basis of the experimental evidence and the homogeneous complexes detected. The obtained tool is then useful for the small scale estimation of ground motion amplification at site, not only in the Molise Region, but eventually, it can be exported in the rest of the Italian Apennines, because of the similar geolithological settings.

The relationship between simple geotechnical parameters, namely N_{SPT} and V_S was explored and new empirical correlations, which account for the structured features of these deposits, were proposed. This process was based on the analysis of lithostratigraphic properties of the

geolithological complexes outcropping in the area. In this way, three different correlations were produced and related to the main detectable lithofacies, namely Structured Soils Deposit (SSD), All soils (AS), and Weathered soils (WS). Even if only a sector of the Apennine chain is concerned, the proposed correlation could reasonably be applied in different sector of the same chain or in similar geological terrains whenever the uncertainties and the features of this simplified tool fit the aim of the analysis and the scale of the engineering problem of interest.

The zoning at Grade II developed in this work dealt with the elaboration of thematic maps that pictured the vulnerability of physical environment on regional scale. In this context, the natural slope instability due to seismic events and their impact on the roadway network is accounted. Two approaches were developed: a simplified geomorphologic approach, which did not rely upon the database of geotechnical test collected, and a more rigorous dataset-based approach.
The first is based on a geomorphological-geotechnical coupled approach, which was implemented in a GIS environment. It was based on a 200x200 m DEM and the strength parameters were attributed on the basis of the relative erodibility of each geolithological complex. The results given by this simplified approach were compared with another widespread simplified procedure, which is the HAZUS method. It is evidenced a linear decreasing trend of the critical acceleration with the slope, while HAZUS presents a stepwise trend, due to its well-known approach. In all the classes, the saturated conditions of this study give the lowest and most safety values. In dry conditions, every geological class at very low angles of slope presents higher yield acceleration values, but increasing the steepness at the slope threshold respectively of 25° (B class) and 10° (C class), the results are more safety than the ones of Hazus. The maps obtained from this approach, in terms of permanent displacements were inserted in vulnerability functions to assess the performance of the roadway network. They were also adopted in a study with the partnership of the Campobasso district for the definition of the intervention priorities in

the seismic vulnerability assessment of 13 masonry bridges, through the compilation of a euristic weighted method.

The engineering geology approach was based on the soil strength characterization and a 50x50 m DEM. The implemented procedure presents interesting elements of novelty, which updates the pre-existing approaches. In particular, the strength parameters were differentiated to account for cohesive and frictional soils behavior. In the first case the undrained shear strength s_u was adopted, while in the second, the classical Mohr-Coulomb φ' and c' parameters were employed. The seismic input was modified for both stratigraphic amplification and topographic amplification, following the most recent seismic codes in force. The first was reliant on both soil class and PGA, while the second considered both amplification and deamplification as function of the cliff shapes, through the parameter curvature, which can be easily developed at territorial scale.

The permanent displacements maps give an accurate picture of the areas that can be most likely affected by landslides in the selected shaking scenario. The method adopted is effective to characterize the seismic slope behavior, and can be improved in order to quantify PGD in a "performance based design" approach. It can be adopted as planning and zoning tools, permitting to quantify critical areas and to identify intervention priorities, in which to increase the degree of knowledge and analysis.

Finally, a detailed seismic slope stability analysis at grade III was carried out to compare and validate the results obtained in the II grade engineering geological approach.

The investigated phenomenon affected a neighboring roadway and is typical of the landslides, which seasonally occur in Molise. The geological and geomorphological features were retrieved by field surveys and permitted to identify the subsoil model, which was validated by the geotechnical characterization by laboratory tests of the soil samples. The stability analysis was

performed solving the rigorous Newmark approach for two static slope conditions, which are pre-failure and incipient failure. The calculated displacements on eight recorded accelerograms resulted differently matched by the several literature relationships, but all of them resulted contained by the chosen upper bound relationship. Furthermore, the maximum value of displacement retrieved by the rigorous Newmark analysis is in agreement with the results of the II grade study. Hence the choice to adopt in the II grade analysis an upper bound relationship appears well suited in the view of safety advantage.

REFERENCES

Akin, M. K., Kramer, S. L., Topal, T., (2011). *Empirical correlations of shear wave velocity (Vs) and penetration resistance (SPT-N) for different soils in an earthquake-prone area (Erbaa-Turkey).* Engineering Geology 119, 1-17.

ALA, American Lifeline Alliance. (2001). *Seismic fragility formulations for water system*. American Society of Civil Engineers (ASCE) and Federal Emergency Management Agency (FEMA).

Ambraseys N.N. (1988). *Engineering seismology*. Earthquake Engineering and Structural Dynamics, 17, 1-105.

Ambraseys, N.N., Menu, J.M., (1988). *Earthquake-induced ground displacements*. Earthquake Engineering and Structural Dynamics, 16, 985–1006.

Ambraseys, N.N. (1995). *The prediction of earthquake peak ground acceleration in Europe*. Earthquake Engineering and Structural Dynamics, 24(4), 467-490.

Ambraseys, N. Srbulov, M. (1995). *Earthquake induced displacement of slopes*. Soil Dynamics and Earthquake Engineering 14, 59-71.

Anbazhagan, P., Parihar, A., Rashmi, H.N., (2012). *Review of correlation between SPT-N and shear modulus: a new correlation applicable to any region*. SoilDyn and EarthqEng, 36, 52-69.

Andrighetto R. (1994). *Applicazione di sistemi informativi geografici (GIS) a problematiche di rischio e vulnerabilità in zone sismiche*. Relazione finale, CNR-GNDT / IG, ottobre 1994.

Argyroudis, S., Pitilakis, K. (2012). *Seismic fragility curves of shallow tunnels in alluvial deposits*. Soil Dynamics and Earthquake Engineering, 35, 1-12.

Arias, A., (1970). *A measure of earthquake intensity*, in Hansen, R.J. (Editor), Seismic design for nuclear power plants: Massachusetts Institute of Technology Press, Cambridge, Mass., 438-483.

Aucelli, P.C., Robustelli, G., Rosskopf C.M., Scarciglia F., Di Paola, G., Lucà, F. (2010). *Geomorphological Map of the area between Frosolone and Trivento (Molise, Italy)*. Journal of Maps,6,1, 423-434.

Aucelli, P. C., Amato, V., Cesarano, M., Pappone, G., Rosskopf, C.M., Russo Ermolli, E., Scarciglia, F. (2011). *New morphostratigraphic and chronological constraints for the*

Quaternary paleosurfaces of the Molise Apennine (Southern Italy). Geologica Carpathica, 62, 1, 17-26.

Aucelli, P.C., Casciello, E., Cesarano, M., Perriello Zampelli, S., Rosskopf, C.M. (2013). *A deep, stratigraphically and structurally controlled landslide: The case of Mount La Civita (Molise, Italy).* Landslides, DOI 10.1007/s10346-012-0351-7

Ausilio E., Silvestri F., Troncone A. Tropeano G. (2007). *Seismic displacement analysis of homogeneous slopes: a review of existing simplified methods with reference to Italian seismicity*. IV ICEGE, Thessaloniki.

Barnhardt, W.A., Kayen, R.E. (2000). *Radar Structure of Earthquake-Induced, Coastal Landslides in Anchorage, Alaska.* Environmental Geosciences, 7, 1, 38-45.

Bernard, P. Zollo, A.: (1989). *The Irpinia (Italy) 1980 earthquake: detailed analysis of a complex normal faulting.* J. Geophys. Res. 94(B2), 1631–1647.

Bindi, D., Pacor, F., Luzi, L., Puglia, R., Massa, M., Ameri, G., Paolucci, R. (2011). *Ground motion prediction equations derived from the Italian strong motion database.* Bull. Earthquake Eng., 9, 1899-1920.

Biondi G., Condorelli A., Mussumeci G., Maugeri M. (2004). *Il metodo degli spostamenti nella valutazione in ambiente GIS del rischio sismico di frana su vasta scala*. IARG, Incontro Annuale dei Ricercatori di Geotecnica, Trento, 7-9 luglio 2004.

Bishop, A.W. (1955). *The Use of the Slip Circle in the Stability Analysis of Slopes*. Geotechnique, Great Britain, 5, 1, 7-17.

Boiano, U. (2000). *La Formazione torbiditica di S. Bartolomeo (Appennino meridionale): revisione litostratigrafica, analisi sedimentologica ed implicazioni sui caratteri dei bacini legati a prismi di accrezione.* Boll. Soc. Geol. It., 119, 39-62.

Bommer, J., Rodríguez, C.E., 2002. *Earthquake-induced landslides in Central America*. Engineering Geology 63, 189–220.

Boni A., Casnedi, R., Centamore, E., Colantoni, P., Cremonini, G., Elmi, C., Monesi, A., Selli, R., Valletta, M. (1969). *Note illustrative della Carta Geologica d'Italia alla scala 1:100.000 S. Severo*, Servizio Geologico d'Italia, 46 pp.

Bozzano, F., Martino, S., Naso, G., Prestininzi, A., Romeo, W.R., Scarascia-Mugnozza, G. (2004). *The Large Salcito Landslide Triggered by the 2002 Molise, Italy, Earthquake*. Earthquake Spectra, 20, S1, S95–S105.

Bozzano, F., Lenti,L., Martino, S., Paciello,A., Scarascia-Mugnozza, G. (2008). *Self-excitation process due to local seismic amplification responsible for the reactivation of the Salcito landslide (Italy) on 31 October 2002*. Journal of Geophysical Research, 113, B10312, 1-21.

Bracone, V., Amorosi, A., Aucelli, P.C., Rosskopf, C.M., Scarciglia, F., Di Donato, V., Esposito, P. (2012a). *The Pleistocene tectono-sedimentary evolution of the Apenninic foreland basin between Trigno and Fortore rivers (Southern Italy) through a sequence stratigraphic perspective*. Basin Research, 24, 213-233.

Bracone, V., Amorosi, A., Aucelli, P.C., Ciampo, G., Di Donato, V., Rosskopf, C. M.(2012b). *Palaeoenvironmental evolution of the Plio-Pleistocene Molise Periadriatic Basin (Southern Apennines, Italy): insight from Montesecco Clays*. Ital. J. Geosci. (Boll. Soc. Geol. It.), 131, 2, 272-285.

Brancaccio, L., Cinque, A., Di Crescenzo, G., Santangelo, N., Scarciglia, F. (1997). *Alcune osservazioni sulla tettonica quaternaria nell'alta valle del f. Volturno (Molise)*. Il Quaternario, It. Jour. Quat. Sci, 10 (2), 321-328.

Brancaccio, L., Di Crescenzo, G., Rosskopf, C.M., Santangelo N., Scarciglia F. (2000). *Geological map of Quaternary deposits and geomorphological map of the Volturno river valley (Molise, southern Italy)*. Descriptive notes. Quaternario, Ital. J. Quat. Sci. 13, 1-2, 81-94.

Bray, J. D., Rathje, E. M., (1998). *Earthquake-induced displacements of solid-waste landfills*. J. Geotech. Geoenviron. Eng. 124, 242–253.

Building Seismic Safety Council, BSSC. (2001). *NEHRP Recommended Provisions for Seismic Regulations for New Buildings and Other Structures,* FEMA 368, Part 1, (Provisions): developed for the Federal Emergency Management Agency , Washington D.C.

Butcher, G.W., Beetham, R.D., Millar, P.J., Tanaka, H. (1993). *The Hokkaido-Nansei-Oki Earthquake - Preliminary report of the NZNSEE Reconnaissance Team.* Bulletin of the New Zeland National Society for earthquake engineering, 26, 3, 284-291.

Calcaterra, D., Ramondini, M., Di Martire, D. (2006). *Studi preliminari sulla frana di Colle Lapponi - Piano Ovetta nel Comune di Agnone (IS).* IARG, Incontro Annuale dei Ricercatori di Geotecnica, Pisa, 26-28 Giugno 2006.

Casnedi, R., Crescenti, U., D'Amato, C., Mostardini, F., Rossi, U. (1981). *Il Plio-Pleistocene nel sottosuolo molisano*. Geol. Romana, 20, 1‑42.

Cello, G., Paltrinieri, W., Tortorici, L. (1987). *Caratterizzazione strutturale delle zone esterne dell'Appennino molisano.* Mem. Soc. Geol. It., 27, 44-50.

Cello, G., Mazzoli, S. (1999). *Apennine tectonics in southern Italy: A review.* Journal of Geodynamics 27, 191–211.

Cherubini, C., Giasi, C.I., Guadagno, F.M. (1989). Il coefficiente di spinta a riposo delle argille azzurre subappennine di Matera. Rivista Italiana di Geotecnica, 4/1989.

Chigira, M., Wu, X., Inokuchi, T., Wang, G. (2010). *Landslides induced by the 2008 Wenchuan earthquake, Sichuan, China.* Geomorphology, 118, 225-238.

Chiodo, G., Dramis, F., Gervasi, A., Guerra, I., Sorriso-Valvo, M. (1999). *Frane sismo-indotte e pericolosità di sito: primi Risultati dello studio degli effetti di forti terremoti Storici in calabria centro-settentrionale*. GNGTS, Atti del 18° Convegno Nazionale / 13.07.

Cinque, A., Patacca, E., Scandone, P., Tozzi, M. (1993). *Quaternary kinematic evolution of the Southern Apennines. Relationships between surface geological features and deep lithospheric structures.* Spec. Issue on the Workshop: «Modes of crustal deformation: from the brittle upper crust through detachments to the ductile lower crust» (Erice, 18-24 November 1991), Ann.Geofis., 36, 249-260.

Civita, M., Govi, M., Maugeri, M. (1985). *La franosità dei versanti nella valutazione del rischio sismico globale. Indagini sul terremoto del Friuli (1976)*. Geologia applicata e Idrogeologia, 20 (II), 503-530.

Cocco, E., Pescatore, T. (1968). *Scivolamenti gravitativi (olistostromi) nel flysch del Cilento (Campania).* Boll. Soc. Nat. Napoli, 9, 102 pp.

Cocco, E., Cravero, E., Ortolani, F., Pescatore, T., Russo, M., Sgrosso, I., Torre, M. (1972). *Les faciès sedimentaires miocènes du Bassin Irpinien (Italie Meridionale).* Atti dell'Accademia Pontaniana, Volume XXI, International Symposium on the flysch problems, Sedimentological Commission of the CBGA, Sofia 14-26 October 1972 (*In French*).

Colleselli, F., Colosimo, P. (1977). Comportamento di argille Plio-Pleistoceniche in una falesia del litorale adriatico. Rivista Italiana di Geotecnica 1/77.

Comegna, L. (2005). Proprietà e comportamento delle colate in argilla. Ph. D. thesis.

Corbi, I., De Vita, P., Guida, D., Guida, M., Lanzara, R., Vallario, A. (1999). *Evoluzione geomorfologica a medio termine del vallone in località Covatta (bacino del fiume Biferno, Molise).* Geogr. Fis. Din. Quat., 22.

Corniello, A., Santo, A. (1994). *Geologia e fenomeni gravitativi nell'area dell'alto corso del fiume Trigno (Molise).* Geol. Rom., 30, 67-74.

Cotecchia, V., Guerricchio, A., Melidoro, G. (1986a). *The Geomorphogenetic Crisis Triggered by the 1783 Earthquake in Calabria (Southern Italy)*. Proceedings of the International Symposium on Engineering Geology Problems in Seismic Areas, Bari, Italy, 6, 245–304.

Cotecchia, V., Del Prete, M., Federico, A., Fenelli, G.B., Pellegrino, A. E, Picarelli, L. (1986b). *Studio di una colata attiva in formazioni strutturalmente complesse presso Brindisi di Montagna Scalo (PZ)*. XIV Convegno Italiano di Geotecnica, Bologna, 1, 253-264.

Cotecchia V., Melidoro G. (2002). *Movimenti franosi nel comune di Petacciato (CB) – Studi, rilevamenti dell'area in frana, indagini e orientamenti progettuali*. Incarico Presidenza Consiglio dei Ministri ‐ Dipartimento Protezione Civile ‐ Presidenza Regione Molise.

Cotecchia, F., Mitaritonna, G., Lollino, P., Elia, G. (2011). *Interventi di stabilizzazione nei pendii dell'Appennino Dauno: analisi dello stato esistente e proposta di criteri innovativi*. XXIV Convegno AGI, Napoli.

Croce, A. (1977). Opening adress. Proceed. Int symp. "*The geotechnics of strutturally complex formations*". Capri , Gen., Rep. Vol 2, 148-151.

Crostella, A., Vezzani, L. (1964). *La geologia dell'Appennino foggiano*. Boll. Soc. Geol. It., 83, 121-142.

Cruden, D.M., Varnes, D.J. (1996). *Landslide types and processes*. In Landslides - Investigation and Mitigation,Transportation Research Board Special Report No. 247 (A.T. Turner &. R.L. Schuster ed.), National AcademyPress, Washington DC, 36-75.

D'Argenio, B., Pescatore, T., Scandone, P. (1972). *Schema geologico dell'Appennino Meridionale Campania e Lucania)*. Atti del Conv. Moderne vedute sulla geologia dell'Appennino (Roma 16-18 Febbraio 1972), Accad. Naz. Lincei, Quad., 183, 49-72.

D'Elia, B. (1983). *La stabilità dei pendii naturali in condizioni sismiche.* XV Convegno Nazionale di Geotecnica, AGI, Spoleto 4-6 Maggio.

D'Elia, B., Federico, G., Pescatore, T., Rippa, F. (1986). *Occurrence and development of large landslide (Andretta, Italy) reactivated by the November 23rd 1980 earthquake*. Geologia Applicata e Idrogeologia, vol. XXI (2), 365-381.

D'Elia, B., Picarelli, L., Leroueil, S., Vaunat, J. (1998). Geotechnical characterization of slope movements in structurally complex clay soils and stiff jointed clays. Rivista Italiana di Geotecnica, 3/1998, 5-47.

Decanini, L., Di Pasquale, G., Galli, P., Mollaioli, F., Sanò, T. (2004). *Seismic Hazard and Seismic Zonation of the Region affected by the 2002 Molise, Italy, Earthquake*. Earthquake Spectra, 20 (S1), 131-165.

Delgado, J., Garrido, J., Lopez-Casado, C., Martino, S., Pélaez, J.A. (2011). *On far field occurrence of seismically induced landslides.* Engineering Geology, 123, 204-213.

Del Gaudio V., Wasowski J. (2004). *Time probabilistic evaluation of seismically induced landslide hazard in Irpinia (Southern Italy)*. Soil Dyn. Earthq. Eng., 24, 915-928.

Del Gaudio V., Wasowski J. (2010). *Advances and problems in understanding the seismic response of potentially unstable slopes.* Engineering Geology, 122, 1-2, 73-83.

De Marchi (Commission), (1970). *Commissione interministeriale per lo studio della sistemazione idraulica e la difesa del suolo*. Atti della Commissione, I, Roma, http://www.censu.it/relazione-de-marchi/.

Di Bucci, D., Corrado, S., Naso, G., Parotto, M., Praturlon, A. (1999), *Evoluzione tettonica neogenico-quaternaria dell'area molisana.* Boll. Soc. Geol. It., 118, 13-30.

Di Bucci, D., Mazzoli, S. (2003). *The October-November 2002 Molise seismic sequence (southern Italy): an expression of Adria intraplate deformation*. Journal of the Geological Society, London, 160, 503-506.

Di Bucci, D., Massa, B., Tornaghi, M., Zuppetta, A. (2005). *Structural setting of the Sannio 1688 earthquake epicentral area (Southern Italy) from surface and subsurface data*. Journal of Geodynamics, 40, 2-3, 294-315.

Di Carluccio, A., Fabbrocino, G., Fabbrocino, S., Santucci de Magistris, F., Todisco, F. (2009) *Approccio metodologico alla valutazione di vulnerabilità per infrastrutture distribuite: aspetti geologici e geotecnici*. Anidis XIII, L'ingegneria sismica in Italia, Bologna 28 Giugno - 2 Luglio.

Dikmen, U., (2009). *Statistical correlations of shear wave velocity and penetration resistance for soils*. Journal of Geophysics and Engineering 6, 61–72.

Di Nocera, S., Matano, F., Pescatore, T., Pinto, F., Quarantiello, R., Senatore, M., Torre, M. (2006). *Schema geologico del transetto Monti Picentini orientali-Monti della Daunia meridionali: unità stratigrafiche ed evoluzione tettonica del settore esterno dell'Appennino meridionale*. Boll. Soc. Geol. It., 126, 39-58.

Di Luzio, E., Paniccia, D., Pitzianti, P., Sansonne, P. Tozzi, M. (1999). *Evoluzione tettonica dell'Alto Molise.* Bol. Soc. Geol. It., 118, 287-315.

Di Paola, G., Filocamo, F., Rosskopf, M.C. (2011). *Carta di sintesi dei geositi molisani*. http://www.regione.molise.it.

Di Rosario, F. (2008). *Comportamento di grandi frane in argille*. Ph. D. Thesis, Università Roma La Sapienza.

Douglas, J. (2004). *Ground motion estimation equations 1964–2003*. In: Reissue of ESEE Report No. 01-1: A comprehensive worldwide summary of strong-motion attenuation relationships for peak ground acceleration and spectral ordinates (1969 to 2000) with corrections and additions, Research report number: 04-001-SM, www.imperial.ac.uk.

d'Onofrio, A., Vitone, C., Cotecchia, F., Puglia, R., Santucci de Magistris, F., Silvestri F. (2009). *Caratterizzazione geotecnica del sottosuolo di San Giuliano di Puglia*. Rivista Italiana di Geotecnica, 3, 43-61.

d'Onofrio A., Mastrangelo A., Penna A., Santo A., Silvestri F. (2013). *Seismic risk analysis of buried pipelines: the case of L'Aquila gas network*. Rivista Ita-liana di Geotecnica, 4/2013.

Duncan, J.M., Wright, S.G. (2005). *Soil Strength and Slope Stability*. Gohn Wiley & Sons Inc.

EC8. (2003). Eurocode 8: *Design of Structures for Earthquake Resistance, Part 1: General Rules, Seismic Actions and Rules for Buildings*, December 2003, CEN Central Secretariat, Bruxel, ENV 1998-1-1.

Eckel, E.B. (1970). The Alaska earthquake March 27, 1964: Lessons and Conclusions. Geological Survey Professional Paper, 546, pp. 64.

Eidinger, J. (1998). *Lifelines, water distribution systems in the Loma Prieta, California, earthquake of October 17, 1989.* Performance of the built environment e Lifelines. US Geological Survey Professional Paper 1552-A (pp. 63e80

EN-1997-1, Eurocode 7 (2004). *Geotechnical design – Part 1: General rules*. CEN European Committee for Standardization, Brussels, Belgium.

EN-1997-2, Eurocode 7 (2007). *Geotechnical design – Part 2: Ground investigation and testing.* CEN European Committee for Standardization, Brussels, Belgium.

EN 1998-1 (2006). *Eurocode 8: Design of structures for earthquake resistance – Part 1: General rules, seismic actions and rules for buildings.* CEN European Committee for Standardization.

Esposito E., Luongo G., Marturano A., Porfido S. (1987). *Il terremoto di S.Anna del 26 Luglio1805*. Mem. Soc. Geol. It., 37, 171-191

Esu, F., Martinetti, S. (1965). *Considerazioni sulle caratteristiche tecniche delle argille Plio-Pleistoceniche della fasia costiera adriatica tra Rimini e Vasto*. VII Convegno di Geotecnica, Trieste.

Esu, F.(1977). *Behavior of slope in structurally complex formations*. Proceed. Int symp. "The geotechnics of strutturally complex formations". Capri , Gen., Rep. Vol 2, 292-304.

Evangelista L., Fabbrocino S., Lanzano G., Todisco F., Santucci de Magistris F., Fabbrocino G. (2011). *Integrated geotechnical characterization of distributed sites in the Molise Region (Italy) for seismic vulnerability analysis.* 5ICEGE 5th International Conference on Earthquake Geotechnical Engineering, January 2011, Santiago, Chile.

Fabbrocino, G., Di Fusco, A., Manfredi, G. (2005). *In situ evaluation of concrete strength for existing constructions: critical issues and perspectives of NDT methods.* Symposium "Keep Concrete Attractive", Budapest 22- 25 May.

Fabbrocino S., Lanzano G., Forte G., Santucci de Magistris F., Fabbrocino G. (2014). *SPT blowcount versus shear wave velocity relationship in the structurally complex formations of the Molise region (Italy).* A paper submitted to Engineering Geology.

Fabbrocino S., Paduano P., Forte G., Lanzano G., Santucci de Magistris F., Fabbrocino G. (2014). *Engineering Geology Model for seismic vulnerability assessment of critical infrastructures*. A paper submitted to London Geological Society Special Publication

Farr, T.G., Kobrick, M. (2000). *Shuttle radar topography mission produces a wealth of data*. Eos, Transactions American Geophysical Union, 81, 48, 583–585.

Federico, G., Tancredi, G. (1980). *Osservazioni sulle proprietà meccaniche in sede delle argille varicolori molisane.* Rivista Italiana di Geotecnica, 1/80.

Fell, R., Hungr, O., Leroueil, S., Riemer, W. (2000). *Keynote lecture – Geotechnical engineering of the stability of natural slopes, and cuts and fills in soil*. GeoEng 2000 Congress, 19-24 November, Melbourne, Australia.

Fellenius, W. (1936). *Calculation of the Stability of Earth Dams*. Proceedings of the Second Congress of Large Dams, 4, 445 - 463.

Fenelli, G.B., Paparo Filomarino, M., Picarelli, L., Rippa, F. (1982). Proprietà fisiche e meccaniche di argille varicolori dell'Irpinia. Rivista Italiana di Geotecnica, 3/82.

Festa, A., Ghisetti, F., Vezzani, L. (2006). *Carta Geologica del Molise scala 1:100,000. Note illustrative*: Regione Molise Presidenza della Giunta, Litografia GEDA, Nichelino (TO) ISBN 88-902635-0-4.

Fiorillo, F. (2003). *Geological features and landslide mechanisms in an unstable coastal slope (Petacciato, Italy).* Engineering Geology, 67, 255–267.

Forte, G., Fabbrocino, S., Santucci de Magistris, F., Silvestri, F. (2013). Seismic Permanent Ground Deformations: earthquake triggered landslides in Molise Apennines. Rend. Online Soc. Geol. It., 24, 134-136.

Forte, G., Fabbrocino, S., Santucci de Magistris, F., Silvestri, F., Fabbrocino, G. (2014). Earthquake triggered landslides: the case study of a roadway network in Molise Region (Italy). IAEG Conference proceedings in press.

Fracassi, U., Valensise, G. (2007). *Unveiling the Sources of the Catastrophic 1456 Multiple Earthquake: Hints to an Unexplored Tectonic Mechanism in Southern Italy*. BSSA, 97, 3, 725-748.

Frazzetta, G., Lanzafame, G. (1977). *I dissesti del medio e basso bacino del F. Biferno*. Geol. Rom., 16, 87-111.

Fruzzetti, V.M.E., Scarpelli, G., Ruggeri, P., Segato, D., Vita, A. (2013). *Caratterizzazione geotecnica delle argille Grigio-azzurre calabriane.* IARG, Incontro Annuale dei Ricercatori di Geotecnica, Perugia, 16-18 Settembre 2013.

Galeandro, A., Doglioni, A., Guerricchio, A., Simeone, V. (2013). *Hydraulic stream network conditioning by a tectonically induced, giant, deep-seated landslide along the front of the Apennine chain (south Italy).* Nat. Hazards Earth Syst. Sci., 13, 1269–1283.

Garcìa-Rodriguèz M.J., Havenith H.B. Benito B. (2002). *Evaluation of Earthquake- triggered landslides in El Salvador using a Gis based Newmark model*. 14th Conference on Earthquake Engineering, October 12 - 17, 2008, Beijing, China.

Gilbert, G.K., Humphrey, R.L., Sewell, J.S., Soule, F. (1907*). The San Francisco Earthquake and Fire of April 18th, 1906 And Their Effects On Structures And Structural Materials*. Washington: Government Printing Office.

Grana, F. (2007). *Caratterizzazione geotecnica dei movimenti lenti e profondi delle coltri detriche e di frana delle formazioni marnoso-calcaree dei Monti Martani.* Ph. D. Thesis, Università Roma La Sapienza.

Gruppo di Lavoro MS. (2008). *Indirizzi e criteri per la microzonazione sismica*. Conferenza delle Regioni e delle Province autonome, Dipartimento della protezione civile, Roma, 3 vol. e Dvd. (*in Italian*).

Guadagno, F:M:, Palmieri, M., Siviero, V., Vallario, A. (1987). *La frana del Febbraio 1984 in località fonte Griciatta nel Comune di Agnone (Isernia).* Mem. Soc. Geol. It., 37, 127-134.

Guerricchio, A., Melidoro, G., Simeone, V. (1996). *Le grandi frane di Petacciato sul versante costiero adriatico (Molise).* Mem. Soc. Geol. It., 51, 607-632.

Guerriero G. (1995). *Modellazione sperimentale del comportamento meccanico di terreni incolata*. Ph. D. Thesis, Università degli Studi di Napoli Federico II.

Hancox, G.T., Perrin, N.D., Dellow, G.D., (2002). *Recent studies of historical earthquake induced landsliding, ground damage, and MM intensity in New Zealand*. Bulletin of the New Zealand Society for Earthquake Engineering, 35, 59–95.

Hasançebi, N., Ulusay, R., (2007). *Empirical correlations between shear wave velocity and penetration resistance for ground shaking assessments*. Bulletin of Engineering Geology and the Environment 66, 203–213.

Harp, E.L., Jibson, R.W. (1996). *Landslides triggered by the 1994 Northridge, California, earthquake*. BSSA, 86, S319-S332.

Harr, M.E. (1987). *Reliability-based design in Civil Engineering.* McGraw-Hill Book Company.

Havenith H.B. (2002). *Experimental studies in the Tien Shan mountains (central Asia) and dynamic modelling*. Ph. D thesis, Universitè de Liège.

Hippolyte, J.C., Angelier, J., Roure, F. (1994). *A major geodynamic change revealed by Quaternary stress patterns in the Southern Apennines (Italy)*. Tectonophysics, 230, 199-210.

Hutchinson, J.N. (1988). *Morphology and geotechnical parameters of landslides in relation to geology and*

hydrogeology. Proc. 5th Int. Symp. On Landslides, Lausanne, Editor C. Bonnard, Balkema, Rotterdam, 3-35.

IAEG (1990). *IAEG Commission on landslides, suggested nomenclature for landslides*. Bulletin of the International Association of Engineering Geology, 41, 13-16.

Idriss, I.M. (1985). *Evaluating seismic risk in engineering practice.* Theme Lecture, Proceedings of the Eleventh International Conference on Soil Mechanics and Foundation Engineering, San Francisco, 265-320.

Idriss I.M., Boulanger R.W., (2004). *Semi-Empirical Procedures for Evaluating Liquefaction Potential During Earthquakes*. Proc.11th ICSDEE & 3rd ICEGE, Berkeley, CA, USA, Doolin et al. (Eds), 1, 32-56.

Iervolino, I., Galasso, C., Cosenza, E. (2010). *REXEL: computer aided record selection for code-based seismic structural analysis*. Bull Earthquake Eng., 8, 339–362

Ippolito, F., D'Argenio, B., Pescatore, T. Scandone, P. (1975). *Structural-Stratigraphic Units and Tectonic Framework of Southern Apennines*. In Squyres C. Ed., Geology of Italy, Earth Sci. Soc. Lybian Arab Republ., 317-328.

ISPRA (2005). *Rapporto sulle frane in Italia - Capitolo 19 Molise*. A cura di Rosskopf M.C. & Aucelli P. http://www.isprambiente.gov.it/it/pubblicazioni/rapporti/Rapporto-sulle-frane-in-Italia.

ISSMGE. (1999). *Manual for Zonation on Seismic Geotechnical Hazards (revised version)*. Technical Committee for Earthquake Geotechnical Engineering, TC4, International Society for Soil Mechanics and Geotechnical Engineering. The Japanese Geotechnical Society, Tokyo.

Iysian, R., (1996). *Correlation between shear wave velocity and in-situ penetration test results*. Digest 96, December, 371-374.

Jafari, M.K., Asghari, A., Rahmani, I., (1997). *Empirical correlation between shear wave velocity (Vs) and SPT-N value for south of Tehran soils*. Proceedings of 4th International Conference on Civil Engineering (Tehran, Iran) (in Persian).

Janbu, N. (1954). *Applications of Composite Slip Surfaces for Stability Analysis*. Proceedings of the European Conference on the Stability of Earth Slopes, Stockholm, 3, 39 - 43.

Japanese Geotechnical Society (1998). *Geotechnical aspects of the January 17, 1995 Hyogoken-Nambu earthquake*. Soils & Foundations; 2 (special issue).

Jibson, R.W., Keefer, D.K., (1993). *Analysis of the seismic origin of landslides: Examples from the New Madrid seismic zone*. Geological Society of America Bulletin, 105, 521-536.

Jibson, R.W., Edwin, L.H., Michael, J.A. (1998). A *Method for Producing Digital Probabilistic Seismic Landslide Hazard Maps: An Example from the Los Angeles, California, Area*. USGS Open-File Report 98-113.

Jibson, R.W., Crone, A.J. (2001). *Observations and Recommendations Regarding Landslide Hazards Related to the January 13, 2001 M-7.6 El Salvador Earthquake*. USGS Open-file Report, 01-141.

Jibson, R.W., Michael, J.A. (2009). Maps showing the seismic landslide hazards in Anchoredge, Alaska. U.S. Geological Survey Scientific Investigations Map 3077, scale 1:25,000, 11-p. pamphlet. [Available at URL http://pubs.usgs.gov/sim/3077]

Jibson, R.W. (2011). Methods for assessing the stability of slopes during earthquakes—A retrospective: Engineering Geology, 122, 43-50.

Kalteziotis, N., Sabatakakis, N., Vasiliou, I., (1992). *Evaluation of dynamic characteristics of Greek soil formations.* Proc. 2nd Hellenic Conference on Geotechnical Engineering, Thessaloniki, Oct. 1992, Vol. II, pp. 239-2 (in Greek).

Keefer, D.K. (1984). *Landslides caused by earthquakes.* Geological Society of America Bulletin, 95, 406-421.

Keefer, D.K., Wilson, R.C., (1989). *Predicting earthquake-induced landslides, with emphasis on arid and semi-arid environments, in Landslides in a Semi-arid environment*. Inland Geological Society, Riverside, California, 2, 118-149.

Keefer, D.K. (2000). *Statistical analysis of an earthquake induced landslides distribution-1989 Loma Prieta, California event*. Engineering Geology, 58, 231-249.

Keefer, D.K. (2002). *Investigating landslides caused by earthquakes - A historical review*. Surveys in Geophisics, 23, 473-510.

Kieffer, D.S., Jibson, R., Rathje, E.M., Kelson, K. (2006). *Landslides Triggered by the 2004 Niigata Ken Chuetsu, Japan, Earthquake.* Earthquake Spectra, 22, S1, S47-S73.

Kramer, S.L. (1996). *Geotechnical Earthquake Engineering*. ISBN-10:0133749436.

Kulhaway, F.H., Maine, P.W., (1990). *Manual on estimating soil properties for foundation design.* Electric Power Research Institute, EPRI EL6800, Project 1493-6, Final Report.

Kuribayashi, E. Tatsuoka, F. (1975). *Brief review of liquefaction during earthquakes in Japan*. Soils and Foundations, 15, 4, .81-92.

Lacasse, S. Nadim, F. (1996). *Uncertainties in characterizing soil properties*. Uncertainty in the Geologic Environment. From Theory to Practice. Madison, ASCE,49–75.

Lambe T.W., Whitman, V.W. (1969). *Soil Mechanics*. Massachussets Institute of Technology.

Landolfi, L., Caccavale, M., d'Onofrio, A., Silvestri, F., Tropeano, G. (2011). *Preliminary assessment of site stratigraphic amplification for shakemap processing*. 5th ICEGE, 10 - 13 January, Santiago, Chile.

Lanzafame, G., Tortorici, L. (1976). *Osservazioni geologiche sul medio e basso bacino del fiume Biferno (Molise, Italia centro-meridionale).* Geol. Rom., 15, 199-222.

Lanzano, G., Salzano, E., Santucci de Magistris, F., Fabbrocino, G. (2013). *Seismic vulnerability of gas and liquid buried pipelines.* Journal of loss prevention in Process Industries, 28, 72-78.

Lee, I. K., White, W. Ingles, O. G. (1983). *Geotechnical Engineering*. Boston, Pitman.

Legg, M.R., Slosson,J.E. (1984). *Probabilistic approach to earthquake-induced landslide hazard mapping.* In Proceedings of Eighth World Conference on Earthquake Engineering, San Francisco, CA, 445-452.

Lemoine A., Douglas J., Cotton F. (2012). *Testing the Applicability of Correlations between Topographic Slope and VS30 for Europe.* Bulletin of the Seismological Society of America, 102, 6, 2585–2599.

Lomnitz, C., Rodríguez E., S. (2001). *El Salvador 2001: Earthquake disaster and disaster preparedness in a tropical volcanic environment*. Seismological Research Letters, 72, 346-351.

Lumb, P. (1974). *Application of statistics in soil mechanics*. Soil Mechanics: New Horizons. Lee, I. K., ed., London, Newnes-Butterworth: 44–112, 221–239.

Luzi L., Pergalani F. (1996). *Applications of statistical and GIS techniques to slope instability zonation (1:50,000 Fabriano geological map sheet).* Soil Dyn. and Earth. Eng., 15(2), 83–94.

Luzi L., Pergalani F. (2001). A correlation between slope failures and accelerometric parameters: the 26 September 1997 earthquake (Umbria-Marche, Italy), Soil Dynamics and Earthquake Engineering, 20, 5-8, 301-313.

Mankelow, J.M., Murphy, W. (1998). Using GIS in the probabilistic assessment of earthquake triggered landslide hazards. Journal of Earthquake Engineering, 2:4, 593-623.

Martino, S., Scarascia-Mugnozza, G. (2005). *The role of the seismic trigger in the Calitri (Italy) landslide: historical reconstruction and dynamic analysis*. Soil Dyn. Earth. Eng., 25, 933-950.

Mavrouli,O., Fotopoulou, S., Pitilakis, K., Zuccaro, G., Corominas, J., Santo, A., Cacace, F., De Gregorio, D., Di Crescenzo, G., Foerster, E., Ulrich, T. (2014). Vulnerability assessment for reinforced concrete buildings exposed to landslides.Bulletin of Engineering Geoly and Environment, DOI:10.1007/s10064-014-0573-0.

Meletti, C., Galadini, F., Valensise, G., Stucchi, M., Basili, R., Barba, S., Vannucci, G., Boschi, E. (2008). *A seismic source zone model for the seismic hazard assessment of the Italian territory.* Tectonophysics, 450, 85-108.

Michelini, A., Faenza, L., Lauciani V., Malagnini, L. (2008). *ShakeMap implementation in Italy*. Seismol. Res. Lett. 79, 5, 688–697.

Miles, S.B., Ho, C.L., (1999). *Rigorous landslide hazard zonation using Newmark's method and stochastic ground motion*. Soil Dynam. Earthq. Eng. 18, 305–323.

Mora, S., Mora, R., (1994). *Los deslizamientos causados por el terremoto de Limón: Factores de control y comparación con otros eventos en Costa Rica.* Revista Geologica de America Central, 139–152 (Vol. esp. Terremoto de Limón).

Morasca, P., Zolezzi, F., Spallarossa, D., Luzi, L. 2008. *Ground motion models for the Molise Region (Southern Italy).* Soil Dynamics and Earthquake Engineering, 28, 198-211.

Marchi, F., Kaynia, A.M., Gottardi, G., Nadim, F. (2011). *Role of numerical model and parameter variability on seismic response of slopes: the case of Las Colinas Landslide*. 5th ICEGE, January 2011, 10 -13 Santiago, Chile.

Marinos, P., Hoek, E. (2001). *Estimating the geotechnical properties of heterogeneous rock masses such as Flysch*. Bull. Eng. Geol. Env., 60, 85-92.

Morgenstern, N. R. (1992). *The Evaluation of Slope Stability- a 25 Year Perspective*. In Stability and Performance of Slopes and Embankments, Geotechnical Special Publication 31, ASCE, New York, 1, 1-26.

Mostardini, F., Merlini, S. (1986). *Appennino centro meridionale. Sezioni geologiche e proposta di modello strutturale.* 73° Congr. Soc. Geol. It. Roma 30.9/4.10.86, 1-59.

Newmark N.M. (1965). *Effects of earthquakes on dams and embankments*. Geotechnique, 15, 2, 139-160.

NIBS, National Institute of Building Science. (2004). *Earthquake loss estimation methodology.* HAZUS Technical manual. FEMA, Washington D.C.

NTC, (2008). *Approvazione delle nuove norme tecniche per le costruzioni (Italian Building Code)*, Gazzetta Ufficiale della Repubblica Italiana, n. 29 del 4 febbraio 2008 – Suppl. Ordinario n. 30, 2009 (in Italian).

Ogniben, L. (1963). *Le formazioni tipo Wildflysch delle Madonie (Sicilia centro-settentrionale)*. Mem. Ist. Geol. Mineral. Univ. Padova, 24, 58 pp.

Ogniben, L. (1969). *Schema introduttivo alla geologia del confine calabro-lucano.* Mem. Soc. Geol. Ital., 8, 453-763.

Olivares, L. (1996). Caratterizzazione dell'Argilla di Bisaccia in condizione monotone, cicliche e dinamiche e riflessi sul comportamento del Colle a seguito del terremoto del 1980. Ph. D. thesis, University of Naples Federico II.

Ohta, T., Hara, A., Niwa, M., Sakano, T., (1972). *Elastic shear moduli as estimated from N-value.* Proc. 7th Ann. Convention of Japan Society of Soil Mechanics and Foundation Engineering, 265-268.

Ohta, Y., Goto, N., (1978). *Empirical shear wave velocity equations in terms of characteristics soil indexes*. EarthquakeEngineering and Structural Dynamics 6, 167-187.

O'Rourke T.D. (1998). *An Overview of Geotechnical and Lifelines Earthquake Engineering*. ASCE Geotechnical Special Publication, 75, Eds., Reston.

Pagliaroli, A. (2006). *Studio numerico e sperimentale dei fenomeni di amplificazione sismica locale di rilievi isolati.* Ph. D. Thesis, Università di Roma La Sapienza.

Panico, A., Lanzano, G., Salzano, E., Santucci de Magistris, F., Fabbrocino, G. (2013), Seismic *Vulnerability of Wastewater Treatment Plants*. Chemical Engineering Transactions, 32, 13-18, DOI: 10.3303/CET1332003

Paolucci, R., (2002) *Amplification of earthquake ground motion by steep topographic irregularities.* Earthquake Engineering and Structural Dynamics, 31, 1831-1853.

Papadopoulos, G.A., Plessa, A., (2000). *Magnitude-distance relations for earthquake–induced landslides in Greece.* Engineering Geology 58, 377–386.

Patacca, E., Scandone, P. (2004). *The 1627 Gargano earthquake (Southern Italy): Identification and characterization of the causative fault.* Journal of Seismology, 8, 259-273.

Patacca, E., Scandone, P. (2007). *Geology of the Southern Apennines.* Boll. Soc. Geol. It, (Ital. J. Geosci.), Spec. Issue 7, 75-119.

Pellegrino, A., Picarelli, L. (1982). *Contributo alla caratterizzazione geotecnica di formazioni argillose intensamente tettonizzate.* Convegno del progetto finalizzato Conservazione del suolo - Fenomeni franosi, Roma.

Pellegrino, A., Picarelli, L., Bilotta, E. (1985). *Caratteristiche geotecniche e stabilità dei pendii in formazioni strutturalmente complesse*. In: Geotechnical Engineering in Italy, An Overview, AGI, 195-214.

Pertusati, S., Buonanno, A. (2009). *Structural evolution of a foreland basin succession : the Dauna Unit in the Sannio-Molise sector of the Southern Apennines*. Ital. J. Geosci. 128(2): 551 – 564.

Pescatore, T., Sgrosso, I., Torre, M. (1969). *Lineamenti di tettonica e sedimentazione nel Miocene nell'Appennino campano-lucano.* Mem. Soc. Nat. in Napoli, suppl. al Boll., 78, 337-408.

Pescatore, T. (1988). *La sedimentazione miocenica nell'Appennino Campano-Lucano.* Mem. Soc. Geol. It., 41, 37-46.

Pescatore, T., Di Nocera, S., Matano, F., Pinto, F. (2000). *L'unità del Fortore nel quadro della geologia del settore orientale dei Monti del Sannio (Appennino meridionale)*. Boll. Soc. Geol. It., 119, 587-601.

Pescatore, T., Di Nocera, S., Matano, F., Pinto, F., Quarantiello, R., Amore, O., Boiano, U., Civile, D., Fiorillo, L., Martino, C. (2008). *Geologia del settore centrale dei monti del Sannio: nuovi dati stratigrafici e strutturali.* Mem. Descr. Carta Geol. d'It., 77, 77-94.

Phoon, K. K., Kulhawy, F. H. (1999). *Characterization of geotechnical variability*. Canadian Geotechnical Journal, 36(4), 612–624.

Pisanò, F. (2011). *Seismic performance of infinite earth slopes: numerical modelling, constitutive issues and theoretical considerations*. Ph. D. Thesis, Politecnico di Milano.

Pitilakis, K., Alexoudi, M., Argyroudis, S., Anastasiadis, A. (2006) *Seismic risk scenarios for an efficient seismic risk management: the case of Thessaloniki (Greece)*. In Advances in Earthquake Engineering for Urban Risk Reduction, Nato Science Series: IV: Earth and Environmental Sciences Volume 66, 229-244.

Postpischl, D., Branno, A., Esposito, E., Ferrari, G., Maturano, A., Porfido, S., Rinaldis, V., Stucchi, M. (1985). *The Irpinia earthquake of November 23, 1980, in Atlas of Isoseismal Maps ofItalian Earthquakes,* CNR-PFG 114(2B), 152–157.

Porfido, S., Esposito, E., Vittori, E., Tranfagla, G., Michetti, A.M., Blumetti, M., Ferreli, M., Guerrieri, L., Serva, L. (2002). *Areal distribution of ground effects induced by strong earthquakes in the Southern Apennines (Italy).* Surveys in Geophisics, 23, 529-562.

Porfido, S., Esposito, E., Guerrieri, L., Vittori, E., Tranfaglia, G., Pece, R. (2007). *Seismically induced ground effects of 1805, 1930, 1980 earthquakes in Southern Apennines (Italy).* Ital. J. Geosci. (Boll. Soc. Geol. It.), 126 (2), 333-346.

Prestininzi, A., Romeo, R. (2000). *Earthquake-induced ground failures in Italy*. Engineering Geology, 58, 387–397.

Puglia, R. (2008). *Analisi della risposta sismica locale di San Giuliano di Puglia*. Ph. D. Thesis.

Rapolla, A., Paoletti, V., Secomandi, M. (2010). *Seismically-induced landslide susceptibility evaluation: Application of a new procedure to the island of Ischia, Campania Region, Southern Italy*. Eng. Geol., 114, 10-25.

Rasulo A., Goretti A., Nuti, C. (2004). *Performance of Lifelines During the 2002 Molise, Italy, Earthquake*. Earthquake Spectra, 20, S1, 301-314.

Regione Molise (2001). *Studio del Rischio Idrogeologico nella Regione*. Europrogetti & Finanza, Sudgest, Physis.

Rivieccio, M. (2013). *Fattori geologico – geomorfologici per la definizione della suscettibilità da frana a cinematismo lento in aree ad alta sismicità: analisi e confronti di casi studio.* Ph. D. Thesis, University of Naples.

Rizzi Zannoni, G. A. (1809). *Atlante Geografico del Regno di Napoli, map no. 7*, Stamperia Reale, Napoli (edited by: Valerio, V., Società Uomini e Istituzioni Cartografiche nel Mezzogiorno d'Italia, Firenze, Istituto Geografico Militare, 1993).

Rodriguez, C.E., Bommer, J.J., Chandler, R.J. (1999). *Earthquake-induced landslides: 1980–1997.* Soil Dynamics and Earthquake Engineering, 18, 325–346.

Rodríguez, C.E., (2006). *Earthquake-induced landslides in Colombia*. ECI Conference on Geohazards, Lillehammer, Paper 38.

Romeo, R., Delfino L. (1997). *Catalogo nazionale degli effetti deformativi del suolo indotti da forti terremoti*. Rapporto Tecnico SSN/RT/97/04, Roma, Maggio 1997.

Romeo, R. (2000). *Seismically induced landslide displacements:a predictive model.* Engineering Geology, 58, 337–351.

Rosskopf, M. C., Aucelli, P. C. (2007). *Analisi del dissesto da frana in Molise.* In: Rapporto sulle frane in Italia. Il progetto IFFI. Metodologia, risultati e rapporti regionali. Rapporti APAT 78:493–508.

Rovida, A., Camassi R., Gasperini, P., Stucchi, M. (2011). *CPTI11, the 2011 version of the Parametric Catalogue of Italian Earthquakes*. Milano, Bologna, http://emidius.mi.ingv.it/CPTI. DOI: 10.6092/INGV.IT-CPTI11

Sabetta F. Pugliese A. (1996). *Estimation of Response Spectra and Simulation of Nonstationary Earthquake Ground Motions*. BSSA, 86, 2.

Salvador, A. (1994). *International stratigraphic guide*. The geol. Soc. of Am., 2nd edition, 214 pp., Boulder (Colorado USA).

Sanchez-Sesma, F.J. (1990). *Elementary solutions for response of a wedge-shaped medium to incident SH and SV waves.* Bulletin of Seismological Society of America, 80, 737-742.

Santaloia, F., Cotecchia, F., Polemio, M. (2001). *Mechanics of a tectonized soil slope: influence of boundary conditions and rainfall.* Quarterly Journal of Engineering Geology and Hydrogeology, 34, 165 - 185.

Sarconi, M. (1784). *Osservazioni Fatte Nelle Calabrie e Nella Frontiera di Valdemone sui Fenomeni del Tramoto del 1783 e Sulla Geografia Fisica di Quelle Regioni.* Reali Accademia delle Scienze e Belle Lettere. Napoli.

Sassa, K., Fukuoka, H., Scarascia-Mugnozza, G., Evans, S. (1996). *Earthquake-induced landslides: distribution, motion and mechanisms.* Soils & Foundations, Special Issue for the Great Hanshin Earthquake Disaster, 53–64.

Scrocca, D., Tozzi, M. (1999). *Tettonogenesi mio-pliocenica dell'Appennino molisano*. Boll. Soc. Geol. Ital., 118, 255-286.

Seed, H.B. (1968). *Landslides during earthquake due to soil liquefaction*. Fourth Terzaghi Lecture, Journal of Soil Mech. Found. Div., ASCE, 94 (SM5), 1053-1122.

Selli, R. (1962). *Il Paleogene nel quadro della geologia dell'Italia centro-meridionale*. Mem. Soc. Geol. It., 3, 737-789.

Serva, L., Esposito, E., Guerrieri, L., Porfido, S., Vittori, E. V., Comerci. (2007). *Environmental effects from five historical earthquakes in Southern Apennines (Italy) and macroseismic*

intensity assessments: Contribution to the INQUA EEE Scale Project. Quaternary International, 173 -174, 30-44.

Sgrosso, I., (1986). *Criteri ed elementi per una ricostruzione paleogeografica delle zone esterne dell'Appennino centro-meridionale.* Atti 73° Congr. Soc. Geol. It., 167-170.

Sgrosso, I. (1988). *Nuovi elementi per un più articolato modello paleogeografico nell' Appennino Centro-Meridionale*. Mem. Soc. Geol. It. 41, 225-242.

Sgrosso, I. (1998). *Possibile evoluzione cinematica miocenica dell' Orogene centro-sud appenninico*. Boll. Soc. Geol. It. 117, 679-724.

Silvestri F., Aiello V., Barile A., Costanzo A., Puglia R., Pescatore T.S., Lo Russo E., Pinto F., Tornesello D. (2006). *Analisi e zonazione di pendii in condizioni sismiche: applicazione di metodi tradizionali ed avanzati ad un'area di studio*. Questioni di Ingegneria Geotecnica - Scritti in Onore di Arturo Pellegrino, Hevelius, Benevento.

Simonelli, A.L., Fortunato E. (1996). *Effects of earth slope characteristics on displacement based seismic design*. Proc. 11 World Conference on Earthquake Engineering, Acapulco, Pergamon, Oxford.

Sitar N., Khazai B. (2000). *Landsliding in native ground: A GIS based approach to regional seismic stability Assesment*. GSA Cordilleran Section, 31, InterNet http://www2.ced.berkeley.edu:8002/.

Skempton, A.W. (1953). *The Colloidal "Activity" of Clays*. Proceedings of Third International Conference on Soil Mechanics and Foundation Engineering, Switzerland, Aug 1953, 57-61.

Skempton, A.W. Hutchinson, J.N. (1969). *Stability of natural slopes and embankment foundations*. Procs., 7th International Conference of Soil Mechanics and Foundation Engineering, Mexica, State of the Art volume, 291-340.

Stewart, J.P., Brey, J.D., Seed, R.B., Sitar, N. (1994). *Preliminary report on the principal geotechnical aspectsof the January 17, 1994 Northridge Earthquake*. Report No. UCB/EERC 94-08, University of California at Berkley.

Stewart, J.P., Blake, T.F., Hollingsworth, R.A. (2003). *A Screen Analysis Procedure for Seismic Slope Stability.* Earthquake Spectra, 19,3, 697–712.

Sykora, D.W., (1987). *Examination of Existing Shear Wave Velocity and Shear Modulus Correlations in Soils.* Department of the Army, Waterways Experiment Station, Corps of Engineers, Miscellaneous Paper GL, 87-22.

Terzaghi, K., Peck, R.B., (1948). *Soil Mechanics in Engineering Practice*. J. Wiley, New York, 549 pp.

Torgoev, A., Havenith, H.B., Lamair, L. (2013). *Improvement of seismic landslide susceptibility assessment through consideration of geological and topographic amplification factors*. JAG 2013, 17-18/09 Grenoble, France.

Tortorici, L. (1975). Osservazioni geologiche sul Flysch di S. Bartolomeo nell'area compresa tra il F. *Trigno e Benevento (Italia Meridionale).* Boll. Soc. Geol. It., 94, 1791-1809.

Tosatti, G., Castaldini, D., Barbieri, M., D'Amato Avanzi, G., Giannecchini, R., Mandrone, G., Pellegrini, M., Perego, S., Puccinelli, A., Romeo, W.R., Tellini, C. (2008). *Additional Causes of Seismically-Related Landslides in the Northern Apennines, Italy.* Revista de geomorfologie,10, 5-21.

Tozzi, M., De Corso, S., Antonucci, A., Di Luzio, E., Lenci, F., Scrocca, D. (1999). *Assetto geologico della Montagnola di Frosolone.* Geol. Rom., 35, 89-109.

Tropeano, G., Ausilio, E., Silvestri, F., Troncone, A. (2007). *Analisi sismica di pendii omogenei: revisione di un metodo semplificato esistente con riferimento alla sismicità italiana*. IARG, Incontro Annuale dei Ricercatori di Geotecnica, Salerno 4-6 Luglio 2007.

Tropeano, G., Ausilio, E., Costanzo, A., Silvestri, F. (2009). *Valutazione della stabilità sismica di pendii naturali mediante un approccio semplificato agli spostamenti.* XIII Convegno Nazionale "L'Ingegneria Sismica in Italia (ANIDIS 2009)", Bologna.

Tropeano, G. (2010). *Previsione di spostamenti di pendii in condizioni sismiche*. Ph.D. Thesis, University of Calabria.

Valensise, G., Pantosti, D., Basili, R. (2004). *Seismology and tectonic setting of the 2002 Molise, Italy, Earthquake.* Earthq. Spectra, 20, 23-37.

Varnes, D.J. (1978). *Slope movements. Types and processes.* In: Schuster, R.L., Krizek, R.J. (Eds.), Landslides: Analysis and Control. Special Report, vol. 176. National Academic of Sciences, Transportation Research Board, Washington, pp. 11‐35.

Vezzani, L., Festa, A., Ghisetti, F. (2010). *Geology and Tectonic Evolution of the Central Southern Apennines.* Italy. Geological Society of America Special Paper, 469, pp. 58. doi: 10.1130/2010.2469.

Videpi Project. *Visibility of petroleum exploration data in Italy*. World Wide Web Address: 588 http://unmig.sviluppoeconomico.gov.it/videpi/en/; last access August 13th, 2013.

Vitone, C., Cotecchia, F. (2011). *The influence of intense fissuring on the mechanical behavior of clays*. Geotechnique, 61, 12, 1003-1018.

Wald, D.J., Earle P.S, Lin, K., Quitoriano V., Worden B. (2006). *Challenges in rapid ground motion estimation for the prompt assessment of global urban earthquakes*. Bull. Earthq. Res. Inst. 81, 272-281.

Wald, D.J., Allen, T.I. (2007). *Topographic slope as a proxy for seismic site conditions and amplification*. Bull. Seismol. Soc. Am. 97, no. 5, 1379–1395.

Wieczorek, G.F., Wilson, R.C., Harp, E.L., (1985). *Map Showing Slope Stability During Earthquakes in San Mateo County, California.* U.S. Geological Survey Miscellaneous Investigations Map I-1257-E, scale 1:62,500.

Wilson, R.C., Keefer, D.K., (1983). *Dynamic analysis of a slope failure from the 6 August 1979 Coyote Lake, California, earthquake*. Bulletin of the Seismological Society of America, 73, 863-877.

WP/WL1 (1993) *Multilingual Landslide Glossary*. Bi Tech Publishers, Richmond, British Columbia, Canada.

Yamagishi, H. (2000). *Recent Landslides in Western Hokkaido, Japan*. Pure appl. geophys., 157, 1115-1134.

Yokota, K., Imai, T., Konno, M., (1991). *Dynamic deformation characteristics of soils determined by laboratory tests.* OYO Tee. Rep. 3, p. 13.

Youd, T.L., Hoose, S.N. (1977). *Liquefaction susceptibility and geologic setting.* World Conference on Earthquake Engineering, 6th New Delhi, Proceedings v 3, 2189-2194.

Youd, T.L., Hoose, S.N. (1978). *Historic ground failures in northern California triggered by earthquakes*. U.S. Geological Survey professional paper 993, U.S. Govt. Print. Off., Washington, IV, 177 pp.